A computational framework for analysis and optimisation of automated solar shading systems

Document status and date:
Published: 16/02/2022

Document Version:
Publisher's PDF, also known as Version of Record (includes final page, issue and volume numbers)

Please check the document version of this publication:

• A submitted manuscript is the version of the article upon submission and before peer-review. There can be important differences between the submitted version and the official published version of record. People interested in the research are advised to contact the author for the final version of the publication, or visit the DOI to the publisher's website.
• The final author version and the galley proof are versions of the publication after peer review.
• The final published version features the final layout of the paper including the volume, issue and page numbers.

Link to publication

A computational framework for analysis and optimisation of automated solar shading systems

WITHIN HIGH PERFORMANCE BUILDING FACADES

Samuel de Vries

Bouwstenen   Nr.329

A computational framework for analysis and optimisation of automated solar shading systems

Within high performance building facades

PROEFSCHRIFT

ter verkrijging van de graad van doctor aan de Technische Universiteit Eindhoven, op gezag van de rector magnificus prof.dr.ir. F.P.T. Baaijens,

voor een commissie aangewezen door het College voor Promoties, in het openbaar te verdedigen op woensdag 16 februari 2022 om 13:30 uur

door

Samuel Bruno de Vries

geboren te Amsterdam

Dit proefschrift is goedgekeurd door de promotoren en de samenstelling van de promotiecommissie is als volgt:

voorzitter	prof.dr.ir. A.S.J. Suiker
1e promotor	prof.dr.ir. J.L.M. Hensen.
Copromotor	dr.ir. R.C.G.M. Loonen.
Promotie-commissieleden	prof.dr. M. Overend (Technische Universiteit Delft)
	prof.dr.ir. M. Aries (Jonkoping University)
	prof.dr. F. Goia (Norwegian University of Science and Technology)
	prof.ir. W. Zeiler

A computational framework for analysis and optimisation of automated solar shading systems

Within high performance building facades

To:

Meta Hees & Geert de Vries

Table of contents

Summary

Automated shading systems have the potential to substantially reduce building energy consumption, increase occupant exposure to natural daylight and reduce visual and thermal discomfort. The performance of automated solar shading systems, however, greatly depends on how these screens or slats are operated. Conventional control strategies for automated shading systems, that tend to follow binary close-open approaches, are ill-equipped to respond to the large variety of environmental conditions and shifting performance goals in managing the indoor climate of office buildings. Consequently, they inadequately satisfy the visual comfort requirements of occupants and are frequently associated with user dissatisfaction.

Recently, a series of enabling developments has led to promising comfort-driven control strategies being proposed that seek to maximise the admission of daylight by closing shading devices only to the extent that is necessary to prevent daylight glare or thermal discomfort. If these strategies are to be deployed successfully at scale, however, there are several challenges that need to be overcome. For the development and application of such comfort-driven automated shading strategies there is a need for detailed insight into how control and design parameters can be leveraged to influence building performance trade-offs. Additionally, there is a need for generically applicable and scalable workflows for the development of control strategies and their successful deployment in specific buildings.

This doctoral dissertation investigates how computational analyses and optimisation can be used to support the development and application of comfort-driven shading strategies. More specifically, the objective of this research is to develop and test a computational framework for performance evaluation and optimisation of advanced automated shading strategies. Firstly, this framework consists of a virtual test bed (VTB) aimed at analysing the performance of (i) advanced shading controls, (ii) materialisation and shading design features, and (iii) applications of dynamic solar shading systems within performance-driven façade design processes. Secondly, this framework encapsulates a set of computational support methods, aimed at performance analysis, optimisation, and quality control in the application of the VTB.

Because of the fragmented façade design and delivery process, the design and control parameters that define the building performance effects of automated shading systems are specified by various decision makers at different positions in the supply chain. In addition, these design and control parameters vary in their physicality and scale (e.g., from control parameters to detailed shading device properties, to the design of the overall façade). The requirements for the computational framework are therefore investigated through an iterative process

involving four application studies. This process includes feedback from stakeholders in the shading industry. In each application study, the computational framework is developed and tested by applying it to analyse and optimise a series of design and control aspects that are specific to a particular type of shading system and decision-maker perspective.

The development of the computational framework starts by analysing the characteristics of the problem at hand. A literature review identifies the needs and possibilities for applying building performance simulation (BPS) effectively to support decision making in this domain. This literature review is focussed on: (i) the challenges and opportunities in the development and application of comfort-driven automated shading systems and (ii) the state of the art and knowledge gaps in computational analyses and optimisation of advanced fenestration systems.

Based on the identified needs and possibilities, and the findings of the four application studies, a set of requirements for the computational framework were obtained. These requirements point out the need for a multi-domain tool that is able to describe interactions between indoor daylighting and thermal conditions and how these are affected by shading systems with time-varying optical and thermal behaviour. Additionally, it is concluded that the VTB must have the ability to accommodate complex control methods as well as describe the automated shading system at different levels-of-scale. Finally, the VTB must be configurable in accordance to: (i) the perspective of varying decision makers, (ii) automated shading systems with various characteristics, (iii) the purpose of the simulation study, (iv) the available input information.

The main contribution of the research is the developed computational framework. This framework consists of a VTB for analyses and optimisation of automated shading systems and a set of computational support methods that facilitate the effective use of this VTB. The VTB follows a modular structure and is envisioned as a continuously evolving toolchain that can be applied in new configurations and extended to fulfil new desired functionalities. The VTB is designed for multi-domain and multi-scale simulation of automated shading systems. It employs a co-simulation approach between high-resolution domain specific tools using middleware software. These domain specific tools are used for transient thermal building simulation, daylighting and glare simulation, and control system simulation. Additionally, the VTB uses a stepped approach where sub-system simulations are used to describe the physical behaviour of shading materials, shading devices, and the overall fenestration system. The emergent physical behaviour predicted by subsystem simulations at the lower levels of scale is used to define input parameters for models that describe the fenestration system at a higher level of abstraction and predict performance effects on the building level. The VTB

also includes multiple features for modelling energy systems at varying levels of detail. These energy system models allow building designers to investigate interactions between the indoor climate effects of shading controls, HVAC system performance, and time-of-use dependent on-site or grid electricity characteristics. In addition, these models are demonstrated to be suited for quantifying uncertainties regarding future electricity grid characteristics. The novelty of the VTB can be found in the combination of existing simulation techniques into a coherent simulation environment aimed at their application in the context of product development, which is a relatively new field of application for BPS.

Each VTB module is individually verified and validated throughout the four application studies. In addition, the four application studies show that the modular structure of the VTB allows it to be configured to fulfil various simulation objectives and describe a variety of shading systems. Furthermore, these studies illustrate fit-for-purpose application of the VTB and provide guidance in the selection of model complexity and resolution. Through these studies, this research contributes to the knowledge on performance modelling of complex fenestration systems.

The analyses and optimisation support methods that are developed in this research use statistical classification techniques to identify high performance sensor configurations, detection algorithms and control parameters. The application studies show that the presented support methods are generically applicable and not tied to a particular type of shading system or building application. Additionally, these methods require only a small number of simulations and relatively little effort from a developer. Therefore, it is concluded that the support methods fit well within the constraints imposed by the current practice of shading control development. The support methods contribute to the body of knowledge on the simulation-based development of advanced shading strategies. Their novelty can be found in the beneficial trade-off between (i) their replicability, (ii) their effectivity in finding control strategies that optimally exploit non-intrusive and non-ideal sensors, and (iii) the time, effort, and skill that are required of developers in their application. Many existing approaches tend to perform particularly well in only a subset of these three aspects. Because the support methods place due emphasis on all three aspects, however, they allow the creation of control strategies that are potentially more scalable in the current context.

The computational framework has gone through usability testing in a broad variety of representative applications that illustrate the most significant ways of it. The application studies address: optimisation of design and control aspects on the five most relevant levels-of-scale (i.e.: sensor deployment strategy, control strategy, shading material, shading system, façade configuration), various types of shading systems (e.g., sun-tracking roller shades and vertical blinds), and the perspectives of

various decision makers that are positioned at varying places within the façade design and delivery process (e.g., control developers and façade designers).

A novel aspect of this research is that it presents examples of simultaneous optimisation of control and design features of automated shading system and building facades. In the existing body of research, and in engineering practice, optimisation of these aspects is predominantly approached either consecutively or in isolation. This research shows that that the presented co-optimisation approach can lead to outcomes that offer increased visual comfort, improved energy performance and lower costs than the solutions that are found using traditional approaches.

Finally, this research contributes insights into the causal relationships between solar shading design and control features and building performance effects. These insights give reason to reconsider the often thermally driven approach to the design of facades, the specification of solar shading devices and the development of control approaches.

Nomenclature

3PHS	Radiance three phase method
-ab	Radiance rendering parameter: Ambient bounces
-ad	Radiance rendering parameter: Ambient divisions
-lw	Radiance rendering parameter: Limit weight
-c	Radiance rendering parameter: Number of rays to accumulate
ACC	Accuracy
ACH	Air changes per hour
ANSI	American National Standards Institute
AOI	Angle of incidence
ASHRAE	American Society of Heating, Refrigerating and Air-Conditioning Engineers
ASHWAT	ASHRAE Window Attachment model
ASTM	American Society for Testing and Materials (reference spectral distribution for solar irradiance)
AU	Always Up
BCVTB	Building controls virtual testbed
BL	Baseline control strategy
BPS	Building Performance Simulation
bRA	Blind rotation angle
BRTDfunc	A radiance material modifier based on a bi-directional reflection transmission distribution function
BSDF	Bidirectional scattering distribution function
CD	Cooling demand
cDA_{300lx}	Continious daylight autonomy using 300 lux as a performance criterion
CDD	Cooling degree days
CEN	European Committee for Standardization
CFS	Complex fenestration system
CGDB	Complex glazing database
CM	Control mode
COA	Cutt-off angle
COP	Coefficient of performance
CSV	Comma-separated values
CT	Classification Tree
CT_{CM}	Classification Tree for detecting glare for a particular control mode
$CT_{SM;SP}$	Classification Tree for detecting glare for a particular control mode designated by its shade mode and shade position
D_{opt}	Optimal facade design solution

5

D_{300lx}	Daylit area fraction using 300 lux as a cutt-of criterion
DA	Daylight autonomy
DAL	Dalec, a tool for integrated day light and artificial light and energy calculation
DAYSIM	a tool for simulation of daylight and artificial lighting
DC	building design characteristics used as inputs for a CT control strategy
DGP	Daylight Glare Probability
DGP_{Rpict}	Daylight Glare Probability simulated using the Radiance Rpict program
DGPs	Daylight glare probability simplified
$DGPs_{0.4;0deg;exc.}$	$DGPs_{0.4;exc.}$ for the viewing direction facing into the 0 degree direction. Maximum of two occupant positions
$DGPs_{0.4;exc}$	Share of office hours that a DGPs of 0.4 is exceeded
DMX	Radiance three phase method daylight matrix
$D_{rcontrib}$	Rcontrib program parameters for generating view matrices
e	Opening area between two blinds projected parallel onto window surface
EL	The eye-level control mode
E_{light}	Lighting energy demand
EMS	Energy Management System
EP	EnergyPlus
E_{prim}	Primary energy consumption for heating, cooling and lighting
Ev	Indoor vertical illuminance sensor readings
EWF	Exposed window fraction
$EWF_{40\%;exc.}$	Share of office hours that an EWF of 40% is exceeded
EX	Exceedance
EXT	Exterior
FN	False negatives
FP	False positives
GHG	Greenhouse gass
HD	Heating demand
HDD	Heating degree day
HDR	High definition range
HG	High gain low-E coated glazing system
Hi	Range in sensor measurements where E_v > 30000 lx
HVAC	Heating, ventilation and air conditioning
IBPSA	International Building Performance Simulation association
IDF	Energyplus input data file
IEA	International Energy Agency

IEA SHC	IEA Solar Heating and Cooling program
IES	Illuminating Engineering Society
IGDB	International glazing database
IR	Infra red
ISO	International Organization for Standardization
IWEC	International Weather for Energy Calculations
LBNL	Lawrence Berkeley National Laboratory
LIR	Longware infrared
Lo	Range in sensor measurements where E_v < 6400 lx
Low-E	Low emissivity
MF	Sky discretisation in the 3PHS method
MF3	Reinhart 3 half sphere discretisation
Mi	Range in sensor measurements where 6400 lux ≤ E_v ≤ 30000 lx
Mn	Most closed sun tracking blind control logic
MNL	Manual shading system operation
MPC	Model predictive control
Mx	Most open sun tracking blind control logic
N	North
NMBE	Normalized mean bias error
NREL	National Renewable Energy Laboratory
NRMSE	Normalized root mean square error
OF	Openess factor
Op	Most open blind position
PBC	Performance based control
PC	Performance Classification
PEF_{nonRE}	Primary fossil energy factor
PF	Penalty function
PV	Photovoltaic
PVC	Polyvinyl chloride
Rb	Reflectance of the back of the blind
RBC	Rule-based control
REHVA	Federation of European Heating, Ventilation and Air Conditioning associations
Rf	Reflectance of the front of the blind
ROC	Receiver operating characteristic
RPICT	A Radiance program
Rsol	Solar reflectance

Rvis	Visual reflectance
s	Blind area projected parallel onto window surface
S	Radiance three phase method sky matrix
SA	Shade actuation
SC	Solar cut-off control logic
$sDA_{300/50\%}$	Spatial daylight autonomy using 300 lux and 50% as cutt-of criteria
SEER	Seasonal energy efficiency ratio
SHGC	Solar heat gain coefficient
SM	Shade Mode
SOL	Solar heat gain energy
SPF	Seasonal Performance Factor
STVB	Sun-tracking vertical-blind
Ti	Indoor drybulb temperature
TN	True Negative
TP	True Positive
TPR	True Postive Rate
Tsol	Solar transmittance
Tvis	Visual transmittance
VB	Vertical Blind
VCI	View clarity index
VCT	Visual comfort time
VMX	Radiance three phase method view matrix
VPPA	Vertical projection profile angle
Vrcontrib	Rcontrib program parameters for generating view matrices
VSA	Vertical Shading Angle
VTB	Virtual Testbed
WN_y	Azimuth angle of window normal
WWR	Window-to-wall Ratio

1 Introduction

1.1 Background

Dynamic solar shading systems are an indispensable element of contemporary office buildings. Such shading systems help manage the admission of solar energy into office buildings and are therefore instrumental for achieving a visually and thermally comfortable indoor climate and reducing building energy consumption (Konis and Selkowitz 2017; Kuhn 2017; Reinhart 2004; Reinhart 2018). Occupants of office spaces generally have limited freedom in choosing their seating position in a space and cannot easily adapt to visually or thermally uncomfortable conditions resulting from exposure to direct solar radiation. Solar exposed office space without dynamic shading devices therefore lead to frequent occurrences of daylight glare (Goia 2016; Ochoa et al. 2012b; Mangkuto et al. 2016; Wienold 2007). Dynamic shading devices also reduce solar heat gains, lower indoor convective and surface temperatures, protect occupants from exposure to direct solar radiation (Luna Navarro et al. 2019), and prevent excessive cooling energy consumption (Goia 2016).

Using dynamic shading devices rather than static shading elements has the benefit that these devices can, in principle, be adapted to varying environmental conditions and occupant preferences. Such devices can be retracted, for instance, under overcast sky conditions to increase the admission of daylight. Additionally, glare discomfort cannot be fully prevented with static shading devices, particularly at low solar altitude angles, without severely impacting the functioning of the window in providing natural daylight and a view to the outdoors (Bodde 2020). Dynamic shading devices therefore get installed in most solar exposed office spaces during their operation. A large variation of dynamic shading devices is used in practice, each with their own benefits and limitations that result from the applied actuation mechanism, the shading device geometry and materialisation. Frequently used typologies are (i) roller shades where a flexible sheet is retracted vertically through a rolling mechanism, (ii) horizontal- and (iii) vertical blinds where rigid slats can be rotated or retraced fully. Although these devices are present in many office buildings, they are often not considered in the building design process. Particularly shading devices on the interior of the glazing system are usually not treated as an integral part of the building skin and their design, installation and operation are considered the responsibility of the user of the building rather than that of the building design team. Consequently, most studies aimed at the optimisation of façade design choices assume that no dynamically operated shading devices are present (Méndez Echenagucia et al. 2015; Mangkuto et al. 2016; Pilechiha et al. 2020; Susorova et al. 2013).

In most buildings these dynamic shading devices are operated manually by users. Monitoring of user interactions with manually operated shading devices (O'brien et al. 2013; Reinhart and Voss 2003; Reinhart 2004; Haldi and Robinson 2010) showed

that, although the behaviour of occupants varies greatly, most occupants operate shading devices infrequently (e.g., weekly of less) and mainly on arrival or when exiting office spaces. Operation is driven mainly by visual stimuli and users position shading devices in a way that minimizes further devices operations and disturbance or discomfort of other users (O'brien et al. 2013; Sadeghi et al. 2018; Cohen et al. 1999; O'brien and Gunay 2015). This means that users tend to close shading devices to an extent that prevents visual discomfort throughout a longer duration for multiple users whilst preserving a minimal degree of view to the outdoors (Haldi and Robinson 2010; Konis 2013; Sadeghi et al. 2016). The situation that is found in many office buildings with manually operated shading devices, has been characterised by Cohen et al. (1999) as "*blinds closed - lights on*", indicating how manual operation of shading devices often does not exploit the benefits of natural daylight and views and leads to high lighting energy consumption.

Automated solar shading systems can manage the admission of solar energy more actively in response to varying environmental conditions than manually operated or static shading solutions. This ability can be used to achieve an indoor climate that offers more beneficial trade-offs between conflicting performance goals (Kuhn 2017; Lee et al. 1998; Shen and Tzempelikos 2012; Atzeri et al. 2018; Beck et al. 2010; De Vries et al. 2019). The increased indoor comfort conditions that automated shading systems can enable have been shown to positively contribute to the health (Lucas et al. 2014; Rea and Figueiro 2018; Figueiro et al. 2019), well-being (Aries et al. 2010; Heschong 2003b; Hellinga and Hordijk 2014; Wienold 2009a), and productivity of office workers (Wargocki et al. 2007; Knoop et al. 2019; Heschong 2003b, 2003a). Additionally, previous research showed that automated shading systems can substantially reduce building energy consumption compared to situations with manually operated shading devices or no solar shading. Reductions of 12-40% in the energy demand for space cooling, 0-17% for space heating and 4-8% in electric lighting are reported in literature (Bakker et al. 2011; Hutchins 2015; Sabine and Eleanor 2015; Beck et al. 2010). The International Energy Agency (IEA) has identified dynamic solar control solutions as key technologies for transitioning to a low energy consumption built environment in developed countries where there is a strong emphasis on the tertiary industry (Lafrance 2013; Iea 2019). In summary, automated solar shading systems can potentially play an important role in reducing operational greenhouse gas (GHG) emissions of office building in a cost-effective manner. Additionally, these systems can positively contribute to the health, well-being, and productivity of office workers.

The performance of automated solar shading systems, however, greatly depends on how these shades or slats are being operated (Tzempelikos and Shen 2013; Lee et al. 1998; Shen and Tzempelikos 2012; Daum and Morel 2010; Yao et al. 2016; Correia Da Silva et al. 2015; Mahdavi et al. 2008; Gunay et al. 2016). In practice, simple shading

control strategies are usually applied. These strategies involve full open and close actions in response to a single sensor and a control threshold (Yun et al. 2017; Beck et al. 2010; Favoino et al. 2016a; Tabadkani et al. 2020a). Such conventional control strategies often do not live up to the potential of automated shading systems and they are frequently associated with user dissatisfaction (Meerbeek et al. 2014; Stevens 2001; Karlsen et al. 2015). This dissatisfaction has been attributed to the limited opportunities for user feedback to the control system (Luna-Navarro et al. 2020; Meerbeek et al. 2014; Kwon et al. 2019; Stevens 2001; Bakker et al. 2014; Bluyssen et al. 2011) and the inadequacy of control strategies to satisfy the visual comfort requirements of occupants (Shen and Tzempelikos 2012; Karlsen et al. 2015; De Vries et al. 2019; Atzeri et al. 2018). Additionally, the binary close-open control approach limits the system to two optical and thermal states and is thus ill-equipped to respond to the large variety of environmental conditions and shifting performance goals that characterise office buildings (Loonen et al. 2013; Karlsen et al. 2015).

Recently, a series of enabling developments led the scientific community to propose comfort-driven control strategies that seek to maximise the admission of daylight and views to the outdoors by dynamically closing shading devices only to the extent that is necessary to prevent daylight glare or thermal discomfort (Shen and Tzempelikos 2017; Seong et al. 2014; Motamed et al. 2020; Coffey 2013; Bueno et al. 2020). These strategies use knowledge of their environment (Seong 2015; Mcneil 2020) and climatic conditions to classify when and to what extent shading devices should close to prevent discomfort.

The further development and application of such strategies, however, is faced with several challenges that need to be overcome if they are to be deployed successfully at scale. These advanced comfort-driven shading strategies, enabling developments and the challenges they face will be discussed in more detail in Chapter 2.

1.2 Automated shading terminology

In the literature, various terms are used to describe automated shading systems. No widely accepted terminology exists to denote the components that make up the overall shading system and various terms tend to be used interchangeably. To reduce ambiguity, the terminology that is used in this research is presented in Table 1.1. These terms will be discussed in more detail in the following chapters.

Table 1.1 The employed terminology related to automated shading systems

Term	Meaning in this work
Shading device	The physical device that blocks incoming solar radiation, e.g., blinds, shades, etc.
Control logic	A low-level function for determining the position of the shading device based on control inputs. Can be a single control mode within a multi-mode strategy.
Control strategy	An algorithm that can employ various control logics that are activated in response to sensor measurements.
Automated shading system	The physical shading device, actuation mechanisms and motorisation devices.
Automated shading strategy	The shading system combined with the control strategy and the sensor strategy aimed at operating the system.
Sensor strategy	An algorithm and sensors that are used to detect and classify indoor comfort and energy performance conditions.
Detection algorithm	An algorithm that is used to classify indoor conditions based on sensor measurements.
Shading concept	An initial idea that is to be developed and tested before it can be deployed. Refers to high level control concepts, e.g., sun-tracking behaviour.

1.3 Research and design needs for the realisation of comfort-driven automated shading systems

Developing automated solar shading systems requires making decisions regarding a large number of design parameters involving control sensors, the control logic, actuation mechanisms, and the design of the shading device (Kuhn 2017; Ochs et al. 2020b). For the most ideal operational performance, control settings additionally need to be tuned to a specific building application when a shading system is deployed.

In order for advanced automated shading solutions to be adopted by the market and applied effectively in high performance buildings, there is a need for insight into the benefits of advanced automated solar shading strategies for both end-users as well as developing parties (Loonen et al. 2019). In the traditional fragmented façade delivery process, different decision makers decide upon different design and control parameters. Most decision makers are therefore faced with a situation where they can only influence a small subset of parameters, whilst others are either fixed because of earlier design decisions, or yet undecided but beyond the responsibility of the decision maker (Ochs et al. 2020b). Considering the aforementioned opportunities, however, there is also the juxtaposed need to look beyond the traditional roles and responsibilities and obtain insight in the performance gains that could be obtained from more integrated decision making. In such an integrated approach, automated shading solutions and their control parameters would be assessed together with other façade design parameters in early-stage design (Ochs et al. 2020b).

In summary, for the development and effective application of high-performance automated shading strategies, that overcome the aforementioned challenges, there is a need for:

- Detailed insight into how design and control parameters can be leveraged to influence building performance trade-offs (Loonen et al. 2013).
- Generically applicable and scalable workflows (Loonen et al. 2019) for the development of control strategies and their successful deployment in specific buildings.
- To obtain high performance outcomes, these workflows should enable developers to effectively navigate the performance effects related to the vast control space (Kuhn 2017) that is defined by the nearly infinite number of possible sequences of shading system actuations.
- In order for the resulting control strategies to be practically applicable and scalable, the aforementioned workflows should be compatible with low-cost control hardware and software, and conventional deployment practices (Fontoynont et al. 2021; Coffey 2013). Additionally, these workflows should minimise the effort and skill that is required to develop and deploy advanced automated shading systems (Coffey 2013).

1.4 Challenges in simulation and optimisation of automated solar shading systems

Most academic studies that develop and test advanced solar shading solutions rely on building performance simulation (BPS) (Tzempelikos and Shen 2013; Atzeri et al. 2018; Wienold 2007; Shen et al. 2014; Seong et al. 2014; Coffey 2013; Huchuk et al. 2016; Gunay et al. 2014; Daum and Morel 2010; Yun et al. 2017; Shen and Tzempelikos 2012). BPS can provide detailed insight into building performance aspects that are difficult and costly to measure or reproduce in-situ or in experimental set-ups (De Klijn-Chevalerias et al. 2017). Findings from in-situ and experimental set-ups are difficult to translate to another context where the climate, building characteristics and users are different. To draw conclusions regarding cause-and-effect relationships many physical parameters need to be measured. Particularly challenging aspects of this are the measurement of physical parameters at the point of the user (e.g., the luminance distribution seen by an actual user) and the disaggregation of measured quantities (e.g., various energy end-uses). Additional challenges arise from the large number of unknown parameters that potentially influence performance aspects (e.g., material properties at various levels of scale) and the fact that any counter factual scenarios need to be considered and implemented in the design of the set-up a priori. Within the research and development (R&D) process, BPS has some distinct advantages over the alternative research methods. With relatively little effort BPS can be used to evaluate the effects of design decisions on multiple spatial scales, from the material to the whole-building level. BPS provides insight into the behaviour of systems characterised by contradicting physical effects that are hard to predict based on simplified approaches or engineering intuition, and difficult to disentangle in measurements (Loonen et al. 2017; Loonen et al. 2019). Additionally, with BPS, the effects of automated shading strategies can be evaluated for a large variety of buildings, types of users, climates and solar shading types (e.g., blinds, roller shades, shutters). This makes BPS a promising tool for exploring high potential shading concepts and identifying risks in the context of automated solar shading (Loonen et al. 2017; Ochoa et al. 2012a).

Although there are many BPS studies that propose promising advanced automated shading concepts, there is a lack of uptake of these advanced solutions in practice (Ochs et al. 2020b; Bonato et al. 2019). One of the explanations for this lacking uptake is that the prevalent approach is too focussed on building performance effects of advanced automated shading strategies and places too little emphasis on factors that are defining for the practical implementation of these strategies at scale. The development of solar shading controls using BPS currently tends to follow a trial-and-error process where simulations are used to test a preconceived strategy using post-hoc analyses (Loonen 2018). As an alternative to this process, there is a need for

generically applicable approaches that structure the use of BPS to identify high performance solutions in an effective manner.

In addition, there are several issues hindering the effective application of BPS to assess and optimise advanced automated shading strategies. Methods have been developed to overcome some of these challenges (Section 2.5) but there is no coherent framework that combines their individual functionalities. Additionally, most BPS software was originally developed for the design of buildings and the context of product development and the creation of control strategies are relatively new fields of application (Loonen et al. 2017; Loonen et al. 2019). To summarise the challenges to apply BPS effectively in this context include:

- **Conventional shading devices in binary states:** BPS tools were developed when simple close-open control strategies were the norm. These tools offer limited flexibility for describing advanced multi-state shading systems that can be configured in a multitude of thermal and optical states by partially closing shading devices or switching between different sets of optical and thermal properties.
- **Simple control behaviour:** The operation of dynamic shading devices in BPS tools is usually limited to a small number of predefined conventional control strategies and offer limited possibilities to describe more advanced control behaviour involving for instance: elaborate logical structures, run time execution of external programs, the use of external hardware controllers, and a large variety of sensors types and configurations that measure parameters in different physical domains.
- **Focus on the building scale:** BPS tools tend to describe shading systems at the macro-level. To leverage detailed material properties and design features at the milli and micro scale for improving building performance requires new multi-scale workflows. Shading fabrics, for instance, are often specified using a limited set of input parameters that define their optical behaviour on the level of the shading device but do not describe the weave of the fabric explicitly.
- **Separation of domains:** The performance of advanced shading solutions is determined by interactions between the thermal and the daylight domain; two physical domains that are largely separated across different BPS tools (Taveres-Cachat et al. 2021).
- **Design and control:** The performance of facades with automated shading systems depends on building and shading system design parameters as well as control behaviour. Although these aspects have been investigated individually, the concept of co-optimisation of façade design and shading controls is largely unexplored and there is a need for enabling simulation workflows.

- **Assumptions and uncertainties:** In performing computational design support studies, practitioners inevitably must make a great number of assumptions. The influence of such assumptions has been insufficiently explored.
- **Occupant behaviour:** The building performance effects of automated shading strategies depend on how occupants interact with such systems. Existing BPS tools greatly simplify this behaviour and offer little insight into how likely occupants are to accept certain automated strategies.

This research contributes to filling the aforementioned knowledge gaps in the use of BPS to describe the performance of advanced automated shading products. This research seeks out to combine the existing state-of-the art in simulation methods (discussed in Section 2.5) within a coherent framework designed specifically for this context. Additionally, contributes insights into how BPS can be applied in a more replicable and scalable way in developing new advanced strategies.

1.5 Research goals and objectives

The aim of this research is to expedite the transition to high-performance buildings by aiding the scalable development and deployment of advanced automated shading strategies. The objective of this research is to develop and test computational approaches for performance evaluation and optimisation of advanced automated shading strategies. This research focusses on a computational approach rather than experimental or in-situ methods because the beneficial features of BPS (discussed in Section 1.4) make this approach for developing automated shading strategies more scalable. This objective of this research is divided into the following subobjectives:

O.1. To develop and test a virtual test bed (VTB) for advanced automated shading strategies aimed at analysing the performance of (i) advanced shading controls, (ii) materialisation and shading system design features, and (iii) applications of dynamic solar shading systems within performance-driven façade design processes.

O.2. To develop computational support methods, aimed at performance analysis, optimisation, and quality control in the application of the VTB.

O.3. To illustrate, through a series of application studies, how the VTB and the support methods can be used to identify scalable high-performance design and control solutions.

O.4. To better understand the causal relationships between solar shading design/control parameters and building performance effects.

The VTB is conceived as a continuously evolving tool chain that should be upgraded whenever new requirements arise from new applications. The goal of this research is to develop a first working prototype of this VTB. For brevity, the VTB and the computational support methods that are discussed in point 1 and 2 will together be referred to in this thesis as computational approaches or the computational framework.

By developing the computational framework this research will contribute to the knowledge gaps in simulation and optimisation of automated shading systems that were identified in Section 1.4. These knowledge gaps will be further explored further by a review of the state-of-the art in simulation and optimisation in Section 2.5.

1.6 Scope of the work

The development and application of automated shading systems forms a multi-disciplinary research topic. This research targets a specific area within a larger research field and requires some clarification of the scope of this work.

Performance aspects: In the assessment of building performance, the focus in this research lies on visual comfort, the admission of sufficient daylight and views, building energy consumption, and its associated costs and environmental impacts. Thermal comfort is implicitly addressed through the analysis of cooling energy consumption.

Building performance domain: The successful wide-spread deployment of the shading strategies that are analysed in this research depends on many factors that do not directly influence the building performance aspects that are central to this thesis. This research was caried out in collaboration with industry partners that do address these factors. Possible constraints posed by factors outside of the building performance domain will be discussed in the application studies that are presented in the following chapters.

Existing products: In the selected application studies, the focus lies on supporting the development of high-performance shading strategies that employ commonly accepted types of shading devices, such as roller shades or blinds, in an advanced manner. This emphasis is aimed at supporting the development of high-performance solutions that can benefit from economies of scale and match existing consumer preferences.

Software prototype: The VTB that is developed in this research should be considered as a software prototype and not as a software tool with a user-friendly interface and extensive documentation.

Office buildings: This research is focussed on the application of the computational framework for improving the indoor climate of office buildings. The framework can, however, also be applied for developing shading solutions for other types of buildings in the tertiary sector or even for residential buildings.

1.7 Research methodology

The exact requirements for the VTB and the accompanying support methods were not known a priori. These requirements and the VTB were therefore developed through an iterative process following four application studies that were executed in collaboration with decision makers from companies in the solar shading industry (Figure 1.1). This methodology is inspired by the Use Case methodology (Jacobson 1987; Bittner and Spence 2003) that is commonly used to define requirements in systems engineering. In this approach, system requirements are defined using a set of usage scenarios that define how a user will employ a system to achieve a particular goal.

In this research, a set of initial requirements for the computational framework are defined from a review of the literature on (i) the state of the art in advanced automated shading systems, (ii) the challenges and (iii) opportunities surrounding their development and deployment, and (iv) the state of the art in computational performance assessment of advanced fenestration systems. This literature review will be discussed in detail in Chapter 2. Based on the initial requirements, a first version of the computational framework is developed.

In each application study, the framework is extended and refined by applying it to a practical problem that is defined together with decision makers from industry partners. The requirements for the computational framework are defined based on the goals of these application studies. Additionally, the modelling features designed to fulfil these requirements are developed and tested within these studies. The companies Kindow B.V. and Verosol Nederland B.V. and the automated shading systems that they develop form the inspiration for the application studies that are investigated in this research. Additionally, these companies could be viewed as potential future users of the computational framework. The application studies, however, were not specifically designed to support current company R&D.

Kindow B.V. is a Dutch company that focusses on the development of advanced automated shading control solutions and has developed sun-tracking roller blind and vertical blind systems. Verosol Nederland B.V. specializes in metallised solar shading fabrics and also offers automated shading solutions. The company is part of Kvadrat, a Danish textile manufacturing company.
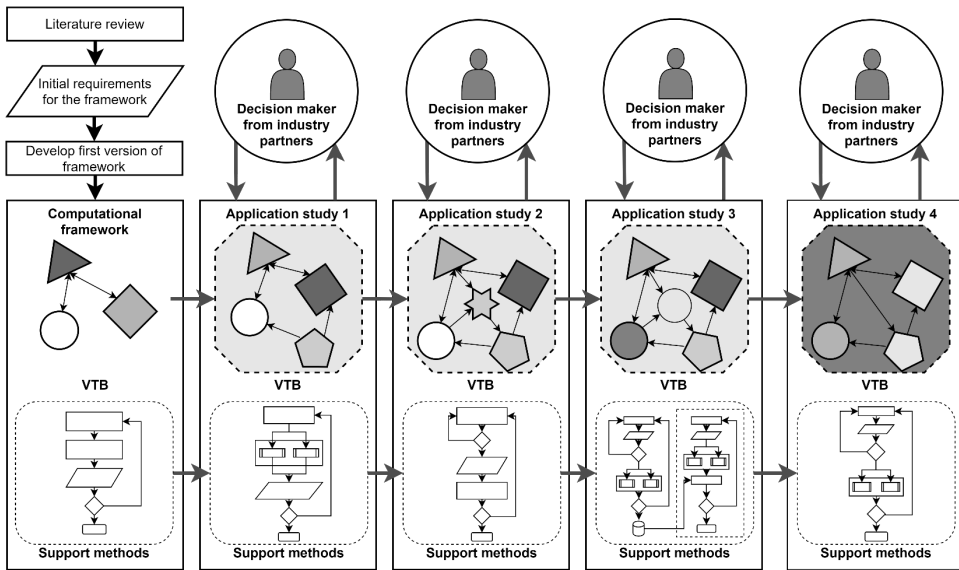
Figure 1.1 Overview of the research methodology.
An initial version of the computational framework is developed based on a review of literature. The framework is developed further in an iterative process involving four application studies and consultation with decision makers from the shading industry.

Figure 1.2 describes the approach that is followed in each application study in more detail. In each study, a control or design goal is defined together with the decision makers. Additionally, each study starts with an initial automated shading concept that will be evaluated or improved. In the next step, a fit-for-purpose simulation strategy is defined based on the parameters that are to be optimised and the performance aspects of interest.
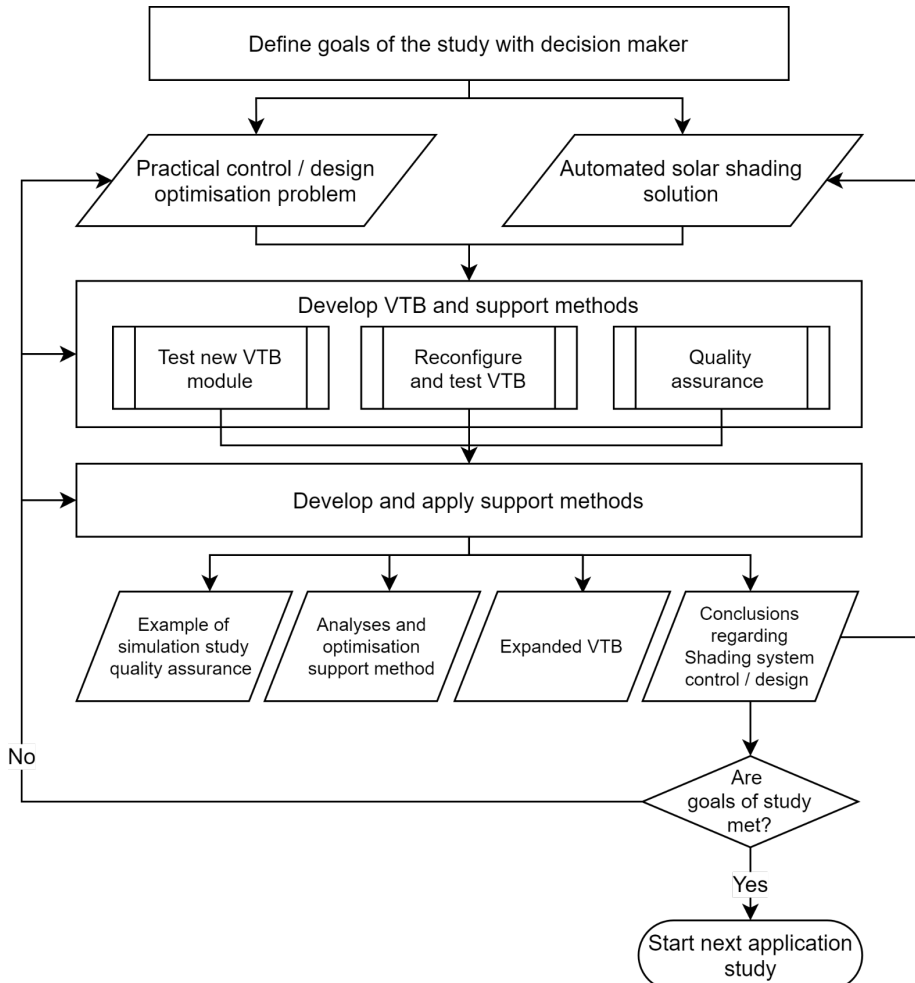
Figure 1.2 Research steps that are taken in each application study

The VTB has many features that are contained within dedicated VTB modules. Depending on the problem that need to be addressed, a different set of features is required. A particular study might not require the full suite of existing VTB modules and possibly new modules are required. The VTB is therefore reconfigured to fit the needs of the study and new modelling capabilities are added. Whenever a new module is added to the VTB, verification and validation studies are executed to confirm the correct functioning of the VTB module. Additional quality assurance tests are executed, such as sensitivity analyses, to define the required modelling resolution. The outcomes of these quality assurance tests are, in some cases, specific

to the particular application study. These tests mainly provide an example of how errors can be identified and minimised in the application of the VTB.

The VTB is then used to analyse or optimise the automated solar shading concept. In this step, new support methods for effectively improving and optimising the initial shading concept are developed and tested. From this analysis, conclusions are drawn regarding the performance of the automated shading solutions and directions for further improvement of the system are identified. These outcomes are discussed with the industry partners to assess whether the problem was sufficiently addressed. Depending on this assessment, the problem formulation is adjusted, or the applied simulation, optimisation and quality assurance methods are refined further. After multiple iterations the shading system optimisation problem is sufficiently addressed and an updated VTB and accompanying support methods are obtained.

Figure 1.3 gives an overview of the four application studies. Developing and testing the support methods and VTB within these four studies ensures a broad applicability and usability of the outcomes of this research. The figure shows the type of design and control parameters that describe properties and system behaviour at different levels of scale. These parameters will be discussed in more detail in Section 2.2. Each application study focusses specifically on one level of scale and the design parameters on that level of scale are optimised, whilst keeping the parameters at the other levels of scale constant. A different decision maker is central in each application study. Additionally, the type of shading system that is optimised is varied to contribute to the broad applicability of the developed VTB. It should be noted that, as is common with informal applications of the use case approach (Bittner and Spence 2003), the application studies presented in this research illustrate the most significant ways of using the computational framework but other applications are also possible. The VTB is thus developed as a continuously evolving tool chain that should be upgraded whenever new requirements arise from new applications (i.e., possible applications and upgrades are discussed in Chapter 10).

The studies focused on three types of decision makers in the solar shading product supply chain: control developers, solar shading system developers and façade designers. In practice, the types of design and control aspects that are decided upon by these actors is not always clearly delineated and may vary depending on how particular companies position themselves in the market. The studies were defined to include the design and control aspects that are most defining for the effects of automated shading solutions on building performance aspects and to address that decision making regarding these aspects takes place at different positions in the shading system supply chain.

	System	A. Sensors	B. Controls	C. Shade material	D. Shading system	E. Facade design
Application study 1		BMS				
Application study 2		BMS			?	
Application study 3		BMS				
Application study 4		BMS				
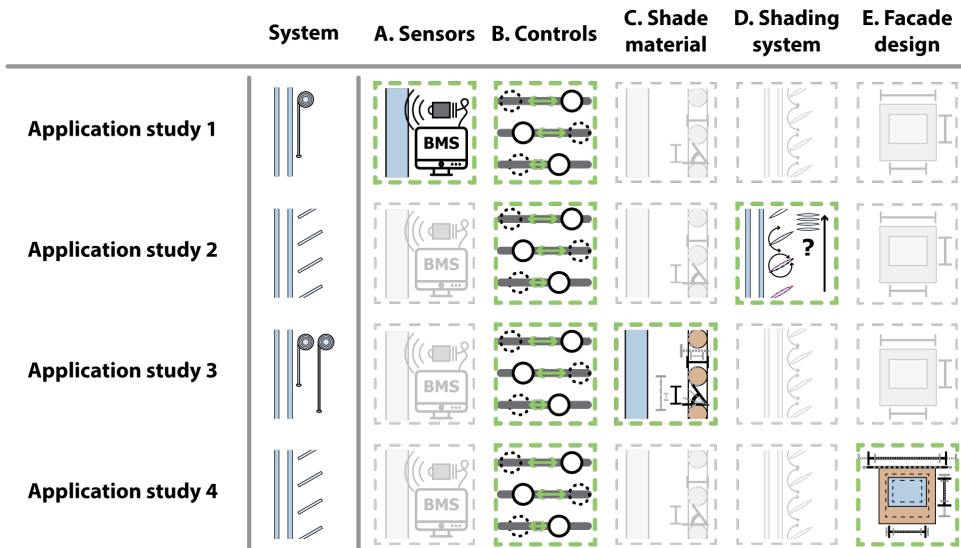
Figure 1.3 The four application studies. In each study a different design and control aspect is optimised (green) whilst keeping other parameters constant (grey)

In this research, the control developer is assumed to decide upon the control strategy and the sensors that are employed but not to have an active role in the design of the motorisation system or the selection of fabrics. Rather this decision maker combines existing products in an overall system that is to be deployed in a building. The shading system developer is focussed on developing an integrated automated solar shading product and is assumed to design the physical shading system, including the actuation mechanisms and the shading device. The façade designer is assumed to select the glazing system and design windows and exterior static shading devices. Different approaches to the way the façade designers include automated shading systems in their decision-making framework will be explored.

1.8 Thesis outline

Figure 1.4 gives an overview of the structure of this PhD thesis. In chapters 5 to 8 the four application studies are presented. The sections of the application study chapters each have the following general structure:

1. **Introduction** - Discusses the topic and goals of the application study
2. **An initial concept** - Presents an initial shading concept that will be improved, describes characteristics of this shading system, and gives a summary of the aspects that will be optimised, and which will be assumed constant.
3. **Methodology and simulation strategy**
   3.1. Investigated design and control options
   3.2. Performance indicators
   3.3. Configuration of the VTB
   3.4. Assumptions and input parameters.
4. **Support methods** – Discussion of new support methods applications
5. **Quality assurance** – Verification and validation studies aimed at testing new VTB modules and configurations
6. **Results** – Application of the VTB to optimise the initial shading concept
7. **Application discussion and conclusion** – Practical lessons regarding the performance of the investigated shading concept.
8. **Concluding remarks** – Conclusions regarding new VTB modules and support method and their role within the overall computational framework

The four application studies were executed in a consecutive manner and new insights were progressively obtained. Chapter 9 presents a reflection where some of the assumptions that were made in the earlier chapters are reviewed in light of new insights. Chapter 10 summarises the conclusions of this research and reviews the functionalities, strengths, and limitations of the developed simulation framework. In addition, it suggests directions for future work.

Chapter 1: Introduction
Describes the research background, objectives and methodology.

Chapter 2: Identification of requirements for the simulation framework
Presents an analysis of the opportunities and challenges facing the development and application of advanced automated shading systems. In addition, a review of literature representing the state of the art in automated shading systems is presented. Based on the literature review and the insights obtained in the application studies, a set of requirements for the computational framework is presented. The chapter concludes with an overview of the performance aspects that are addressed in this research and presents the indicators that are used to assess them.

Chapter 3: The virtual testbed
Presents the overall simulation tool chain and its components along with an overview of the quality assurance tests that are executed to validate and verify each component.

Chapter 4: The IEA SHC Task 56 reference office: model description and validation
This chapter presents the Task-56 Reference office that is used throughout this research. Additionally, two validation studies are presented that validate the daylighting (A) and thermal (B) simulation modules through inter-model comparison.

The application studies

Chapter 5: Simulation-based support for sensor and control strategy development using performance mapping and statistical classification	Chapter 6: Design and control optimisation of a multi-state vertical-blind solar shading system	Chapter 7: Design and control optimisation of a multi-state double roller blind system	Chapter 8: Co-optimisation of façade design and automated solar shading systems

Chapter 9: Reflection

Chapter 10: Conclusions and future research

Figure 1.4 Graphical outline of this work

2 Identification of requirements for the simulation framework

2.1 Introduction
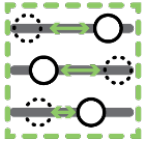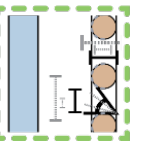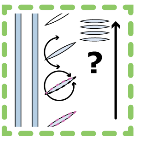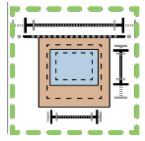
This chapter presents the requirements for the simulation framework that was obtained through un-systematic literature review and the iterative research process involving four application studies. Section 2.2 presents a review of the literature on the state-of-the art in advanced automated shading technologies. Sections 2.3 and 2.4 analyse the opportunities and challenges in the development and application of comfort-driven automated shading systems. Section 2.5 discusses the literature on simulation and optimisation of automated shading systems, with a particular emphasis on existing methods for overcoming some of the issues that were raised in Section 1.4. Section 2.6 present the formulated requirements for the simulation framework and Section 2.7 discusses the performance aspects and indicators that will be used in this research.

2.2 State of the art in automated solar shading technologies

Promising automated solar shading concepts have been proposed aimed at improving indoor environmental quality and reducing building energy consumption. The literature on this topic can be classified in terms of the level of scale (A to E in Table 2.1) of the aspects that are novel or optimised.

Table 2.1 Levels of scale in the design and control aspects that can be used to improve the performance effects of automated shading strategies

| A. Sensors and connectivity | B. Control rules and parameters | C. Shade material | D. Shading system and actuation mechanisms | E. Façade system |

To summarise the literature using these levels of scale:

A. Some research has focussed on new enabling connectivity between different building technologies and novel sensing capabilities. Arnesano et al. (2019) proposed and tested a façade integrated sensing system that measures indoor and outdoor conditions at the window level and that uses serial and wireless modules for communication with other building systems. Böke et al. (2020) developed and tested a communication system for synchronising the operation of façade integrated shading, ventilation, heating and cooling systems. Yun et al. (2020) and Shen and Tzempelikos (2017) proposed methods for predicting indoor work plane illuminance using low-cost and

non-intrusive window mounted sensors. Allen et al. (2019) prosed a high-resolution network of wearable sensors for measuring the visual environment and controlling shading systems.

B. Novel and optimised control approaches have been proposed, including: advanced rule-based control (e.g. sun-tracking behaviour) (Shen and Tzempelikos 2017; Seong et al. 2014; Tzempelikos et al. 2007b; Oh et al. 2012), proportional control of actuation responses to sensor measurements (Shen and Tzempelikos 2017; Kristl et al. 2008; Motamed et al. 2020), and model-based performance weighing approaches (Piscitelli et al. 2019; Oldewurtel et al. 2012; Coffey 2012; Coffey 2013; Huchuk et al. 2016; Gunay et al. 2014; Wu et al. 2019a; Wu et al. 2019b; Gehbauer et al. 2020; Katsifaraki et al. 2017; Bueno et al. 2018).

C. Some research has focussed on the micro and milli-scale through the development of novel materials with beneficial optical and thermal behaviour (Mashaly et al. 2021; Saini et al. 2018; Goia et al. 2013b) or optimising material properties (Mangkuto et al. 2019; Yi and Malkawi 2009) and design features of materials for shading devices (Bueno et al. 2020; Chi et al. 2017).

D. The performance effects of automated shading devices can also be influenced by design properties at the level of the shading system. Research efforts have been focussed on optimising the geometry of shading devices such as blinds (Tsangrassoulis et al. 2006; Tzempelikos 2008; Santos et al. 2018; Konis and Lee 2015; Taveres-Cachat et al. 2019), as well as on actuation mechanisms that allow complex movements and geometries (Hashemloo et al. 2015; Saini et al. 2018), automated operation of new types of shading devices (Mettanant 2013), or the ability to dynamically switch between different materials on their sun-facing sides (Oh et al. 2012) to manipulate the admission of solar energy.

E. Finally, novel and optimised concepts have been proposed in which automated shading systems are an integral component within a novel overall façade design (Tzempelikos et al. 2007a; Favoino et al. 2016b; Denz et al. 2018; Aslihan and Eleanor 2006; Do and Chan 2020, 2021)

2.3 Opportunities for automated solar shading systems

Currently, several enabling developments can be identified that could bring automated solar shading closer to fulfilling its potential (Fedrizzi 2020). High reflectance metals coatings have made interior shading products more effective at reducing solar heat gains (Bakker and Van Dijk 2015; Van Uffelen 2014). Compared to their exterior counterparts, interior shading devices can be actuated in a fine-tuned manner using silent and low-cost motorisation systems. Additionally, glass coating technologies have enabled glazing systems that can substantially reduce the admission of near infra-red (IR) solar radiation with only small effects on the transmittance of light in the visible range (Bakker et al. 2019; Roos et al. 2001; Mohelnikova 2009). The utilisation of high reflectance glass coatings allows for a greater emphasis on effective daylight management in the control of automated shading devices.

Reduced cost of sensor technology and microcontrollers and increased possibilities in communication between different devices has led to an increasingly all-encompassing 'internet of things' (IoT). This IoT offers new possibilities in terms of information gathering and management of devices (Jankowski et al. 2014; Jia et al. 2019) that can be utilised to improve the indoor climate and reduce energy consumption in the design and operation of Smart Buildings (Buckman et al. 2014; Jia et al. 2019). These developments will enable automated shading systems to be controlled in a more fine-tuned way using more granular sensor data. The ability to adjust the position of shading devices in a fine-tuned manner opens up the ability to configure shading devices in a multitude of thermal and optical states, allowing the admission of daylight and solar energy to be adjusted in a more gradual manner and even vary in relation to individual user preferences. Such multi-state systems offer more opportunities for balancing conflicting performance goals and responding to varying environmental conditions (Loonen et al. 2013; Favoino et al. 2016a; Favoino et al. 2015; Giovannini et al. 2019; Bui et al. 2020; Oh et al. 2012; Mangkuto et al. 2019). The increased granularity and accuracy in sensing indoor environmental conditions and the ability to actuate shading devices in a more fine-tuned manner are promising because they enable comfort-driven control strategies. In contrast to their conventional counter parts, these strategies seek to maximise the admission of daylight by closing shading devices only to the extent that is necessary to prevent daylight glare or thermal discomfort.

The advent of daylight dimming controls for electric lighting systems forms another enabling development. The increased application of daylight dimming controls has made effective daylight utilisation an important strategy in reducing building energy consumption (Ochs et al. 2020b).

2.4 Challenges for automated solar shading systems

Although promising automated shading concepts have been proposed, the further development and successful application of these solutions is not straight forward and currently, there is a lack of uptake of advanced solutions (Ochs et al. 2020b; Bonato et al. 2019). Both technological and non-technological causes can be identified for this lack of market uptake (Bonato and Fedrizzi 2019; Fedrizzi and Fassaden 2018):

- Developing comfort-driven automated shading systems is complex because it requires detailed insight into how design and control parameters influence the comfort conditions of occupants and trade-offs between conflicting performance aspects (Loonen et al. 2013). Additionally, these aspects are affected by highly dynamic environmental conditions and can interact differently depending on the specific application in terms of e.g., building type, facade properties and interior lay-out (Favoino et al. 2016a; Loonen et al. 2014; Kuhn 2017; Loonen et al. 2013; Silva Da et al. 2012). Consequently, one-size-fits-all shading solutions will perform sub-optimal and there is a need for customisation.
- Potential solutions for addressing this complexity need to be compatible with the currently available control hardware (Coffey 2013; Piscitelli et al. 2019) and software, sales and commissioning practices (Motamed et al. 2020), and the preferences of purchasing parties (Maurer et al. 2020).
- The façade design and delivery process is characterized by fragmented roles and responsibilities. Traditionally, different parties are consecutively tasked with specifying solar shading devices, designing, and implementing (smart) lighting systems, and programming and commissioning automated shading controls. This means that the design features that can be leveraged to maximize the benefits of automated solar shading systems are often designed by different decision makers at different moments in the life cycle of a building and not addressed integrally within the façade design process (Attia et al. 2018).
- Technologies like daylight dimming, high reflectance coatings and advanced control systems have led to a situation where interactions between the thermal and visual physical domains are defining for the indoor climate and energy consumption of office buildings. Within the fragmented façade design process there is, however, insufficient awareness of these interactions. In this context, solar shading devices are often viewed as either a means for reducing solar heat gains when glazing alternatives are being considered, or as glare protection devices and considered when deciding upon interior furnishing.

2.5 State of the art in simulation and optimisation of automated solar shading systems

In this section, the building performance simulation (BPS) literature is reviewed in a non-systematic manner to identify the existing approaches aimed at overcoming some of the challenges in the simulation and optimisation of automated shading systems, that were discussed in Section 1.4.

This literature review forms the inspiration for the initial requirements of the framework. The solutions presented in the literature each address a subset of the identified challenges. Additionally, there are limitations to capabilities of the available tools and gaps in the knowledge around their effective application. The requirements for the computational framework presented in the next section are therefore aimed at combining the solutions from this literature review within a cohesive framework that overcomes the limitations that are identified in this review. In addition to the literature review presented here, some aspects will be elaborated upon in the introductions of the application study chapters. The following approaches have been proposed in literature to address the challenges that were identified in Section 1.4:

Separate domains: Different methods for overcoming the separation of the daylighting and thermal domains in BPS have been presented (Taveres-Cachat et al. 2021). Some methods rely on a stepped simulation approach (Roudsari et al. 2013; Jakubiec and Reinhart 2011; Bueno et al. 2015; Bustamante et al. 2017). Loonen (2018) has presented a co-simulation framework and multiple research teams have focussed efforts on developing new simulation environments, tailored for specific advanced fenestration solutions (Shen and Tzempelikos 2012; Bueno et al. 2015; Werner et al. 2017).

Conventional shading devices in binary states: The shading models in existing BPS tools tend to focus on the most common types of shading devices in conventional applications. To be able to describe fine-tuned operation of conventional shading devices, earlier studies have relied on dividing the window surface into multiple sub surfaces (Wienold 2007; Atzeri et al. 2018; Gunay et al. 2016). This approach allows conditions where a shading device covers only parts of the window to be described used the traditional binary (shaded or unshaded) fenestration system models. Additionally, this approach has been used to describe equivalent degrees of admission of solar energy for complex non-coplanar shading device geometries (Choi et al. 2017; Tabadkani et al. 2020b). The errors associated to this modelling approach and the chosen resolution in discretising window surfaces, however, has not been investigated. In addition, methods are available for describing the physical effects of systems with time-varying optical and thermal properties (Santos et al. 2018) and non-conventional geometrically complex shading devices (Molina et al.

2015; Santos et al. 2018). These methods distributed across various simulation tools, however, that need to be coupled to assess whole-building performance effects. The successful application of these approaches requires tooling that facilitates this coupling as well as more knowledge on quality control in this context.

Complex control behaviour: To describe complex control logics, Atzeri et al. (2018) have used graphical programming environments to create schedules that can be used by BPS tools to describe deterministic open-loop control strategies. Others (Tabadkani et al. 2021; Van Moeseke et al. 2007), seeking to describe closed-loop control behaviour have used application programming interfaces, based on simplified programming languages, that are built-in to particular domain specific BPS tools. Shen and Tzempelikos (2012) and Loonen (2018) have included scripting environments within co-simulation frameworks, allowing the use of more advanced mathematical methods and external programs in the control strategy. Additionally, this approach allows sensor variables predicted by multiple domain specific BPS tools to be used within a single strategy.

Trial-and-error process: As an alternative to the ad-hoc application of BPS in the development of shading control strategies some generically applicable approaches have been proposed. For example, exhaustive-search simulation studies (Yun et al. 2017; Van Moeseke et al. 2007) and self-learning methods (Gunay et al. 2014) have been applied to relate sensor measurements to performance goals by optimising control thresholds for simple rule based control (RBC) strategies. This optimisation does require, however, exploring a vast space of possible control thresholds. Additionally, the approach remains limited to the constraints of the initially assumed control concept and does not provide the deeper level of understanding that is needed to guide the development of a more advanced control logic. The model predictive control (MPC) approach does not have this limitation. Although MPC has been shown to be a promising solution for high-performance building controls (Oldewurtel et al. 2012; Mahdavi 2001; Mahdavi et al. 2005; Huchuk et al. 2016), it is not commonly applied in practice (Coffey 2013; Piscitelli et al. 2019). A possible explanation for this is that much effort and skill is required of a developer every time that a control strategy needs to be developed for a new type of solar shading system or when a system is commissioned into a new building (Killian and Kozek 2016). Potentially, self-learning behaviour can reduce this effort but setting up the model architecture and parametrising the model remain costly. Additionally, MPC is computationally expensive and complex during operation. Researchers have developed techniques to significantly reduce the computational complexity of MPC by rule-extraction and the mapping of operational conditions to MPC control responses (Coffey 2013; Piscitelli et al. 2019). This process, however, requires more effort from developers and is computationally expensive in the preparation phase. Additionally, a fitness function with relative weights for different performance

indicators must be defined beforehand when applying the MPC to the multi-objective solar shading control problem. This is not easily done based on engineering intuition and tuning these weights towards the desired performance outcomes therefore requires extensive sensitivity analyses (Mahdavi 2001; Oldewurtel et al. 2012). To conclude: there is need for generally applicable methods that guide the use of BPS towards high performance control solutions. For such methods to be scalable, they need to require little effort from developers whenever a system is to be applied in a building.

Building scale: Although detailed models (Hart et al. 2018; Carli 2006) are available for describing the optical and thermal behaviour of complex shading systems in evaluating fenestration systems on the building-component level, these models are not yet directly accessible in whole-building simulation environments (Santos et al. 2018). Additionally, quality assurance efforts of these simulation models have focussed on commonly used devices in simple configurations. Multi-scale modelling methods are available that simulate the component behaviour of shading systems in a detailed manner and provide inputs for whole-building simulations (Bueno et al. 2015; Curcija et al. 2018; Lbnl 2019b, 2019a; Bustamante et al. 2017; Sun et al. 2018).

Fit-for-purpose: Modelling methods of varying complexity are available for describing the elements that determine the performance of automated shading systems. Individual models tend focus primarily on one of the separate levels of scale in Table 2.1. In addition, various performance indicators and simulations methods are available. How applicable these methods are to solve particular simulation problems depends on the goal of the decision maker, the characteristics of the system being investigated and the available input information (Trčka and Hensen 2010). In supporting the development and application of advanced automated shading systems it is unclear how fit-for-purpose modelling approaches can be selected that match the various perspectives of decision makers in the façade delivery process. This topic, and the associated literature, was explored further for each relevant modelling domain in the application study chapters.

2.6 Requirements for the computational framework

From the review of the literature, a set of initial requirements for the computational framework were formulated (R.1 to R.4). Through the iterative research process, described in section 1.7, additional requirements were identified (R.5-R.9), and the following list was defined:

R.1. The virtual testbed (VTB) must enable a meaningful performance comparison between design and control alternatives in terms of their effects on daylight sufficiency, visual comfort, view to the outdoors, thermal comfort, and building energy consumption including its associated costs and environmental impacts. More specifically, the VTB should facilitate the evaluation of the performance effects of design and control parameters related to (i) the employed control sensors (ii) the shading control strategy, (iii) the design and materialisation of the shading device, and (iv) the design of the building façade.

R.2. The VTB must have the ability to describe the mutual interactions between indoor daylighting conditions, indoor thermal conditions, dynamic operation of shading systems, occupant behaviour, and energy systems.

R.3. The VTB must have the ability to describe shading systems with multi-state behaviour involving partial closing of shading devices and alternating optical and thermal properties.

R.4. The VTB must have the ability to describe complex control behaviour involving elaborate logical structures, run time execution of external programs and various sensor configurations and placements that measure physical quantities in different domains (e.g., temperatures, visual spectrum, solar spectrum, etc.).

R.5. The VTB must have the ability to the describe the automated shading system at different levels-of-scale (e.g., from detailed shading fabric characteristics, to the design of shading devices and actuation mechanisms, to their behaviour in an overall fenestration system).

R.6. The VTB must be configurable in accordance to: (i) the perspective of varying decision makers in the façade delivery process, (ii) the automated shading system that will be investigated, (iii) the purpose of the simulation study, and (iv) the available input information.

R.7. The simulation framework must facilitate a fit-for-purpose modelling approach where the configuration and the complexity of the applied models (R.5) can be tuned to the goals of the simulation study (R.6).

R.8. The simulation framework must facilitate experiments that allow a comparison of building performance effects resulting from different sensor strategies, control approaches, shading, and façade design options.

R.9. The simulation framework needs to give detailed insight into how these interactions (R.2) and multi-scale effects (R.5 and R.7) can be influenced using shading control and design aspects.

2.7 Performance aspects and indicators

The performance aspects of interest in this research are daylight sufficiency, visual comfort, view to the outdoors, building energy consumption, thermal comfort and finally, system costs and financial benefits. This section will discuss the performance metrics that will be used to assess these aspects.

2.7.1 Daylight quality, quantity, and sufficiency

Exposure to daylight positively contributes to the health and well-being of occupants (Knoop et al. 2019; Lucas et al. 2014; Rea and Figueiro 2018; Figueiro et al. 2019; Aries et al. 2013). The extent to which the admission of daylight contributes to building occupant health and well-being, however, is hard to quantify and there is no scientific consensus regarding the required minimum light exposure or duration and spectra for positive effects to be obtained. The current generation of daylighting performance indicators therefore primarily focuses on the visual aspects of daylight and quantify these aspects in terms of the quantity of daylight that is admitted to the indoors and the distribution of daylight illuminance across the indoor space.

Climate based daylight metrics (Brembilla and Mardaljevic 2019) allow designers to evaluate the distribution of daylight spatially across an interior work plane as well as across a whole year. These indicators are referred to as being 'climate-based' because they allow daylighting performance to be expressed under variable sky-conditions. Several climate-based daylighting performance indicators will be used in this research:

1. **Spatial daylight autonomy (sDA):** Expresses the annual sufficiency of daylight levels across an area of interest. It is defined as the percentage of the task area that meets a minimum degree of daylight autonomy (DA), where DA is the percentage of total occupied hours that a minimum daylight illuminance level is exceeded (Heschong et al. 2012). In this research 300 lux and 50% of occupied time are used as cut-off criteria for defining acceptable daylight performance ($sDA_{300/50\%}$). These cut-off criteria have been shown to correspond well with subjective assessments by building occupants of daylight quality and quantity (Reinhart et al. 2014; Saxena et al. 2010; Nezamdoost and Van Den Wymelenberg 2017). For the $sDA_{300/50\%}$ metric, the IES-LM-83 standard suggests $sDA_{300/50\%} \geq$ 55% as an indication of nominally acceptable daylight sufficiency and $sDA_{300/50\%} \geq 75\%$ as preferred daylight sufficiency.

2. **Daylit area fraction (D_{300lx}):** This indicator is defined in this research to be able to evaluate instantaneous daylighting performance and assess the effectivity of different possible shading control actions at a particular control interval. D_{300lx} gives the percentage of floor area that receives at least 300 lux at a point in time.

3. **Continuous daylight autonomy (cDA$_{300lx}$):** This metric is similar to DA but attributes partial credit to time steps where daylight illuminance lies below the minimum required level. This partial credit is attributed linearly between 0 and 300 lux where a situation with 150 lux, for instance, gets half the credit of a condition with 300 lux. This approach makes the indicator less sensitive to the chosen illuminance cut-off value.

2.7.2 Visual comfort

Visual comfort is approached in this research as a lack of daylight discomfort glare. Experimental studies on subjective glare assessments of building occupants (Wienold et al. 2019; Wienold and Christoffersen 2006; Konstantzos et al. 2016; Garretón et al. 2018; Tokura et al. 1996) have identified several physical factors, describing the daylight conditions in the field of view of occupants, that determine discomfort glare. These include: (i) the luminance of glare sources, (ii) the solar angle subtended by the glare source (iii) the background luminance, and (iv) the overall vertical illuminance at the position of the occupant (E_v).

Several performance indicators, based on varying combinations of these physical factors, have been developed to predict the probability that occupants would be disturbed by daylight glare under particular visual conditions. In this research the following daylight glare indicators will be used:

Daylight Glare Probability (DGP): This metric was developed based on empirical research by Wienold and Christoffersen (2006) and expresses the probability that a person in a large group of test subjects would declare being 'disturbed' by particular visual conditions. In a subsequent cross-validation comparison between a large number of glare metrics based on a large combination of worldwide experimental datasets, it was concluded that DGP gives the most accurate and robust predictions of the sensation of daylight glare amongst the currently available set of glare metrics (Wienold et al. 2019). DGP is computed from high-definition range (HDR) images made using charge-coupled device cameras or simulations. DGP is computed from these images using an algorithm (Wienold and Christoffersen 2006) based on the equation:

$$\text{DGP} = c_1 \cdot E_v + c_2 \cdot \log\left(1 + \sum_i \frac{L_{s,i}^2 \cdot \omega_{s,i}}{E_v^{c_4} \cdot P_i^2}\right) + c_3 \qquad (2.1)$$

Where: Ev: Vertical illuminance at the position and viewing direction of occupant [lux],
$L_{s;i}$: Luminance of glare source [cd/m²], ω_{si}: Solid angle of source [-],
P_i: Guth's position index (Luckiesh and Guth 1949) [-], s: source, i: source number,
$c_1 = 5.87\cdot10^{-5}$, $c_2 = 9.18\cdot10^{-2}$, $c_3 = 0.16$, $c_4 = 1.87$.

The equation expresses glare probability as a function of daylight saturation (the first E_v term), contrast (the luminance and glare source position related terms), and adaptation (the E_v in the denominator of the contrast terms).

Table 2.2 gives a set of performance criteria from the EN 14501 standard (Cen 2017b) that is commonly used to classify daylight glare conditions based on DGP. Additionally, the table suggests different degrees of glare protection throughout a year and recommends a maximum accepted share of occupied hours that glare classes can be exceeded for each degree of glare protection.

Table 2.2 Glare performance classification according to Cen (2017b). $DGPs_{t;exc.}$: share of occupied hours that a DGP of t is exceeded, t: threshold.

Criterion	Daylight Glare Probability (DGP)		
Glare is mostly imperceptible		DGP ≤	0.35
Glare is perceptible but mostly not disturbing	0.35	≤ DGP ≤	0.40
Glare is perceptible and often disturbing	0.40	≤ DGP ≤	0.45
Glare is perceptible and mostly intolerable	0.45	≤ DGP	

Level of recommended glare protection	
High	$DGPs_{0.35;exc.} ≤ 5\%$
Medium	$DGPs_{0.40;exc.} ≤ 5\%$
Minimum	$DGPs_{0.45;exc.} ≤ 5\%$

Daylight Glare Probability Simplified (DGPs): Wienold and Christoffersen (2006) also proposed the simplified DGPs metric that bases the glare probability prediction on daylight glare saturation alone. DGPs was shown to give reliable predictions of glare sensation in cases where the observer is not exposed to direct solar radiation (Wienold 2007; Konstantzos et al. 2015b). DGPs is computed from E_v at the position of the occupant using the equation:

$$DGPs = c_1 \cdot E_v + c_3 \tag{2.2}$$

Where: $c_1 = 6.22 \cdot 10^{-5}$, $c_3 = 0.184$

2.7.3 View

The availability of views to the outdoors has been shown to positively contribute to the comfort, productivity and well-being of occupants (Heschong 2003b; Wienold 2009a; Aries et al. 2010; Newsham et al. 2009). Additionally, research has shown that both the quantity (the size of the view) and quality of the view (what can be seen and its position) are factors of importance (Heschong 2003b; Hellinga and Hordijk 2014).

Although many methods and indicators for assessing view performance have been proposed in literature (Hellinga and Hordijk 2014; Heschong 2003b; Mardaljevic 2019; Turan et al. 2019; Pilechiha et al. 2020; Wienold et al. 2011; Konstantzos et al. 2015a) only few of these metrics have been empirically validated based on occupant assessments (Heschong 2003b; Hellinga and Hordijk 2014; Konstantzos et al. 2015a). The methods by Hellinga and Hordijk (2014) and Heschong (2003b) were designed for determining appropriate window aperture size and placement and do not account for the effects of dynamically operated shading devices. The method by (Konstantzos et al. 2015a) allows for a comparison of view-through fabric shading devices but there is no empirical basis for predicting the effects that the operation of such device will have on subjective user assessments of the degree of view to the outdoors.

This research therefore takes a simplified and practical approach to view assessment, that is based on the current state of the knowledge on subjective perception of view in a qualitative manner. View to the outdoors is assumed to be only dependent on the position of a shading device and expressed using the fraction of the total window area that is not covered by the shading device if the window were viewed from the front using a parallel projection. This fraction will be called the 'exposed window fraction' (EWF). The way this fraction is computed differs depending on the type of shading device and will be discussed in the corresponding chapters.

2.7.4 Energy consumption and thermal comfort

Building energy performance will be expressed in terms of primary energy consumption for cooling, heating, and lighting. In most studies in this research, primary energy consumption is computed from simulated energy demand using the following equation from Beck et al. (2010):

$$E_{\text{prim.}} = \frac{E_{\text{light}}}{\eta_e} + \frac{E_{\text{cool}}}{\eta_e \eta_c COP_{cool}} + \frac{E_{\text{heat}}}{\eta_h} \qquad (2.3)$$

$E_{prim.}$: primary energy consumption, E_{light}: lighting energy demand,
E_{cool}: cooling energy demand, E_{heat}: heating energy demand
η_e: site to source primary energy ratio for electricity,
η_c: cooling delivery system efficiency, COP_{cool}: chiller coefficient of performance,
η_h: overall heating system efficiency

Final energy consumption and the related operational costs are not assessed explicitly in the four application studies of this research. The simulation framework has been equipped, however, with features to assess operational and lifecycle costs. A description of these additional features can be found in De Vries et al. (2021a).

In this research, thermal discomfort is addressed implicitly through the assessment of cooling energy consumption. In an additional study presented in De Vries et al. (2021a) thermal discomfort is explicitly connected to the sizing of heating, ventilation, and cooling (HVAC) systems and their related costs.

2.7.5 Additional aspects and considerations

In the design of automated shading solutions and high-performance façade systems, whole-building performance effects have to be considered within a larger framework of functional and aesthetic requirements. Some of aspects, such as visual appearance, tend to be subjective and qualitative, and cannot easily be quantified. Many relevant performance aspects are also specific to the shading solution that is being investigated and the position of the decision maker in the façade design and delivery process. Therefore, a set of additional considerations and performance indicators will be discussed within the application study chapters 5 to 8.

3 The virtual testbed

3.1 Introduction

This chapter presents the VTB that was developed in this thesis and gives an overview of the quality assurance tests that were executed to test its proper functioning.

Figure 3.1 shows the VTB in its most extensive configuration. Table 3.1 gives an overview of the main components of the VTB as well as the underlying modules that are aimed at particular functionalities. In the following sections, the main components of the VTB that are used in all application studies, will be presented. These components are denoted by capital letters in the schematic. Certain modules offer higher modelling resolution and additional modelling features, that are only required in particular VTB applications. Whether these additional modules are required depends on the characteristics of the shading system that is being investigated, the purpose of the simulation study and the available simulation input information. These additional modules will be presented in more detail in the application study chapter where they are applied along with an explanation of why they are needed.

Table 3.1 Overview of the VTB components and modules

| Component	Module	Functionality and method
Component A: Daylight simulation	Module A.1:	3phase method
	Module A.3:	DGPs-enhanced method
Component C: Fenestration system simulation	Module B.3.1:	Optical BSDF toolchain
	Module B.3.3:	CFS Optical + absorbed energy toolchain
	Module B.4:	Wienold/Roos fabric model and parametrisation toolchain
Component B: Thermal simulation	Module C.1:	Winkelmann shade model
	Module C.2:	CFS shade model
Component D: Control logic simulation	Module D:	Control functionalities: elaborate logical structures, advanced mathematical methods and execution of external programs
Component E: Data management and co-simulation	Module E:	Framework for data management and co-simulation
Component F: Energy system simulation	Modules F.1.1 & F.2.1:	Energy system description based on performance ratios
	Modules F.1.2 & F.2.2:	Detailed energy system simulation
Support methods S: Control development and decision support methods and algorithms	Module S.1:	Performance mapping and statistical classification method
	Module S.2:	Classification tree method
	Module S.3:	Façade design optimisation methods
	Module S.4:	Method for addressing uncertainties in future electricity grid characteristics
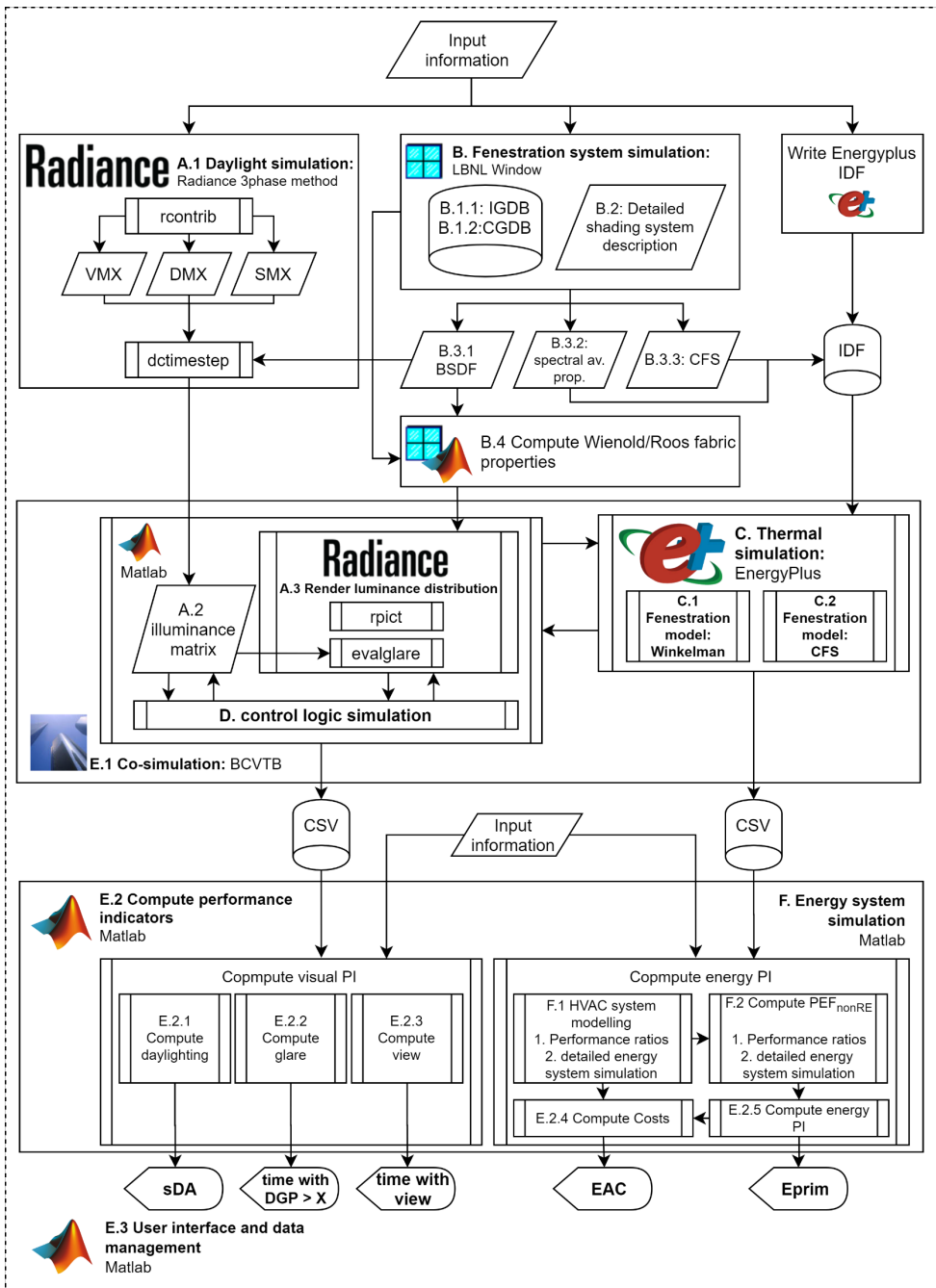
Figure 3.1 The virtual testbed for advanced automated solar shading strategies (VTB).

43

To account for the strong dependence of performance on interactions between the thermal and visual domains, the VTB employs a co-simulation approach using dedicated tools for daylighting simulation, thermal and energy system simulation, and control system simulation. In describing the optical and thermal behaviour of shading devices and the overall fenestration system, the VTB follows a multi-scale strategy where detailed subsystem simulations of the window and shading system are used to compute the emergent behaviour on higher levels-of-scale that are used to assess whole-building performance effects. This multi-scale approach will be discussed in more detail in Section 3.2.3 and Chapter 7.

Figure 3.1 shows two points where input information is entered into the VTB. The point shown at the top refers to inputs that describe the physical characteristics of the system that is being simulated (e.g., the building geometry, material properties, sensor positions). The lower point refers to performance thresholds and system efficiencies. This input information will be described in more detail in Chapter 4.

The VTB and the functions that are used in its support methods are publicly accessible and can be found in the following repository: https://gitlab.tue.nl/bp-tue/solarshading

3.2 The main virtual testbed modules
3.2.1 Component A: Climate-based daylight simulation
The VTB uses Radiance 5.2.0 (Ward et al. 1998) for simulating indoor daylight conditions. Radiance is an open-source suite of programs for predicting global and local illumination. These programs include algorithms for recursive raytracing, combined stochastic and deterministic ray sampling, and describing the optics of various material architypes. The VTB uses several Radiance programs (A in Figure 3.1) from the Radiance suite. The Radiance three-phase (3PHS) method is used for climate-based simulations of the indoor distribution of daylight illuminance (A.1). In certain VTB applications Radiance is also used to simulate the luminance distribution (A.3) in the field of view of occupants and the corresponding simulation methods will be presented in Chapter 7.

The 3PHS method (Ward et al. 2011) offers an effective simulation technique for describing the ambient daylight contribution in a climate-based manner including the effects of dynamically operated façade systems with complex optical properties. The 3PHS method has been validated for the prediction of the indoor illuminance distribution resulting from the dynamic operation of advanced solar shading systems (Mcneil and Lee 2013; Ward et al. 2011). The 3PHS method reduces the computational cost of the simulation by reusing the flux-transfer information

obtained from ray tracing operations, thereby reducing the number of required ray tracing simulations. The 3PHS method starts with a discretised geometrical description of the sky and conceptually splits up the flux-transfer path from the sky to interior sensor points into three components (Figure 3.2). Ray tracing simulations are used to compute each of these flux transfer paths which are stored in the following sets of matrices:

- The View matrix (V) describes flux transfer from indoor sensor points to a discretised description of the window system.
- The Transmission matrix (T) describes flux transfer between incident window directions to exiting directions for the two sides of the window system using a bidirectional scattering distribution function (BSDF).
- The Daylight matrix (D) describes flux transfer from the exterior window system directions and the sky.

Climate-based descriptions of the sky luminous intensity distribution are computed from hourly direct and diffuse solar irradiance values using the Radiance *gendaylit* program based on the Perez all weather sky model (Perez et al. 1990; Perez et al. 1993) and discretised into a sky matrix (S) that describes the luminous contribution for each patch of the sky across the simulation period. A matrix (I) containing the distribution of indoor daylight illuminance across a series of sensor points for each time step can then be obtained through matrix multiplication using the equation:

$$I = VTDS \tag{3.1}$$

Where: V: View matrix, T: Transmission matrix (BSDF), D: Daylight matrix, S: Sky matrix (can also be a vector s for a single time step).

Multiple transmission matrices (T) can be used to describe different optical states of the fenestration system. These states can relate to different blind positions or varying sets of optical properties that the automated control strategy can dynamically switch between. Additionally, the window surface can be divided into multiple segments were V and D matrices are computed to find the relative contribution of each segment. This allows different transmission matrix states to be selected across the window surface. The Radiance 3PHS daylighting simulations are executed before the co-simulation process takes place (module A.1). In this step, a database is created (A.2) containing the daylighting contributions to each sensor point of each segment of the window and each optical T state for all daylit hours of the year.

Figure 3.2 Schematic overview of ray tracing operations and associated daylight flux transfer matrices in the Radiance 3PHS method.

3.2.2 Component C: Transient thermal building simulation

The VTB uses EnergyPlus 8.5 (Crawley et al. 2001) for transient thermal building simulations (C in Figure 3.1). EnergyPlus is an open-source program with a modular structure that offers a multitude of models for describing building physics, HVAC, and energy systems. The program has been extensively validated, with specific emphasis on the effects of the building skin on indoor thermal conditions and building energy consumption (Henninger and Witte 2013, 2011).

EnergyPlus offers the functionality to change thermal and optical properties of building constructions during the simulation run time. Additionally, the energy management system (EMS) allows users to control many features in the operation of the program and execute programs written in the application's run-time language. Within the VTB, EMS programs are used to process information from the other tools, actuate the position of shading devices, and change window constructions during simulation runtime.

EnergyPlus offers multiple window and shading models that vary in terms of their model complexity, required inputs and abilities. Table 3.2 gives an overview of the type of advanced solar shading features that can be described by each model. The VTB is currently set up to work with either the default *Winkelman* glazing and shading models, or the *complex fenestration system model* (CFS) and both these modelling methods will be used in the application studies. The details of the application of these models will be discussed in the application study chapters where they are applied for the first time. The other window and shading systems models can be used in conjunction with the VTB with relatively little ease.

Table 3.2 Window and shading device models in EnergyPlus and possible applications

	Simple glazing indices	Default Winkelman models	Equivalent layer ASHWAT models[1]	Complex fenestration State method
Conventional shading devices:	~	X	X	X
Custom optically complex shading devices:				X
Time varying optical and thermal properties:	X		X	X
Literature:	Arasteh et al. (2009)	Winkelmann (2001)	Barnaby et al. (2009)	Klems (1994)

3.2.3 Component B: Fenestration system simulation

To describe the behaviour of optically complex shading system like blinds and fabric shades, and the way in which they interact with multi-layer glazing systems, the VTB uses the LBNL-Window program (Lbnl 2019b; Curcija et al. 2018). A multi-scale approach is used to describe the physical behaviour of the overall fenestration system. A detailed sub-system simulation (B in Figure 3.1) is executed in LBNL-Window (Bustamante et al. 2017; Klems 1994) before the co-simulation process commences. This simulation computes the angularly dependent optical behaviour of each layer and solves the recursive system of transmission, reflectance and absorption of visible and solar radiation involving all fenestration system layers.

The overall visible transmittance of the multi-layered fenestration system is stored inside the BSDF (B.3.1) that is used for the 3PHS daylighting simulations (A.1). The BSDF contains a matrix that relates flux transfer between a discrete series of 145 incident and outgoing beam directions. If the CFS model is used in EnergyPlus (C.2), a BSDF describing the solar flux transfer (B.3.3), is additionally generated using LBNL-Window. Additionally, the absorptance of each layer of the system in relation to the 145 incident beam directions is stored in a separate absorption matrix. In the VTB configuration that is most detailed in terms of describing the optical characteristics of the shading system (Chapter 7), the LBNL-Window algorithms are also used to compute higher level optical properties (B.4) from a detailed shading system description (B.2).

Through the LBNL-Window program, the VTB allows measured glazing properties from the international glazing database (Mitchell 2018, IGDB: Module B.1.1) and the complex glazing database (Mitchell 2017, CGDB: Module B.1.2) to be accessed.

---

[1] Errors were found within the equivalent layer blind model in this research and reported to the EnergyPlus development team

Throughout this research, measured IGDB glazing data is used. Measured BSDFs from the CGDB, that describe the optical behaviour of shading devices, are only used in Chapter 5. In the other chapters the optical behaviour of shading systems is derived from LBNL-Window simulations.

3.2.4 Component D: Control logic simulation

Matlab (The Mathworks Inc 2017) is used during the co-simulation runtime to simulate solar shading control strategies (D in Figure 3.1), compute the current daylighting conditions using the daylight database, as well as to calculate the resulting interior gains from electric lighting that are sent to EnergyPlus. The program processes incoming sensor information from EnergyPlus and Radiance and calls a set of functions describing rule-based control strategies. In the more elaborate VTB-configurations Matlab is used to call a set of Radiance programs during the co-simulation (A.3). Additionally, a set of advanced Matlab objects representing control features, such as classification trees, are accessed during the simulation.

Matlab was selected for this purpose because it offers a high-level programming language, a flexible modelling environment and a large number of optimisation features.

3.2.5 Component E: Framework for co-simulation and data management

The Building Controls Virtual Testbed 1.6.0 (BCVTB) program (Wetter et al. 2008) is used for directing the co-simulation process and the exchange of information between Matlab and EnergyPlus (E.1 in Figure 3.1). BCVTB uses a loose coupling approach where data are exchanged with a fixed synchronisation time step and where there is no iteration between the client programs (Wetter 2011) within a single time step. Figure 3.3 graphically presents the exchange of information between EnergyPlus and Matlab throughout the co-simulation process.

Within the VTB, a suit of Matlab functions (E.2 and E.3 in Figure 3.1) is used for (i) managing data, (ii) editing and writing input files, (iv) calling simulation programs, (v) computing performance metrics from simulation outputs and (vi) preparing and executing parametric studies. These Matlab function include custom built parallel processing capabilities that reduce simulation time with less parallel overhead time than the default parallel processing features in Matlab.
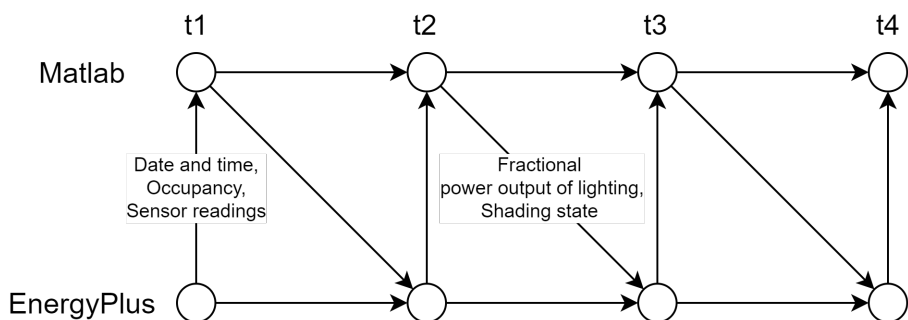
Figure 3.3 Exchange of information in the VTB co-simulation process. T1 stands for time step 1.

3.2.6 Component F: Energy system simulation

In the first three application studies (Chapters 5 to 7), the behaviour of HVAC (F.1.1) and energy systems (F.2.1) is greatly simplified and described using Equation 2.3. The assumptions regarding the efficiency indices in the equation will be presented in Section 4.2.

In Chapter 8, a more detailed approach is used to describe HVAC (F.1.2) and energy systems (F.2.2). The VTB has been equipped with a more detailed air-source heat pump model that is validated through inter-model comparison in Appendix D. Additionally, a method is presented in Chapter 8 and De Vries et al. (2021a) for addressing uncertainties in future electricity grid characteristics. These tools allow building designers to investigate interactions between the effects of advanced shading control solutions on building energy demand, detailed HVAC system performance, local generation of renewables and time-of-use dependent grid electricity characteristics.

3.3 Support methods functions S: A suite of analysis and optimisation algorithms and decision support tools

The VTB additionally offers a set of Matlab functions that are part of the developed support methods. These functions include: (i) statistical classification algorithms that allow optimal control thresholds and rules to be extracted from simulation outputs, (ii) algorithms for identifying pareto-optimal façade design solutions, and (iii) functions for visualising performance effects in relation to design and control aspects. These functionalities will be explained and illustrated in the application studies.

3.4 Quality assurance tests for verification and validation of the VTB modules

To assure that the VTB functions as intended, a series of validation and verification studies were performed that test the functioning of individual VTB components and VTB configurations. These verification and validation studies will be presented as part of the application study chapters in a dedicated quality assurance section. Whenever a new VTB module is used for the first time in this research, the corresponding application study chapter will present quality assurance tests for that module. Table 3.3 gives an overview of the VTB modules that are applied in each application study, and where quality assurance tests were executed. The quality assurance tests were chosen such that each VTB components is tested extensively at least once. The quality assurance sections additionally illustrate how a simulation user can investigate performance sensitivity to modelling resolution and uncertain input parameters.

Table 3.3 Overview of the quality assurance tests of VTB modules in this research

VTB Modules applied:			Chapter 5	Chapter 6	Chapter 7	Chapter 8
Component A: Daylight simulation	Module A.1:	3phase method	X	X		X
	Module A.3:	DGP-enhanced method			X	
Component C: Fenestration system simulation	Module B.3.1:	Optical BSDF toolchain	X	X	X	X
	Module B.3.3:	CFS Optical + absorbed energy toolchain		X	X	X
	Module B.4:	Wienold/Roos fabric model and parametrisation toolchain			X	
Component B: Thermal simulation	Module C.1:	Winkelmann shade model	X			
	Module C.2:	CFS shade model		X	X	X
Component D: Control logic simulation	Module D:	Control functionalities: elaborate logical structures, advanced mathematical methods and execution of external programs	X	X	X	X
Component E: Data management and co-simulation	Module E:	Framework for data management and co-simulation	X	X	X	X
Component F: Energy system simulation	Modules F.1.1 & F.2.1:	Energy system description based on performance ratios	X	X	X	
	Modules F.1.2 & F.2.2:	Detailed energy system simulation				X
Support methods S: Control development and decision support methods and algorithms	Module S.1:	Performance mapping and statistical classification method	X	X	X	
	Module S.2:	Classification tree method			X	X
	Module S.3:	Facade design optimisation methods				X
	Module S.4:	Method for addressing uncertainties in future electricity grid characteristics				X

Legend:

(grey box)	Application of new module. Use-case chapter will include verification, validation and quality assurance sections
X	Module is applied in this study

4 The IEA SHC Task 56 reference office: model description and validation

4.1 Introduction

This research is connected to Task-56 of the International Energy Agency's Solar Heating and Cooling program (IEA-SHC) focussed on Building Integrated Solar Envelope Systems. As part of the Task-56 project, a typical cellular reference office space was defined that is representative of the type of solar exposed office spaces that integrated solar envelope systems seek to improve (D'antoni et al. 2019). The Task-56 reference office will be used, with some minor adjustments, for the assessment of the novel solar shading concepts throughout this research. The primary daylighting (A.1: Radiance 3PHS method), thermal (C: EnergyPlus) and control logic (D: Matlab) simulation components were validated within the Task-56 framework through inter model comparison. This paragraph presents the Task-56 reference office and two validation studies, aimed at testing the aforementioned VTB components.

4.2 Description of the reference office and modelling assumptions

Figure 4.1 (left) shows a geometric overview of the original Task-56 reference office space (D'antoni et al. 2019). In the inter-model comparison studies that are presented in the following sections, the original Task-56 reference office assumptions will be used.
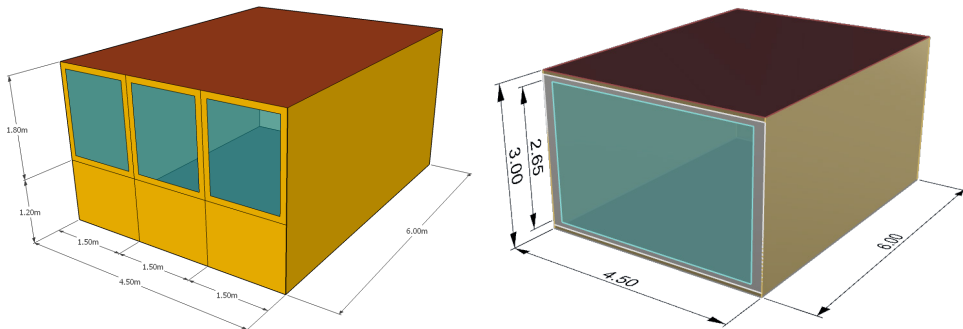
Figure 4.1 Geometric overview of the Task-56 reference office. Left: the original Task-56 office that is used in the validation studies in sections 4.3 and 4.4. Right: The reference office that is used in the application study chapters

Some features of the reference office, such as a high parapet and low window-to-wall ratio (WWR) were developed with the assessment of façade integrated renewable energy generation technologies in mind. These assumptions are not always representative of the type of building applications that developers of

advanced shading strategies are aiming for. Additionally, the application studies in this research are aimed at the Dutch context whereas the Task-56 description only provides climate data and typical construction details for Stuttgart, Stockholm and Rome. Therefore, some minor adjustments are made in the reference office that is used in this research. A larger window is used (Figure 4.1 right), the applied constructions are changed to meet Dutch building codes and practices, and IWEC weather data for Amsterdam is used. Table 4.1 gives a detailed description of the reference office used in this research and other modelling assumptions.

The Task-56 reference office description was developed throughout the duration of this PhD research. Therefore, there are some minor variations between the initial assumptions of the studies that are presented in the application study chapters. The assumptions that are specific to each application study will be discussed in the corresponding chapter. It should be noted that the application studies were not designed to allow for a direct cross comparison between the results that are presented in each application study.

Table 4.1 Reference office details and assumptions

Geometry	Dimensions	width: 4.5m; depth: 6m; height: 3m (27 m²)
	Facade orientation	South
	Window to wall ratio:	80%
Fenestration	Type:	Low-E (pos. 2) double glazing with argon cavity filling
	Glazing:	U_{gl}: 1.2 W/m²K, U_{frame}: 1.5 W/m²K, T_{vis}: 0.82, SHGC: 0.62, CEN
Facade		Rc = 4.5 m²K/W (U_{wall} = 0.22 W/m²K)
Ceiling, walls, floor		Mixed: heavy weight floor/ceiling, lightweight walls
		Ceiling R_{vis}: 0.8, Wall R_{vis}: 0.5, Floor R_{vis}: 0.2
Internal gains	People:	3 (variable occupancy). 120 W/pers.
	Occupancy:	Weekdays: 8:00-19:00 (2860 hours/year)
	Lighting:	10.9 W/m², closed loop linear dimming between 0-500 lux, Two sensors that each control 50% of loads
	Equipment:	7.0 W/m²
HVAC and settings	Infiltration:	ACH: 0.15
	Ventilation:	Constant during occupied hours, 40 m³/(h*pers.), ACH: 1.5
		Sensible heat recovery, efficiency: 70%
	Setpoints:	Lower set point: 21°C, Upper set point: 25°C (constant)
	System efficiencies (Beck et al. 2010)	η_e: 0.47, η_{gas}: 1, The Netherlands 2015 (Niessink and Gerdes 2018)
		$\eta_{cool,deliv}$: 0.7 (Air-based cooling delivery system)
		COP_{cool}: 3 (Chiller with outdoor air condenser)
		η_h: 0.95 (Natural gas condensing boiler)
Weather		IWEC, Amsterdam, The Netherlands (Ashrae 2001)

4.3 Module A: Validation of the daylighting model through inter-model comparison

To validate the VTB components for the 3PHS method daylight simulation (A) and control system simulation (D), the performance predictions of these models will be compared to predictions made using DALEC (Werner et al. 2017). DALEC is a web tool focussed on combined thermal and lighting building simulations in early building design stages. DALEC's daylighting simulation features also utilise the Radiance 3PHS method and have been experimentally validated (Werner et al. 2017). The DALEC simulations were carried out by Martin Hauer from Bartenbach, one of the developing parties of the DALEC tool. A more detailed description of the inter-model comparison that is presented here, can be found in Ochs et al. (2020a).

In this study daylighting performance will be assessed using continuous daylight autonomy (cDA_{300lx}). The two tools use different performance indicators for assessing glare. Glare will be assessed using Daylight Glare Probability Simplified (DGPs) in the VTB and the average luminance of the window in Dalec. Figure 4.2 shows the Radiance model setup that is used in both simulation tools. Because DALEC predicts daylighting conditions at only two sensor points (MP1 and MP2) the comparison between the tools will focus on cDA_{300lx} at these points and not on the sDA_{300lx} indicator that requires a grid of sensor points for its evaluation.
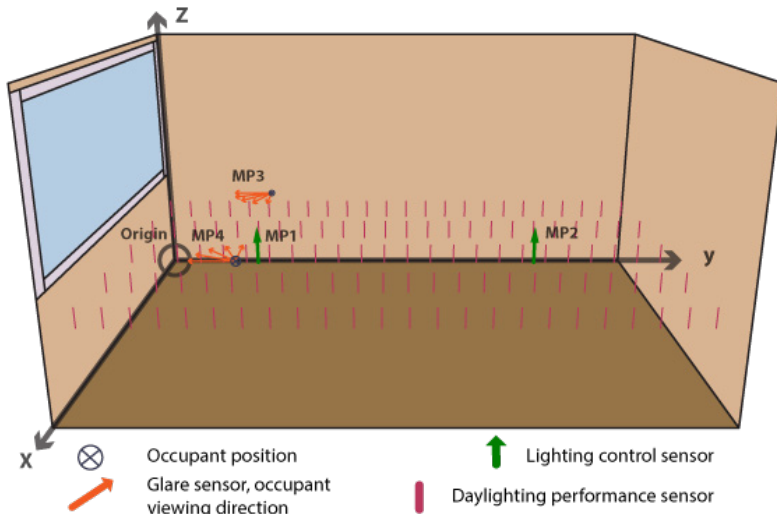
Figure 4.2 Overview sensor positions (MP1 and MP2) that are used to simulate cDA_{300lx} in the inter-model comparison between the VTB and DALEC.

Table 4.2 Overview of assumptions and sensor positions that are used to simulate cDA300lx in the inter-model comparison between the VTB and DALEC.

Sensor point	X Coordinate [M]	Y Coordinate [M]	Z Coordinate [M]
P1	2.25	1.50	0.75
P2	2.25	4.50	0.75
P3	3.50	1.50	1.20
P4	1.00	1.50	1.20
Shading system:			
Solar shading control:		Exterior roller shade:	
If I_{gv}>120 W/m²: Down Else: up		**T**$_{vis}$**:** 30%, fully diffusing	

Table 4.3 shows a comparison of the cDA$_{300lx}$ performance at the two sensors points predicted by the two tools for the three climates from the Task-56 description. Both tools predict similar outcomes and there is generally only 1-3% disagreement in the predicted cDA$_{300lx}$. Only in the climate of Rome there is a larger discrepancy (6%) between the two tools for the sensor point deeper into the space. Even in this case, however, both tools predict a degree of daylighting performance that can be classified as good (cDA300lx ≥ 75%). The differences between the two tools can be explained by:

- Slight differences in the dimensions of the window geometry. DALEC uses a database of pre-defined façade and space design geometries causing slight deviations from the Task-56 description.
- Difference in the sky models that are used to predict vertical irradiance that is used as an input for the shading control strategy.
- Differences in Radiance render settings.

Table 4.3 Comparison of predicted daylighting performance in terms of continuous daylight autonomy (cDA$_{300lx}$) at two work plane illuminance sensors by DALEC and the VTB

	cDA$_{300lx}$ at Point 1:		cDA$_{300lx}$ at Point 2:	
	VTB	DALEC	VTB	DALEC
Stuttgart	87%	90%	78%	79%
Rome	89%	90%	85%	79%
Stockholm	79%	77%	69%	66%

Overall, the agreement between the two tools is sufficient to conclude that the VTB modules A and E function properly. It can be noted that very good daylighting performance is predicted for the reference office, even though a conventional shading control strategy is used. This is because the reference office assumes a shading fabric with a high transparency (T_{vis}: 30%). Both tools predict that this situation would lead to an unacceptable degree of glare protection (Figure 4.3). A

more representative baseline scenario using a fabric with a lower openness will therefore be assumed in the application study chapters.
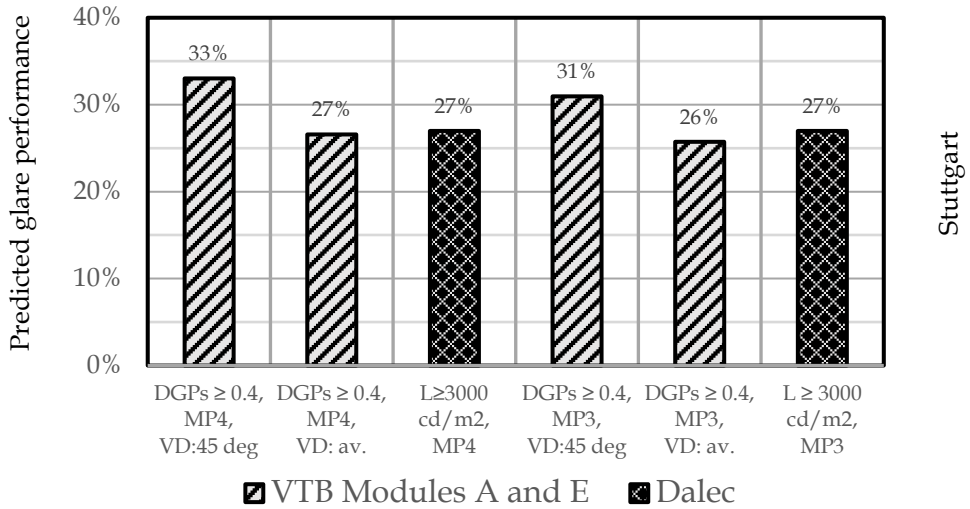
Figure 4.3 Glare performance, predicted by the two tools for the Task-56 reference office. Where: L = Average luminance of the window predicted by DALEC, VD: Viewing direction, 45Deg: Viewing direction facing the window at 45 degree, av.: average DGPs across all viewing directions predicted by the VTB.

4.4 Module C: Validation of the thermal model through inter-model comparison

To validate the EnergyPlus (VTB component C) reference office model, the performance predictions of this model were compared to the seven other validated and widely used building energy simulation tools: TRNSYS (TRN), Simulink CarnotUIBK (SIM_IBK):, Simulink ALMAbuild (SIM_BO), IDA ICE (IDA), Dalec (DAL), Modelica (MOD), and the Passive house planning package (PHPP). Annual simulations were executed with each tool for each of the three Task-56 climates and construction alternatives. The zone heat balance components predicted by each tool (legend in Figure 4.4) were then compared to assess the agreement between the tools. The comparison is presented in detail by Magni et al. (2021) and Ochs et al. (2020a). In this comparison the VTB component C is labelled as EnergyPlus (EP).
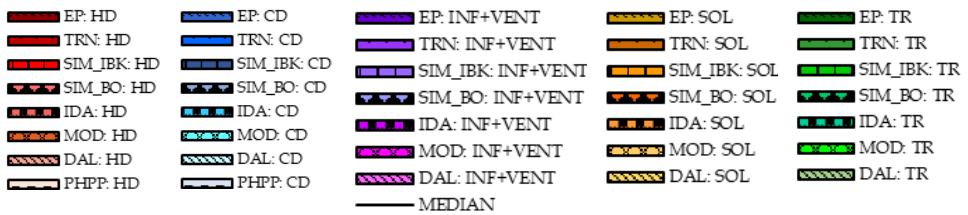
Figure 4.4 Overview of the simulation tools that are used in the inter-model comparison and legend to Figure 4.5. HD: heating demand, CD: cooling demand,
VV: ventilation and infiltration losses, TR: transmission losses, SOL: solar gains.
EP: EnergyPlus, TRN: TRNSYS, SIM_IBK: CarnotUIBK, SIM_BO: ALMAbuild,
IDA: IDA ICE, DAL: Dalec, MOD: Modelica, PHPP: Passive house planning package

Figure 4.5 shows monthly sums of the main components of the zone thermal balance that are predicted by each tool compared to the median value amongst all tools, for the three climates. For each month the thermal balance components for all tools are grouped next to each other. VTB component C (EnergyPlus) is shown as the set of stacked bars that are shown on the far left for each month. The graph suggests a good overall agreement between the different tools. Within the comparison studies, these zone thermal balance components were compared at an annual, monthly, and hourly level. For each of these time steps, the normalized mean bias error (NMBE) and normalized root mean square error (NRMSE) of the predictions of each of the tools were compared to the median prediction of all tools in Magni et al. (2021). Using the requirements set by Ashrae (2014), the study concluded that the agreement between the different tools was acceptable. From the inter-model comparison, it can additionally be concluded that VTB module B functions as intended.
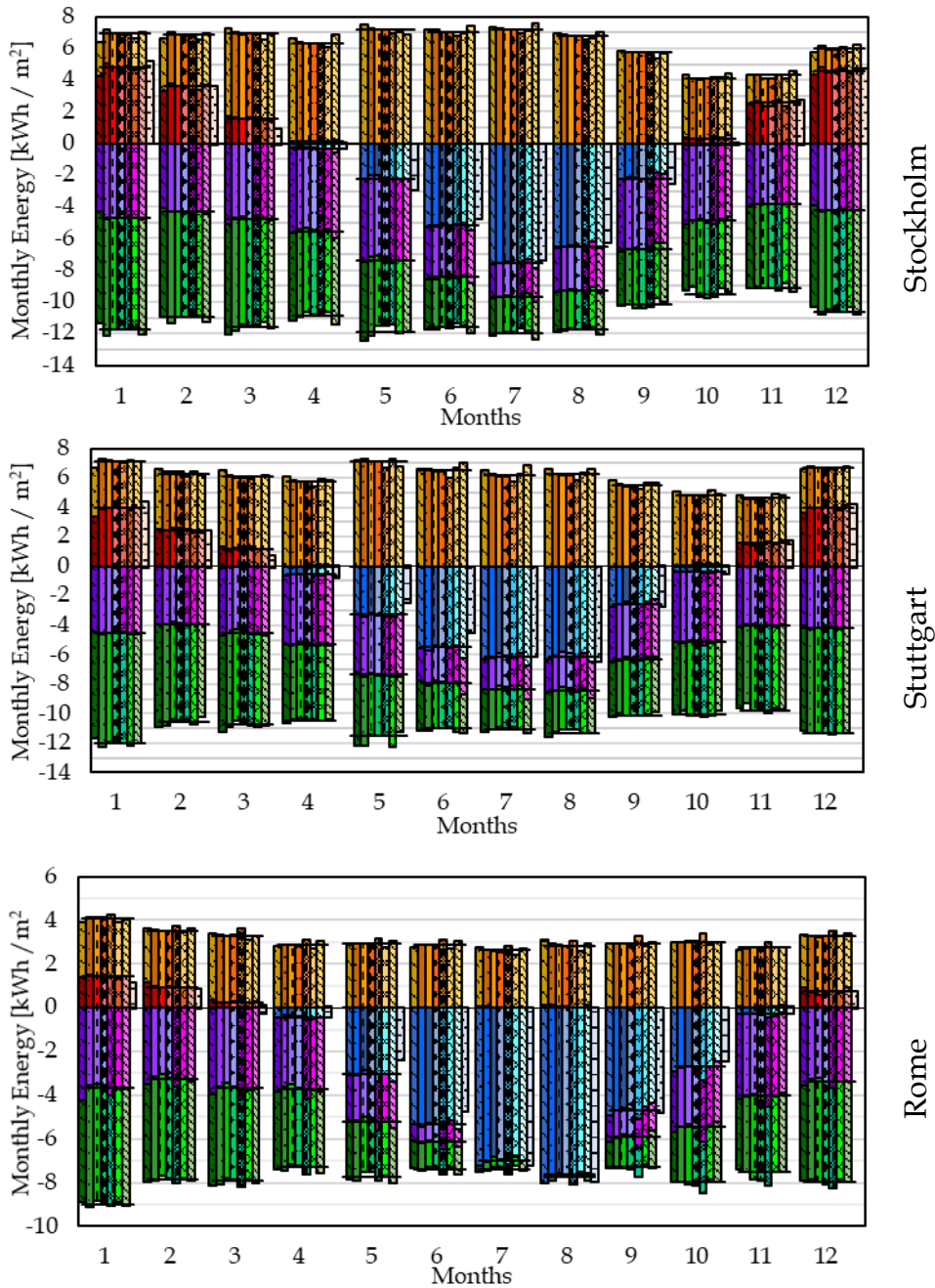
Figure 4.5 Monthly thermal balance of the reference office space predicted by the EnergyPlus model (VTB component B, stacked bars furthest on the left) and the other building energy simulation tools. Image from Magni et al. (2021).

5 Simulation-based support for sensor and control strategy development using performance mapping and statistical classification

5.1 Introduction

Developing an automated shading control strategy requires specifying control sensors and defining control rules and parameters. When the system is deployed in a building, additional decisions have to be made regarding the placement of control sensors and the tuning of control parameters. This chapter focusses on optimization of the applied shading control sensors, control rules and control parameters (the A and B levels-of-scale in Table 2.1). The specification of these control and sensor aspects is generally positioned late in the overall façade delivery process, taking place after the design of the building has been completed. The task of specifying these aspects generally requires collaboration between a solar shading contractor, an electrical contractor and a control and monitoring contractor (Beck et al. 2010). Some developers offer integrated automated shading solutions, allowing the motorization system, sensors, and a control concept to be purchased from a single contractor.

This application study takes the perspective of the developer of an integrated solution, or a shading contractor collaborating with the other responsible parties, as a decision maker that is tasked with specifying control sensors and developing a control strategy for a newly designed or existing building. The starting point of this study is a sun-tracking control concept for an automated indoor roller blind system. The study assumes that an existing motorisation concept has been developed that uses a silent motor that allows the position of the shade to be varied continuously. To develop the sun-tracking control concept into a high-performance control strategy, and apply it in a specific building, it needs to be extended with more elaborate control rules and equipped with sensors. The simulation purpose of the developer is to:

i.   Select a sensor deployment strategy that offers beneficial trade-offs considering multiple performance aspects.
ii. Identify control algorithms that optimise comfort conditions using non-ideal sensors.

The shading control strategy will use radiation sensors to classify indoor comfort conditions and decide upon control actions (Tabadkani et al. 2020a; Beck et al. 2010). Sensors need to be non-intrusive to occupants and are usually placed in non-ideal locations. Therefore, they cannot measure comfort conditions of occupants and building performance indicators directly (Yun et al. 2020; Tzempelikos and Shen 2013). For detecting a risk of daylight discomfort glare, for instance, it is not practically feasible to use the luminance distribution and illuminance at the position of occupants as direct control variables and only non-intrusive light sensors can be used. Additionally, it is important that a risk of glare resulting from a control action is predicted beforehand and prevented rather than retroactively corrected. The type of sensor that is used, its position and orientation influence the effectivity of the

control strategy in addressing building performance aspects (Yun et al. 2017; Tzempelikos and Shen 2013). In the development of the sensor strategy, a trade-off therefore must be made between the complexity and costs of the strategy on the one hand, and its positive effects on building performance on the other. An additional consideration is that, whilst control rules can always be easily changed, it is undesirable to change sensing equipment after it has been installed.

The goal of this study within the overall research is to verify the initial configuration of the VTB. An additional goal of the study is to develop and test a simulation-based support method for the development of performance-driven rule-based solar shading control strategies and the optimisation of sensor selection, control thresholds and detection algorithms. The requirements for this method are the following:

  i.   It supports the selection of control rules, parameters and sensors based on performance goals, gives detailed insight into performance trade-offs, and provides a structured approach to identifying high performance solutions inside the control space.
  ii.   It identifies solutions that are compatible with the currently available control hardware.
  iii. It is generically applicable and not tied to a particular type of shading system or building application.
  iv.   Applying the support method requires little effort from a developer. This feature allows the method to be used to customise a control strategy for a particular building design.

The proposed support method will be presented in Section 5.4. The method simplifies the task of developing an advanced control logic by guiding a developer in identifying a set of simple control actions, aimed at balancing trade-offs between a subset of performance aspects under specific representative environmental conditions. These control actions will later form the individual control modes of a multi-mode control strategy. The effects of these control modes on occupant comfort conditions are then graphically mapped to sensor measurements, such that the most beneficial conditions for activating each control mode can be identified. The effectivity of detection algorithms, sensors and control thresholds are then evaluated using statistical classification techniques and visualised in a confusion matrix. This allows the effectivity of non-intrusive sensors to be optimised. The graphic nature of this method allows the performance effects of all possible values for a single control threshold to be visualised in a single image using the results of only two full-year simulations. The method builds on, generalises and structures some of the ad-hoc research tasks observed in literature on advanced solar shading case studies

(Chan and Tzempelikos 2013; Oh et al. 2012; Shen and Tzempelikos 2017; De Vries et al. 2019).

The proposed support method will be illustrated and tested by applying it to the development of the sun-tracking roller blind concept and the selection of appropriate sensors and sensor thresholds. The research presented in this chapter can be found in a conference paper (De Vries et al. 2019), presented at the Building Simulation 2019 conference, and a journal article published in the Journal of Building Performance Simulation (De Vries et al. 2021c).

5.2 The initial concept: a sun-tracking control logic for automated indoor roller blinds

The initial sun-tracking control concept is based on a review of the literature on control strategies for shading systems (Tzempelikos and Shen 2013). This control logic, titled the solar cut-off logic (SC), balances the goal of limiting daylight discomfort glare with the competing goal of admitting daylight and views to the outdoors. The algorithm controls the roller blind in relation to the sun's position to block direct sunlight from hitting an occupant's desk (Figure 5.1) using Equation 5.1. The edge of an occupant's desk is assumed to be at 75 centimetres height (workplane height, wph) and positioned 75 centimetres from the façade (workplane depth, wpd).

$$sh = \frac{wpd}{cos(\gamma - 180)} \cdot tan\,\alpha\ + wph \qquad (5.1)$$

wpd: distance between the edge of the work plane and the façade, wph: height of the work plane from the floor,
sh: distance between bottom of the shade and the floor (shade height)
γ: solar azimuth in degrees (clockwise from North convention), α: solar altitude in degrees.
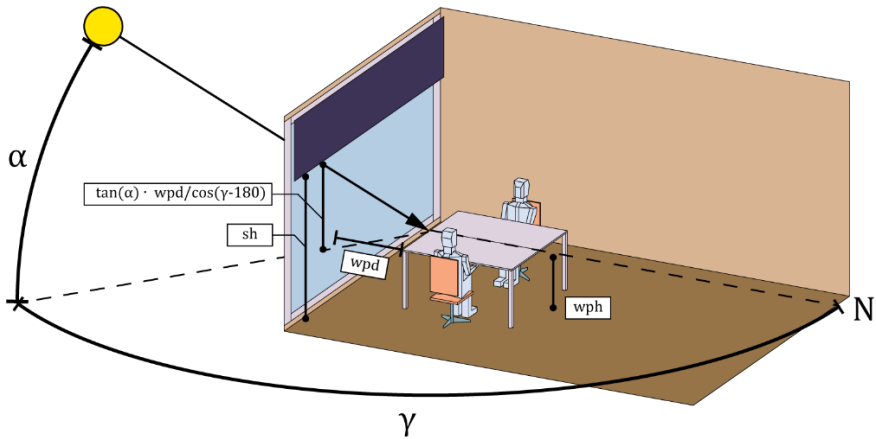
Figure 5.1 Parameters and solar position angles used in the solar cut off control logic

The control developer in this study is assumed to not be involved in the selection of the solar shading fabric or the design of the façade. It is assumed that a metal coated shading fabric is used that has a high solar reflectance and a low openness (Table 5.1). A conventional control strategy for indoor roller blinds will be used as a benchmark. In this baseline strategy (BL), the roller blind is controlled using an outdoor global vertical irradiance sensor where the shade is either fully raised or lowered in response to a threshold of 200 W/m² (Beck et al. 2010).

Table 5.1 Shade fabric properties

	T_{vis}:	$R_{vis;front}$:	T_{sol}:	$R_{sol;front}$:	OF:	ε_{front}	ε_{back}
Shade properties:	0.013	0.719	0.025	0.740	0.008	0.230	0.858

Table 5.2 gives an overview of the main goals and assumptions in this study in addition to the characteristics of the shading system that is investigated.

Table 5.2 Goals, assumptions and system characteristics in application study 1

Optimise:	Assume:	System:
Control rules	Shading fabric	Variable height roller shade system
Control thresholds	Motorisation system	Constant thermal/optical properties
Sensors	Glazing system	Complex control logic
	Building	

5.3 Methodology and simulation strategy

Based on the aspects summarise in Table 5.2, the methodology and simulation strategy (Figure 5.2) were defined. Figure 5.2 gives an overview of this methodology, the subsequent steps, and the corresponding sections where they will be discussed in this chapter.
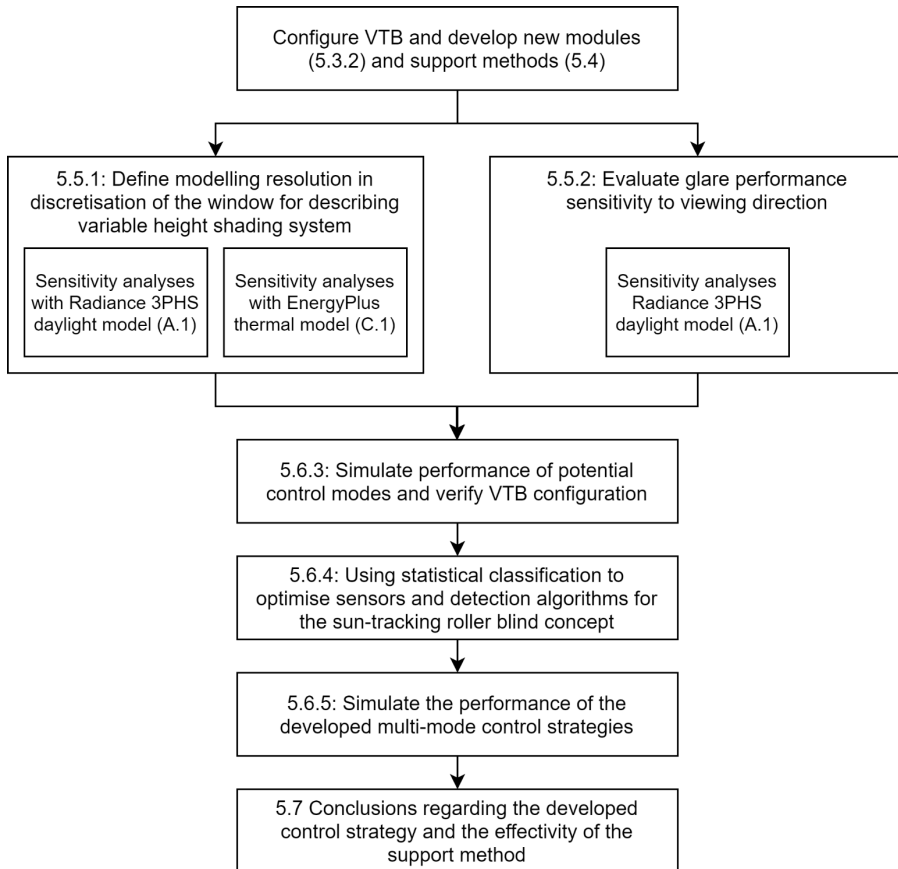
Figure 5.2 Overview of the methodology followed in this study

5.3.1 Performance aspects and indicators

Spatial daylight autonomy is used as an indicator for daylighting performance, with 300 lux and 50% of occupied hours as cut-off criteria (sDA300/50%). To evaluate instantaneous daylighting performance, the daylit area fraction D_{300lx} is used. For quantifying visual discomfort, daylight glare probability simplified (DGPs) is used as a performance indicator. In this study, DGPs is considered sufficiently reliable because the sun-tracking control strategy and low-openness fabric ensure that occupants are not exposed to sunlight.

In this study, view to the outdoors is assumed to be only dependent on the position of the shade. The exposed window fraction (EWF) is used as a performance indicator. Research investigating occupant operation of operable roller shades has shown that users tend to leave the lower portion of a window unshaded to maintain a visual connection with the outdoors (Haldi and Robinson 2010; Konis 2013; Sadeghi et al. 2016). Based on this observation, conditions where the shade is positioned above the eye level of a seated occupant (at 1.2 meters from the floor relating to a 40% EWF) are counted as offering a view to the outdoors. The percentage of occupied hours where this condition is met is used as a performance indicator and is abbreviated as $V_{1.2m;exc}$.

Energy performance is quantified as primary energy consumption for cooling, heating, and lighting, and computed from energy demands using Equation 2.3.

5.3.2 Configuration of the virtual testbed

Figure 5.3 shows how the VTB was configured to address the simulation study objectives, performance indicators and shading system characteristics. The main simulation modules for thermal simulation, daylight simulation, and control logic simulation have been discussed in Chapter 3. The elements that were added for this study are the modules for describing the variable height roller shade system in EnergyPlus (C.1) and Radiance (part of A.1) and a set of statistical classification functions for evaluating the effectivity of detection algorithms, sensors and control thresholds.

To simulate a variable height shading system using the Radiance three-phase method, the fenestration system needs to be divided into a number of horizontally oriented segments (Figure 5.4) that are either fully shaded or unshaded (Subramaniam 2018). In this study, the illuminance matrix, that is generated using the Radiance three-phase method, contains daylighting contributions of each segment of the window for all day lit hours of the year and both the shaded, as well as the unshaded states.

In EnergyPlus the default glazing and shade models (Dariush et al. 1989; Finlayson et al. 1993) are used, which are described in the paper by Winkelmann (2001) and hence referred to as the 'Winkelman' models in this work. The Winkelman model implemented in a single zone EnergyPlus model was validated by Loutzenhiser et al. (2007) using empirical methods and inter model comparison. The shading models in EnergyPlus do not allow for partially shaded window states to be directly implemented. Here, a similar modelling approach was chosen as with Radiance, where the window is divided into segments.
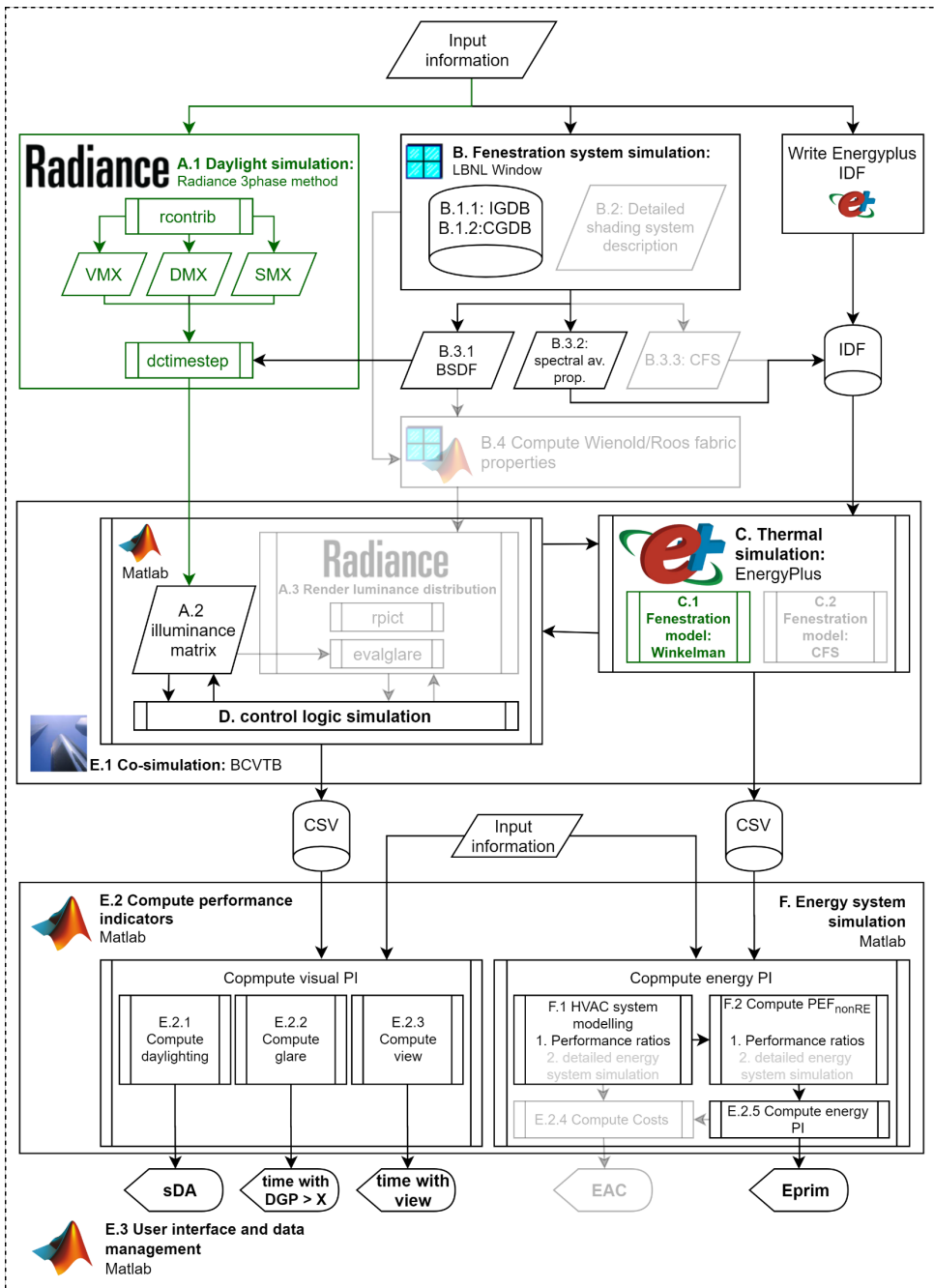
Figure 5.3 Configuration of the VTB for this application study. VTB components that are not used in this configuration are shown in light grey. New VTB modules that will be tested in this chapter are shown in green. The input information refers to the geometry and parameters that are specified in Figure 5.4 and Sections 5.3.3.

Glare sensor   Lighting control sensor

Glare sensor in sensitivity analyses   Daylighting performance sensor
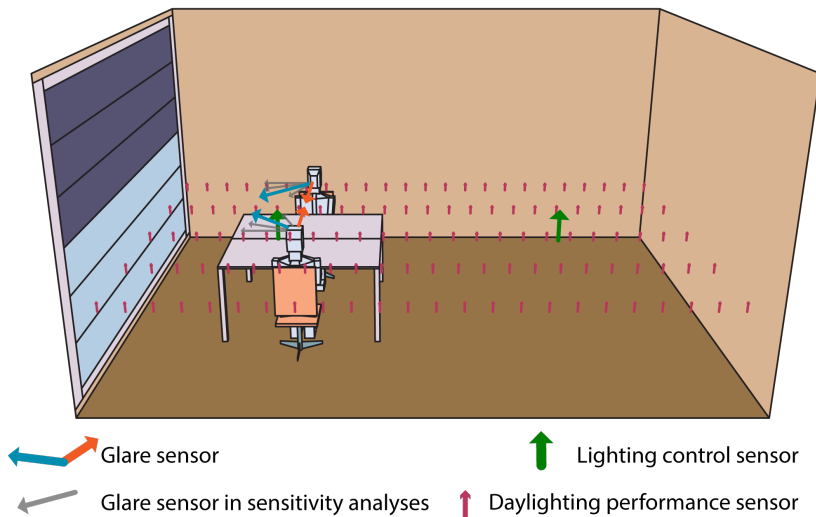
Figure 5.4 Overview of the Radiance three-phase method daylighting model

5.3.3 Assumptions and simulation input parameters

The details of the office cell model used in this study are summarised in Table 5.3. In addition, Table 5.4 gives and overview of simulation settings.

To assess glare probability, two seating positions as shown in Figure 5.4 are assumed. This a conservative assumption, because seating arrangements closest to the window are the most sensitive to the occurrence of glare (Giovannini et al. 2020). Additionally, the likelihood of discomfort glare is strongly influenced by viewing direction (Jakubiec and Reinhart 2012; Bian et al. 2018). For each seating position, glare is assessed in two viewing directions: one where the occupant is facing a wall, and one where the occupant is facing the window at 45 degrees as recommend in EN 14501 Cen (2017c). Annual aggregated performance is quantified using the percentage of occupied hours that a DGPs of 0.40 (disturbing glare) is exceeded. This annual indicator is separately assessed for both viewing directions ($DGPs_{0.4;0deg;exc}$ and $DGPs_{0.4;45deg;exc}$), where at each time step the maximum DGPs value of both occupant positions is used. $DGPs_{0.4;0deg;exc}$ thus gives the share of occupied hours that at least one of the two occupants perceives 'disturbing' glare if they were facing a wall (Figure 5.1) whilst $DGPs_{0.4;45deg;exc}$ assumes both occupants are facing the window at 45-degrees. In this case study, $DGPs_{0.4;0deg;exc}$ is considered the most critical as it is representative for instances where the occupants are facing their computer monitors and cannot easily adjust their viewing direction. Disturbing glare in this viewing direction is likely to lead to occupants overruling the automated control system. Therefore, preventing disturbing glare in this viewing direction is stated as a performance goal of the strategy that is going to be developed.

DGPs$_{0.4;45deg;exc}$ is considered less critical than DGPs$_{0.4;0deg;exc}$ because the occupants have more freedom to avert from this viewing direction. DGPs$_{0.4;45deg;exc}$ will therefore be treated as a performance indicator that is undesirable, but trade-offs with other aspects, such as daylighting performance, are considered acceptable. The influence of the assumptions regarding the viewing direction of the occupants on glare performance are also evaluated in the sensitivity analyses, presented in Section 5.5.2..

Hourly weather data for Amsterdam (IWEC) is used in this study. For EnergyPlus, a 5-min time step is chosen, as a sub-hourly resolution helps to increase the reliability of the heat balance algorithms as well as limit the effect of errors deriving from BCVTB's loosely coupled co-simulation approach. Within Radiance an hourly time step is chosen to describe sky conditions because of the unavailability of sub-hourly weather data.

Table 5.3 Study details and assumptions

Geometry	Dimensions	width: 4.5m; depth: 6m; height: 3m (27 m²)
	Window	80% Window to wall ratio facing South
Fenestration	Type:	Low-E (pos. 3) double glazing with argon cavity filling
	Glazing:	U$_{gl}$: 1.2 W/m²K, U$_{frame}$: 1.5 W/m²K, T$_{vis}$: 0.82, SHGC: 0.62, CEN
HVAC and settings	Infiltration:	ACH: 0.15
	Ventilation:	Demand driven, 40 m³/(h*pers.), ACH: 1 (average)
		Sensible heat recovery, efficiency: 70%
	Setpoints:	Lower set point: 21°C, Upper set point: 25°C (constant)
Weather		IWEC, Amsterdam, The Netherlands (Ashrae 2001)

Table 5.4 Simulation parameters and assumptions

	EnergyPlus	Radiance
Fenestration	Glazing optical properties from IGDB: Lay 1: IGDB# 1608 Lay 2: IGDB# 11560 Shade properties from CGDB# 20032: anisotropic optical model	BSDF created with LBNL-Window Lay 1: IGDB# 1608 Lay 2: IGDB# 11560 Shade: CGDB# 20032
Interior surfaces		Lambertian reflectors: Ceiling, r$_{vis}$: 0.8, Wall, r$_{vis}$: 0.5 Floor, r$_{vis}$: 0.2
Simulation settings	Idealised HVAC system: unlimited capacity and ideal response	Sensor grid: 5x25
		V$_{rcontrib}$: -ab 12 -ad 5·10⁴ -lw 2·10⁻⁶,
		D$_{rcontrib}$: -ab 2 -ad 10³ -lw 5·10⁻⁴ -c 3000
		s and D sky resolution: MF3
	5 min. time step	hourly time step

5.4 Support method: developing shading control strategies using performance mapping and statistical classification

Figure 5.5 gives an overview of the proposed support method. A developer starts with five preparatory steps (1.1-1.5). These steps include defining a set of performance aspects, indicators and goals (1.3) that the control strategy will seek to balance. Additionally, the developer defines an initial set of control modes (1.1). In each of these control modes, the shading device is dynamically operated according to a distinct logic that focuses on pursuing a subset of the overall performance goals. The different control modes should vary in terms of how far the shading device is opened and, consequently, in the amount daylight, sunlight and solar radiation that is admitted. The developer then defines several potential sensors alternatives (1.2), that the multi-mode control strategy will use to switch between control modes. Additionally, the developer defines a description of a representative office space (1.4) that is considered representative for the final application of the system. A simulation model is then developed (1.5) to predict the performance of each of the control modes and the corresponding sensor readings for each sensor alternative.

A simulation of a typical year is executed for each of the initial control modes, where the specific control mode is followed continuously (2). These simulations offer the developer a quantification of the overall annual performance of each control mode, the instantaneous performance at each time step and lists of corresponding simulated sensor readings.

The developer then evaluates, using annual performance indicators, if the individual performance goals are each met by at least one of the control modes and whether they provide the desired performance trade-offs (3.1). The most promising control modes are now selected and ordered in terms of the amount of solar energy that is admitted, with control mode 1 (CM_1) being the most open mode of operation and subsequent control modes (CM_2 to CM_n) being more closed. If the initial control modes do not offer the desired performance, new control modes can be added. The developer can find possible improvements by analysing the instantaneous time step performance of the initial control modes (3.2). If after multiple iterations of testing potential control modes the desired performance goals and trade-offs cannot be achieved, this gives reason to review the feasibility of the initially assumed goals, the proper functioning of the simulation model and the constraints that are posed by the selected dynamic shading system and its physical properties.
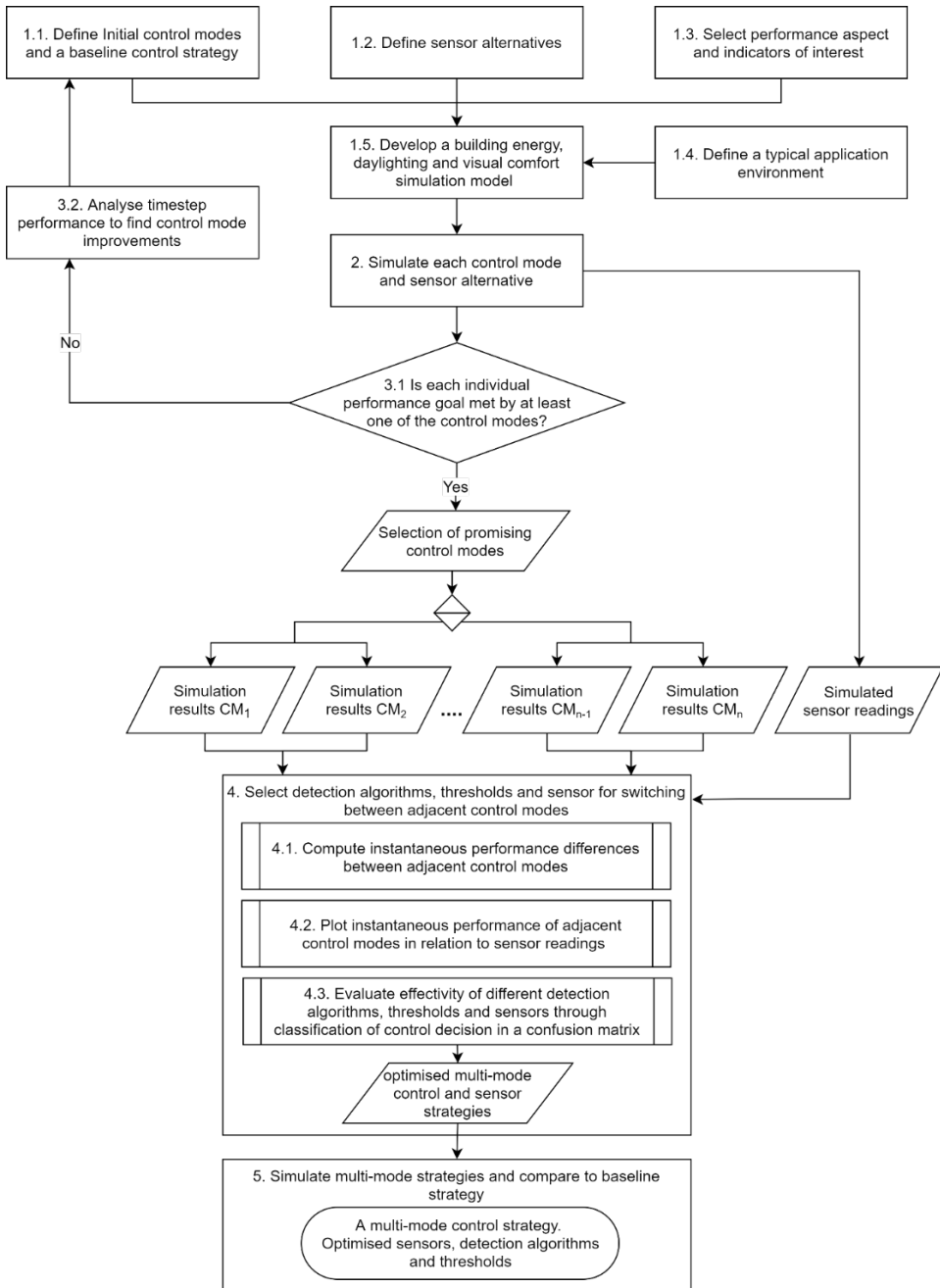
Figure 5.5 Overview of the computational method for developing high performance solar shading control and sensor strategies.

In the next step (4), a sensor strategy is developed. This strategy is defined by the detection algorithms, thresholds and sensors that are used to detect the boundaries of conditions where the control system will switch between two adjacent modes of operation. Adjacent here relates to the order in the admittance of solar energy. Each adjacent set of control modes will get a detection algorithm that determines when CM_n leads to poor performance and CM_{n+1} should be activated. The approach in step 4 is to relate the instantaneous performance, or the performance difference, of two adjacent control modes to sensor readings (4.2) and test detection algorithms using statistical classification techniques. In this application study, control decisions are classified in a confusion matrix (4.3) (Fawcett 2006). By relating the decisions of potential detection algorithms to simulated performance predictions, the effectivity of these algorithms can be evaluated. Potential sensor strategies can be evaluated from a multi-objective perspective by using the confusion matrix method for each performance indicator.

All steps will be graphically illustrated using the application study example. Additionally, a set of indicators that aid the developer in refining detection algorithms will be presented. This set includes indicators that are commonly used in the field of statistical classification as well as quantities developed in this research. The outcome of this process is a multi-mode control strategy, or multiple strategies, with optimised sensors and sensor thresholds. The performance of these strategies is then simulated and compared to a baseline strategy (step 5). The effectivity of the proposed support method will be investigated in the discussion section (5.7) using the results of the application study.

5.5 Quality assurance

This section highlights quality assurance of the new VTB features. The performance sensitivity to the chosen modelling resolution in subdividing the window to describe the variable height shading system will be investigated in Section 5.5.1. Additionally, the performance sensitivity to assumed occupant viewing directions will be investigated Section 5.5.2. The configuration of the overall testbed is additionally verified in the results section (5.6).

5.5.1 VTB Module A.1 and C.1: Sensitivity analysis of variable height roller blind models

The modelling approach, in which the window is split into segments, causes the actual position of the roller blind to be rounded to the height of the nearest segment. The rounding of the shade's position will lead to errors in the predicted flux of visual and thermal radiation. The magnitude of these errors can be decreased by increasing the number of window subdivisions. Within the daylight model, however, the number of subdivisions is proportional to the required computational effort. In EnergyPlus, errors could be introduced by an inappropriate application of the underlying models. The shade model in EnergyPlus explicitly describes heat and mass exchange between the air cavity, the shade, the zone, and the window. The chosen application of this model is therefore likely to give errors in convective solar gains.

Figure 5.6 presents a sensitivity analysis investigating an appropriate modelling resolution for the amount of window divisions. Figure 5.6A shows the sensitivity of performance predictions by the daylighting model. Within Radiance, increasing window subdivisions will better approximate the amount of transmitted daylight, as is illustrated by the flattening of predicted performance for the solar cut-off (SC) case. Spatial daylight autonomy is the most sensitive indicator, flattening only at 35 divisions. Because simulation time increases strongly beyond this point (Figure 5.6C) 35 divisions were chosen in this study. Figure 5.6B shows the sensitivity of predicted primary energy consumption to the number of window divisions in EnergyPlus. In this analysis, daylight dimming of lighting was disabled. The always up (AU) and always down (AD) cases show that the predicted E_{prim} changes only slightly as the number of window divisions are varied. This indicates that the errors introduced by the modelling approach have a small effect on performance predictions. The predicted performance of the solar cut-off (SC) strategy flattens out from 20 window divisions onward. For consistency, however, 35 divisions was chosen in EnergyPlus.
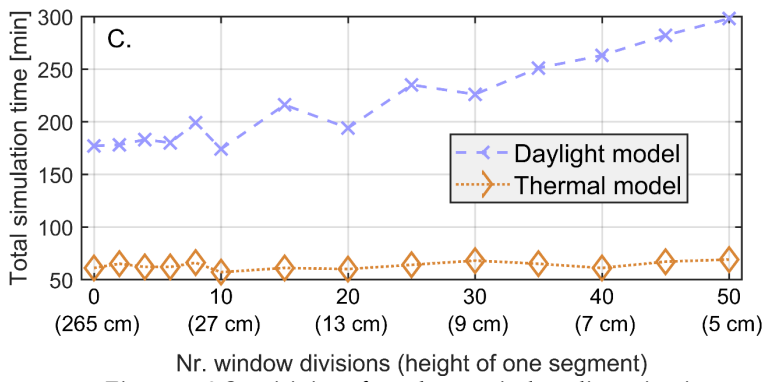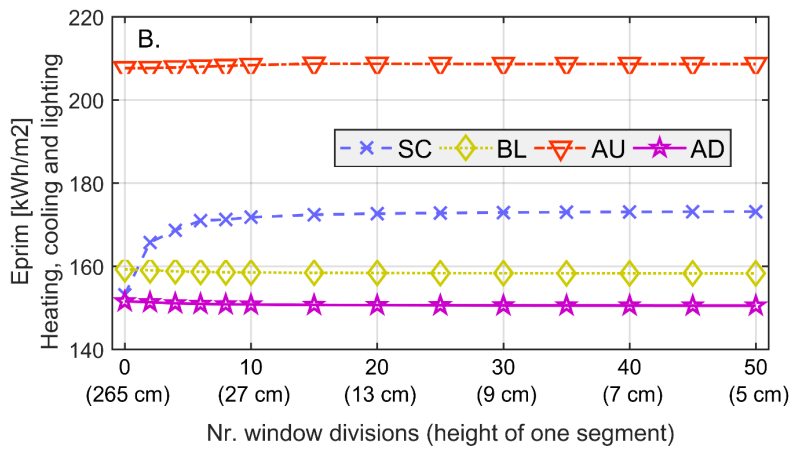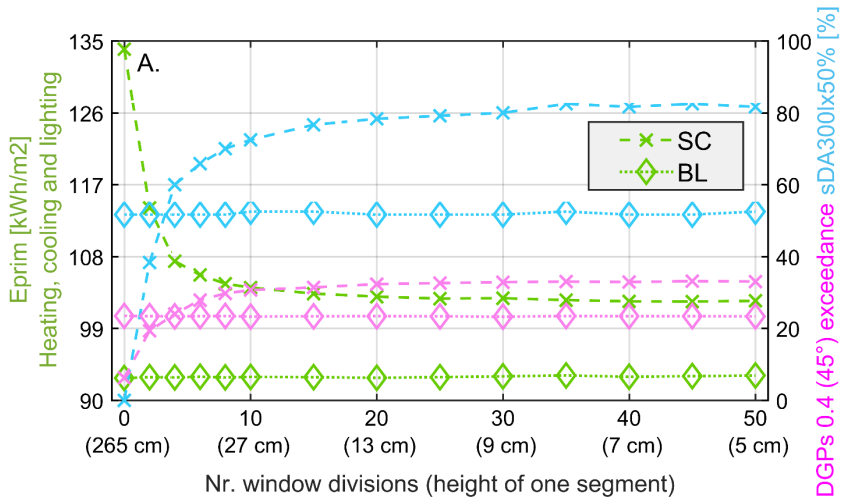
Figure 5.6 Sensitivity of results to window discretization.

A. Daylight model, B. Thermal model, C. Sensitivity of simulation time for both models

5.5.2 VTB Module A.1: Glare performance sensitivity to occupant viewing direction

Figure 5.7 presents a series of glare duration curves, resulting from annual simulations of the initial solar cut-off (SC) concept and the conventional baseline (BL) strategy. For each control strategy the viewing direction of the two occupants is varied at 22.5-degree intervals between 0 (facing a wall) and 90 degrees (facing the window). In the graphs glare results for the different viewing directions are ordered from high to low and plotted in relation to a vertical axis that indicates the share of occupied hours that a particular DGPs value is exceeded.
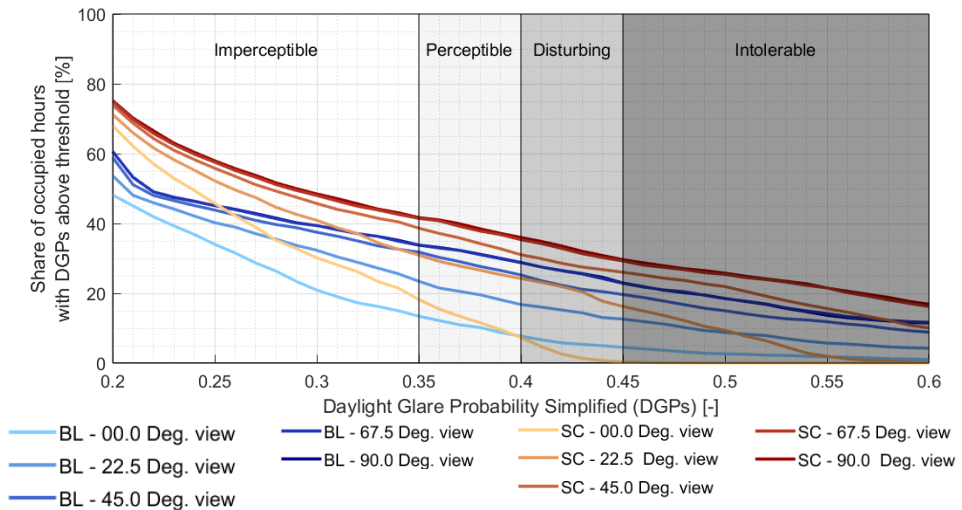
Figure 5.7 Glare duration curve for the SC and BL control strategies. DGPs simulation results for different viewing directions varying between the direction where the occupants are facing the window (00.0 Deg.) to the direction where the occupants are facing a sidewall (90.0 Deg.)

The figure confirms that predicted glare performance is very sensitive to the assumed viewing direction. Additionally, the two control strategies have a distinct glare load duration pattern that causes differences in the annual glare exceedance between the two strategies to depend strongly on the chosen glare class (e.g., perceptible, disturbing, or intolerable). For the viewing direction where occupants are facing their desktop monitors (00.0 Deg.), a small rotation of their viewing angle (22.5 Deg.) causes large differences in predicted annual glare performance (e.g., 7% $DGPs_{0.4;exc;00.0Deg}$ versus 24% $DGPs_{0.4;exc;22.5Deg}$ for SC) and different conclusions regarding which strategy performs best (e.g., the BL strategy gives 8% $DGPs_{0.4;exc;00.0Deg}$ and 17% $DGPs_{0.4;exc;22.5Deg}$). The viewing directions between 45 and

90 degrees, however, do not show much variation in terms of the shape of the glare duration curves and the overall degree of glare that is experienced. The graph confirms that the 00.0 and the 45.0 degree viewing directions give a representative overview of how the different strategies perform in terms of disturbing glare exceedance, relative to each other across the different viewing directions.

5.6 Application of the support method to sensor selection and control strategy development for the sun-tracking concept

In the following sections, the proposed support method is applied to further develop the sun-tracking roller blind concept. The sections are labelled using steps 1.1 to 5 from the flow-diagram in Figure 5.5. Some intermediate steps of the support method (1.3, 1.4, 1.5) that are shown in the diagram, involve defining performance indicators and the development of a simulation model. These steps have already been discussed in the methodology section of this chapter and will therefore be skipped here.

5.6.1 Define a set of initial control modes and a baseline strategy (Step 1.1)

In this study, preventing daylight discomfort glare is the control goal with the highest priority. In this step, a large part of the control space will be excluded based on experience and the body of knowledge on preventing glare with shading devices. By assuming a set of rule-based control modes based on initial analyses in step 3 and optimizing the conditions under which they are activated in step 4, the control space is greatly decreased, and the problem made more manageable.

To maximize the admission of daylight and views, a developer can start with a control mode where the shading system is placed in the most open position. Here, this means fully raising the shade. To minimise cooling energy consumption and glare, a control mode is added where the shading system is placed in the most closed position. In this case, this means fully lowering the shade.

The sun-tracking SC control logic, that was the starting point of this study, forms an additional control mode that balances multiple conflicting performance objectives. Solar cut-off algorithms can be geometrically defined for most commercially available types of shading devices (Tzempelikos et al. 2007b; Seong et al. 2014) and are a good starting point in defining control modes. Previous research (Atzeri et al. 2018; Tzempelikos and Shen 2013; De Vries et al. 2019) showed that the sun-tracking strategy can lead to undesirable degrees of glare and cooling energy consumption because it causes the shade to be nearly fully raised at mid-day in summer when solar altitude is high. An additional control mode, titled EL, will therefore be included. The EL control mode follows the same sun tracking behaviour as SC but now the maximum allowable shade height is limited to a seated eye-level height of 1.2 meters.

5.6.2 Define potential sensor alternatives (Step 1.2)

In this study, the focus lies on sensors and algorithms for detecting different ranges in incident solar energy. In literature, a wide variety of sensors are used for this purpose, ranging from outdoor or indoor irradiance and illuminance sensors, to glare sensors at the position of an occupant (Silva Da et al. 2012; Yun et al. 2017). In this study, three sensors are evaluated: an exterior global horizontal irradiance sensor (E-$I_{g;h}$), an exterior global vertical irradiance sensor (E-$I_{g;v}$), and an indoor vertical illuminance sensor (I-$E_{g;v}$). The placement of these sensors is illustrated in Figure 5.8. The sensors are set up in an open-loop configuration and are selected because they are non-intrusive to occupants and easily commissioned on-site.

The outdoor irradiance sensors are chosen as this type of sensor is commonly installed for integration in building management systems. The indoor illuminance sensor is positioned in between the glazing and roller blind. This alternative is chosen because it is generally cheaper than the outdoor pyranometers. Additionally, this sensor is expected to better approximate the perception of daylight by occupants as it measures radiation in the visual spectrum, is affected by glazing characteristics, and its vertical position aligns reasonably well with the viewing direction of multiple occupants. Using this selection of sensors, the importance of both the positioning of a sensor and the part of the solar spectrum it measures, will be tested.
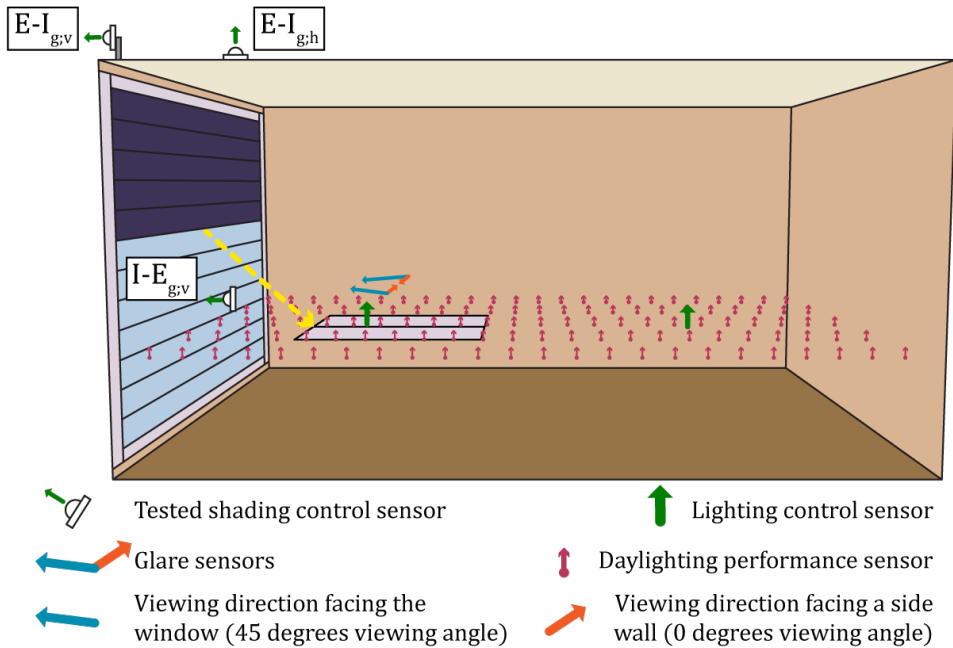
Figure 5.8 Overview of the reference office illustrating the placement of the investigated sensors and the set-up of the daylighting simulation model

5.6.3 Simulate and evaluate the performance of each control mode (Steps 3.1 and 3.2)

The performance of the initial control modes is now simulated. In these simulations the shading system follows one of the envisioned control modes continuously throughout the year. A case is simulated where the shades are always up (AU), one where the system follows the solar cut-off logic (SC), one where the shade is always down (AD) and one where the solar cut-off logic shade height is limited to the seated eye-level (EL).

Figure 5.9 shows the performance of each of the cases in relation to the baseline. Here, the performance indicators are reformulated such that the most desirable situation is reached if all performance indicators are as low as possible. View and glare performance are shown as the share of occupied hours that their required criterion was not met. Daylighting performance is presented as the complementary percentage to $sDA_{300/50}$: the floor area that does not receive at least 300 lux for 50% of occupied time.

The graph shows that each of the control modes successfully addresses a single performance aspect but performs badly on the other aspects. As expected, the AU case offers the best $sDA_{300/50}$ and $V_{1.2m;exc}$ but performs less well than the BL in terms of $DGPs_{0.4;exc}$ and E_{prim}. The SC case offers a more beneficial trade-off between the different performance aspects. Compared to the BL strategy, it offers superior $sDA_{300/50}$ and a slight improvement in E_{prim} which can be attributed to reductions in lighting energy consumption. The SC logic performs similar to the BL strategy in terms of the other indicators, and does not satisfy the defined requirement of 0% $DGPs_{0.4;0deg;exc}$. The EL logic does fulfil the 0% $DGPs_{0.4;0deg;exc}$ requirement and greatly reduces $DGPs_{0.4;45deg;exc}$. With regards to daylighting and energy performance, the EL strategy performans similar to the BL. The AD case fully eliminates disturbing glare in both viewing directions but performs very badly in all other performance indicators.

These results suggest that combining the AU, SC, and EL control logics into a multi-mode control strategy could provide a strategy that performs significantly better than the baseline. In this multi-mode control strategy, the SC control mode would be activated under conditions where the AU mode leads to glare or an unacceptable amount of cooling energy consumption. Likewise, the EL strategy would be activated when excessive admission of solar energy in the SC mode would cause undesired performance. The AD case does not appear to offer any additional beneficial performance trade-offs in relation to the other cases and it will therefore not be considered as a potential control mode for the multi-mode strategy.
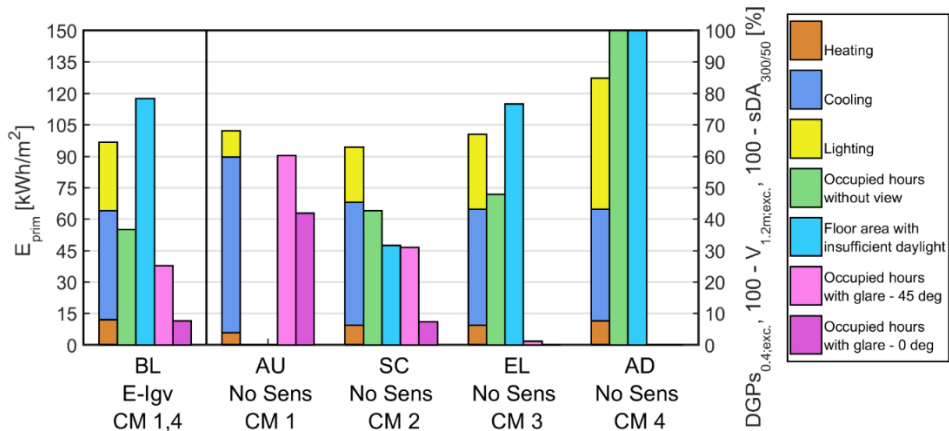
Figure 5.9 Summary of whole building performance for each control mode and the baseline strategy. BL: Baseline, AU: Always up, SC: Solar cut-off, EL: Solar cut-off with maximum height at eye level, AD: Always down. The control mode (CM) are numbered and ordered in terms of the amount of solar energy that they admit

The development of more refined control actions can be supported by analysing the instantaneous time step performance of the initially simulated cases (step 3.2). In this research, for instance, the EL strategy was added after analysing the contour plots in Figure 5.10. These plots show the time step performance of the SC strategy and indicate that the EL strategy leads to excessive cooling energy consumption and glare when the shade is positioned very high at mid-day in summer.

The three most promising cases (AU, SC, EL) have now been identified. In Figure 5.9 these cases are ordered and numbered in terms of the amount of solar energy that they admit. As control modes in a multi-mode strategy, they will be respectively referred to as CM_{1AU}, CM_{2SC} and CM_{3EL}.

The analyses of the different cases in step 3 can also be used to verify the proper functioning of the VTB configuration. The results in Figure 5.9 show that as less solar energy is admitted (e.g., from CM_{1AU} to CM_{3EL}), $sDA_{300/50}$, lighting and cooling energy consumption decrease whilst heating energy consumption and $DGPs_{0.4;exc}$ rise. Additionally, analysing time step (Figure 5.10 with results for the SC case) or monthly (Appendix A, Figure A.1) aggregated simulation outputs can assist the modeller in verifying the simulation model.
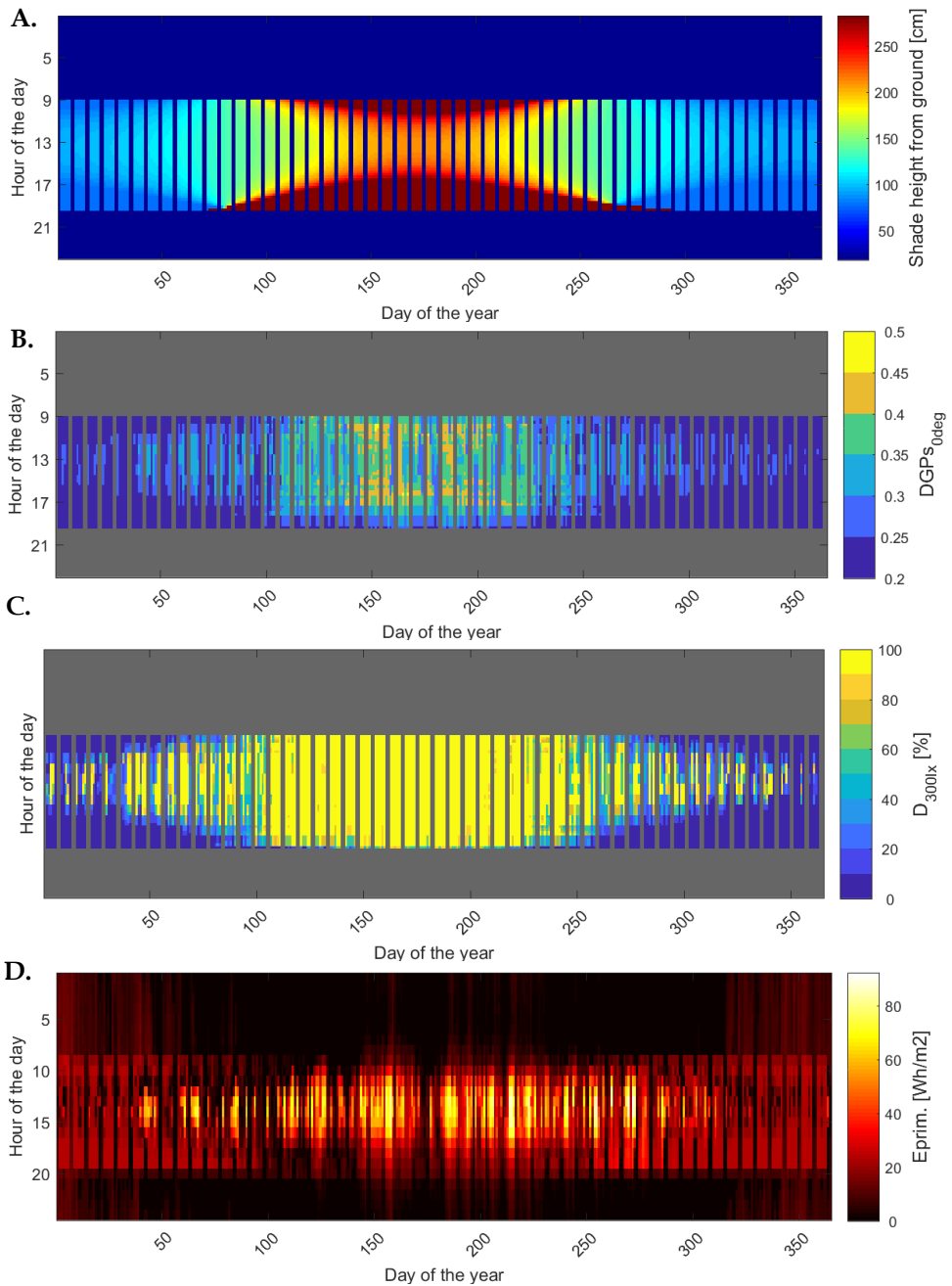
Figure 5.10 Behaviour and performance of the SC case.
A: shade height, B: Maximum DGPs for both occupants in the 0-degree viewing direction,
C: Floor area receiving at least 300 lux, D: Primary energy consumption for heating
cooling and lighting.

5.6.4 Optimise sensor strategy through mapping of performance effects to sensor measurements and statistical classification of detection algorithms (Step 4)

The goal of this step is to develop a sensor strategy that identifies the most ideal conditions to activate each control mode. In this study, two detection algorithms were defined: one for activating CM_{2SC} and one for activating CM_{3EL}. The CM_{2SC} detection algorithm determines when the system will switch between the CM_{1AU} and the CM_{2SC} control modes and the CM_{3EL} detection algorithm determines when the system switches between $CM_{2;SC}$ and $CM_{3;EL}$.

5.6.4.1 *The confusion matrix approach: a detection algorithm for switching between the CM_{1AU} and the CM_{2SC} control modes*

To develop the CM_{2SC} detection algorithm, instantaneous performance results from the AU and SC cases are related to the simulated sensor measurements and the effectivity of potential detections algorithms, and sensors, is evaluated using confusion matrices. A confusion matrix is a table that is used in statistical classification to evaluate the performance of a, usually imperfect, classification algorithm in separating various groups in a dataset (Fawcett 2006). All datapoints allocated to various cells in the table according to their classification by to classifier that is to be tested in one dimension, and their true classification in the other. By counting the datapoint in each cell various metrics can be computed that give insight into how the classification algorithm performs in various aspects.

Figure 5.11 illustrates how the confusion matrix approach works using the CM_{2SC} detection algorithm and the $I\text{-}E_{g;v}$ sensor as an example. Simulated glare performance ($DGPs_{0.4;0deg}$ and $DGPs_{0.4;45deg}$) from the AU case is plotted in relation to the $I\text{-}E_{g;v}$ sensor measurements. Figure 5.12 and Figure 5.13 show the same simulation results ($DGPs_{0.4;45deg}$ in relation to $I\text{-}E_{g;v}$) but underline the generic features of the approach and clarify the steps involved in making the confusion matrix. Earlier, $DGPs >= 0.4$ was defined as a criterion for undesired glare performance. Here, a conservative approach will be taken by focussing on preventing glare in the 45-degree viewing direction (coloured circles in Figure 5.11).
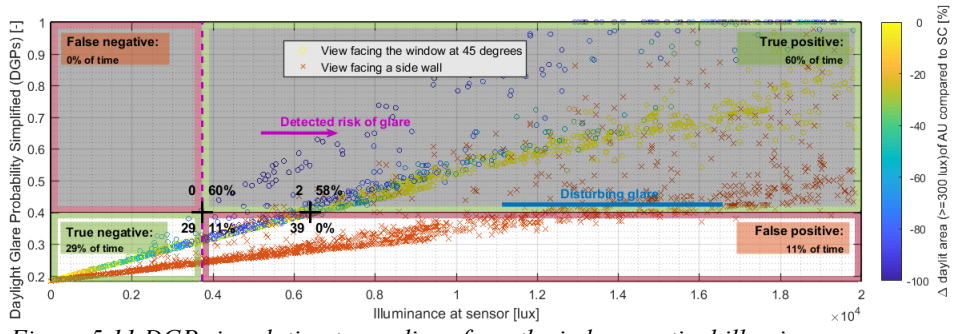
Figure 5.11 DGPs in relation to readings from the indoor vertical illuminance sensor. Simulated results for the AU case. $\Delta D_{t;300lx;2SC;1AU}$ is displayed using the colour of the circles for the 45-degree viewing angle
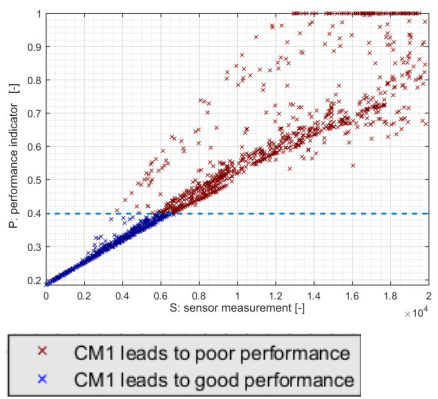
Figure 5.12 Actual performance classification of instantaneous performance of CM1 based on a performance criterion
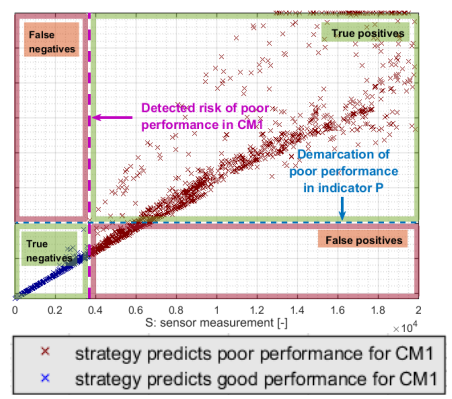
Figure 5.13 Performance classification by a simple detection algorithm (if: S > 3700 then: positive) and evaluation of its effectivity using a confusion matrix

Using the performance criterion, each instance is tested for the condition $DGPs_{45deg} >= 0.4$ classifying them into 'positives' (P) or 'negatives' (N), where positive stand for the occurrence of glare. This classification is called the true performance classification (PC_{true}). In the images it is represented by a horizontal line (Figure 5.12). The goal of the sensor strategy is to predict this performance classification using a detection algorithm and sensor measurements S creating a $PC_{detected}$ that separates all instances into predicted P and N classes. An ideal sensor strategy (Figure 5.12) would be one that always classifies performance conditions correctly ($PC_{true} = PC_{detected}$). Actual sensor strategies are generally less effective and will classify some instances incorrectly. The effectivity of a sensor strategy can be evaluated by relating the detected classification to the true classification and binning

all instances in one of the four cells of a confusion matrix. Figure 5.11 and Figure 5.13 illustrate this graphically. Here, a potential detection algorithm that uses a single sensor threshold of 3700 lux is used, and $PC_{detected}$ can be represented by a vertical line. The threshold is chosen because it always prevents disturbing glare, as will be clarified later. The two lines now graphically define a confusion matrix where all instances are contained within one of four quadrants:

- The true positives (TP): the sensor algorithm correctly detected glare in CM_{1AU}. CM_{2SC} is activated to prevent glare.
- The true negatives (TN): the sensor algorithm correctly detected no glare in CM_{1AU}. CM_{1AU} is activated to maximise the admission of daylight and views.
- The false positives (FP): the sensor algorithm wrongly detected glare in CM_{1AU}. CM_{2SC} is activated and the shade is lowered further than what would be necessary to prevent glare.
- The false negatives (FN): the sensor algorithm wrongly detected no glare in CM_{1AU}. CM_{1AU} is activated and this causes occupants to be exposed to glare.

5.6.4.2 *Evaluating the effectivity of the CM_{2SC} detection algorithm in detecting glare*

The effectivity of different sensor strategies can be quantified by looking at the share of occupied hours that are contained in each confusion matrix region. The share of all positives that were detected by the sensor strategy, or true positive rate (TPR), gives an idea of how well the strategy detects conditions where the occupants perceive glare. Here, a TPR of a 100% means that all instances with disturbing glare were detected. The 'accuracy' (ACC) quantifies the frequency of the system making correct performance classifications and is defined as the ratio between the number of instances contained in the 'true' regions to the number of total instances. In this example, a greater ACC indicates better performance trade-offs between daylighting performance and visual comfort. The 3700-lux sensor threshold that is evaluated in the confusion matrix in Figure 5.11 is defined such that false negatives, where activating $CM_{1;AU}$ would cause glare in the 45-deg viewing direction, never occur. This threshold can be found by selecting all datapoints in where glare actually occurs (TP+FN) and selecting the minimal sensor value that is associated to this datapoint. The accuracy of this strategy is not ideal (89%) due to a substantial number of false positives (11%) that lead to an unnecessary decline in daylighting and view performance.

ACC and TPR only quantify the frequency of false control decisions but not the severity of the effects on other performance aspects. The impact of false control decisions can be large or small, however, depending on environmental conditions. More detailed insight into performance trade-offs can be obtained by looking at the

84

effects of false control decisions on daylighting performance. To quantify these effects, the instantaneous difference in $D_{t;300lx}$ between the SC and AU cases is computed for each time step (Equation 5.2). This performance difference ($\Delta D_{t;300lx;2SC;1AU}$) is visualized in Figure 5.11 using the gradient colour scale of the 45-degree viewing angle. The dark blue colour of the instances contained in the false positive (FP) region indicates that these instances will have a particularly strong negative effect on daylighting performance.

$$\Delta D_{t;300lx;2SC;1AU} = D_{t;300lx;SC} - D_{t;300lx;AU} \tag{5.2}$$

$D_{t;300lx;SC}$: *floor area (%) receiving more than 300 lux, at time step t, for the SC case*
$D_{t;300lx;AU}$: *floor area (%) receiving more than 300 lux, at time step t, for the AU case*
$D_{t;300lx;2SC;1AU}$: *change in instantaneous daylighting performance when switching from*
$CM_{1;AU}$ to $CM_{2;SC}$

Table 5.5 summarizes the effectivity scores (TPR:100% and ACC:98%) associated to the 3700-lux threshold along with the resulting overall daylighting performance (sDA_{actual}: 74%) if this detection algorithm would be implemented in a two-mode strategy ($CM_{1;AU}$ + $CM_{2;SC}$). In addition, the table shows the ideal daylighting performance that could be achieved (sDA_{ideal}: 100%) with a two-mode strategy if the detection algorithm would make no false classifications ($PC_{detected}$ =PC_{true}). Together, the collection of indicators quantify how well the detection algorithm can isolate instances with undesired performance, what the effects are of wrong control decisions, and what could be gained by improving the algorithm further. By comparing sDA_{actual} to sDA_{ideal} it becomes clear that, although sDA_{actual} is significantly better than that of the BL (sDA:22%), there is still a lot of room for further improvement.

Figure 5.11 suggests that a better trade-off between glare and daylighting performance can be obtained by moving the threshold closer to the point where the linear regression line of the scatter plot intersects the 0.4 DGPs disturbing glare line. This approach is illustrated with the second cross. Here, the choice is made to accept that 3% of all $DGPs_{0.4;45deg}$ exceedance goes undetected (TPR: 97% and 2% FN) by using a control threshold of 6400 lux. The graph shows that this reduces the occurrence of FP to 0%. Table 5.5 summarises the positive effects of changing the detection threshold, where sDA_{actual} increases to 100%, matching sDA_{ideal}. Note that, although $DGPs_{0.4;45deg}$ increases, the more critical $DGPs_{0.4;0deg}$ indicator remains almost unchanged. This means that the disturbing visual discomfort that is introduced by this new threshold, could be mitigated by a change in the viewing direction of the occupant. In this case study, this is considered an acceptable trade-off for improving daylighting performance.

Table 5.5 Summary of the effectivity of tested sensors, thresholds and detection algorithms for switching between the CM_{1AU} and CM_{2SC} control modes

Sensor:		Exterior horizontal irradiance		Exterior vertical irradiance		Interior vertical illuminance	
Threshold based on:		**30 W/m²**		**50 W/m²**		**3700 lux**	
DGPs₄₅ deg >= 0.4	Glare:	TPR: 100%	ACC: 78%	TPR: 100%	ACC: 91%	TPR: 100%	ACC: 89%
		DGPs 0.4;45deg 31%	DGPs 0.4;0deg 7%	DGPs 0.4;45deg 31%	DGPs 0.4;0deg 7%	DGPs 0.4;45deg 31%	DGPs 0.4;0deg 7%
	sDA:	Actual: 69%	Ideal: 100%	Actual: 78%	Ideal: 100%	Actual: 74%	Ideal: 100%
		Negative	Positive	Negative	Positive	Negative	Positive
	E_{prim}: kWh/m²	∑TN: 1.1	∑FP: 10.6	∑TN: 4.7	∑FP: 7.0	∑TN: 4.5	∑FP: 7.2
		∑FN: -0.5	∑TP: -8.7	∑FN: -0.9	∑TP: -8.3	∑FN: -0.7	∑TP: -8.4
		totN: 0.7	totP: 1.9	totN: 3.8	totP: -1.3	totN: 3.8	totP: -1.3
	Saved:	Actual: 0.7	Ideal: 11.7	Actual: 3.8	Ideal: 11.7	Actual: 3.8	Ideal: 11.7
Threshold based on:		**80 W/m²**		**80 W/m²**		**6400 lux**	
DGPs₄₅deg[2°] >= 0.4	Glare:	TPR: 97%	ACC: 87%	TPR: 97%	ACC: 97%	TPR: 97%	ACC: 98%
		DGPs 0.4;45deg 33%	DGPs 0.4;0deg 8%	DGPs 0.4;45deg 33%	DGPs 0.4;0deg 7%	DGPs 0.4;45deg 33%	DGPs 0.4;0deg 8%
	sDA:	Actual: 83%	Ideal: 100%	Actual: 99%	Ideal: 100%	Actual: 100%	Ideal: 100%
		Negative	Positive	Negative	Positive	Negative	Positive
	E_{prim}: kWh/m²	∑TN: 5.5	∑FP: 6.2	∑TN: 7.2	∑FP: 4.5	∑TN: 7.9	∑FP: 3.8
		∑FN: -0.7	∑TP: -8.5	∑FN: -1.2	∑TP: -8.0	∑FN: -1.1	∑TP: -8.1
		totN: 4.8	totP: -2.3	totN: 6.0	totP: -3.5	totN: 6.8	totP: -4.3
	Saved:	Actual: 4.8	Ideal: 11.7	Actual: 6.0	Ideal: 11.7	Actual: 6.8	Ideal: 11.7

5.6.4.3 *Evaluating the effectivity of the CM$_{2SC}$ detection algorithm in identifying beneficial energy performance*

The confusion matrix approach can also be used to assess how well the detection algorithm identifies instances where switching from the CM$_{1AU}$ to CM$_{2SC}$, would improve energy performance. This process is visualised in Figure 5.14. In this case, control decisions are evaluated as if the only goal of the control is to minimize energy consumption. The effects of switching between the two control modes is quantified using the difference in instantaneous primary energy consumption for heating, cooling and lighting ($\Delta E_{t;prim}$) between the AU and SC cases. This $\Delta E_{t;prim}$ is computed using the equation:

$$\Delta E_{t;\text{prim}.;2SC;1AU} = E_{t;\text{prim}.;AU} - E_{t;\text{prim}.;SC} \qquad (5.3)$$

$E_{t;prim;SC}$: *instantaneous primary energy consumption for heating, cooling and lighting, at time step t, for strategy SC*

$E_{t;prim;AU}$: *instantaneous primary energy consumption for heating, cooling and lighting, at time step t, for strategy AU*

Instances where activating CM$_{2SC}$ saves energy are now labelled as 'positives' and the PC$_{true}$ is based on the performance criterion $\Delta E_{t;prim}$<0. This criterion is represented in the graph by the horizontal line at $\Delta E_{t;prim}$=0. The graph is used to evaluate the effectivity of the previously defined 6400-lux threshold from an energy perspective. This detection algorithm is again represented by a vertical line that defines PCdetected and the two lines delineate the regions of the confusion matrix. The colour scale is used to visualise $\Delta D_{t;300lx;2SC;1AU}$ and highlights the relationship between energy and daylighting performance. To obtain a quantification of the total effects of the wrong and correct control decisions, the $\Delta E_{t;prim}$ of all instances contained within each of the four regions of the confusion matrix are summed. The four regions, denoted with the subscript e, can be interpreted as follows:

- The true positives (TP$_e$): the sensor algorithm activates CM$_{2SC}$. This reduces E$_{t;prim}$ compared to activating CM$_{1AU}$. A negative value for $\sum$TP$_e$ quantifies this reduction.
- The true negatives (TN$_e$): the sensor algorithm activates CM$_{1AU}$. This reduces E$_{t;prim}$ compared to activating CM$_{2SC}$. A positive value for $\sum$TN$_e$ quantifies this reduction.
- The false positives (FP$_e$): the sensor algorithm activates CM$_{2SC}$. This increases E$_{t;prim}$ compared to activating CM$_{1AU}$. A positive value for $\sum$FP$_e$ quantifies this increase.
- The false negatives (FN$_e$): the sensor algorithm activates CM$_{1AU}$. This increases E$_{t;prim}$ compared to activating CM$_{2SC}$. A negative value for $\sum$FN$_e$ quantifies this increase.
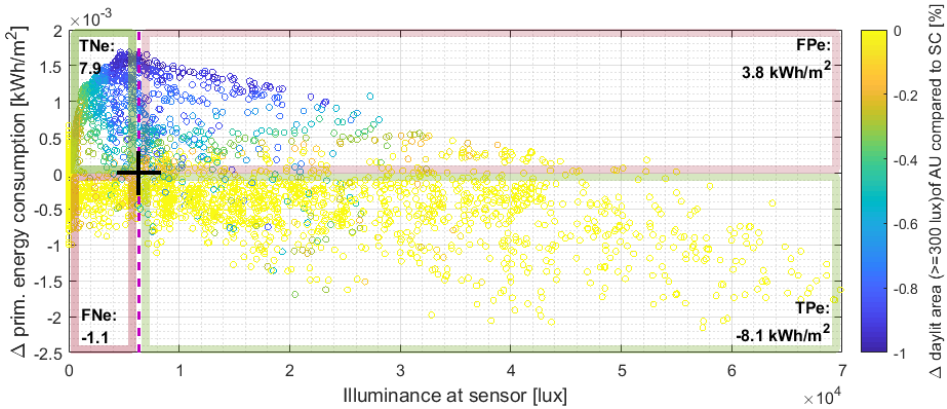
Figure 5.14 Evaluation of the effectivity of the illuminance sensor strategy in addressing energy performance. Vertical axis: difference in instantaneous primary energy consumption of AU and SC strategies. Colour: difference in instantaneous daylighting performance of AU and SC strategies.

The sums of two of the four matrix cells can be used to assess the effects that potential detection algorithms would have in a two-mode strategy ($CM_{1;AU} + CM_{2;SC}$) compared to the initial AU or SC cases. By summing all the detected 'negatives' ($totN_e$) the effects can be compared in relation to the SC case and by summing all the detected 'positives' ($totP_e$) the effects can be compared in relation to the AU case. The 6400-lux threshold $CM_{1;AU;2;SC}$ solution has a $E_{t;prim}$ that is 6.8 kWh/m² ($totN_e = TN_e + FN_e$) lower than that of the SC case. This net effect is a consequence of the instances where raising the shade saved energy (TNe: 7.9 kWh/m²) and the instances where doing so would lead to more energy consumption (FNe: -1.1 kWh/m²). For the initial 3700-lux threshold, the reduction in $E_{t;prim}$ compared to SC is only 3.8 kWh/m² (Table 5.5). This shows that the 6400-lux threshold is also more beneficial in terms of energy performance.

5.6.4.4 *Benchmarking the CM_{2SC} detection algorithm against the ideal case*

The four regions also allow the performance of a detection algorithm to be benchmarked against an ideal sensor strategy that always activates the CM with the lowest $E_{t;prim}$ ($PC_{detected} = PC_{true}$). With an ideal strategy $E_{t;prim}$ would be 11.7 kWh/m² ($TN_e + FP_e$) lower than that of the SC case. This means that 58% of the $E_{t;prim}$ reduction that could potentially be achieved by optimising the detection algorithm has been realised with the 6400-lux algorithm. To facilitate these comparisons, the totNe score that is obtained by each sensor strategy is summarized under the header 'actual' next to the 'ideal' score.

Combining Figure 5.11, Figure 5.14 and Table 5.5, some observations can be made. Figure 5.14 suggests that raising the shade fully saves energy in almost all instances where doing so would improve indoor daylighting conditions. In almost all instances where raising the shade would not cause such an improvement, the increase in solar heat gains would lead to an increase in total primary energy consumption. In this case, there appears to be little conflict between the goal of improving daylighting performance and the goal of improving energy performance.

The indicators in Table 5.5 show that compared to the original, 3700-lux threshold, the 6400-lux threshold offers more beneficial performance trade-offs between visual comfort and the other performance aspects. With this approach, both daylighting and energy performance come quite close to the ideal performance that is achievable using the selected control actuations. This suggests that there is little need for testing more complex detection algorithms.

To be able to compare the effectivity of different sensors, control thresholds were determined for each type of sensor using both the 0% and the 2% $DGPs_{0.4;45deg}$ exceedance approaches. In Table 5.5, these thresholds are summarised along with the corresponding effectivity of each sensor strategy. The variation in daylighting and energy performance amongst the sensors show that they vary in the effectivity with which they can classify instances with glare. It is concluded that the $E-I_{g;h}$ sensor is less effective in classifying glare than the other sensors. Meeting the visual comfort requirement with this sensor leads to a 2 kWh/m^2 higher E_{prim} and a 17% lower $sDA_{300lx;50\%}$ than with the other sensors. Although the differences between the $E-I_v$ and the $I-E_{g;v}$ are less pronounced, the $I-E_{g;v}$ sensor does perform better in terms of both daylighting (1%) and energy consumption (0.8 kWh/m^2).

5.6.4.5 *A detection algorithm for switching between the CM$_{2SC}$ and the CM$_{3EL}$ control modes*

In determining the detection algorithm for switching between CM$_{2;SC}$ and CM$_{3;EL}$, the goal of prohibiting discomfort glare is again given priority. Measurements from the three sensors are used to detect when CM$_{2;SC}$ leads to glare and decide that CM$_{3;EL}$ should be activated. Figure 5.15 and Figure 5.16 show simulated glare performance in relation to sensor measurements from the SC case. Two sensor types are shown to illustrate the differences in the effectivity with which the sensors classify visual discomfort. Figure 5.15 shows results for the I-E$_{g;v}$ sensor and Figure 5.16 shows results for the E-I$_{g;h}$ sensor. The colour scale is again used to plot instantaneous effects on daylighting performance ($\Delta D_{t;300lx;3EL;2SC}$) of switching between the two control modes, computed using the equation:

$$\Delta D_{t;300lx;3EL;2SC} = D_{t;300lx;EL} - D_{t;300lx;SC} \qquad (5.4)$$

$D_{t;300lx;EL}$: percentage of floor area that receives more than 300 lux, at time step t, for the EL case; $D_{t;300lx;SC}$: percentage of floor area that receives more than 300 lux, at time step t, for the SC case; $D_{t;300lx;3EL;2SC}$: change in instantaneous daylighting performance when switching from CM2;SC to CM3;EL

The top graphs (A and C) show a detection algorithm where the control threshold is chosen such that disturbing glare is always prevented for the view facing the wall (0% FN). The relationship between glare probability and sensor measurements is less linear than in the previous example. As a result, there are many instances (35%) contained within the FP region. These instances have a strong negative effect on daylighting performance as can be seen from their negative $\Delta D_{t;300lx;3EL;2SC}$ values and the performance that is achieved compared to the ideal (Table 5.6).

The occurrence of glare in the SC case can be attributed to a large fraction of the window being exposed at high solar altitude giving occupants a large view of the sky. This situation can lead to glare at instances with high luminance sky conditions. A detection algorithm based on both illuminance and the amount of window area that is visible to the occupant therefore seems like a promising direction for further improvement. The bottom C and D graphs illustrate this approach. Here the illuminance, or irradiance, measured by the sensors is multiplied by the unshaded height of the window. The relationship between DGPs and these manipulated sensor measurements are more linear than in the cases using the unmanipulated sensor measurements. Consequently, the performance trade-offs that can be achieved are more beneficial as can be seen by the improvement in the effectivity indices shown in Table 5.6.
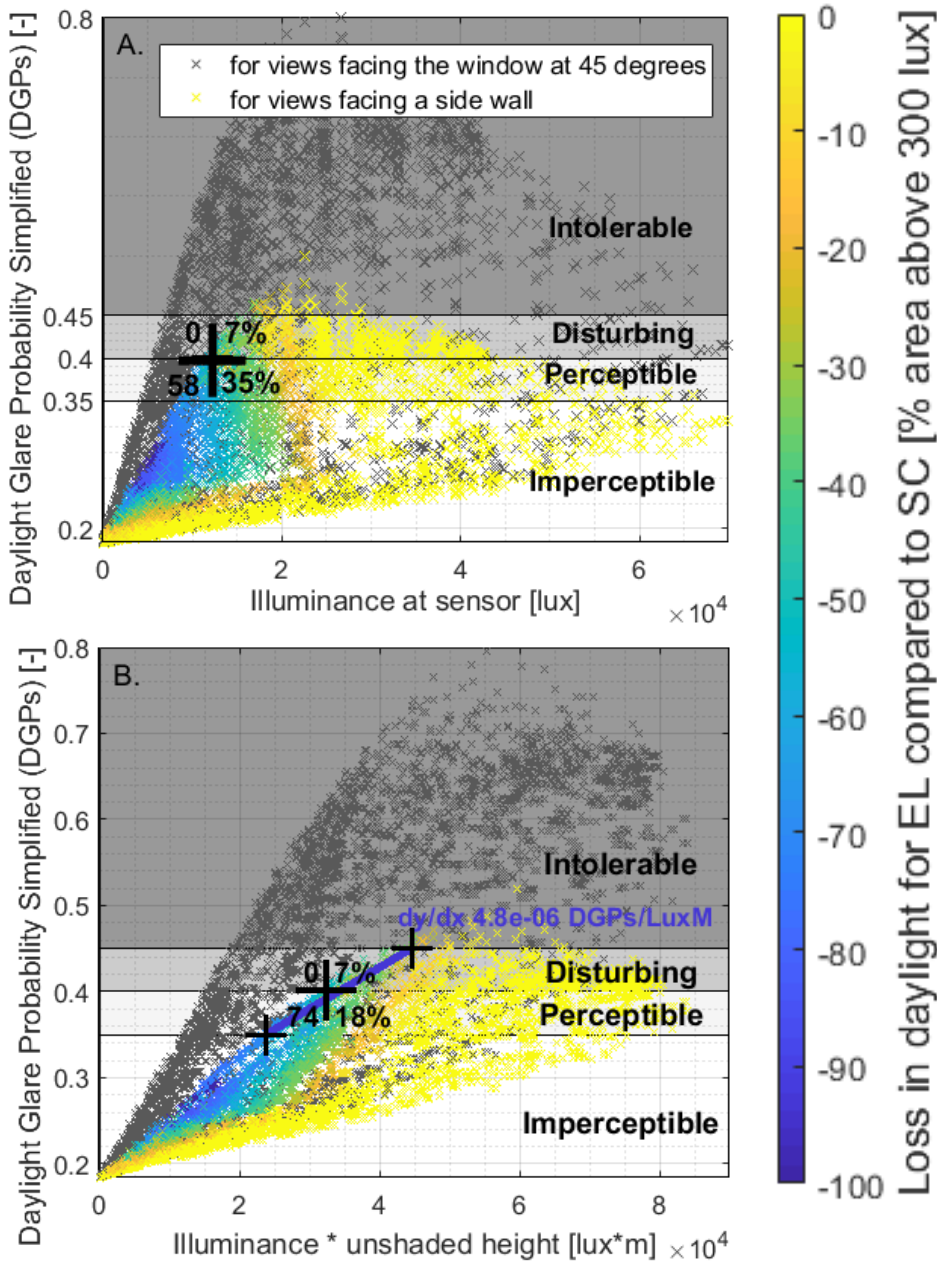
Figure 5.15 Simulated DGPs from the SC case in relation to:
A. Indoor vertical illuminance, B. Indoor vertical illuminance multiplied by the unshaded window height
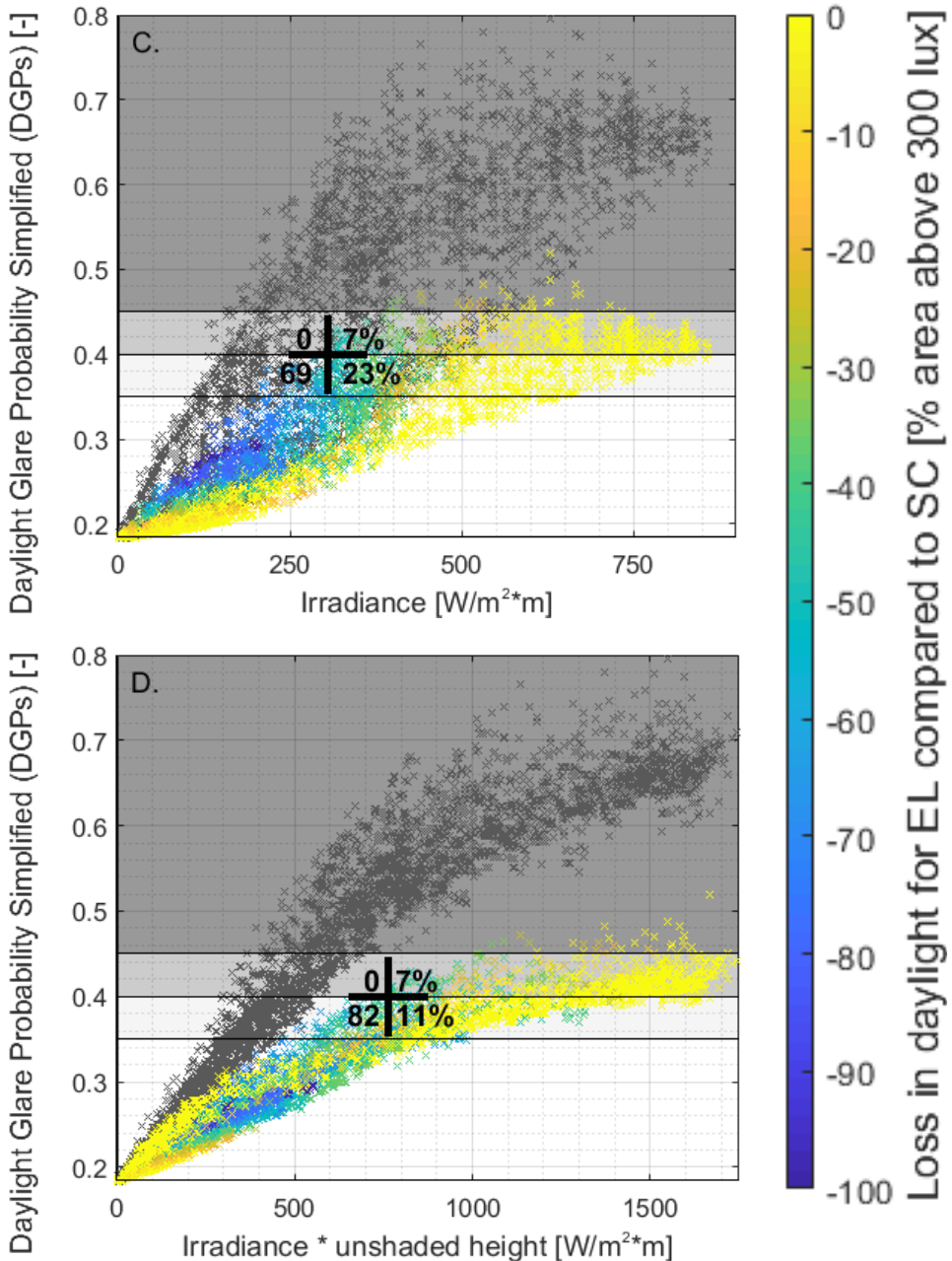
Figure 5.16 Simulated DGPs from the SC case in relation to:
C. Exterior horizontal irradiance, D. Exterior horizontal irradiance multiplied by the
unshaded window height. Colour represents the loss in daylit area
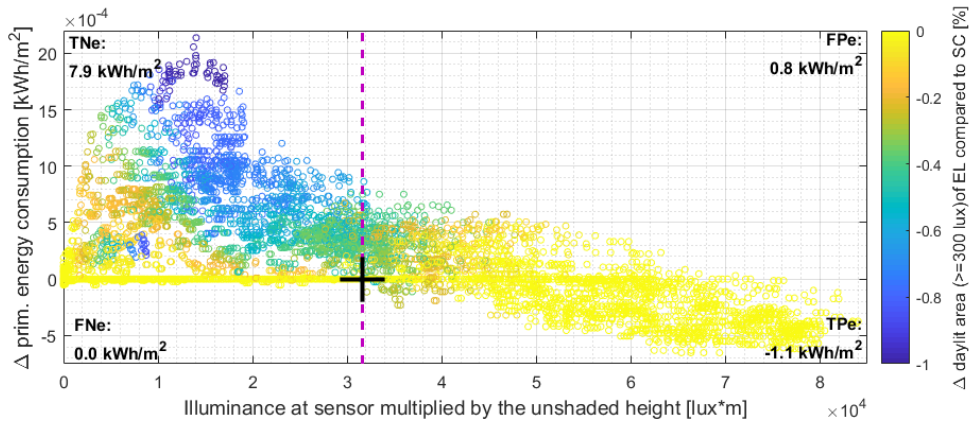
Figure 5.17 Evaluation of the effectivity of sensor strategy in addressing energy performance. Vertical axis: difference in instantaneous primary energy consumption of SC and EL strategies. Colour: difference in instantaneous daylighting performance of SC and EL strategies

For assessing the effects of the different detection algorithms on energy performance, the following equation is used:

$$\Delta E_{t;\text{prim.};3EL;2SC} = E_{t;\text{prim.};SC} - E_{t;\text{prim.};EL} \qquad (5.5)$$

$E_{t;prim;EL}$: *instantaneous primary energy consumption for heating, cooling and lighting, at time step t, for strategy EL.* $E_{t;prim;SC}$: *instantaneous primary energy consumption for heating, cooling and lighting, at time step t, for strategy SC*

Figure 5.17 visualises the results for the detection algorithm where the I-$E_{g;v}$ sensor is used, and measurements are multiplied by the unshaded height. The net effects of each alternative, shown in Table 5.6, are again expressed relative to the SC case and are obtained by summing the instances contained in the TPe (switching to CM$_{3;EL}$ saved energy) and FPe (switching to CM$_{3;EL}$ used more energy) regions. This totP$_e$ score is again summarized next to the cell labelled 'actual'.

The energy and daylighting scores of the different sensors in Table 5.6, show that the I-$E_{g;v}$ sensor identifies visual discomfort most effectively. The differences between the sensors are less pronounced here than in the previous case with CM$_{1;AU}$ and CM$_{2;SC}$. By comparing the scores of the two approaches for switching between CM$_{2;SC}$ and CM$_{3;EL}$ it becomes clear that the most beneficial performance trade-offs can be achieved when sensor measurements are multiplied by the unshaded height of the window. Although there is some room for additional improvement, the achieved daylighting performance is reasonably close to the ideal. The graphs suggest that further improvements could be found by reducing the amount, or the

93

negative effects, of the FPs shown in Figure 5.15. The amount of FPs can be reduced by improving the detection approach. Reducing the negative effects can be done by adjusting control response.

Table 5.6 Summary of the effectivity of tested sensors, thresholds and detection algorithms for switching between the $CM_{2;SC}$ and $CM_{3;EL}$ control modes

Top section

Threshold based on:	Exterior horizontal irradiance sensor — 310 W/m²		Exterior vertical irradiance sensor — 150 W/m²		Interior vertical illuminance sensor — 12000 lux	
Glare:	TPR: 100%	ACC: 77%	TPR: 100%	ACC: 64%	TPR: 100%	ACC: 64%
DGPs0 deg >= 0.40	DGPs 0.4:45deg 7%	DGPs 0.4:0deg 0%	DGPs 0.4:45deg 7%	DGPs 0.4:0deg 0%	DGPs 0.4:45deg 7%	DGPs 0.4:0deg 0%
sDA:	Actual: 57%	Ideal: 69%	Actual: 55%	Ideal: 69%	Actual: 53%	Ideal: 69%
	Negative	Positive	Negative	Positive	Negative	Positive
E_{prim} kWh/m²	TN_e: 7.2	FP_e: 1.6	TN_e: 7.1	FP_e: 1.7	TN_e: 7.0	FP_e: 1.7
	FN_e: 0.0	TP_e: -1.1	FN_e: 0.0	TP_e: -1.1	FN_e: 0.0	TP_e: -1.1
	$totN_e$: 7.2	$totP_e$: -1.1	$totN_e$: 7.1	$totP_e$: 0.6	$totN_e$: 7.0	$totP_e$: 0.6
Saved:	Actual: -1.1	Ideal: 1.1	Actual: -0.6	Ideal: 1.1	Actual: -0.6	Ideal: 1.1

Bottom section

Threshold based on:	Exterior horizontal irradiance sensor — 760 (W/m²)·m		Exterior vertical irradiance sensor — 380 (W/m²)·m		Interior vertical illuminance sensor — 31600 lux·m	
Glare:	TPR: 100%	ACC: 89%	TPR: 100%	ACC: 79%	TPR: 100%	ACC: 80%
DGPs0 deg >= 0.40 and sensor value * unshaded height	DGPs 0.4:45deg 14%	DGPs 0.4:0deg 0%	DGPs 0.4:45deg 11%	DGPs 0.4:0deg 0%	DGPs 0.4:45deg 11%	DGPs 0.4:0deg 0%
sDA:	Actual: 61%	Ideal: 69%	Actual: 62%	Ideal: 69%	Actual: 63%	Ideal: 69%
	Negative	Positive	Negative	Positive	Negative	Positive
E_{prim} kWh/m²	TN_e: 7.9	FP_e: 0.9	TN_e: 7.9	FP_e: 0.9	TN_e: 7.9	FP_e: 0.8
	FN_e: -0.1	TP_e: -1.0	FN_e: 0.0	TP_e: -1.1	FN_e: 0.0	TP_e: -1.1
	$totN_e$: 7.8	$totP_e$: -0.1	$totN_e$: 7.9	$totP_e$: -0.2	$totN_e$: 7.9	$totP_e$: -0.3
Saved:	Actual: 0.1	Ideal: 1.1	Actual: 0.2	Ideal: 1.1	Actual: 0.3	Ideal: 1.1

5.6.5 Simulate the performance of the developed multi-mode control strategies (Step 5)

A multi-mode control strategy with optimised detection algorithms has now been developed. The previous steps have focussed on evaluating and improving the performance of the individual detection and actuation algorithms. In this step, the performance of the complete multi-mode control strategy is assessed and compared to the baseline strategy. To evaluate if the confusion matrix method ranks the different sensors correctly, all sensors are included in this comparison. Only the best performing detection algorithms from the previous section are now evaluated. CM_{2SC} is activated using the 2% allowed $DGPs_{0.4;45deg}$ exceedance sensor threshold and the algorithm where the sensor measurements are multiplied by the unshaded height is used to activate CM_{3EL}.

Figure 5.18 presents a summary of whole building performance for the developed control strategies and the three sensor alternatives. The performance indicators are defined as in Figure 5.9 where the goal is to get each indicator as low as possible. To also evaluate the benefits of the individual control modes and detection algorithms, scenarios that include only two of the three proposed control modes are included for each sensor alternative.
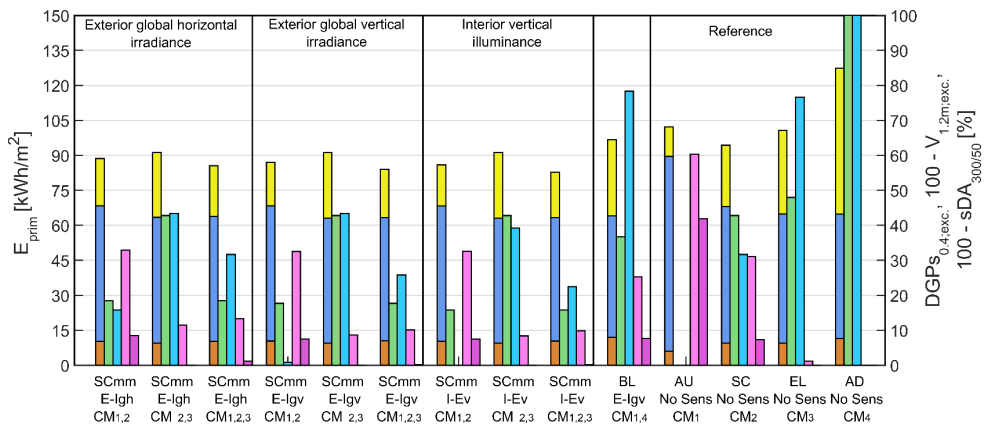
Figure 5.18 Summary of whole building performance predicted using simulations of the multi-mode SCmm strategy in combination with different sensors. Performance indices defined as in figure 5.9.

For all sensor types we see a similar pattern in performance improvements. Compared to the SC only strategy, fully raising the shade in the two-mode $CM_{1AU;2SC}$ strategies improves daylighting (by 16-32% $sDA_{300lx;50\%}$) and energy performance (by

6-11%) as well as the time with a view to the outdoors (by 24-27%) without causing a significant change in visual discomfort. The improvements in energy performance can be attributed to reductions in lighting energy consumption as well as to slight improvements in cooling energy consumption due to reduced lighting gains. The CM_{3EL} improves overall energy performance and reduces the time that the visual discomfort criterion is met to 0% (a 7% reduction) for the 0-degree viewing direction. These improvements do have a negative effect on daylighting performance (8-12% relative reduction in $sDA_{300lx;50\%}$). Compared to the SC only alternative, implementation of both the CM_{1AU} and CM_{3EL} control modes has a beneficial effect on all performance aspects. The only exception to this is the alternative using a horizontal irradiance sensor, where there is no improvement in daylighting performance.

Overall, substantial differences can be observed between the three sensors, where the indoor illuminance sensor stands out as the best performing alternative for all performance indicators. Compared to the worst performing alternative, the horizontal exterior irradiance sensor (E-Igh $CM_{1AU;2SC;3EL}$), the illuminance sensor (I-Ev $CM_{1AU;2SC;3EL}$) offers a 3% lower E_{prim}, a 9% higher $sDA_{300lx;50\%}$, 3% reduction in $DGPs_{0.4;45deg}$ exceedance and 3% more $V_{1.2m;exc}$. The large differences in daylighting performance between these two sensors can mainly be explained by the horizontal irradiance sensor's poor performance when it comes to detecting low-light conditions. This is not surprising as this threshold marks the lower boundary of conditions characterised as being partly cloudy or slightly overcast. Under such conditions, the contribution of the direct component will start becoming more significant in the overall sensor measurements and a vertically oriented sensor is better equipped to identify such instances.

Amongst the investigated alternatives I-Ev-$CM_{1AU;2SC;3EL}$ strategy offers the best trade-off in performance aspects. Compared to the conventional BL strategy it offers significant improvements for all indicators: 14% reduction in E_{prim}, a 56% higher $sDA_{300lx;50\%}$, 21% more $V_{1.2m;exc}$ and 15% reduction in $DGPs_{0.4;45deg}$ exceedance. Additionally, the I-Ev-$CM_{1AU;2SC;3EL}$ strategy can mitigate disturbing glare in the most critical viewing direction completely.

5.7 Application discussion and conclusion

In this study, the support method was used to select a sensor deployment strategy for the automated indoor roller blind system. The vertical indoor illuminance sensor was shown to offer substantial performance benefits (3% lower E_{prim}, 9% higher $sDA_{300lx;50\%}$, 3% lower in $DGPs_{0.4; exc.;45deg}$ and 3% more $V_{1.2m;exc}$) over the other sensor configurations. Additionally, the support method was used to develop a multi-mode

sun-tracking control strategy and the algorithms and control parameters for activating each control mode were optimised for the specific building application.

Using the results of the application study, this section will evaluate the efficiency and limitations of the support method. Additionally, this section discusses how the method can be used to customise controls for other building applications.

In the confusion matrix method, instantaneous performance results of two separate simulations are used to identify ideal circumstances for switching between adjacent control modes. This approach has the limitation that it only quantifies the immediate performance effects of control actions. In assessing energy performance effects, this does not accurately describe the transient effects of shade actuations, and the admission of solar energy, on energy performance. This causes an error in the estimated energy reductions that are used to assess the individual control improvements. To explore the extent to which this limitation influences the conclusions of the confusion matrix evaluations, the energy reductions that were estimated using this method (step 4) are compared to the results from the multi-mode simulations (step 5). If we compare the energy performance results shown in Figure 5.18 to the estimated energy performance improvements, obtained by summing instantaneous E_{prim} in the confusion matrix quadrants (Table 5.5 and Table 5.6), it can be seen that both evaluations lead to the same ranking of options for all sensors, detection algorithms and control mode alternatives. From this it can be concluded that the confusion matrix approach can reliably rank amongst alternatives and identify high performing solutions.

Although the relative hierarchy of the different options is predicted correctly, the predicted energy savings are less accurate. The summation of confusion matrix quadrants suggest that the $CM_{1;AU,2;SC}$ strategy would have a 6.8 kWh/m² lower E_{prim} than the SC only strategy (Table 5.5) whereas the results from step 9 show this reduction to be 8.5 kWh/m² (Figure 5.18). The $CM_{2;SC,3;EL}$ strategy is estimated to lead to a 0.3 kWh/m² reduction in E_{prim} relative to SC whereas Figure 5.18 shows that this difference should be 3.2 kWh/m². Overall, the conclusions drawn from the multi-mode simulation study are in line with those based on the confusion matrix method. There are some discrepancies in predicted energy savings in absolute terms, but it is not the goal of the method to give an exact prediction of potential energy savings. Rather, the goal is to be able to rank the relative merits of different options and identify high performing solutions. This comparison showed that the confusion matrix method can meet this goal in a reliable way.

The most promising alternative that was identified in the case study, the SC_{mm}-$CM_{1AU;\ 2SC;3EL}$ multi-mode strategy using an indoor illuminance sensor, offers a reduction of 14% in E_{prim}, 56% more $sDA_{300lx;50\%}$, and 8-15% reduction in $DGPs_{0.4}$

exceedance in relation to the conventional baseline solution (Figure 5.18). This shows that the support method can identify high performance control rules, detection algorithms, thresholds and sensors using only a limited number of simulations. In this study, many simulation results were presented to illustrate and test the proposed method. For identifying the best performing SC_{mm}-$CM_{1AU;\ 2SC;3EL}$ alternative and comparing it against a baseline, only five simulations would have to be executed in practice.

The presented correlations between sensor measurements and performance effects depend on building design characteristics, occupant positions and contextual factors such as climate. Ideally, the proposed method is used to optimise control thresholds for specific building applications. To illustrate this, the support method was applied for three different buildings, varying in terms of their fenestration design and window-to-wall ratios (WWR: 40%, 60% and 80%). This additional study, shown in Appendix A, is not discussed in detail but the main conclusions can be summarised as follows. The scatter plots in Figure A.4 and Figure A.5 show how the correlation between sensor measurements and glare and energy performance changes with the varying WWR. The graph shows that only the 40% WWR case leads to different conclusions regarding the control thresholds that are needed to satisfy required comfort conditions. In Figure A.6, the I-Ev-$CM_{1AU;2SC;3EL}$ strategy is evaluated within the 40% WWR building using both generic control thresholds, defined using the initial 80%WWR case, and control thresholds customised to the specific building application. These results show that, although the I-Ev-$CM_{1AU;2SC;3EL}$ strategy with generic control thresholds gives significant performance improvements over the BL strategy, additional improvements in daylighting (18% higher $sDA_{300lx;50\%}$) and energy performance (8% lower E_{prim}) can be obtained by customising control thresholds to the 40%WWR application. By making scatter plots for multiple representative building applications, like in Figure A.4, developers can obtain insight and intuition into how the mapping of sensor measurements and performance effects are influenced by different building characteristics and adjust control thresholds on the basis of this insight.

With the proposed method the control space is constrained to the behaviour described by the initially selected control modes and ideal performance therefore cannot be guaranteed. To test the extent to which this constraint limits the performance potential of the resulting strategies Figure 5.19 shows a performance comparison between the best performing $SC_{mm\text{-}IEv\text{-}CM1AU;2SC;3EL}$ strategy and a performance-based control (PBC) strategy that is not constrained to a limited set of control modes. The PBC strategy selects the most open shading position at each control interval that does not lead to disturbing glare for both viewing directions ($DGPs_{45deg} \leq 0.4$ and $DGPs_{45deg} \leq 0.4$). The graph shows that the constrained strategy, that is developed using the support method, approximates the performance of the

PBC strategy quite closely. Further analyses of the behaviour of the two strategies additionally showed that the PBC often employs sun-tracking similar to the RBC and that this behaviour follows from seeking to maximise the admission of daylight whilst meeting the visual comfort constraints.
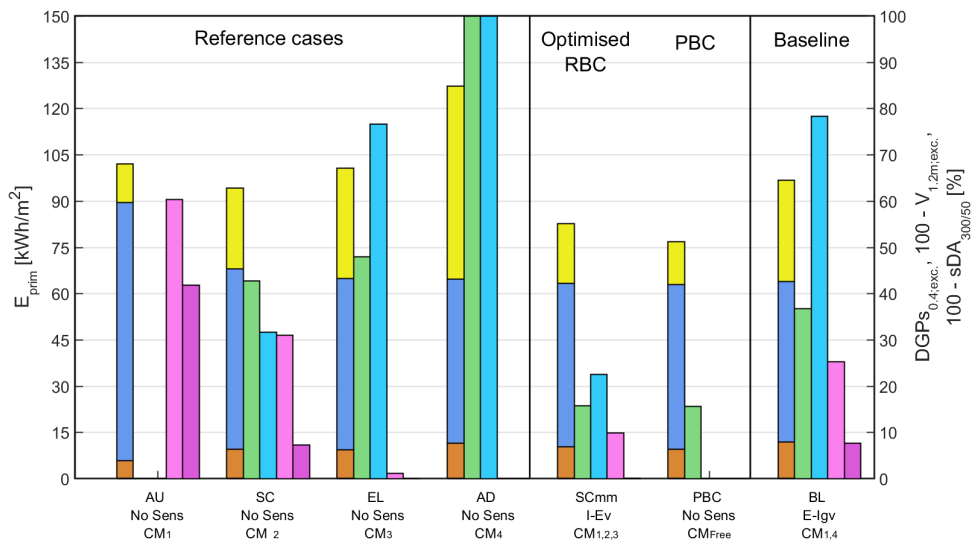
Figure 5.19 Summary of whole building performance of the multi-mode sun tracking strategy (SCmm-CM$_{1,2,3}$), developed using the support method, to a performance-based control strategy (PBC) and the reference cases.

5.8 Concluding remarks

The presented study showed that the VTB is able to fulfil some of the initial requirements that were defined in Section 2.6. The VTB was used to describe the performance effects of complex control behaviour resulting from interactions between indoor daylighting conditions and indoor thermal conditions.

Using this application study, a support method was developed that structures the use of BPS to support the development of comfort-driven control strategies for automated solar shading systems. The structured method was used to guide the development of a multi-mode sun-tracking control strategy. Confusion matrices were used as a tool to assess the effectivity of control decisions and optimise the sensor strategy that is used to switch between control modes. A series of scatter plots, relating sensor measurements to performance effects, combined with confusion matrices and a set of associated indicators were introduced to navigate the control space. These tools help quantify performance trade-offs and guide

decision making in developing a sensor strategy. The mapping of sensor measurements to performance effects allows performance criteria to be directly translated to control thresholds. The visualisation of this mapping in a set of scatter plots allowed the effects of moving control thresholds to be visualised in a single image and optimal control thresholds to be identified. The graphic nature of this mapping allows developers to investigate the performance effects of changing the relative weight of evaluation criteria without having to run additional simulations. Additionally, the plots visually support the developer in extracting detection algorithms from simulation data. Using the confusion matrix as a control decision classification tool, the performance of an existing concept could be analysed in a way that illustrated the constraints of a detection algorithm in relation to a more ideal unconstrained case. Being able to benchmark a potential concept in relation to an ideal control concept allows developers to weigh the costs of increasing control and sensor strategy complexity to potential gains in choosing research and development directions.

The application study focussed on using single control thresholds for switching between control modes, only a single radiation sensor was used to inform the system in each alternative and the actuation algorithms were intentionally kept simple. It should be noted that the presented algorithms and sensor combinations are not part of the support method. The support method was applied to single type of solar shading system (roller blinds) with a limited degree of control freedom. In the following chapters the support method will be applied and extended using different types of solar shading systems including systems with more degrees of freedom.

A few applications of the method, that go beyond the current application study, are recommended for further research. The performance mapping approach is not limited to using a single sensor and for developing detection algorithms based on multiple sensors, multi-dimensional plots can be used. Additionally, multiple performance criteria can be used with the confusion matrix method to identify threshold ranges that relate to different degrees of occupant sensitivities and comfort preferences. The 'disturbing' and 'perceptible' glare criteria can be used, for instance, to define the upper and lower boundaries of a threshold range that can be adjusted by users.

Different statistical classification techniques could be used as an alternative, or in addition to, the confusion matrices presented in this research. The confusion matrix approach has the advantage that different weights can be assigned to different types of false control decisions (e.g. causing glare is worse than decreasing the admission of daylight). A disadvantage of the current approach is that sensors are evaluated using specific control thresholds. For assessing sensors in a way that is not tied to a specific control threshold an ROC-curve could be used.

In the support method the control space of possible control actuations is constrained to a select number of control modes, that are selected based on engineering knowledge and structured analyses. Hereby the control space is made smaller and more manageable. A disadvantage of this constraint is that, although the method leads to high performance outcomes, ideal performance cannot be guaranteed. The support method is, however, also suited for developing actuation algorithms that exploit a larger part of the control space by using a proportional control approach (Shen and Tzempelikos 2017). To illustrate this point, Figure 5.15B shows how this could be approached in the application study. The graph indicates a slope that can be used in the $CM_{3;EL}$ mode to define the maximum shade height proportionally to sensor measurements, as an alternative to using seated eye level. Another possible application would be to discretize the control space and treat every shading system state as if it were a separate control mode. The mapping of sensor measurement to performance effects requires that distinct simulation alternatives are used but potentially a large number of control modes can be used. In the case study this would mean using annual simulations of discrete shade height positions in step 2 and 3. In this application the error in the assessment of instantaneous energy performance effects would have to be carefully assessed.

6 Design and control optimisation of a multi-state vertical-blind solar shading system

6.1 Introduction

In the previous chapter, effective management of solar energy was achieved through partial closing of the shading device. The optical and thermal properties of the shading device, however, were assumed to not change over time and only a single shading material was investigated. The review of the literature on the state of the art in automated shading systems indicated that multi-state shading systems that can change their thermal and optical properties are a promising research direction. Additionally, the review of the literature on simulation of automated shading devices indicated the limitations in many existing BPS tools in describing the physical effects of systems with time-varying optical and thermal properties.

This chapter focusses on optimization of the control strategy and the design of the shading system and its actuation mechanisms (the B and C levels-of-scale in Table 2.1). The goal of this application study is to develop and test VTB modelling-features for describing the performance effects of time-varying thermal/optical properties and design choices regarding the materialisation of the shading device. The application study takes the perspective of a developer of an integrated automated shading solution encompassing the motorisation system, the shading device, and a control strategy. The starting point of this study is a rudimentary initial version of a sun-tracking vertical-blind (ST-VB) concept. Developing the rudimentary concept into a deployable control strategy requires the specification of control rules, sensors, components and materials.

For the development of such an integrated shading strategy, it is important to consider that certain design and control decisions need to be made early in the development process whereas others can be reconsidered later. Actuation mechanisms are generally designed once by a product developer and cannot easily be changed once a production line is set up or when shading systems are applied in buildings. Contrary to the overall automation concept, which should be determined at an early stage, control rules and thresholds can easily be changed at a later stage. Additionally, it is desirable that materialisation and visual appearance of the shading device can be adapted to particular projects.

The simulation purpose of the shading product developer is to inform decision making in the development of an automation strategy for interior vertical blinds that involves both the selection of features to include in the actuation mechanism, as well the selection of control rules that exploit these features. Additionally, there is a need to evaluate the performance benefits of different system features within a larger framework of functional and aesthetic requirements. To this end, the developer also seeks insights into the performance benefits and challenges associated with the use of different types of blind materials in relation to different control concepts.

The research presented in the chapter was published in an article in the Journal of Building Engineering (De Vries et al. 2021b).

6.2 The initial concept: a sun-tracking control logic for automated interior vertical blinds

The initial ST-VB concept utilises a silent motorisation system that allows a set of interior vertical blinds to be rotated continuously without disturbing occupants. This enables the blinds to be operated using a sun-tracking control logic that prevents direct sunlight from reaching an occupant whilst preserving a large unobstructed view to the sky (Figure 6.1) for a large part of the day. The position of the blinds, expressed using the blind rotation angle (bRA), is adjusted in relation the solar azimuth angle using different control approaches that will be discussed further in paragraph 6.3.1. To obtain a generic control logic, that is independent of window orientation, solar azimuth (γ) is expressed relative to the window surface normal (WN_γ) using the vertical projection profile angle (VPPA): the angle between solar azimuth and a vertical surface projecting from the facade.
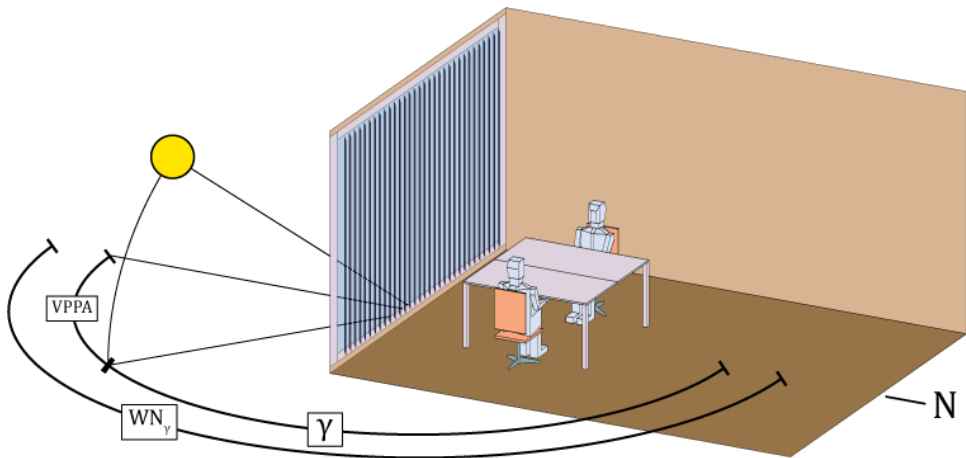
Figure 6.1 The sun-tracking vertical-blinds (ST-VB) concept, with solar azimuth angle (γ), the vertical projection profile angle (VPPA) and the azimuth angle of the outward surface normal of the window ($WN\gamma$)

Table 6.1 gives an overview of the main goals and assumptions in this study along with the characteristics of the shading system that is investigated.

Table 6.1 Goals, assumptions and system characteristics in application study 2

Optimise:	Assume:	System:
Control rules and parameters	Sensors	Variable rotation angle vertical blind system
Shading material (macroscale)	Glazing	Time-varying thermal/optical properties
Motorisation system	Building	Complex control logic

6.3 Methodology and simulation strategy

Figure 6.2 gives an overview of the workflow and the subsequent steps that will be discussed in this chapter.

Configure VTB and develop new modules (6.3.3)

6.5 Verify simulation toolchain:
Verify modules for generating BSDF (B.3.1) and CFS (B.3.3) that describe the optical behaviour of the combined shading and window system under varying blind positions and optical properties:

6.5.1: Verify CFS implementation in EnergyPlus. Compare SHGC predicted by EnergyPlus to SHGC predicted by LBNL-Window for varying blind positions

6.5.1: Verify dynamic control of CFS and interactions with the building model. Analyse effects of different control strategies on energy performance

6.5.2: Verify overall toolchain configuration by analysing performance effects of different control alternatives

Simulate performance of conventional roller blind baseline strategies and of each control strategy and materialisation alternative for the vertical blinds

6.6.1: Evaluate the effects of different control concept alternatives

6.6.2: Evaluate performance sensitivity to blind materialisation

6.7: Evaluate potential of ST-VB concept. Give recommendations regarding different features for the actuation mechanism and different blind materialisations

Figure 6.2 Overview of the workflow followed in this chapter

107

6.3.1 Investigated control rules, slat properties and design considerations

This section gives an overview of design and control aspects that will be investigated in this chapter. The performance effects of different potential control logics will be tested in Section 6.6. These control rules will be implemented as control modes in a multi-mode strategy and different configurations of this strategy will be evaluated. Additionally, the benefits and challenges associated with the use of different types of blind materials will be explored in relation to different concepts that determine the rotational freedom of the blind. This section will discuss each alternative and its associated design considerations. Table 6.2 summarizes these control rules in pseudo code along with the abbreviations that will be used for the corresponding control modes in the results section.

Table 6.2 Investigated control rules and the abbreviations used to describe them

ST-VB	**Sun-tracking vertical-blind**
Op-Mx	**If E_v > 6400 lx And VPPA < 90:** *Most open sun-tracking (Mx)* **Else:** *low-light sky response (Op)*
Op-Mn	**If E_v > 6400 lx And VPPA < 90:** *Most closed sun-tracking (Mn)* **Else:** *low-light sky response (Op)*
Op-Mx-Mn	**If E_v > 30000 lx And VPPA < 90:** *Most closed sun-tracking (Mn)* **Else if E_v>6400 lx And VPPA<90:** *Most open sun-tracking (Mx)* **Else:** *low-light sky response (Op)*
Reflect always	**Always:** *Reflecting side of blind always facing sun*
Reflect if morning	**If solar time is morning:** *Reflecting side of blind facing sun* **Else:** *Absorbing side of blind facing sun*
Reflect if afternoon	**If solar time is afternoon:** *Reflecting side of blind facing sun* **Else:** *Absorbing side of blind facing sun*
Reflect if cooling season	**If month is [Jan. Feb. Nov. Dec.]:** *Absorbing side of blind facing sun* **Else:** *Reflecting side of blind facing sun*
Reflect if cooling season or Ti>23	**If month is [Jan. Feb. Nov. Dec.] and Ti < 23°C:** *Absorbing side of blind facing sun* **Else:** *Reflecting side of blind facing sun*
Start retracted	**If first occupied hour of the day and E_v < 6400 lx:** *fully retract blind* **If E_v > 6400 lx:** *expand blinds and start sun-tracking response* **if E_v < 6400 lx and blinds have already been expanded today:** *most open blind rotation*
BL	**Baseline:** conventional automated roller-blind strategy.
Up-Down 200 W/m²	**If $I_{g;v}$ > 200 W/m²:** *fully lower roller blind* **Else:** *fully raise roller blind*
Up-Down 6400 lx	**If E_v > 6400 lx:** *fully lower roller blind* **Else:** *fully raise roller blind*

6.3.1.1 *Sensor strategy*

In the multi-mode strategies, the indoor illuminance (E_v) sensor that was selected for the roller blind strategy in Chapter 5, will be used to decide when the system should

activate each control mode (Figure 6.7). As with the previous study, three ranges are distinguished in the illuminance sensor measurements that are each associated to a different degree of risk for discomfort glare (Table 6.3). These ranges are titled **Lo, Mi** and **Hi**. The investigated control modes vary in the degree to which the blinds are opened and their ability to prohibit discomfort glare. Each control mode will therefore be activated only in response to corresponding sensor measurement ranges.

Table 6.3 Glare risk sensor ranges

	Lo	Mi	Hi
E_v sensor range	$E_v < 6400$ lx	6400 lx $\leq E_v \leq 30000$ lx	$E_v > 30000$ lx

6.3.1.2 *Sun-tracking control concepts*

There are different ways in which sun-tracking behaviour can be employed to block direct sunlight using vertical blinds. The performance of two sun-tracking approaches, and combinations thereof will be explored. In the most open form of sun-tracking the vertical edges of the blind are aligned with the VPPA (Figure 6.3) according to the equation:

$$\textbf{If } \gamma \leq \textbf{\textit{WN}}_\gamma\textbf{: } bRA = 90 + 2*VPPA$$
$$\textbf{Else: } bRA = 90 - 2*VPPA$$

(6.1)

This control logic uses the blind rotation angle (bRA) that maximises the amount of sky that is visible from the interior whilst not admitting direct sunlight and will be abbreviated as **Mx**. This strategy is inspired by a control strategy for horizontal blinds proposed by Konstantzos et al. (2015b). In the most closed form of sun-tracking, the surface normal of each individual blind is aligned with the VPPA following the equation:

$$\textbf{If } \gamma \leq \textbf{\textit{WN}}_\gamma\textbf{: } bRA = 90 + VPPA$$
$$\textbf{Else: } bRA = 90 - VPPA$$

(6.2)

This approach shades a larger portion of the bright circumsolar region of the sky and will be referred to as **Mn**. It is designed to offer more protection from discomfort glare (Motamed et al. 2020; Katsifaraki et al. 2017) but also admits less daylight and offers less view to the outside. The Mx and Mn control modes will be activated under Mi and Hi conditions using different configurations.
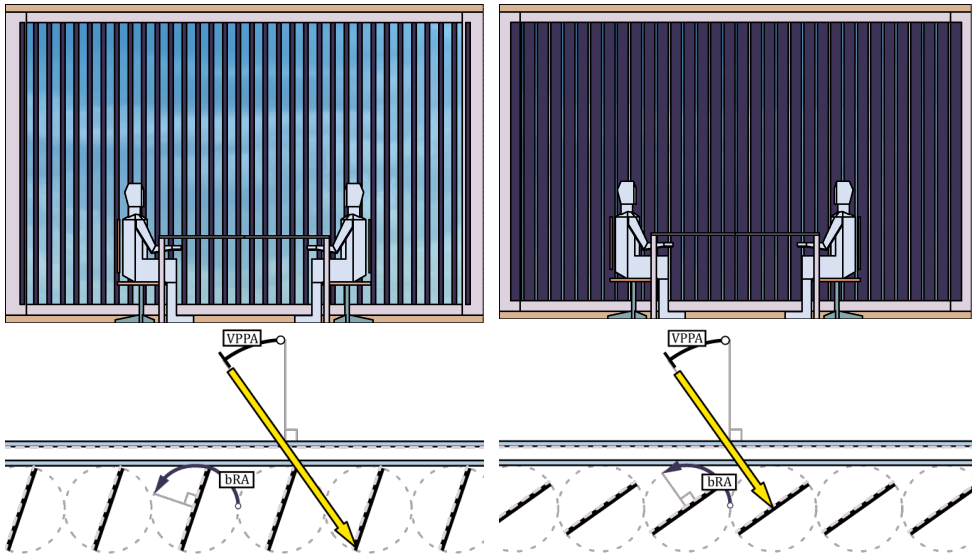
Figure 6.3 Two different forms of sun-tracking.
Mx (left): the most open strategy that aligns the edges of the blind with the VPPA.
Mn (right): the most closed strategy that aligns the surface normal of the blind with the VPPA

6.3.1.3 *Opening the blinds*

Sun-tracking behaviour would lead to an unnecessary loss of daylight admission under overcast conditions, or when the sun is not visible at any point from the interior. All strategies therefore include a control mode, referred to as **Op**, that responds to these conditions by opening the shading system. The Op control mode will be activated under Lo conditions (Table 6.3). Two different actuation alternatives will be investigated. One where the blinds are rotated to the most open position, and one where the blinds are retracted fully (Figure 6.4).

In the retracting alternative, the blinds are fully retracted once at the start of the day. Once Mi sensor conditions (Table 6.3) are detected, the blinds are expanded and positioned according to one of the sun-tracking control modes. For the remainder of the day, the blind cannot be retracted again, and the open bRA position will be used if Lo conditions occur. This limitation was chosen to avoid many large movements of the blinds, that could be distracting to users. The ability to automatically retract the blinds would require an additional actuation mechanism that would be more expensive and complex than the initial concept where only rotations are supported. By quantifying the performance benefits of the retracting alternative, decision makers can investigate whether it is worth investing time and money to develop this system feature.
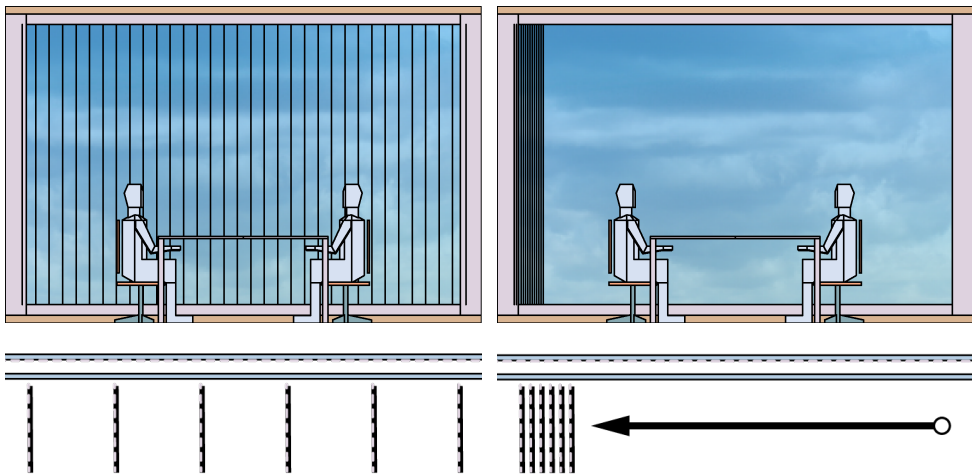
Figure 6.4 Control actuations in the open control mode (Op). Left: Rotating the blinds to the most open position.
Right: Retracting the blinds fully at the start of each day (Start retracted)

6.3.1.4 *Using the front and back blind reflectance to dynamically adjust the admittance of solar energy*

In principle, the ST-VB concept allows the blinds to be rotated 360 degrees. Both sides of the blind can therefore be used to face the sun in the sun-tracking modes. This offers the opportunity to use a different solar reflectance for the two sides of the blind and switch between the two sides to either admit or reflect more solar energy. A low reflectance could be used in the heating season to reduce heating energy demands whilst a high reflectance could be used in the cooling season to reduce solar heat gains and cooling energy demands. The potential of this concept will be tested using different control rules for switching between the reflecting and the absorbing side of the blind.

6.3.1.5 *Disturbances by dangling blinds*

A consideration that influences the allowed rotational freedom and chosen materialisation of the blinds is whether the width and spacing of the blinds are chosen such that they overlap or not. Choosing these parameters such that the edges of the blinds touch in a fully closed position, but do not overlap, allows a full 360-degree rotation of the blind and the freedom to orient each of the two sides towards the sun at any moment (Figure 6.5). The downside of this approach is that small dangling movements of the blinds could disturb occupants and possibly cause glare. The disturbing effect of dangling blind movements can be reduced by choosing a

blind width and spacing where the blinds overlap in a fully closed position. The downside of this approach is that it limits the rotational freedom of the blinds to a 0 to 180-degree range.
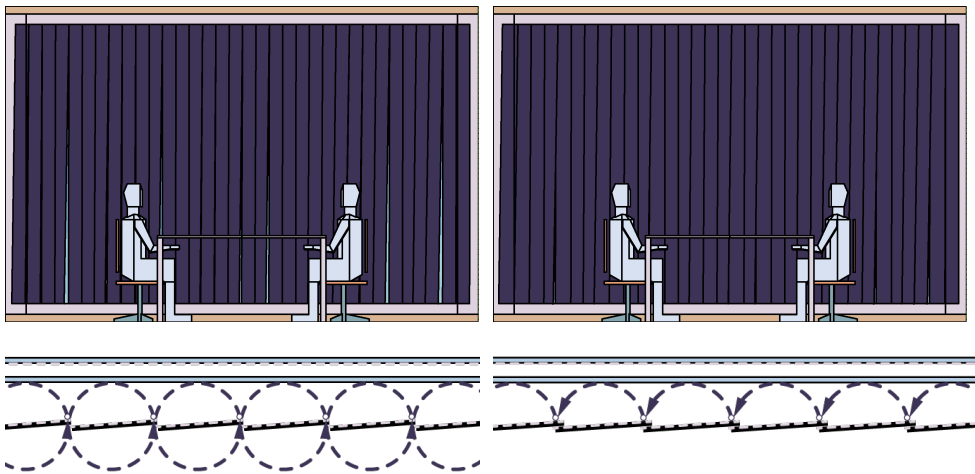
Figure 6.5 Possible disturbance by dangling movements of the blinds, blind width and spacing and the associated rotational freedom

6.3.1.6 *Materialisation of the blinds*

Another important consideration is related to the type of materials that are available in the market. Utilising materials that are readily available for the ST-VB system is preferable because it is less costly than having a blind custom made. Commonly applied products include natural-fibre or synthetic fabrics, fabrics with a metalized coating, solid plastic slats, and metal slats (Table 6.4). Each material is associated with a particular cost and solar reflectance. Visual and solar reflectance are strongly linked and close to identical for most products using the materials in Table 6.4. Specifying the solar reflectance is therefore intrinsically linked to choosing the colour (visible reflectance) and visual appearance of the shading system. The reflectance of the blind can strongly influence daylighting, glare and energy performance and these aspects need to be balanced with the other design considerations. With regards to visual appearance of the blinds, it is preferred to have a large degree of freedom in selecting the colour of the side(s) of the blind that are facing to the interior such that the appearance can be adjusted to desired interior design concept. Additionally, darker colours for the occupant-facing side of the blind can be particularly attractive to end-users because dark colours positively influence the perception of the degree of view to the exterior, due to increased contrast with the exterior luminous environment that is visible between the blinds (Figure 6.6). Off-gassing of volatile organic compounds, fire safety, environmental

impacts and due diligence with associated standards also play a role in defining the materialisation of the blinds. A general qualification based on the type of material is not possible, but it can be noted that some products are more challenging to certify (Well 2019; Greenguard 2013).

Table 6.4 Commonly applied materials for indoor shading products

Name	$R_{vis/sol}$		Emissivity		Cost	Representative
	Front	Back	Front	Back		cases
PVC	0 - 0.8	0 - 0.8	0.9	0.9	Low	Rf80Rb80, Rf55Rb55, Rf20Rb20
Metal slats	0.5 - 0.8	0.5 - 0.8	0.1-0.2	0.1-0.2	High	Rf80Rb80
Fabrics	0 - 0.6	0 - 0.6	0.9	0.9	Low	Rf55Rb55, Rf20Rb55
Metal coated fabrics	0.6 - 0.8	0 - 0.6	0.1-0.2	0.9	Medium	Rf80Rb55, Rf80Rb20, Rf80Rb80

The starting point of this study is a fabric with a metallised coating. The metal coating offers a high solar reflectance, that reduces the admission of solar energy to the interior, as well as a low thermal emissivity. Typically, such fabrics are manufactured for roller-blind applications and coated on one side only. The performance effects of different materialisations, however, will also be explored. Based on the considerations and materials from Table 6.4, the alternatives shown in Table 6.5 will be investigated.
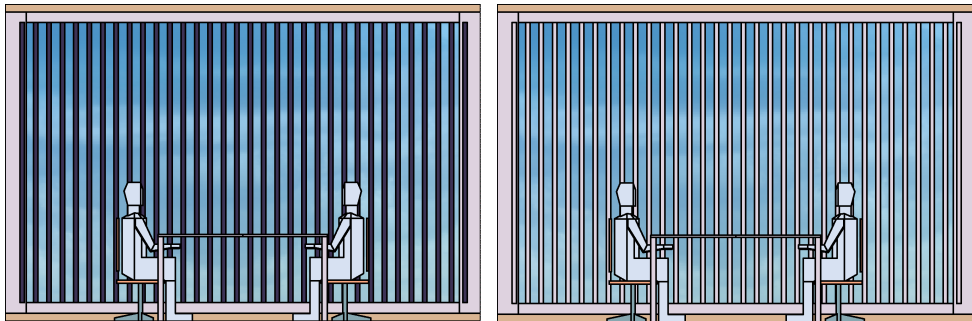
Figure 6.6 Influence visual/solar reflectance (colour) of the blind on the visual appearance the shading system and the perception of the degree of view to the outdoors between the blinds

Table 6.5 Investigated materialisation alternatives

Name	Description	Solar/visible reflectance		Emissivity		Solar/visible transmittance
		Front	Back	Front	Back	
Rf80Rb55	Metallised front light coloured back	80%	55%	0.15	0.9	1%
Rf55Rb55	light coloured front light coloured back	55%	55%	0.9	0.9	1%
Rf20Rb55	dark coloured front light coloured back	20%	55%	0.9	0.9	1%
Rf80Rb80	Metallised front Metallised back	80%	80%	0.15	0.15	1%
Rf80Rb20	Metallised front, dark coloured back	80%	20%	0.15	0.9	1%

6.3.1.7 *The baseline control strategies*

Potential customers purchasing a product like the ST-VB system are likely to compare the product against conventional automated solutions. The automated interior roller-blind system from Chapter 5 will be used as a baseline (BL200W/m²) because such systems are commonly applied in practice. The Rf80Rb55 material will be assumed for the BL strategy. The results from Chapter 5 showed that this conventional strategy is not very effective in mitigating discomfort glare. Occupants are likely to close the shading device when glare occurs, and such interactions will influence the operational daylighting and energy performance of the BL strategy. To give an indication of the extent at which occupant behaviour could influence the performance of the BL strategy, a second baseline (BL6400lx) is added where the shade is controlled using the E_v sensor and the optimised Lo (6400lx) control threshold.

6.3.2 Performance aspects and indicators

The performance aspects of interest in this study are daylight quality, visual comfort, view to the outdoors, and energy efficiency. Daylight quality and quantity are assessed using $sDA_{300/50\%}$. To evaluate instantaneous daylighting performance, the daylit area fraction D_{300lx} is used. The probability of daylight discomfort glare is assumed to be dependent on saturation glare alone because the sun-tracking control logic protects the occupants from exposure to direct solar radiation. DGPs has been shown to give reliable results for blinds with sun-tracking behaviour specifically (Wienold 2007; Konstantzos et al. 2015b). The same occupant positions and viewing

directions as in the Chapter 5 study are assumed to assess DGPs (Figure 6.7). Again, glare is assessed for the two viewing directions, 0-degree and 45-degree, and for each viewing direction the   maximum DGPs of the two positions is used at each evaluated time step. Additionally, 'disturbing' glare exceedance is used as a glare criterion to quantify visual discomfort across a year. $DGPs_{0.4;0deg;exc.}$ and $DGPs_{0.4;45deg;exc.}$ are used as annual performance indicators. $DGPs_{0.4;0deg;exc.}$ is considered to be more critical in this study because occupants cannot easily adjust their viewing direction when glare occurs in the 0-degree viewing direction. The goal is to develop a ST-VB strategy that leads to 0% $DGPs_{0.4;0deg;exc.}$. On the other hand, $DGPs_{0.4;45deg;exc}$ will be treated as an indicator that is undesirable, but here, trade-offs with other performance aspects are considered acceptable.
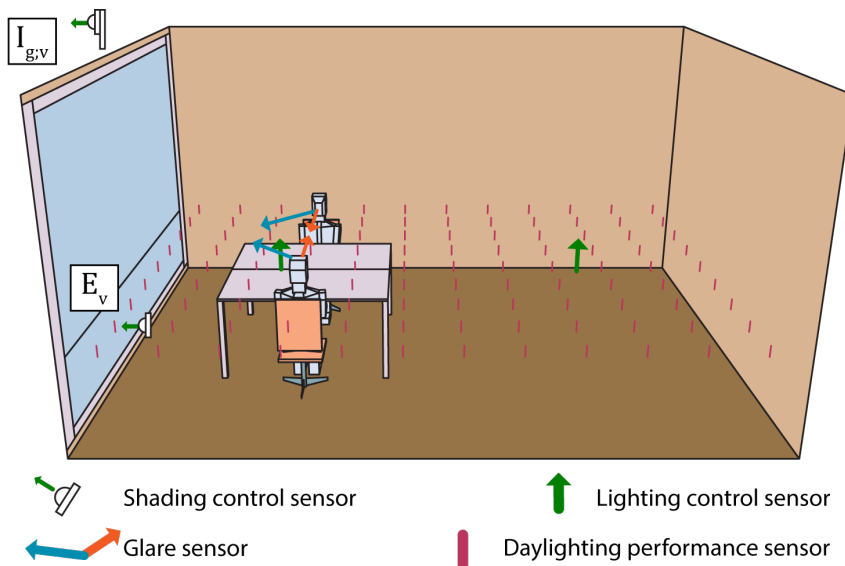
Figure 6.7 Overview of Radiance model set-up. The window is split in two segments to describe flux transfer more accurately in the view matrix

For the ST-VB strategies, the 'exposed window fraction' (EWF) for assessing the degree of view to the outdoors, is computed using simplified version of the method proposed by Tzempelikos (2008) where the effect of slat thickness is disregarded. For these strategies EWF is computed from the bRA using the equation:

$$EWF_{vertical\ blind} = \frac{e}{s+e} = 1 - |\sin(bRA)| \qquad (6.3)$$

Where e: the opening area between two blinds projected along the window surface normal
s: the blind surface area projected along the window surface normal (Figure 6.8)

For the BL strategies, the same approach is taken as in Chapter 5, where EWF is computed at each time step according to the following equation:

$$EWF_{roller\ blind} = \frac{e}{s + e}$$ (6.4)

Where e: the shade height measured from the bottom of the window, s: the shade height measured from the top of the window (Figure 6.8)

For all strategies it is assumed that there is an acceptable degree of view to the outside when EWF is larger than 40% and view performance is expressed as the share of occupied hours when this condition is met. This annual aggregate is denoted by $EWF_{40\%;exc.}$. For the BL strategies, the 40% EWF criterion relates to a shade position above the eye level of a seated occupant (1.2 meters). For the ST-VB strategies, 40% EWF relates to a bRA of 38 degrees (Figure 6.8).

Energy performance is quantified as primary energy consumption for cooling, heating and lighting and computed from energy demands using Equation 2.3.

To assist in the interpretation of the multi-performance graphs that follow in the results section, the $sDA_{300/50\%}$ and $EWF_{40\%;exc.}$ percentages are plotted in terms of their complementary 100% - $sDA_{300/50\%}$ and 100% - $EWF_{40\%;exc.}$ percentages. This allows all performance aspects to be plotted as indicators that are to be minimised.
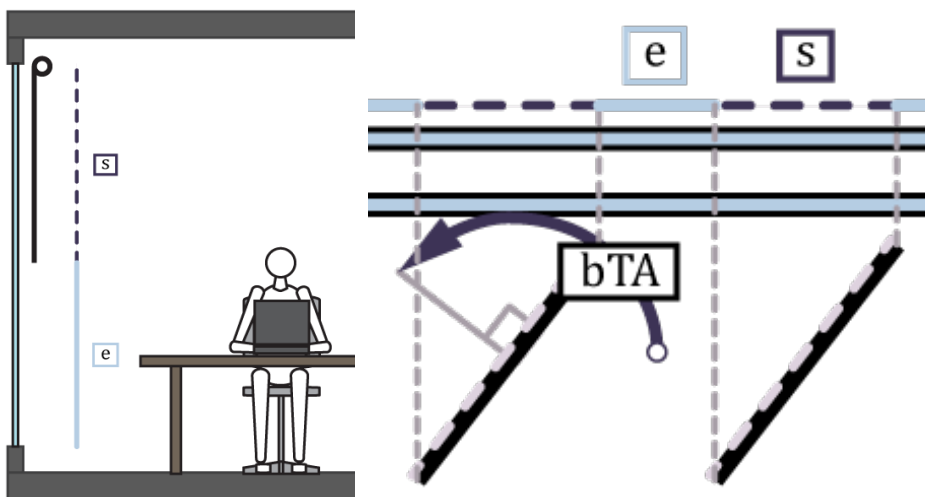
Figure 6.8 Exposed window fraction for the roller blinds (left) and the vertical blinds (right). e: exposed part of the window (in parallel projection), s: shaded part of the window

One of the goals in this study is to assess building performance effects of different system features (e.g., design and materialisation of the blinds, actuation mechanisms) along with other design considerations such as visual appearance, disturbance by dangling blind movements and system costs. The later aspects will not be assessed quantitatively. Rather, the design alternatives in the simulation experiment were selected to allow decision makers to weigh these aspects in a qualitative manner with the associated building performance effects. To facilitate this, some assumed preferences should be considered, that were defined based on stakeholder consultation. These preferences will be discussed in detail in the following section. Regarding system costs, it should be noted that generally these are strongly influenced by the complexity of the actuation mechanism, material type and quality, and the commissioning process.

6.3.3 Configuration of the virtual testbed
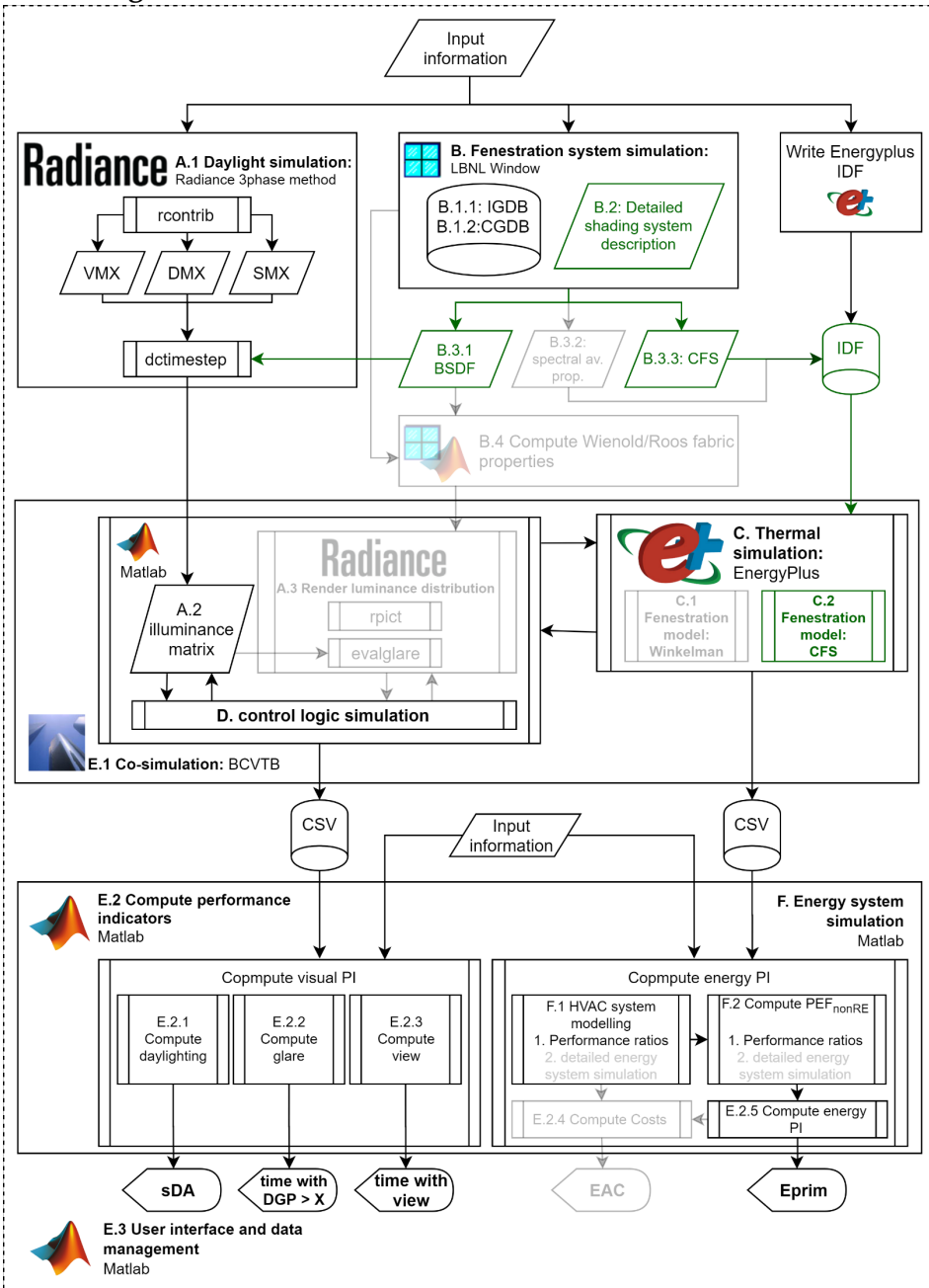
Figure 6.9 Configuration of the VTB in this application study. VTB components that are not used in this configuration are shown in light grey. New VTB modules that will be tested in this chapter are shown in green. The input information is specified in Sections 4.2 and 6.3.4.

Figure 6.9 shows how the VTB was configured to accommodate the simulation study objectives, performance indicators and shading system characteristics. In comparison to the VTB configuration from Chapter 5, the VTB was extended with additional features to be able to describe the performance effects of the time-varying thermal/optical properties of the ST-VB system, and give insight into the performance effects of the selected blind materials.

A series of modules were developed describing the combined window and shading system using the complex fenestration systems (CFS) model in EnergyPlus (B.3.3 and C.2). The CFS module in EnergyPlus (C.2) allows for the externally computed BSDFs and absorption matrices to be used to describe the optical behaviour of the fenestration system. The solar flux transfer and absorption matrices are derived from sub-system simulations using LBNL-Window (B.3.3, section 3.2.3). Additionally, a set of Matlab functions was created to facilitate sensitivity analyses of shading device properties, the generation of EnergyPlus CFS descriptions, and BSDFs for simulation with the Radiance 3PHS method.

The employed LBNL-Window blind and glazing models have been validated experimentally by Hart et al. (2018) and through inter-model comparison by Carli (2006). Additionally, Bustamante et al. (2017) have verified the use of the CFS approach in EnergyPlus for describing a dynamic horizontal blind system. The CFS toolchain that is adopted in this thesis and the overall VTB configuration will be verified in a series of quality assurance studies in Section 6.5.
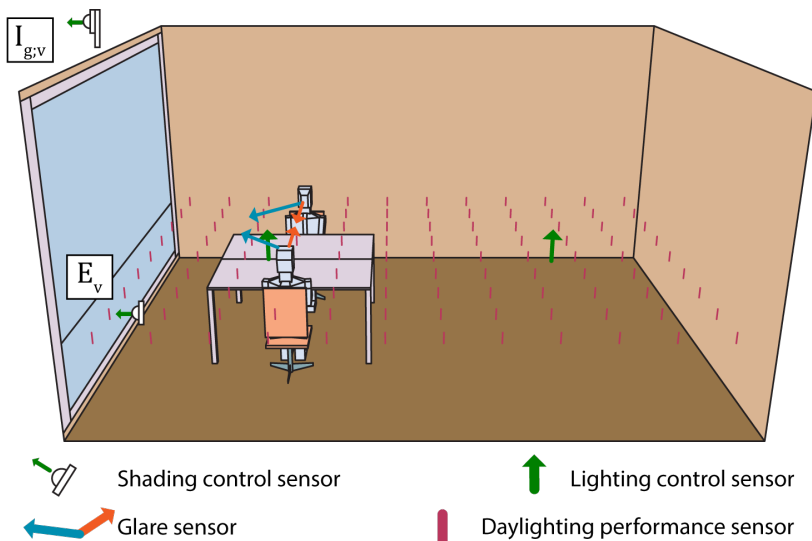
Figure 6.10 Overview of Radiance model set-up. The window is split in two segments to describe flux transfer in the view matrix more accurately

6.3.4 Assumptions and simulation input parameters

This study uses the reference office assumptions that were presented in Section 4.2. Figure 6.10 shows the setup of the Radiance model in this study. The most important simulations input settings can be found in Table 6.6.

Table 6.6 Simulation parameters and assumptions

	EnergyPlus	Radiance
Fenestration	LBNL-Window venetian blind model with glazing properties from IGDB: Lay 1: IGDBnr-11560, Lay 2: IGDBnr-1608	
	CFS	BSDF
Interior surfaces		Lambertian reflectors: Ceiling R_{vis}: 0.8, Wall R_{vis}: 0.5 Floor R_{vis}: 0.2
Simulation settings	Idealised HVAC system: unlimited capacity and ideal response	Sensor grid: 9x12
		$VMX_{rcontrib}$: -ab 12 -ad $5\cdot10^4$ -lw $2\cdot10^{-6}$,
		$DMX_{rcontrib}$: -ab 2 -ad 10^3 -lw $5\cdot10^{-4}$ -c 3000
		S and DMX sky resolution: MF3
	5 min. time step	hourly time step

6.4 Support method

No new support methods are developed for this application study. The method for optimizing control thresholds, that was presented in Chapter 5, is used in this application study to obtain control parameters that are optimized for the ST-VB strategy (Table 6.3).

6.5 Quality assurance

The following sections section highlight quality assurance of the new VTB features contained in VTB modules B.3.3 and C.2 as well as the overall VTB configuration.

6.5.1 VTB Module B.3.3 and C.2: Verification of the complex fenestration modelling toolchain

This section presents a verification study that shows that the toolchain, that is used to set up the CFS model in EnergyPlus and describe the multi-state vertical-blind system, works correctly. To this end, the solar heat gains predicted by the vertical-blind CFS model in EnergyPlus are compared to the heat gains that are predicted by LBNL-Window. Additionally, the behaviour of the model is tested using the initially

defined control concepts. The goal of this verification study is to test that (i) there are no programming errors in the toolchain, (ii) optical data is correctly pre-processed and used in EnergyPlus, and (iii) the radiative and convective surface heat transfer predicted by the CFS model in EnergyPlus gives plausible results. In these simulations, the Rf80Rb20 material is used.

For comparing the heat gains predicted by the two tools at each vertical-blind position, the solar heat gain coefficient (SHGC) is used. The SHGC is generally defined under static boundary conditions and experimentally determined for a particular fenestration system in a controlled laboratory setting. Throughout the EnergyPlus simulation, boundary conditions differ considerably from what is assumed in LBNL-Window (Table 6.7). To verify the toolchain, the Energyplus model is set up to approximate the same SHGC boundary conditions. EnergyPlus does not report an overall SHGC for each vertical-blind position and solar position and incident irradiance cannot be assigned directly. Therefore, the available inputs in EnergyPlus were manipulated such that during a simulation, the boundary conditions at solar noon on the 21st of December would match with the boundary conditions in Table 6.7. The façade of the building was tilted backward 14 degrees to achieve a solar position that is perpendicular to the façade (Figure 6.11). Additionally, the weather data was edited to obtain the desired outdoor temperature and 500 W/m² direct solar radiation on the façade with zero diffuse radiation. Radiative and convective surface heat-transfer coefficients were not changed and are computed using the detailed methods in EnergyPlus to verify that these methods lead to plausible results in this application.

Table 6.7 CEN boundary conditions (Iso 2001) used in LBNL-Window to compute SHGC

	T_i	T_o	Direct Solar radiation	Angle of incidence	Fixed combined surface heat-transfer coefficient	
					inside	outside
CEN boundary conditions	25°	30°	500 W/m²	90°	2.5 W/m²K	8.0 W/m²K

Figure 6.12 shows the SHGC predicted by LBNL-Window and the EnergyPlus CFS model for each bRA. The figure shows that there is generally a good agreement between LBNL-Window and the overall CFS toolchain. The agreement is best when the blinds are in a fully closed position (90° bRA, SHGC difference: 0.003) and becomes slightly worse as the blinds are opened further, giving a maximum difference of 0.029 when the blinds are in the perpendicular positions (0 and 180° bRA). This discrepancy is within the acceptable range of uncertainty in this study. In Appendix B, a similar comparison is presented that illustrates why the

Winkelman blind model (VTB module C.1) does not suffice for describing the double-sided blind system.
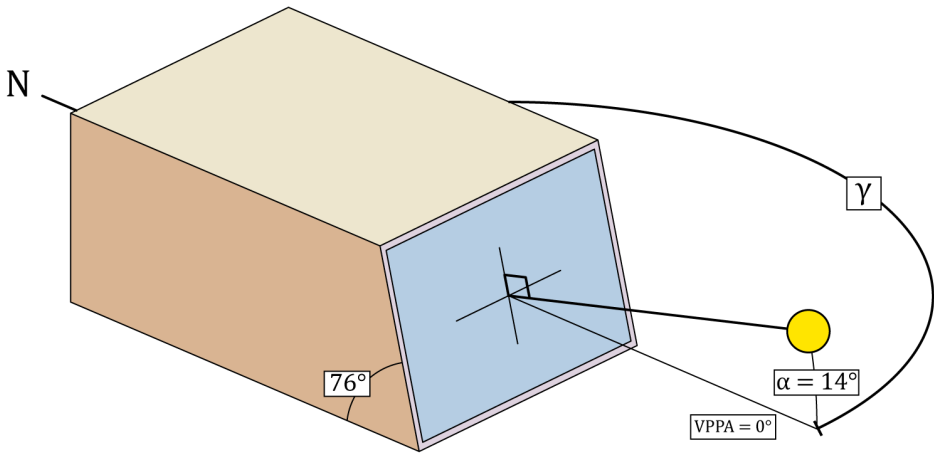
Figure 6.11 Setup of verification experiment. To obtain the 0-degree incidence angle in EnergyPlus, the façade is tilted 14 degrees such that the sun is perpendicular to the façade at solar noon on the 21st of December
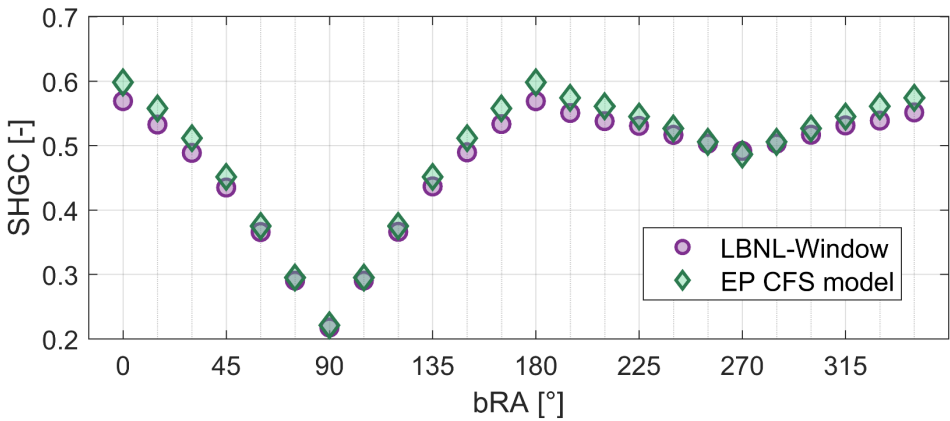
Figure 6.12 SHGC in relation to vertical-blind rotation angle. As predicted by LBNL-Window and the vertical-blind CFS model in EnergyPlus (EP)

The double sided vertical-blind concept (Rf80Rb20) offers a very large variation in the amount of solar energy that is admitted or reflected, ranging from a SHGC of 0.2 in the closed reflecting position (270° bRA) to 0.6 when the blind is in its most open

rotation (90° bRA). By using a highly reflective material for the sun-facing side of the interior blind (90° bRA, R_{sol}: 80%), a substantial portion of the initially transmitted solar radiation is reflected back to the exterior. Overall, the fraction of the incident solar energy that reaches the interior is small, with only 14% being absorbed by the interior shading system and 8% at the interior windowpane. When using the low reflectance side of the blind (270° bRA, R_{sol}: 20%), however, the shading system and the interior windowpane absorb as much as 46% and 4% respectively.

To also verify that CFS states are controlled correctly, and that they interact as expected with the building model a set of dynamically controlled cases will be evaluated. Figure 6.13 shows primary energy consumption for heating and cooling predicted by the CFS toolchain for six validation cases (VD) where daylight dimming of electric lighting was disabled. In each of these cases, one of the control modes that were described before is used throughout a full year. A '3.VD admit sunlight tracking' case is added here, where the blinds are rotated to admit a maximum of direct sunlight (bRA as in Mn but rotated 90-degrees). The label reflecting or absorbing indicates what side of the Rf80Rb20 blind is oriented towards the sun. The results show that the model behaves as expected. Strategies VD2 to VD5 show that cooling energy decreases and heating energy increases when the blinds are in a more closed position. VD3 leads to a small reduction in heating demand compared to the case without blinds (VD2) which can be attributed to a reduction of radiative heat losses associated to the low-emissivity blinds. Additionally, cooling energy increases substantially when the absorbing side of the blind is oriented towards the sun (VD1 in relation to VD5: 34 kWh/m² or 74%). Heating energy consumption, however, is not strongly affected by increasing the absorbed radiation (VD5 in relation to VD1: 1.7 kWh/m² or 22%) and appears to be mainly influenced by the amount of radiation that is transmitted. The latter can be seen in the reflecting cases VD3, VD4 and VD5 where the amount of diffuse solar radiation that is transmitted changes, but the absorbed solar energy remains largely the same (3.7 kWh/m² or 39% difference in $E_{prim;heating}$). The explanation for this is that, for the reference office cell, heating energy consumption mainly occurs outside of daylit hours (Appendix B Figure B.1). During daylit hours, internal gains and a small fraction of solar heat gains are sufficient to heat up the space. Increasing the amount of energy that is absorbed by the blind does not help to reduce heating energy consumption because this leads to convective gains that are immediate and increase indoor temperature at a moment when the heating system is off. If instead the amount of solar energy that is transmitted is increased, this energy will be stored in high-mass internal surfaces and partly released outside of daylit hours where it helps to reduce heating energy consumption.
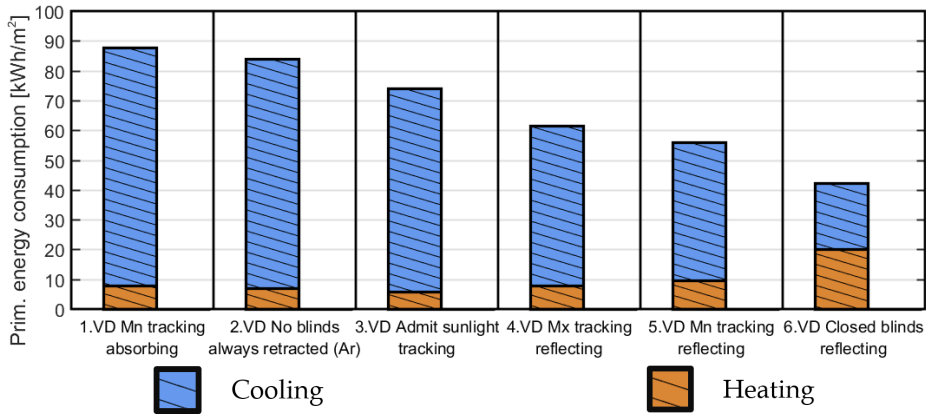
Figure 6.13 Primary energy consumption for heating and cooling for six validation cases

6.5.2 Verification of the overall VTB configuration

In this section, the correct functioning of the overall VTB configuration is verified by analysing the behaviour of one of the ST-VB control alternatives and the resulting performance effects.

Figure 6.14 shows simulation results for the strategy that employs only the most open sun-tracking control logic and always has the reflecting side of the blind facing the sun (1ST-VB Op-Mx-Reflect always). For comparison, the same results are shown for the conventional 14BL roller blind strategy in Figure 6.15. The EWF (A) results show that the sun-tracking control logic in the 1ST-VB strategy, causes the shading device to only partially cover the window for the largest part of the day. It is only during the middle of the day, for roughly an hour around solar noon, that the shading system closes fully. At these instances, the solar azimuth position overlaps with the surface normal of the window (low VPPA) and the blinds have to close fully to block direct sunlight.

During the hours where the ST-VB systems is not fully closed, the admission of daylight is generally high (C), leading to significant improvements compared to the 14BL strategy. This improvement in the amount of admitted daylight also reduces lighting energy consumption (D), and consequently lower overall E_{prim}, compared to the 14BL case. It is only during the short period around solar noon, that both strategies lead to similar daylighting and energy performance. Additionally, the graphs show that, because more solar energy is admitted during the day with the 2ST-VB strategy, less heating energy is consumed in the heating season outside of occupied hours. Consequently, E_{prim} is also lower in these instances.
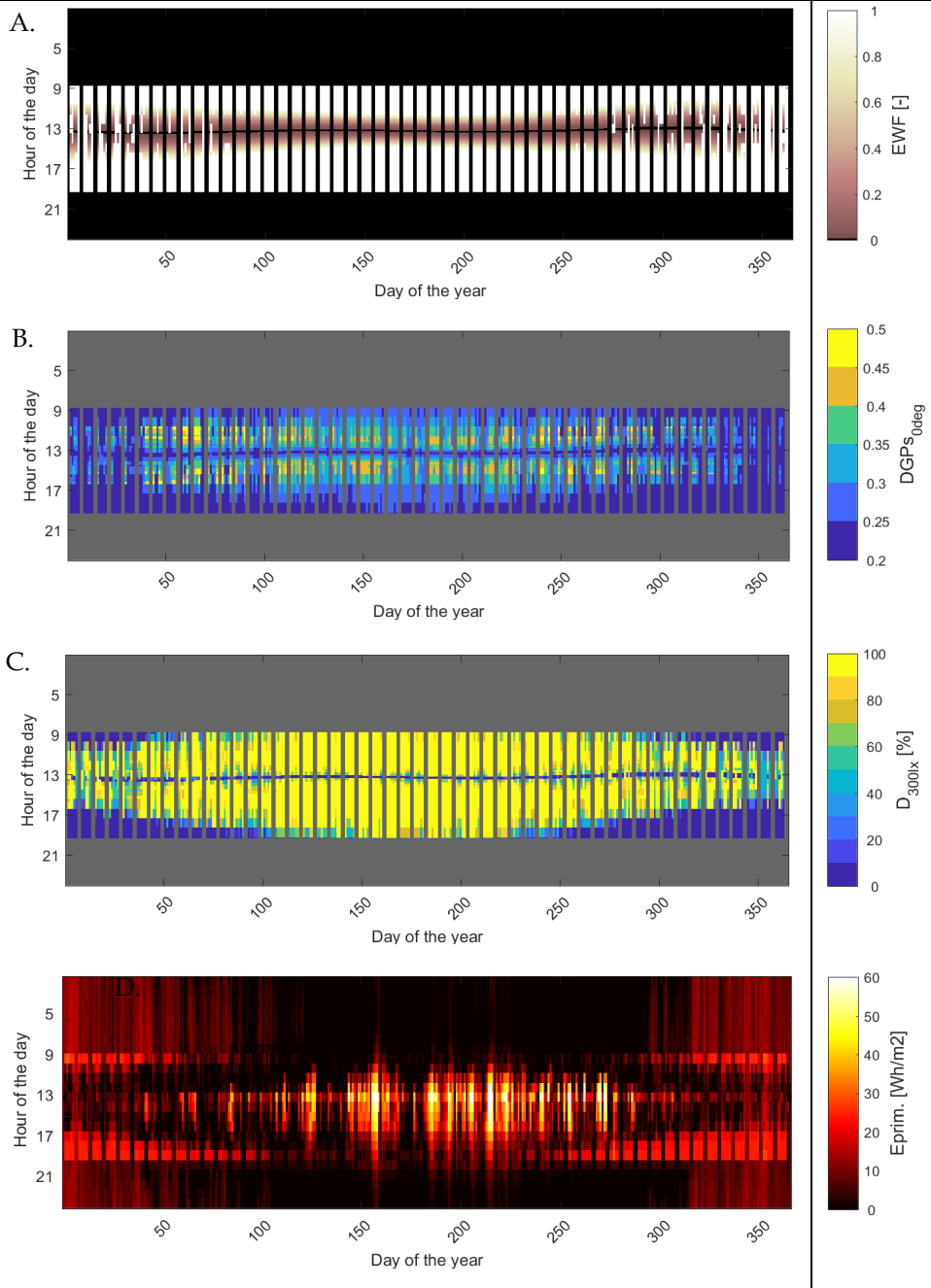
Figure 6.14 Behaviour and performance of the 2ST-VB-Op-Mx-Reflect always strategy. DGPs 0-deg gives the maximum DGPs of both occupants in the 0-degree viewing direction.
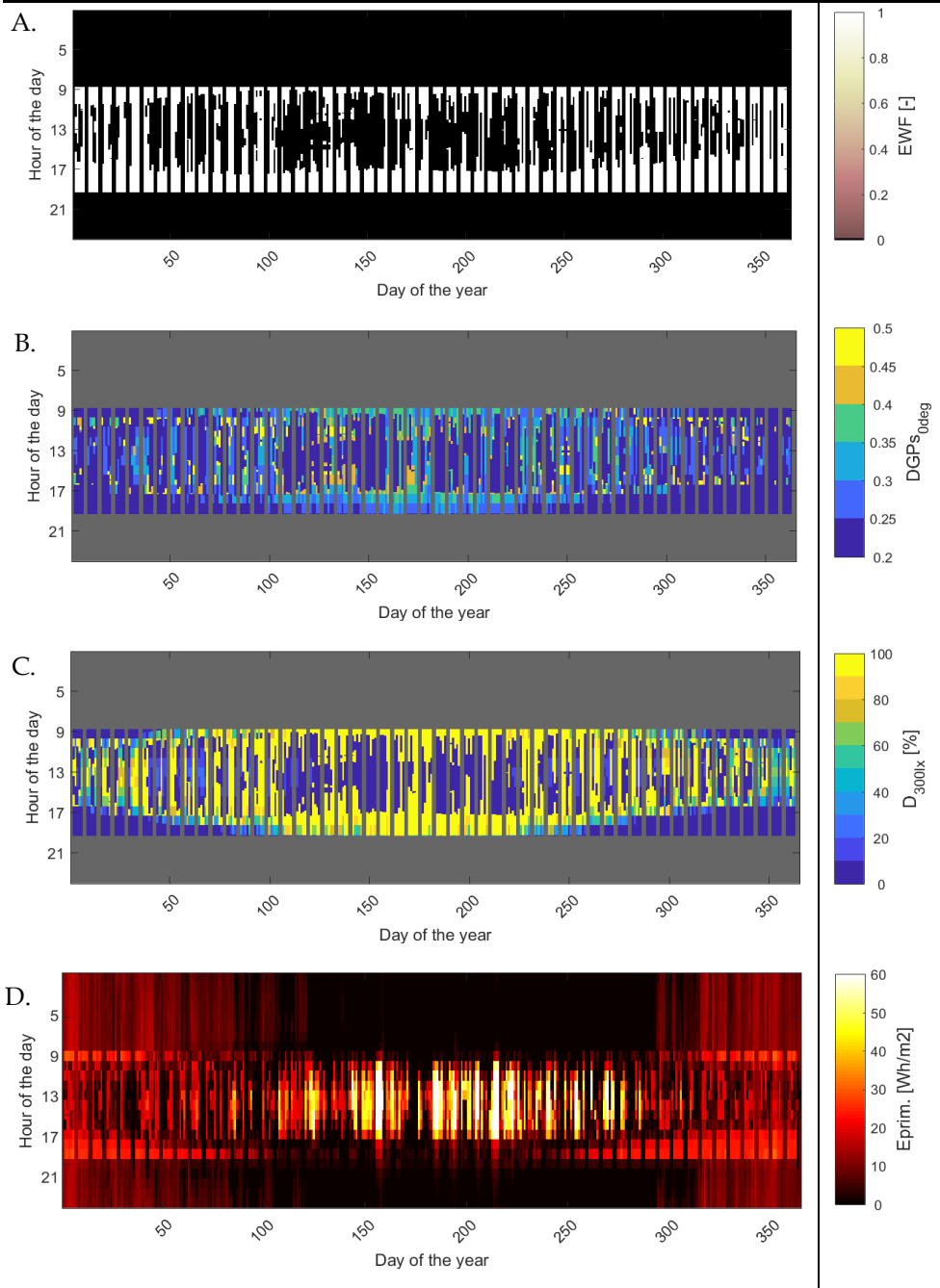
Figure 6.15 Behaviour and performance of the 14BL strategy.
DGPs 0-deg gives the maximum DGPs of both occupants in the 0-degree viewing direction.

With regards to glare performance, the two strategies show contrasting patterns. The instances where the 14BL strategy leads to disturbing glare (DGPs≥0.4) or worse, occur mainly in the early morning and late afternoon. At these instances, direct sunlight is visible to the occupants but due to the oblique incidence angle, vertical irradiance on the façade is too low to exceed the activation threshold. The 2.ST-VB also leads to instances with disturbing glare, but these tend to occur about halfway between sunrise and solar noon, and halfway between solar noon and sunset. At these instances, the VPPA is in the intermediate range (30-60°) and the blinds are in a relatively open position. With the most open sun tracking logic, a large bright region of the sky is visible to the occupants at these instances, which is sufficient to cause glare.

The presented results match well with known principles from building physics and it is concluded that the VTB configuration functions as intended.

6.6 Development and performance evaluation of the multi-state sunt-tracking vertical-blind strategy

In this section, the performance of the ST-VB will be assessed. The performance effects of each control alternative are simulated and evaluated in Section 6.6.1. In Section 6.6.2, the effects of different blind materialisations will be evaluated for each control concept.

6.6.1 Performance assessment of different control concept alternatives

Figure 6.16 shows the performance of the envisioned vertical-blind concept with different sun-tracking approaches, compared to the conventional automated roller-blind strategies. Ideal performance is achieved if all indicators in this graph are zero. The first three strategies in this graph compare the different sun-tracking approaches where the reflecting side of the blind is always facing the sun. All strategies employ the open slat angle position (Op) under Lo sensor ranges.

The strategy that employs only the most open sun-tracking strategy (1ST-VB Op-Mx) offers substantial improvements over the conventional 14BL strategy. 1ST-VB leads to better energy performance (22% less E_{prim}), daylighting performance (76% higher $sDA_{300lx/50\%}$) and more view to the outside (15% higher $EWF_{40\%;exc.}$). For the most critical viewing direction, the 1ST-VB strategy provides similar protection against visual discomfort as the 14BL strategy (8% $DGPs_{0.4exc0deg}$). However, the 1ST-VB performs worse in the 45-degree viewing direction (10% more $DGPs_{0.4exc45deg}$). Employing the more closed sun-tracking (2ST-VB Op-Mn) reduces disturbing discomfort glare, eliminating its occurrence in the most critical viewing direction

altogether (0% DGPs$_{0.4exc0deg}$). This strategy, however, also leads to a 20% decline in sDA$_{300lx/50\%}$ and increases E$_{prim}$ by 4% compared to 1ST-VB.

The multi-mode 3ST-VB-Op-Mx-Mn strategy, that employs both forms of sun-tracking, combines the most beneficial performance traits of 1ST-VB and 2ST-VB. Compared to the two baselines (14 and 15 BL), the 3ST-VB strategy offers a 22-35% reduction in E$_{prim}$, an improvement of 75-99% in sDA$_{300lx/50\%}$ and 8-33% more time with a view to the outdoors. Compared to 14BL, the 3ST-VB strategy leads to a reduction of 8% in the time with disturbing glare for the most critical viewing angle whilst the risk of glare is 5% higher for the viewing angle facing the window. The large variability in performance between the two baseline strategies illustrates the degree of uncertainty associated to conventional shading control strategies that do not provide sufficient protection against visual discomfort.

The 4 to 6 ST-VB strategies explore the performance of a system with overlapping blind edges, where the blinds can only be rotated 180 degrees (Figure 6.16). Because the reflecting side of the blinds can now only be oriented towards the sun for half of the day, a choice must be made to use the reflecting side during the morning or the afternoon. 5ST-VB shows the performance of the Op-Mx-Mn strategy if the reflecting side is used to track the sun during the morning. 5ST-VB shows similar daylighting, view and glare performance to the 3ST-VB strategy, where a full 360-degree rotation is allowed. With 5ST-VB, however, more solar radiation is absorbed by the blinds during the afternoon which increases cooling energy consumption, leading to a total E$_{prim}$ that is 13% higher than that of 3ST-VB. The energy performance of the 5ST-VB strategy is still substantially better than that of 14 and 15BL, offering a reduction of 11-27% in E$_{prim}$. Appendix B provides a more detailed analyses of the time step behaviour of the 5ST-VB strategy (Figure B.1) in comparison to the 14BL (Figure B.2).

In 6ST-VB, the reflecting side of the blind is used during the afternoon, rather than the morning which leads to a 2% increase in E$_{prim}$ compared to 5ST-VB. This shows that, in applying the overlapping blinds concept on a south facing window, it is more beneficial to use the reflecting side during the morning.
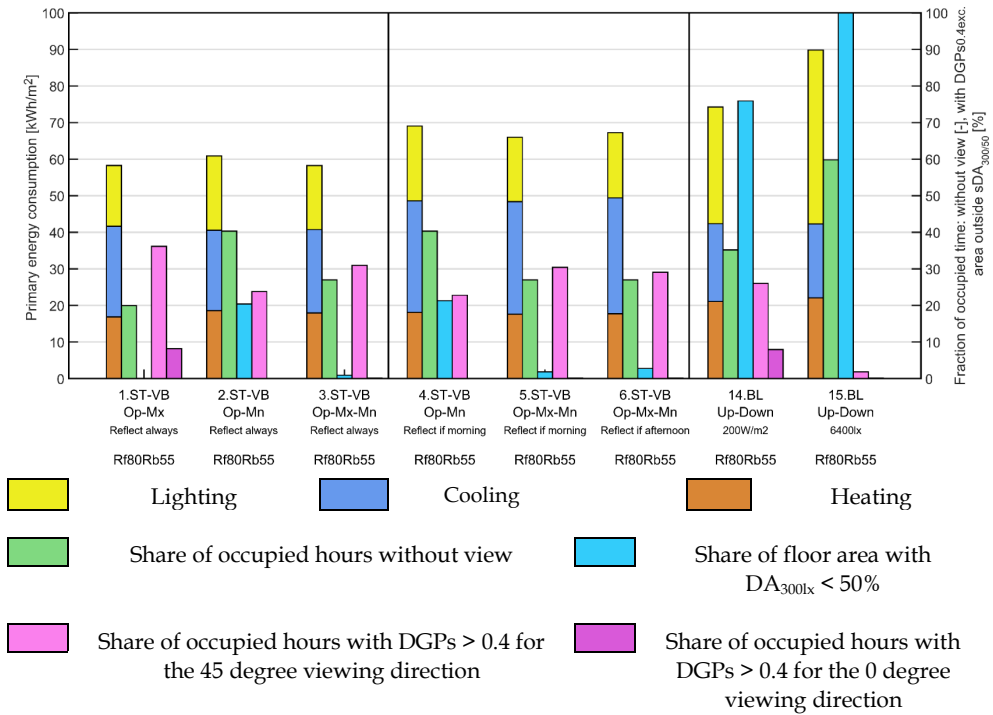
Figure 6.16 Summary of whole building performance predicted using simulations of different sun-tracking approaches for the vertical-blind concept in relation to the automated roller-blind baseline.
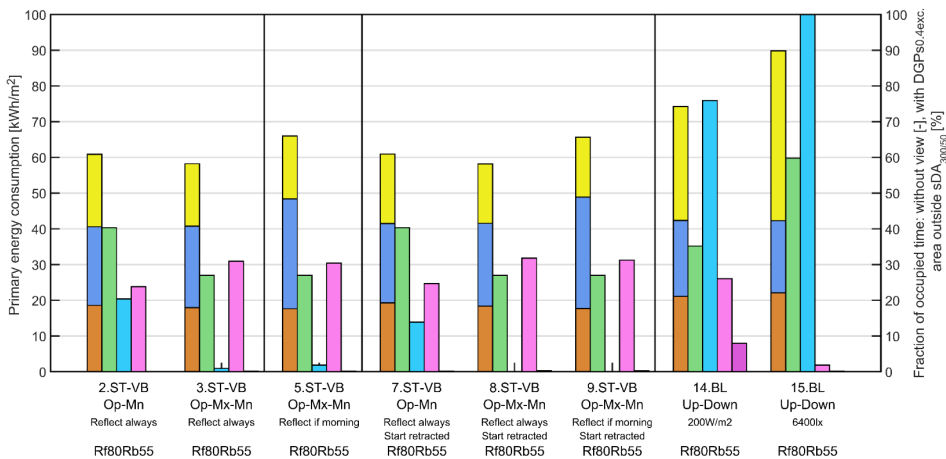
Figure 6.17 Summary of whole building performance of vertical-blind concepts that allow for a full retraction of the blinds (ST-VB7-9) in relation to the sun-tracking concepts that do not offer this functionality (ST-VB1,3,5) and the automated roller-blind baselines (BL 14-15).

In Figure 6.17, the performance of a vertical-blind concept that allows for a full retraction of the blinds (Start retracted) is evaluated. The 7, 8, 9 ST-VB strategies are respectively identical to the 2,3 and 5 ST-VB strategies with the exception that the blinds are fully retracted at the start of the day (Table 6.2). The fully retracting concept only affects daylighting performance and offers only small improvements compared to the previously investigated strategies. The concept increases $sDA_{300lx/50\%}$ by 6, 1 and 2% for 7, 8 and 9 ST-VB respectively.
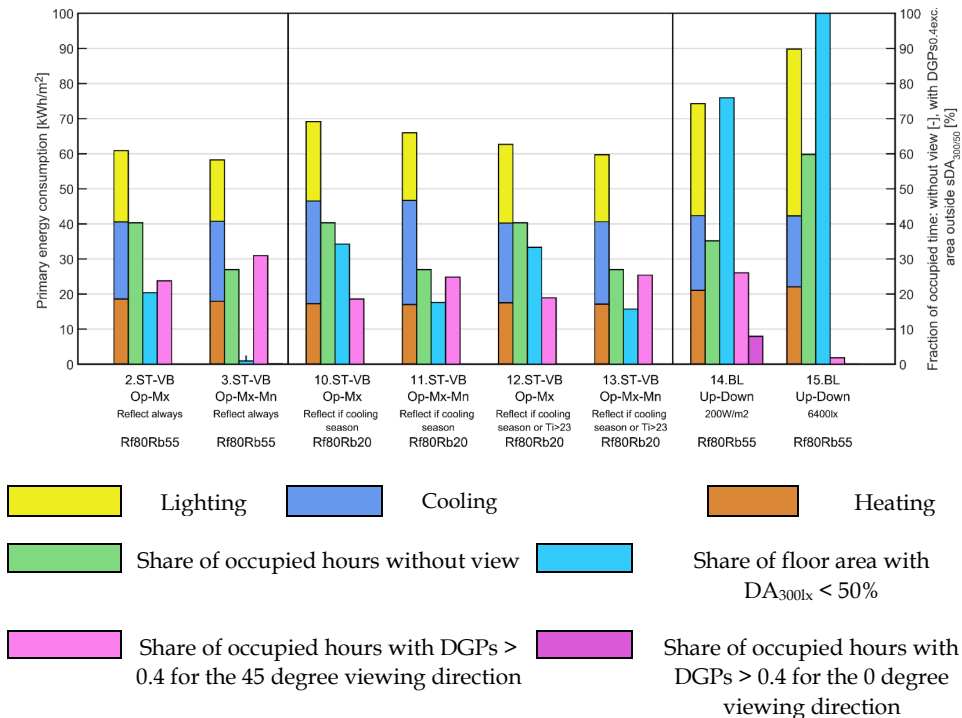
Figure 6.18 Summary of whole building performance of vertical-blind concepts that orient the absorbing side of the blind towards the sun in order to reduce heating energy consumption (ST-VB10-13) in relation to the sun-tracking concepts that do not offer this functionality (ST-VB2,3) and the automated roller-blind baselines (BL 14-15).

Figure 6.18 explores the potential of the concept where the absorbing side of the blind is oriented towards the sun to admit more solar energy and reduce heating energy demand. The Rf80Rb20 material, with a very low reflectance on the backside of the blind, is used and different control rules for switching between the reflecting and absorbing states were tested. 10 and 11 ST-VB follow the same control logic as 2 and 3 ST-VB but now the absorbing side of the blind is oriented towards the sun

during the heating season, which lasts from November until February for the reference office. Using this control logic, the switching concept reduces heating E_{prim} by 1.0-1.3 kWh/m² but increases cooling E_{prim} by 7.7-8.3 kWh/m² due to ineffective control decisions. To avoid such false decisions, the control strategy is improved by adding an indoor convective temperature sensor and only using the absorbing side of the blind if the indoor temperature is below 23 degrees Celsius (12 and 13 ST-VB). Although false control decisions are now reduced, the switching control concept does not offer performance improvements in relation to the original sun-tracking concept. Using the absorbing side of the blind reduces the amount of daylight that is reflected from the blind into the room. This has a detrimental effect on daylighting performance (13-15% less $sDA_{300lx/50\%}$), lighting energy demand and E_{prim} (2.5-2.9% more total E_{prim}).

6.6.2 Performance sensitivity to front and back fabric reflectance

Figure 6.19 shows the performance sensitivity to the blinds' front and back reflectance for the ST-VB strategies where the front side of the blinds is always facing the sun (Reflect always).

The results for the 3ST-VB-Rf80Rb55, 16ST-VB-Rf55Rb55 and 17ST-VB-Rf20Rb55 alternatives show that energy and daylighting performance of the shading system are very sensitive to the solar reflectance of the front of the blind. Both cooling and lighting energy consumption increase strongly for the materials with a lower reflectance. In relation to the high reflectance materialisation (Rf80Rb55), total E_{prim} is 21% higher for the lightly reflecting material (Rf55Rb55) and 55% higher for the dark absorbing material (Rf20Rb55). The 17ST-VB-Rf20Rb55 alternative performs even worse than the baseline scenarios due to its relatively high cooling energy consumption. The daylighting performance of the highly reflecting Rf80Rb55 material is also substantially better, with $sDA_{300lx/50\%}$ being 7% higher than for the Rf55Rb55 material and 24% higher than for the Rf55Rb20 material. With regards to visual comfort, only the 45-degree viewing direction appears to be sensitive to the front reflectance of the blinds and the results show no variations in DGPs for the 0-degree viewing angle.

18ST-VB-Rf80Rb80, 3ST-VB-Rf80Rb55, and 19ST-VB-Rf80Rb20 show that daylighting performance and visual discomfort in the 45-degree viewing angle are the only performance aspects that are sensitive to the back reflectance. Here, only the Rf80Rb20 material leads to a substantial difference in performance (10% lower $sDA_{300lx/50\%}$ and 10% lower $DGPs_{0.4exc45deg}$).
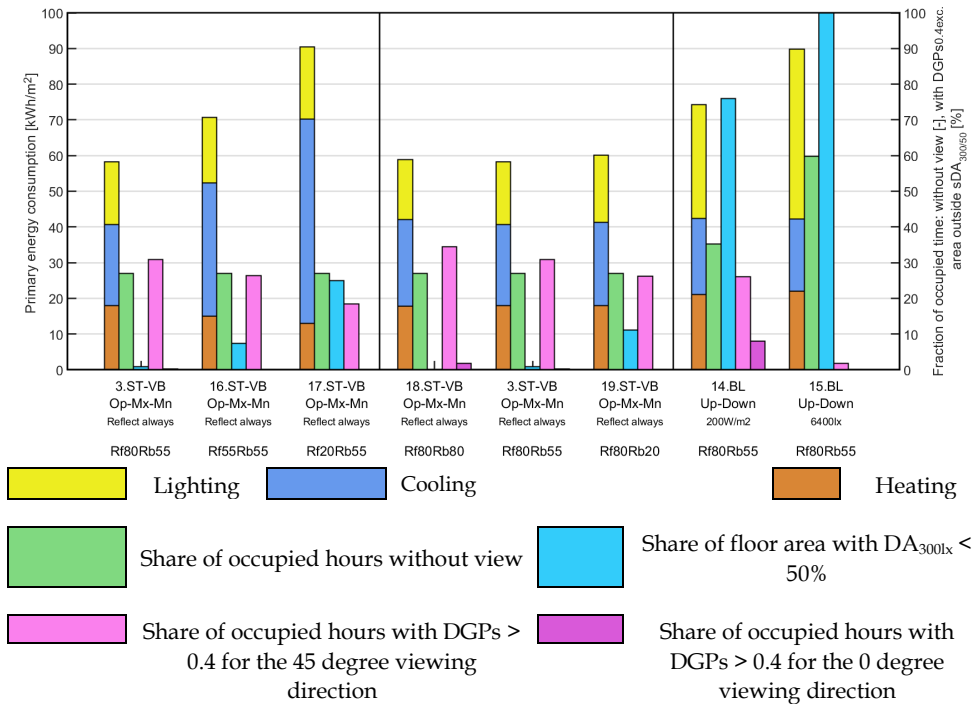
Figure 6.19 Performance sensitivity to fabric front and back reflectance for the sun-tracking control concepts that always use the reflecting side of the blind to track the sun

Figure 6.20 shows the performance sensitivity to the fabric's back reflectance for the ST-VB strategies that switch between using the front and back side of the blind to track the sun. 20ST-VB-Rf80Rb80, 5ST-VB-Rf80Rb55, and 21ST-VB-Rf80Rb20 show that, for the overlapping blinds concept where only a 180-degree rotation is possible, E_{prim}, $sDA_{300lx/50\%}$ and $DGPs_{0.4exc45deg}$ are sensitive to the back reflectance of the fabric. By using a blind that is highly reflecting on both sides (Rf80Rb80) the drawback of the wider blinds concept, increased cooling energy consumption, can be mitigated. There is, however, a trade-off with visual comfort, as with this fabric, there is some occurrence of glare in the most critical viewing direction (2% $DGPs_{0.4exc0deg}$). Using a dark colour for the back of the blind (Rf80Rb20) leads to a situation where the vertical-blinds concept has a higher E_{prim} than BL14.

22ST-VB-Rf80Rb55 and 13ST-VB-Rf80Rb20 show the effects of varying the back reflectance for the concept where the back of the blind is used to absorb solar energy to reduce heating energy consumption. Compared to the Rf80Rb20fabric, the Rf80Rb55fabric offers a better performance trade-off between the ability to absorb solar energy and the admission of sufficient daylight to the interior. The solar absorbing concept (22ST-VB) now offers similar performance to the initial concept

where the reflecting side of the blind is always used to track the sun (3ST-VB) and the reduction (0.3%) in E_{prim} of the absorbing concept is negligible.
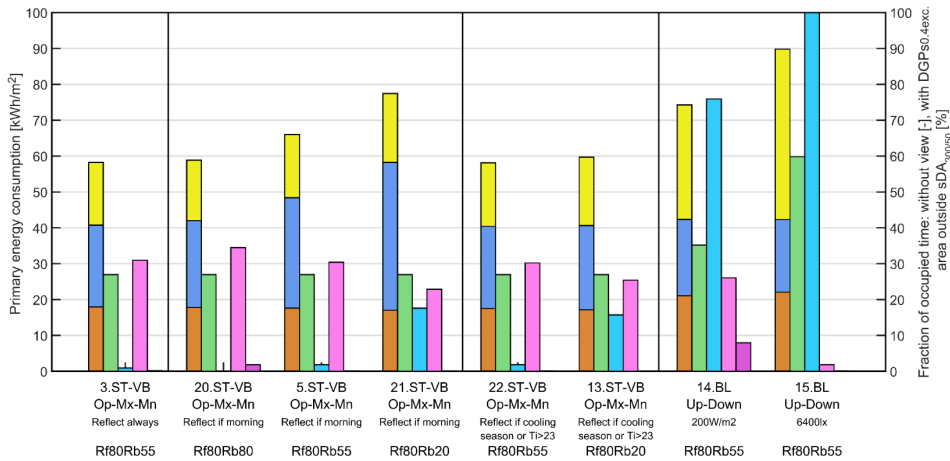
Figure 6.20 Performance sensitivity to fabric back reflectance for the sun-tracking control concepts which switch between using the front and the back of the blind to track the sun

6.7 Application discussion and conclusion

This study evaluated the effects of the ST-VB system on building performance aspects and showed that the ST-VB system offers substantial performance improvements over a conventional automated solar shading solution (22-35% lower E_{prim}, 75-99% higher $sDA_{300lx/50\%}$, 8-33% more $EWF_{40\%;exc.}$ and 8% less $DGPs_{0.4;0deg;exc.}$). Amongst the investigated sun-tracking blind concepts, the 3ST-VB-Op-Mx-Mn-Reflect always alternative, where the reflecting side is always used to track the sun, offers the best performance in terms of E_{prim}, $sDA_{300lx/50\%}$, $DGPs_{0.4exc0deg}$ and $EWF_{40\%;exc}$. This concept also allows for the greatest freedom in choosing the material and visual appearance of the blind. With this concept, using a front reflectance between 55 and 80% offers more beneficial performance than that with the conventionally controlled baselines with a reflectance of 80%. This means that, although using a highly reflecting material offers substantial performance benefits, light-coloured materials such as an uncoated fabric can be used (Rf55Rb55) to improve aspects, such as visual appearance or cost, whilst still offering better building performance than a conventionally controlled highly reflective (Rf80Rb55) roller-blind baseline. Using a dark absorbing material for the front of the blind (Rf20Rb55), however, is not recommended because this greatly increases E_{prim}, causing the ST-VB strategy to perform worse than the baselines. Additionally, with

the 3ST-VB-Op-Mx-Mn-Reflect always strategy, the back reflectance of the blind can be specified without considerable consequences in terms of building performance aspects.

The concept with overlapping blinds, that limits blind rotation to 180 degrees, offers substantial performance improvements over the baseline scenarios (11-27% lower E_{prim}, 72-97% higher $sDA_{300lx/50\%}$, 8-33% more $EWF_{40\%;exc.}$ and 8% less $DGPs_{0.4;0deg;exc.}$). However, this concept does lead to a 13% increase in E_{prim} compared to the strategy where the blinds can make a 360-degree rotation. Here a trade-off will have to be made between reducing disturbances by dangling movements of the blinds or reducing energy consumption. This trade-off can be made on a case-by-case basis because the difference between these two alternatives lies only in the control rules that are applied. With the overlapping blinds concept, energy and daylighting performance are sensitive to the back reflectance of the blind and it is not recommended to use dark absorbing materials (Rb20).

The fully retracting blind concept offered only small improvements in daylighting performance and no substantial benefits in the other performance aspects. Especially for the most promising of the investigated strategies (3 and 5 ST-VB), these improvements do not justify the development of a more complicated motorisation concept.

In this study, the ST-VB concept was tested in a south facing office cell. The presented temporal maps (Figure 6.14) show that the most substantial benefits of the ST-VB strategy occur when the sun is positioned at an oblique azimuth angle in relation to the façade and the VPPA is high. This suggests that the system could potentially offer additional performance benefits for façades that are oriented more towards the west and east, where a low VPPA occurs less frequent during regular daylit office hours.

The solar energy harvesting and reflecting blind concept did not show a substantial reduction in heating energy consumption (0.3% in overall E_{prim}). From this study it can be concluded that there are some inherent limitations to this concept that cannot be easily overcome.

One limitation is that the absorbing fabric, combined with the priority of mitigating daylight discomfort glare, allows solar energy to only be admitted to the inside by means of convective and longwave infrared (LIR) heat gains from the blind surface. The validation cases in Figure 6.13 illustrate that solar energy admitted through these heat-transfer mechanisms, is much less effective at reducing heating energy demand than solar energy admitted as solar radiation. Switching from the situation where the blinds are always closed (6.VD) to the most closed sun-tracking (5.VD) strategy, has a much stronger effect on heating energy consumption (a reduction of

10.6 kWh/m²) than switching from the reflecting to the absorbing (1.VD) state with the sun-tracking strategy (a reduction of 1.8 kWh/m²). These validation cases also show that reducing heating demand by admitting solar radiation causes a smaller penalty in cooling energy consumption than when solar energy is admitted through convection and LIR. The difference between the solar absorbing strategy (1.VD) and the solar admitting strategy (3.VD) shows that cooling energy can even be reduced by admitting beam solar radiation rather than absorbing it. This can be explained by the fact that for this reference office, and many perimeter office spaces exposed to direct solar radiation, there is little space heating demand during the day because solar gains and interior gains are sufficient to heat up the space. In such cases, reducing heating energy demand by increasing convective solar gains is not very effective because these gains are immediate and quickly lead to undesired overheating.

Another limitation of the absorbing blind concept is that there is a strong conflict between wanting to absorb solar energy and wanting to maximise the reflection of daylight into the space. In this study, where visible and solar reflectance are assumed to be closely related, these trade-offs were considerable and reflecting daylight provided the largest daylighting and energy performance benefits. This raises the question of whether this issue could be resolved by applying a spectrally selective material on the absorbing side of the blind. In an ideal case such a material would reflect 100% of the radiation in the visible spectrum and 0% in the near-IR spectrum. Assuming the ASTM G-173 spectral distribution for solar radiation, the solar reflectance of this material would be 0.39 (Nrel 2014). The reductions in heating energy consumption from such a material would lie between the Rb20 and Rb55 fabrics that were tested in this study, and these savings are not sufficient to support further research into this application.

The solar absorbing and reflecting blind concept could potentially be suited for other applications and environments than were tested in this study. The concept is tailored to solar exposed perimeter zones, where daylight glare management is a concern. More promising applications could be found in situations with lower internal gains, lower admission of solar gains, less efficient heating and more efficient, or absent, cooling systems. Possible applications include colder climates, hospital patient rooms, and poorly insulated office spaces with efficient lighting.

In exploring alternative materialisations of the blinds, this study focussed on diffuse solar reflectance. Other design aspects that strongly influence the performance of the system include the direct and diffuse transmittance of the blind. The goal of this study was to support the selection of materials in the early-stage development of the system. Direct and diffuse transmittance can be influenced in each of the material alternatives in Table 6.4 through the application of translucent polymers,

perforations, and fabric openness. It is recommended to investigate the effects of such design modifications in future research.

Some aspects of this case study require further elaboration and should be considered in the interpretation of its conclusions. View is assessed in this study using a simplified approach that focusses only on view quantity and disregards view quality and content, aspects that are known to affect view perception. Additionally, the parallel projection method used in this study has some counter-intuitive characteristics when applied to the vertical blind system. With this method, view performance with the blinds in the most open slat angle position is identical to that when the blinds are fully retracted, and this might not correspond with actual perception of view quantity by occupants in these two instances. Additionally, the method does not address the differences in view to the outdoors that are likely to be perceived from the two occupant positions. Although the applied method has shortcomings, the current state of the knowledge of view quantity and quality is not sufficient to overcome these shortcomings.

In this research, the reflectance of all materialisation alternatives was assumed to be fully diffuse. This assumption is representative for highly diffusing materials (e.g., PVC and metal coated fabrics) it might not be representative for metals with a high specularity (e.g., brushed aluminium) (Mangkuto et al. 2019; De Michele et al. 2018). The influence of blind specularity on the glare and daylighting performance of the ST-VB system is therefore recommended for further research if highly specular materials are considered.

In this study, the prediction of daylight discomfort glare was based on saturation alone. Although research has pointed out that this approach is sufficiently accurate to describe a system where the sun is not in view of an occupant (Wienold 2007), this condition is not always met in the BL14 baseline case. Glare is possibly underestimated in this control alternative.

6.8 Concluding remarks

This study illustrated how the VTB can be used to investigate performance trade-offs in the development of an advanced multi-state solar shading system. The VTB modules for describing systems with time-varying optical and thermal properties were verified. Additionally, a VTB configuration was presented that allows developers to assess the performance effects associated to the selected material properties of the shading device. A series of modules were developed for describing the optical behaviour of the glazing and shading system as an CFS in EnergyPlus using externally computed or measured BSDFs and absorption matrix descriptions.

Additionally, these modules allow the CFS description to be derived for various shading system states from subsystem simulations using LBNL-Window. Although the VTB configuration was only used for straight vertical-blinds and roller shades in this study, it can also describe other types of solar shading devices that are available within the LBNL-Window collection of shading algorithms (screens, horizontal blinds, curved blinds, etc.).

In this study, the performance effects of potential control rules, motorisation concepts and material properties were evaluated within a larger framework of design considerations. As such, this study provided an illustration of how the VTB can be used within the product development context.

The evaluation of the ST-VB concept has provided a number of insights in the causal relationships between shading design parameters and building performance effects and has offered valuable lessons for the development of multi-state solar control systems in general:

- The ability to selectively block direct sunlight whilst admitting daylight from other regions of the sky offers substantial performance benefits. This ability is, however, constrained by the geometry and the degrees of freedom to actuate the position of system. These geometrical features can be exploited if they are designed in accordance with the sun path. For instance, the performance of the ST-VB at low VPPA conditions could potentially be improved by applying a directionally selective blind material (e.g., expanded metal) or combining it with appropriately designed static shading devices. The latter concept will be investigated in Chapter 8.
- The limitation of the investigated absorbing and reflecting blind concept is that the solar, visual and thermal states of the system are coupled, meaning that it is not possible to change the solar reflectance of the system without also changing the amount of daylight admitted to the interior. Multi-state solar shading systems, that can independently adjust the amount of daylight that is transmitted and the amount of solar energy that is admitted, are a promising way forward. Such a system will be explored in Chapter 7.
- For perimeter sun-exposed spaces of office buildings, instances with high incident solar radiation usually do not coincide with a space heating demand. Solar control devices that seek to harvest the benefits of solar energy for reducing heating demands should therefore include mechanisms for energy storage or conversion. Admitting solar radiation to be absorbed by interior surfaces is a more effective mechanism to achieve heating energy reductions than by absorbing this radiation using a shading device with low thermal capacitance. Admitting solar radiation in this way can, however, conflict with the goal of prohibiting daylight glare. Possible strategies for

overcoming these limitations could include: (i) Admitting solar radiation during unoccupied moments or (ii) admitting more solar energy in parts of the space where this would not lead to risk of glare (Rizi and Eltaweel 2021). In the ST-VB concept this could, for instance, be achieved by opening the blinds during weekends in the heating season or splitting the blinds into groups that use different slat angle rotations across a façade.

7 Design and control optimisation of a multi-state double roller blind system

7.1 Introduction

Detailed fabric design features, such as the size, spacing and reflectance of fabric threads, define the optical behaviour of the shading device and its effects on the indoor climate (Bueno et al. 2020; Chi et al. 2017). More open types of fabrics admit more daylight and offer a greater degree of view through the fabric. They do, however, also offer less protection against daylight discomfort glare because of their high specular transmittance of daylight. The potential of using building performance simulation to identify fabric characteristics that offer beneficial performance trade-offs has thus far been largely unexplored. Chapter 6 showed that optimal automated shading performance results from a careful deliberation of both shading design and automated control aspects. Although these aspects have been investigated individually the concept of combined optimisation requires further research.

This chapter focusses on optimization of the control strategy and the design of the shading material (the B and C levels-of-scale in Table 2.1). The study presented in this chapter takes the perspective of the developer of a novel automated shading solution who seeks to leverage the potential of using high openness fabrics to admit more daylight and view to the outdoors whilst protecting against daylight discomfort glare by utilising multiple fabrics with dedicated functions. The starting point of this study is a double roller blind system that uses two shading fabrics that have a different visual transmittance. By lowering the two shades to various heights, the system can take on a variety of optical states to admit more or less daylight, in response to varying outdoor conditions. The system therefore offers more freedom to influence the admission of daylight and potentially better trade-offs between daylighting performance and discomfort glare, than with the systems that were evaluated in the previous chapters. The simulation purpose of the developer of the double roller blind system is to:

i.   Improve the value proposition of the double roller blind concept by co-optimising control behaviour and detailed shading fabric characteristics.
ii.   Identify a control algorithm that exploits the large variety of optical states that the system offers for effective daylight utilisation, whilst being compatible with conventional control hardware and software.

Table 7.1 gives an overview of the main goals and assumptions in this study in addition to the characteristics of the shading system that is investigated.

Table 7.1 Goals, assumptions and system characteristics in application study 3

Optimise:	Assume:	System:
Control rules	Sensors	Variable height double roller shade system
Control thresholds	Motorisation system	Time-varying thermal/optical properties
Shading fabric (miliscale)	Glazing system Building	Complex control logic

The use of high openness fabrics in this study, calls for a different approach to glare assessment than was taken in the previous chapters. With high openness fabrics, situations can occur where the sun is visible through a shading device, causing a large contrast between the specularly transmitted sunlight and the otherwise dark interior conditions. To predict the risk of glare under these conditions both the saturation and the contrast terms of the DGP algorithm (Equation 2.1) are important (Wienold et al. 2019). Simulating the luminance distribution images that are required to assess the DGP contrast term is, however, computationally expensive. This chapter therefore employs and tests a VTB module that allows for computationally efficient simulation of daylight discomfort glare for cases where both contrast and saturation are relevant. Additionally, this Chapter will explore the conditions under this more complex modelling approach is needed and provide insights into fit-for-purpose glare performance assessment.

Predicting the performance effects of design choices regarding detailed shading fabric features, requires fit-for-purpose optical models in each of the modelling domains (e.g., thermal, daylight illuminance, daylight luminance). Additionally, these optical models need to be provided with consistent input information. A toolchain of VTB components is developed and tested in this Chapter for this purpose.

In order to fully exploit the large number of optical states that the double roller blind system offers, the control strategy needs to be able to detect when using a high openness fabric would lead to unacceptable discomfort glare such that it can activate an optical state were less daylight is admitted. This means that the control strategy must accurately classify complex daylighting conditions where discomfort glare is related to the DGP contrast term. This chapter will test a support method for developing performance-based control strategies that are tailored to identify optimal control actions under such complex conditions using only the limited set of sensor and solar position data that would be available during the systems operation. In Section 2.5, promising MPC approaches were reviewed that have been proposed

for controlling automated shading systems in a performance-based manner. This review pointed out that certain features of these approaches limit their scalability in the current context, that is: the skill and effort that is required to deploy such a strategy in a building, and the computational effort that is needed in either the operational or the planning phase (Killian and Kozek 2016; Jain et al. 2018). In addition, the MPC approach creates control strategies that are not easily interpreted making it hard for shading or control contractors to inspect, audit and trust such control strategies (Jain et al. 2018; Killian and Kozek 2016). The support method that is proposed in this chapter is explicitly designed to be more efficient in its application and match better with current control development and deployment practices.

In the support method classification trees are generated from simulation results and used as detection algorithms within the shading control strategy. This approach extends the support method that was presented in Chapter 5 by automating some of its manual tasks and is specifically tailored to systems with a large number of optical states that involve more complex visual comfort conditions than with the shading systems in the previous chapters. The following requirements were defined for the support method in this application:

   i.   It can accurately classify complex visual comfort conditions.
  ii.   It leads to control strategies that are based on performance goals and that can exploit the potential of shading systems that offer many optical states.
 iii.   Its application and the resulting control strategies are scalable, that is:
      a. Compatible with conventional deployment practices and low-cost control hardware and software.
      b. Generically applicable and not tied to a particular type of shading system or building application.
      c. It can be applied efficiently and minimises the effort and skill that is required of a developer.
      d. It leads to control strategies where the control logic is interpretable, allowing them to be audited and adjusted without specialist knowledge.

7.2 The initial concept: a multi-state double roller blind system to achieve an adjustable visible transmittance

7.2.1 Working principle

Figure 7.1 illustrates the double roller blind concept. The concept is based on observations regarding fabrics with varying degrees of visible transmittance that are illustrated in Figure 7.1 and Figure 7.2. Figure 7.2 shows that, although the fabrics with high (20%) and intermediate (5%) transmittance provide sufficient glare protection under certain conditions, they cannot guarantee a glare free environment at all times due their specular transmittance of direct sunlight (Figure 7.1). Therefore, fabrics with a low visual transmittance (1%) are commonly used on solar exposed facades. Figure 7.1 shows, however, that this low transmittance is not always needed, and that daylighting performance can be improved at these moments if a fabric with a higher transmittance is used. The double roller blind concept seeks to exploit this by activating either a high transmittance shade, an intermediate transmittance shade, or both shades simultaneously to obtain the equivalent of a single low transmittance fabric.

A. Only front shade activated
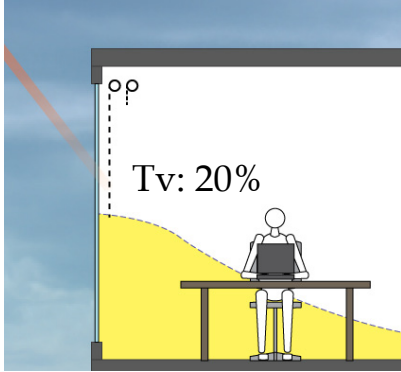
DGP: 0.46, Intolerable glare, D_{300lx}: 100%

Tv: 20%
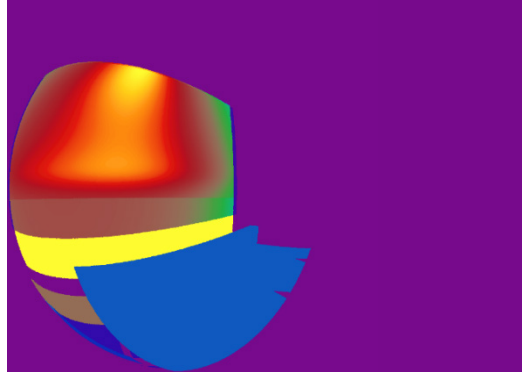
B. Only back shade activated
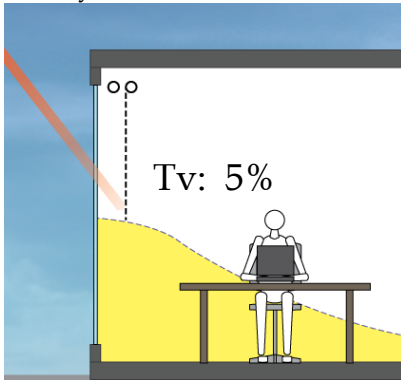
DGP: 0.37, Perceptible glare, D_{300lx}: 97%

Tv: 5%
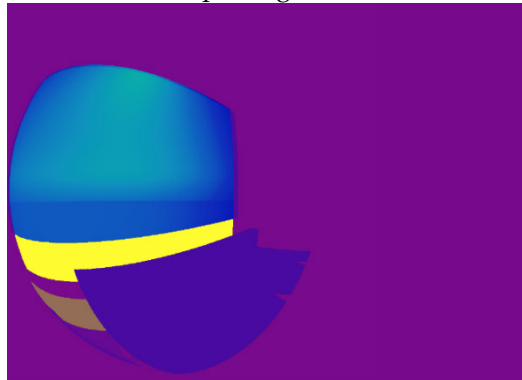
C. Both shades activated
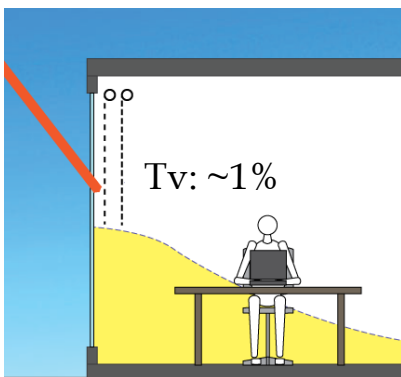
DGP: 0.36, Perceptible glare, D_{300lx}: 69%

Tv: ~1%

Cd/m2
5000
4500
4000
3500
3000
2500
2000
1500
1000
500
0
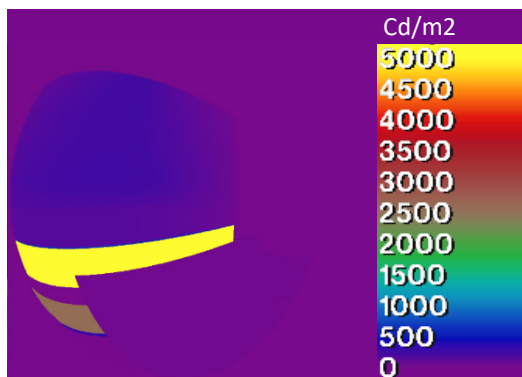
Figure 7.1 Left: working principle of the double roller blind concept. Right: corresponding luminance distribution for each of the shading states under largely clear sky conditions at 14:00, 18th of April

Figure 7.2 Daylighting and glare performance2 of the sun tracking roller blind strategy from Chapter 5 using three fabrics of varying visual transmittance. Results for the 18th of April, a day with largely clear sky conditions
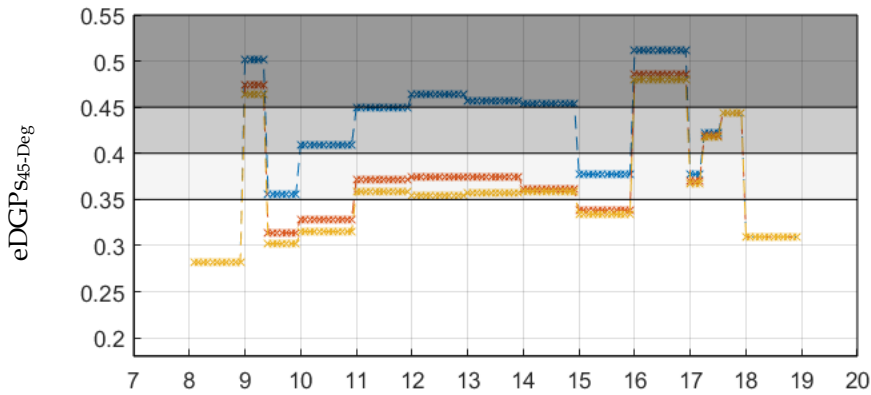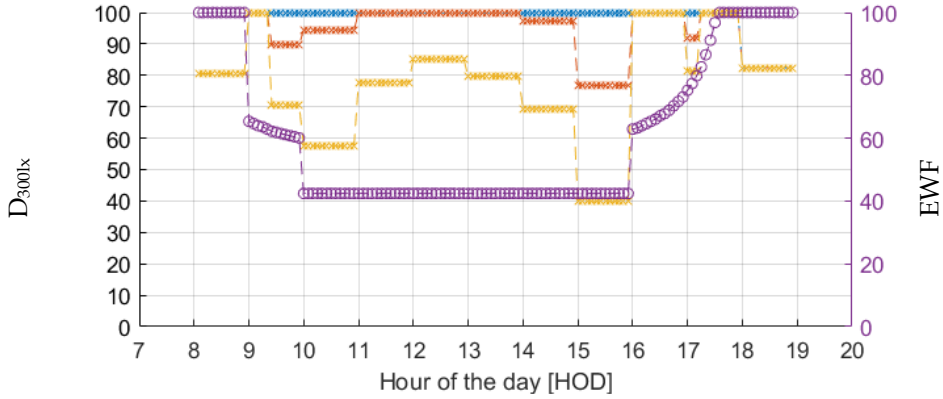
- – –✕– – Performance of front shade only Tv:20%, $SCmm_{CM1AU;2SC;3EL}$
- – –✕– – Performance of back shade only Tv: 5%, $SCmm_{CM1AU;2SC;3EL}$
- – –✕– – Performance of front and back shade Tv: 1%, $SCmm_{CM1AU;2SC;3EL}$
- – –◦– – Exposed window fraction (EWF) in the $SCmm_{CM1AU;2SC;3EL}$ strategy

7.3 Methodology and simulation strategy

Figure 7.3 gives an overview of the workflow that is followed in this application study, its subsequent steps, and the corresponding chapter sections where each step is discussed.

---

2 Two instances can be noted where all fabrics lead to intolerable glare. This is related to the chosen control strategy that was designed to offer protection from 'disturbing' glare only in the 0-Degree viewing direction. In the Chapter 5 study, this was considered sufficiently acceptable.

Configure VTB and develop new modules (7.3.3) and support methods (7.4)

7.5 Verify eDGPs$_{3PHS-Rpict}$ simulation toolchain and parametrisation method:

7.5.1: Validate eDGPs$_{3PHS-Rpict}$ method (A.3) by comparing glare performance predictions with DGP$_{rpict}$ and DGPs$_{3PHS}$

7.5.2:Validate implementation and parametrisation of optical models (B.2, B.3.1 and B.4) by comparing their predicted optical behaviour to measured fabric data

7.5.3:Analyse performance sensitivity to fabric design parameters and verify VTB configuration

7.6.1 Control strategy development using classification trees:

Simulate each mode of operation (SM1CM1 to SMnCMn) for the double roller blind system

Develop classification tree detection algorithms based on simulated glare performance of each mode of operation

Verify the generated classification trees by evaluating the accuracy of their performance classifications based on simulated predictors

7.6.2 Performance assessment of the multi-state double roller blind system:

Simulate the performance of the double roller blind system, controlled using classification trees. Benchmark the system against a single roller blind system controlled using conventional and advanced approaches

7.6.3 Control refinement:

Improve performance trade-offs of the control strategy through analyses of simulation results and addition of heuristic control rules

7.7 Conclusions regarding the potential of the double roller blind concept and recommendations for its further development

Figure 7.3 Overview of the methodology followed in the study that is presented in this chapter

7.3.1 Investigated type of shading fabric

To obtain a shading device that offers a high degree of daylight admission and view to the outdoors, the design of the shading fabric needs to be considered. Solar

shading fabrics are available in a wide variety of weaves and materials that together determine the optical behaviour of the fabric. It is common in the shading industry, however, to specify shading fabrics using a set of optical properties that describe the behaviour of the fabric as a whole. To illustrate these properties, and the resulting optical behaviour, Figure 7.4 shows the measured optical behaviour of five fabrics from the CGDB (Mitchell 2017) with very different types of optical behaviour.
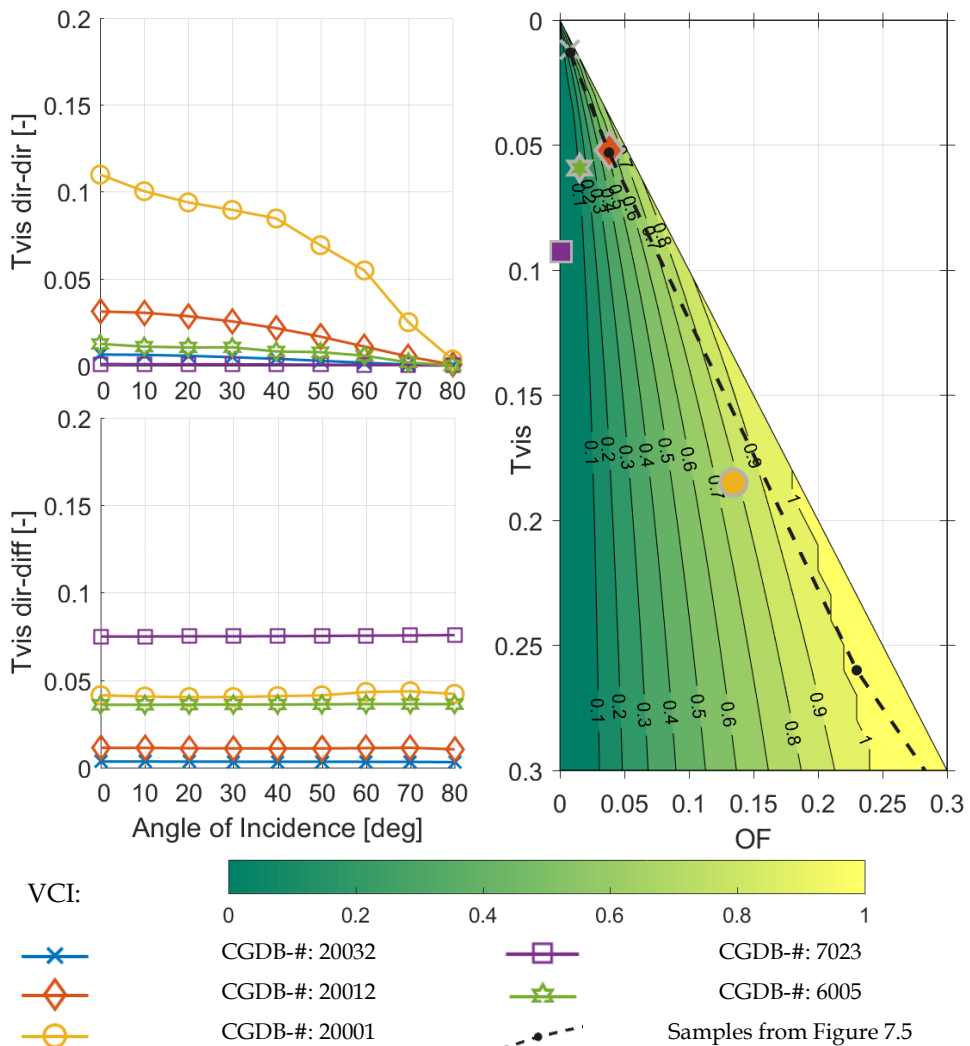
Figure 7.4 Simulated $T_{v;dir\text{-}dir\text{-}\theta}$ and $T_{v;dir\text{-}diff\text{-}\theta}$ using BSDF of measured fabrics (left) and VCI (right) for a selection of fabrics from the IGDB

For mitigating glare, the direct-to-direct transmittance ($Tv_{dir-dir-\theta}$) of the fabric is the most important characteristic. This angularly dependent quantity is often specified using the $Tv_{dir-dir-0}$ at normal incidence also referred to as the openness factor (OF). Additionally, the cut-of-angle (COA) of the fabric is sometimes specified to also describe the angular dependency of the $Tv_{dir-dir-\theta}$ in a simplified manner. The COA is defined (Cen 2017a) as the incidence angle under which direct light transmittance is no longer perceivable ($T_{dir-dir-\theta} < 0.005$), which is 75-80° for the fabrics in Figure 7.4. For daylighting performance, the overall visual transmittance (Tv: $Tv_{dir-dir}$ + $Tv_{dir-diff}$) of the fabric is the most determining property.

Konstantzos et al. (2015a) investigated user assessments of the clarity of view through fully lowered roller shades when viewed frontally. Their research showed that the clarity of view assessment depended strongly on fabric openness and visual transmittance and they proposed the empirically derived view clarity index (VCI), shown in Equation 7.1, for comparing different fabrics. A value of 1 for this index represents a fabric that users assessed as offering a clear view to the outside allowing outside objects and weather conditions to be discerned in vivid colour. A value of 0 represents a fabric that users assessed to offer none of these characteristics.

$$VCI = 1.43 \cdot OF^{0.48} + \left(\frac{OF}{Tv}\right)^{1.1} - 0.22 \qquad (7.1)$$

VCI: View clarity index, OF: Openness factor of fabric, Tv: visual transmittance

Figure 7.4 (right) also shows the VCI for the 5 measured fabrics. The graph shows that a high VCI can be achieved with fabrics that lie close to the diagonal in the image, that is: specularly transmitting fabrics (e.g., #20032, #20012 and #20001), that are characterised by a high OF and a small difference between T_{vis} and OF. This type of fabric is selected for the double roller blind system in this application study in order to maximise the degree of view to the outside when only one of the shades is lowered. These fabrics are characterised by a weave pattern that forms rectangularly shaped openings, where the size of the openings can be used to design fabrics of widely varying OF and Tv. This is illustrated by the images of the fabric samples, shown in Figure 7.5 whose optical properties are indicated by the dashed black line in Figure 7.4.

In this study, a series of sensitivity analyses will be presented where the performance effects of varying shade fabrics will be investigated. In the assessment of the double roller blind system, the two fabrics, summarised in Table 7.2, will be used. These, and other fabrics, will be referred to using their Tv, OF and VCI. For the most open front shade a Tv22OF20VCI100 fabric will be used. For the less open back shade, a Tv07OF05VCI59 fabric will be used. When both shades are lowered this leads to a situation were at most 1% of light is specularly transmitted. Both shades have metallised coating with a high solar reflectance.
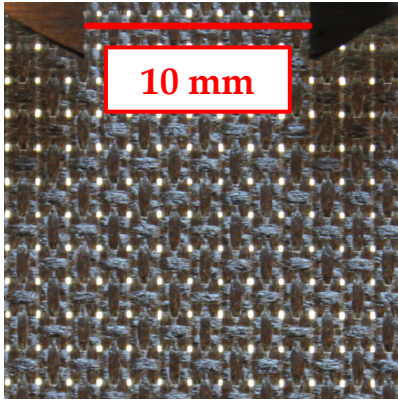
A. CGDB#:20032 | Prod.nr: 802998 | OF: 2%
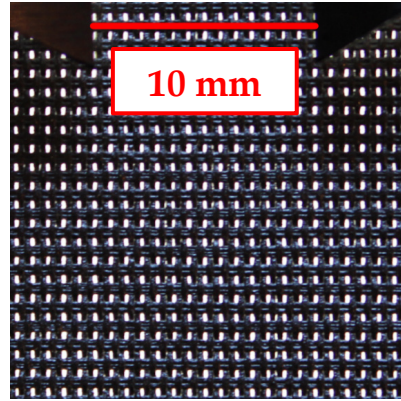
B. CGDB#:20012 | Prod.nr: 205EC01 | OF: 4%
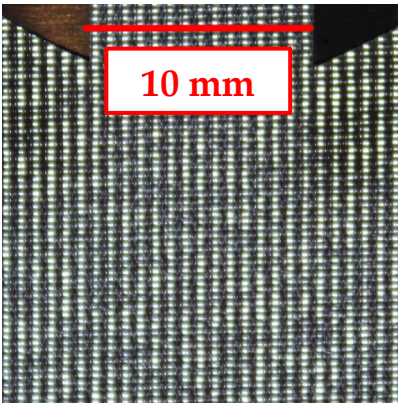
C. Product nr: 816 829 | OF: 23%
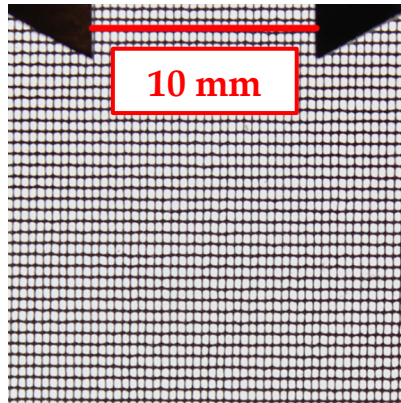
D. Product nr: 858 829 | OF: 51%

Figure 7.5 Close up photographs of four fabrics that are representative for the type of shading devices that are used in this study.

Table 7.2 The two shading fabrics that are used in the double roller blind strategy

	$Tv_{dir\text{-}hem\text{-}0}$	$Tv_{dir\text{-}dir\text{-}0}$	$Tv_{dir\text{-}diff\text{-}0}$	OF	$R_{vis/sol;front}$	$R_{vis/sol;back}$	COA	VCI
Front shade	0.22	0.20	0.02	0.20	0.67	55	75	0.9
Back shade	0.07	0.05	0.02	0.05	0.74	55	75	0.5

7.3.2 Performance aspects and indicators

The performance aspects of interest in this study are daylight quality, visual comfort, view to the outdoors, energy performance and the disturbance of occupants by shade movements. For daylighting performance and energy performance the same indicators are used as in the previous chapters.

Because the double roller blind system employs fabrics with a high specular transmittance, both the saturation and the contrast terms of the DGP algorithm (Equation 2.1) are likely to be relevant in assessing the likelihood of visual discomfort. The DGPs indicator has been shown to give inaccurate predictions in situations where the sun is visible through a shading device (Wienold et al. 2019), causing a large contrast between the specularly transmitted sunlight and the otherwise dark interior conditions (Figure 7.1). Therefore, the regular DGP approach that includes both the saturation, adaptation and contrast terms will be used as a performance indicator in this study.

The same occupant positions and viewing directions are used as in the previous chapters. In this study, however, a more stringent visual comfort performance goal is defined. For the most critical 0-degree viewing direction the double roller blind strategy is to offer the highest degree of glare protection, defined in EN 14501 as having 'perceptible' glare or worse (DGP ≥ 0.35) for at most 5% of all occupied hours (Table 2.2). For the other, 45-degree viewing direction, a medium degree of glare protection (DGP ≤ 0.40 for at least 95% of time) will be the goal.

For both viewing directions, the share of occupied hours were the 'perceptible' and the 'disturbing' glare criteria are exceeded is presented for each shading strategy. When both indicators are presented in a single graph using stacked bars, the $DGP_{0.35exc}$ bar shows the time that is spent within the range that is classified as 'perceptible' but not 'disturbing' glare (0.4 ≥ DGP ≥ 0.35).

The effects of the dynamic operation of the double roller blinds system on view quantity will be assessed using the exposed window fraction (EWF). Additionally, the VCI of each investigated shading fabric will be reported to give an idea of the visibility through the shading device. Because there is insufficient empirical knowledge to substantiate a quantitative combination of the two indicators, this combination will be assed qualitatively. To facilitate this, three indicators based on the EWF method will be reported:

- $EWF_{shFshB;40\%;exc.}$: the share of occupied hours that both shading devices are positioned above seated eye level (1.2 meters height) leaving more than 40% of the window exposed.
- $EWF_{shB;40\%;exc.}$: the share of hours that only the back shade is raised above 1.2 meters and the front shade is positioned lower than that. For the double roller

blind system this means that a user has a view through the Tv22OF20VCI90 front shade and an unshaded view of the window at least below desk height.

- $EWF_{shF;40\%;exc}$: the share of hours that only the front shade is raised above 1.2 meters, leaving the user with a partial view through the Tv07OF05VCI50 back shade.

When both shades are lowered simultaneously below 1.2 meters, the users are assumed to have no view to the outdoors. Also. when a single low openness Tv02OF01VCI20 shade is lowered below 1.2 meters users are assumed to have no view.

Exploiting the increased daylighting potential of the double roller blind system is likely to lead to more movements of the shading devices than with a conventional system. The literature regarding the disturbance of occupants by automated shade movements does not provide a clear quantitative relationship between the severity and frequency of disturbance and the characteristics of shade actuations in terms of their frequency and the magnitude of displacement during an actuation. Based on user assessments of various shading control strategies Bakker et al. (2014) found that users experience infrequent discrete shade movements to be less distracting than more frequent continuous shade actuations. Karlsen et al. (2015), however, found that users were more satisfied with a continuously sun-tracking control logic than with strategies employing discrete full-open and close actuations.

In this study, it is assumed that large shade actuations where one shade goes from a completely raised to a largely lowered state within one time step, have the most potential to be disturbing. This type of control decision will be addressed in this study as a shade actuation (SA). Secondly, it is assumed that shade movements (ShMv) were the system changes the height of an already lowered shade are also disturbing, but to a lesser extent. Sun-tracking shade movements are counted amongst the ShMv, including movements were both shades are moved simultaneously according to a sun-tracking control logic.

Because it is unclear whether the frequency or magnitude of movements are most defining for occupant disturbance, two sets of indicators will be used that each underline the importance of one of these aspects. In the first set, the total distance travelled throughout a year during SA and ShMv will be used as an indicator. Here, a distinction will be made between the distance travelled during small ShMv (less than 20 cm in a single time step) and large ShMv (more than 20 cm). In the second set of indicators, the number of SA and ShMv instances will be counted. The number of large movements will be referred to in terms of the average number of movements per workweek and workday.

7.3.3 Configuration of the virtual testbed

Figure 7.6 shows how the VTB was configured for this study. To be able to give reliable predictions of glare probability for a situation with a fabric shading device with a high specular transmission and give insight into the performance effects of detailed fabric design features, the VTB was extended with additional features.

Predicting the contrast related terms in the DGP formula requires HDR images that describe the luminance distribution in the occupant's field of view. Generating these images using the Radiance *rpict* program, requires many ray tracing operations and is computationally expensive. Using this approach to compare a multitude of design and control alternatives is not practically feasible.

In principle, the 3PHS method can also be used to generate the luminance distribution at shorter simulation times but there are limitations to this approach that cause it to be unsuited to fulfil the goals of this study. The discretisation of the sky in the 3PHS method causes the solid angle that is subtended by the sun, when viewed from an interior sensor point, to be larger than it is in reality. To maintain a physically accurate amount flux transfer, the *genskyvec* program lowers the luminous intensity of each sky patch proportionally. Although this method is sufficiently accurate in predicting the overall distribution of indoor illuminance, it does not describe the luminance, size and position of peaky glare sources accurately enough to predict the glare contribution of the contrast term in Equation 2.1 when a fenestration system with a high specular transmittance is used (Ward et al. 2011).

To overcome these issues, the VTB configuration in this study uses the enhanced Daylight Glare Probability simplified (eDGPs) approach, where different simulation methods are used to compute (i) the contrast related terms and (ii) vertical illuminance ($E_{v;glare}$) that are required for the DGP algorithm (Wienold 2009b). This allows computationally efficient methods to be tailored to each of the formula's components. The prediction of $E_{v;glare}$ requires an accurate description of ambient daylight contribution that results from multiple interior and exterior light reflections. Here, it is not essential to describe the luminance and apparent size of light sources seen by interior points exactly as long as the predicted amount of received luminous flux is predicted accurately. The prediction of the contrast terms, however, does require that the luminance and size of glare sources is accurately described but depends less strongly on the ambient daylight contribution.
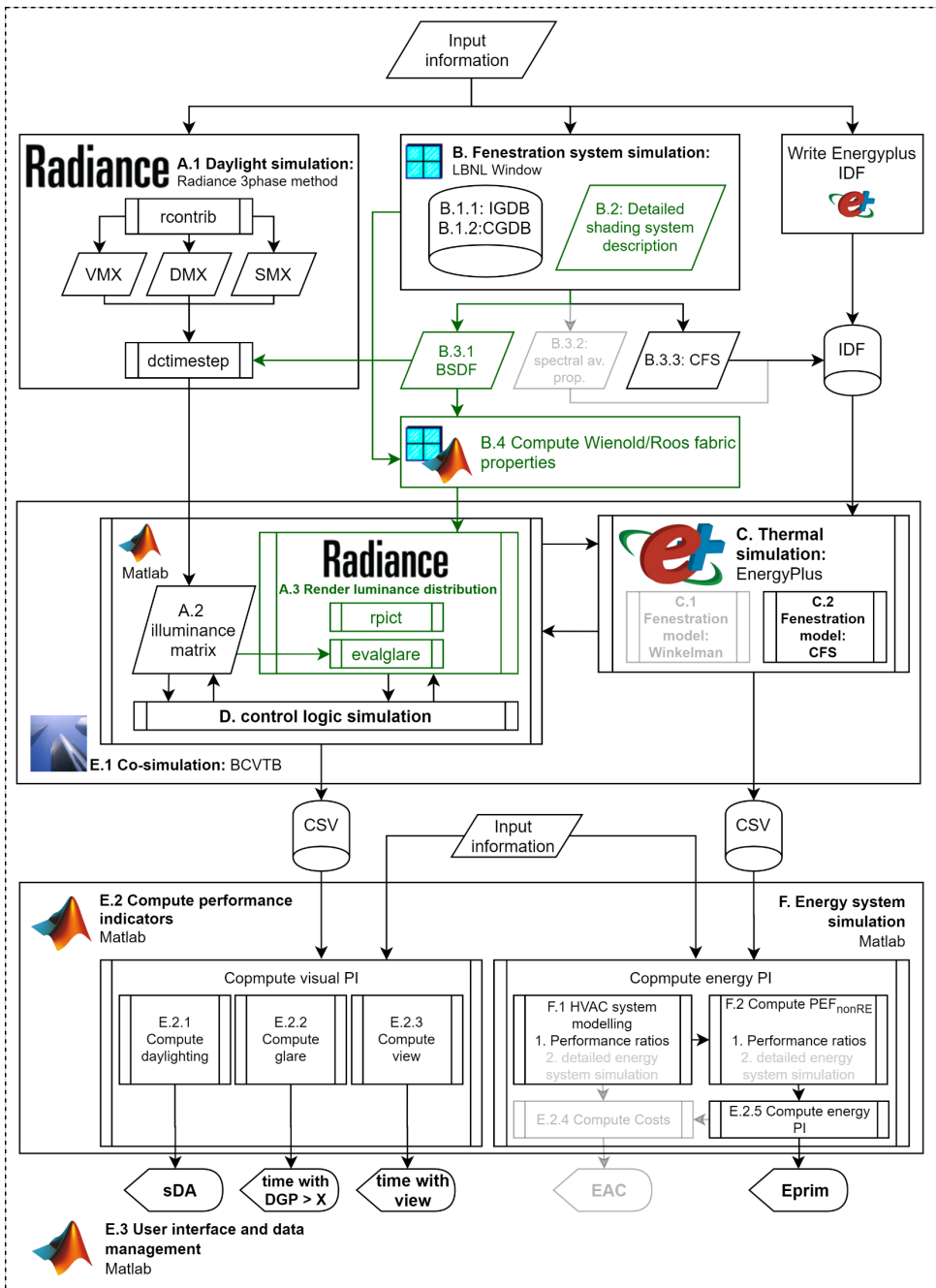
Figure 7.6 Configuration of the VTB for this application study. VTB components that are not used in this configuration are shown in light grey. New VTB modules that will be tested in this chapter are shown in green. The input information refers to the geometry and parameters that are specified in Sections 4.2 and 7.3.4

Table 7.3 The required parameters by different glare metrics, the simulation methods applied in this study and the resulting angular resolution in the prediction of glare sources

Metric	Physical quantities	Method	Daylight component	Simulated sun apex angle	Angular BSDF resolution	Actual sun apex angle
DGPs	E_v	3PHS	Direct + Diffuse	3° (MF:4)	13.5°	Sun: 0.5° Circumsolar: 3°
eDGPs	E_v / L, ω, P	3PHS / Rpict	Direct + Diffuse / Direct	3-13.5° / 0.5°	13.5° / continuous	
DGP	E_v, L, ω, P	Rpict	Direct + Diffuse	0.5°	continuous	

To efficiently fulfil these requirements, the VTB configuration uses the eDGPs$_{3PHS+Rpict}$ approach, proposed and validated by Abravesh et al. (2019), where $E_{v;glare}$ is simulated using the 3PHS method (A.1 in Figure 7.6) and the luminance distribution is simulated using the Radiance rpict program (A.3) with a low number of ambient bounces (the -ab parameter) to reduce simulation time.

Table 7.3 gives an overview of the different glare metrics and simulation methods that are applied in this research and the factors that influence the angular resolution of glare sources as seen from interior sensors. The table clarifies the limitations of the 3PHS method in predicting the luminous distribution. The table also points out the importance of the angular resolution in describing the specular transmittance of light through the shading device. Using the Klems BSDF description as an optical model distributes transmitted sunlight across a large outgoing solid angle, causing an inaccurate description of the luminance and the size of the sun as a glare source. The eDGPs$_{3PHS+Rpict}$ approach therefore uses the Wienold-Roos optical model, that allows the angular transmittance through the shading fabric to be described with a higher angular resolution. This semi-empirical model was initially derived by Roos et al. (2001) to describe the optical behaviour of different kinds of coated glass panes and Wienold et al. (2017) obtained parameters that allowed this model to be used to also describe shading fabrics. The model is described by the *roos_fabric* function and implemented as a *BRTDfunc* material that are not part of the default Radiance distributable. To describe the time-varying optical properties of the double roller blind system the CFS module (C.2), presented in Chapter 6, is used in EnergyPlus.

7.3.4 Assumptions and simulation input parameters
This study uses the reference office assumptions that were presented in Section 4.2. Figure 7.7 shows the setup of the Radiance models that are used in this study. The Wienold-Roos shade model describes the shading system using two material layers.

Each of these layers needs to be assigned to a separate surface that together describe the shading device. To describe the variable height shading system, these two surfaces are split into 10 segments. The window is also described using the Wienold-Roos model that is assigned to two adjacent window surfaces. Table 7.4 summarises the most important simulation settings and assumptions.
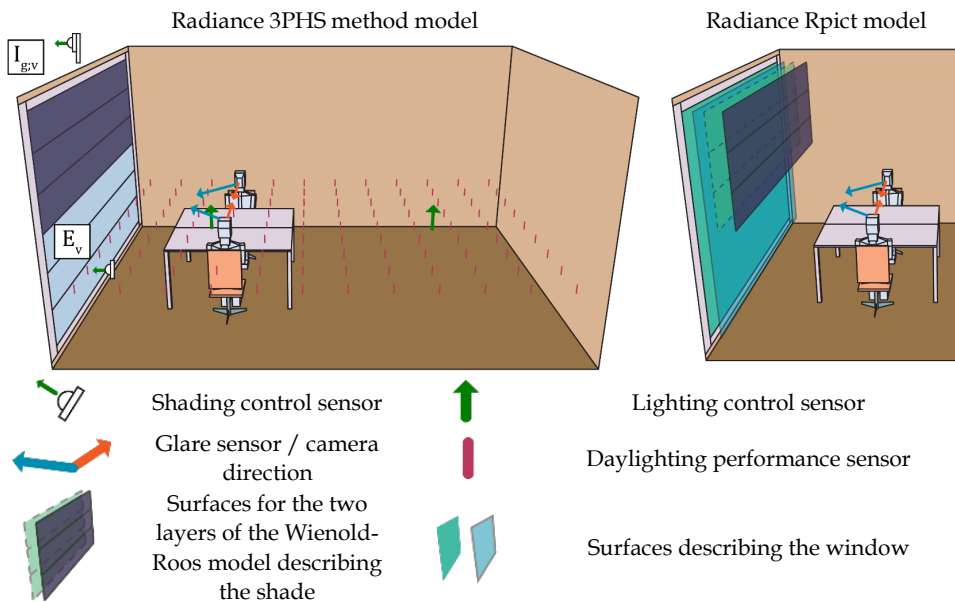
Figure 7.7 Setup of the Radiance models for the 3PHS simulations (left) and the Rpict simulations (right). In the actual models the window and shading system were split into 10 segments.

The double roller blind system will be compared to three baseline strategies:

- The conventional up-down, $I_{g;v} \geq 200$ W/m^2, BL$_{200W}$ strategy, presented in Chapter 5.
- A conventional up-down, $E_v \geq 4500$ lux, BL$_{4500lux}$, where the control threshold is chosen to provide a high degree of glare protection in the 0-degree viewing direction (eDGPs$_{0Deg;0.35;Exc.} \leq 5\%$).
- The SC$_{mm-I-Ev-CM1,2,3}$ optimised sun-tracking control strategy from Chapter 5. The name of this strategy is shortened to SC+ in this study. The control thresholds of the SC+ were again optimised as in in Chapter 5 but now using a more stringent glare performance criterion (eDGPs$_{0Deg} \leq 0.35$).

All baseline strategies will employ a fabric that provides the same degree of glare protection in a fully lowered position as the double roller blind system when both shades are lowered. To achieve identical optical behaviour, the same model is used

as in the double roller blind case but with the baseline strategies, the two shading devices are synchronised according to the BL and SC+ strategies. For reference, the single shading device SC+ strategy will also be investigated with only the front shade or only the back shade of the double roller blind strategy.

Table 7.4 Simulation parameters and assumptions

	EnergyPlus	Radiance	
		3PHS	Rpict
Fenestration		Glazing properties from IGDB: Lay 1: IGDBnr-11560, Lay 2: IGDBnr-1608	
		LBNL-Window perforated screen model	Wienold-Roos shade model
	CFS	BSDF	BRTDfunc
Interior surfaces		Lambertian reflectors: Ceiling R_{vis}: 0.8, Wall R_{vis}: 0.5 Floor R_{vis}: 0.2	
Simulation settings	Idealised HVAC system: unlimited capacity and ideal response	Sensor grid: 9X12	Rpict: -ab 0 -ad 2048 -as 512 -ar 256 -aa 0.13 -lr 6 -st 0.02 -dj 0.00 -ds 0.2 -dp 512
		$VMX_{rcontrib}$: -ab 12 -ad $5 \cdot 10^4$ -lw $2 \cdot 10^{-6}$,	
		$DMX_{rcontrib}$: -ab 2 -ad 10^3 -lw $5 \cdot 10^{-4}$ -c 3000	
		S and DMX sky resolution: MF3	
	5 min. time step	hourly time step	variable time step (if Ev changes)

7.4 Support methods

The following sections present the support methods that were developed for this application study.

7.4.1 A method for developing solar shading control strategies using performance mapping and classification trees

Figure 7.8 gives an overview of the extended support method for the development of performance-driven solar shading control strategies.

The first steps of the approach are identical to those in the support method presented in Chapter 5. The developer defines a set of discrete control modes and orders these in terms of how much solar energy is admitted in their operation. In Figure 7.8, these control modes are denoted using SMSP, an acronym that is specific to the application of the support method to the double roller blind system. This application will be explained in Section 7.6.1. The developer then simulates the performance (P), sensor readings and control variables (S) for each control mode where one control mode is followed continuously throughout a whole year. S contains the readings of sensors that would be available to the actual control system or variables facilitating the classification of performance conditions that are easily predicted using parameters like time and location.

As with the previously presented approach, the developer then maps the performance (P) to sensor readings (S) for each control mode and optimises the detection algorithms that are used to select which control mode gets activated under particular circumstances. This is done by classifying the instantaneous performance of each control mode (PC_{true}) into desired or undesired performance using a performance criterion. In the extended method, this is done by fitting a classification tree (CT) for each control mode to simulation results using S as predictors and PC_{true} as class labels. The classification trees are generated using the Matlab *fitctree* function with the algorithm presented by Breiman et al. (1984). The outcome of this process is a set of classification trees that can be described as elaborate if-else-then structures that allow the performance effects of activating each control mode to be predicted based on new observations of S. For each control mode, a separate classification tree ($CT_{SM;SP}$) is created.

The right-hand side of figure 7.8 shows how the classification trees can be used by the shading control strategy during the operational phase. The control system takes sensor measurements and computes other predictors that together form a set of sensor variables (S). This set can include variables that describe the position of the sun or shading positions that would be set if a particular control mode were to be

activated. This S is then used to predict a performance classification ($PC_{detected}$) for each control mode and the control mode with the most desirable performance is selected and activated. In this study, the control mode that admits the most solar energy, but does not lead to undesired glare, is selected. This selection process can, however, also involve more advanced algorithms.
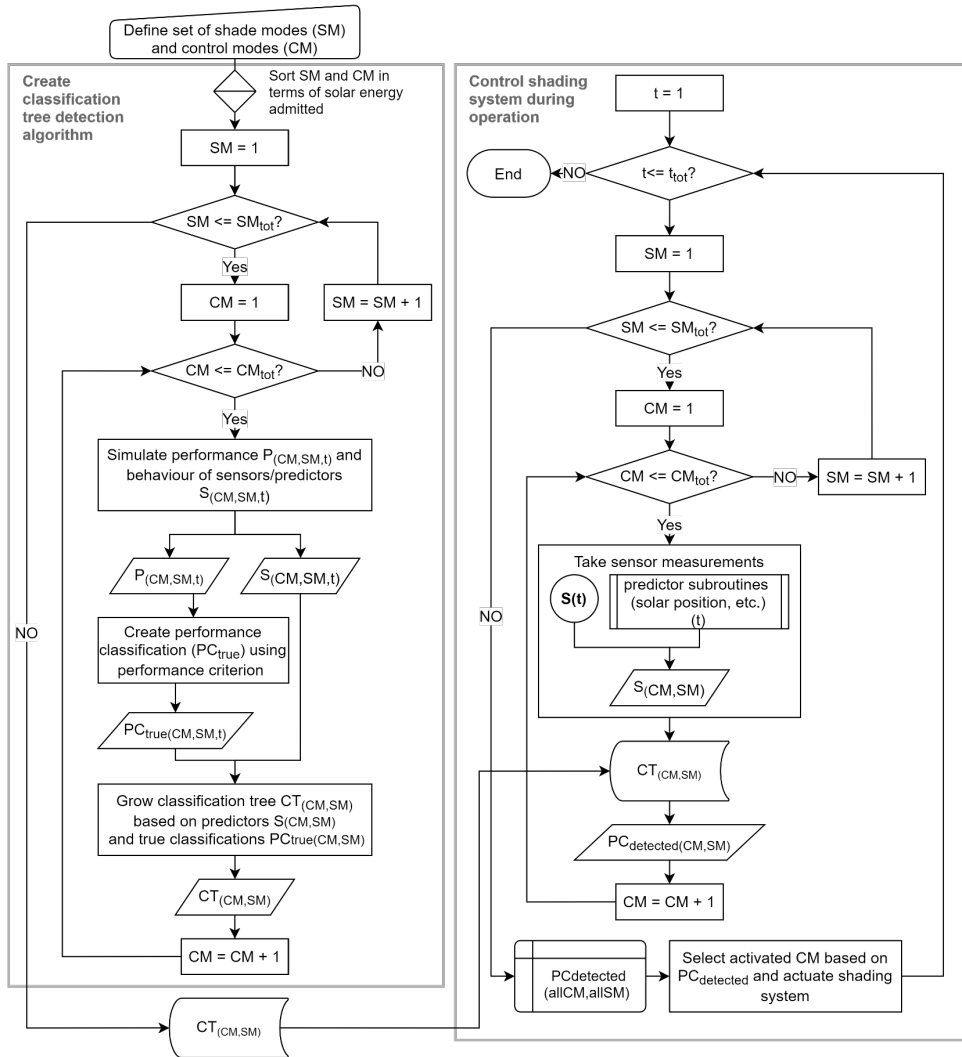
Figure 7.8 Method for developing control strategy classification trees using simulation results. Control modes are designated for the double roller blind system using the CM and SM that will be explained in Section 7.6.1

159

7.4.2 The optical model parametrisation approach

Throughout the VTB, three different optical models are used, that each describe the glazing and shading system at a different level-of-scale and resolution. To provide each of these models with consistent input parameters, a multi-scale approach is used (Figure 7.9).

This study starts with a set of detailed fabric properties (1 in Figure 7.9), at the level of the fabric threads. Additionally, a thickness for the shading device is assumed. A desired COA and $T_{dir-dir-0}$ are selected, that are to be obtained through the design of the fabric weave pattern. For generating the BSDF description of the shade fabric within the 3PHS method and the EnergyPlus CFS model, the LBNL-Window *perforated screen*[3] model is used that describes the shade as a plane with regularly spaced orthogonal openings. The size (x) and spacing (Sx) of these openings are computed (2 in Figure 7.9) from the desired COA and $T_{dir-dir-0}$ using the equations:

$$x = \frac{\sin(COA) \cdot th}{\cos(COA)} \quad (7.2) \qquad Sx = \sqrt{\frac{x^2}{Tv_{dir-dir-0}}} \quad (7.3)$$

x: size of the rectangular opening, Sx: center-to-center distance of openings, COA: cut-of-angle, th: shade thickness, $Tv_{dir-dir-0}$: direct to direct normal transmittance (OF)

Using this detailed description of the shading fabric weave, the optical behaviour of multi-layer fenestration system is simulated with LBNL-Window (4) and described in the BSDF and CFS matrices (5). To obtain the additional diffuse reflectance ($Rv_{dir-diff-0}$) and diffuse transmittance ($Tv_{dir-diff-0}$) input parameters, that are required by the Wienold-Roos model, a Matlab script is used to compute these parameters from the fenestration system BSDFs (6).

---

[3] The VTB also offers support functions for the LBNL-Window *woven shade* and *diffuse shade* models. The *perforated screen* model, however, was found to be most suited for describing metal coated, specularly transmitting fabrics with a high COA
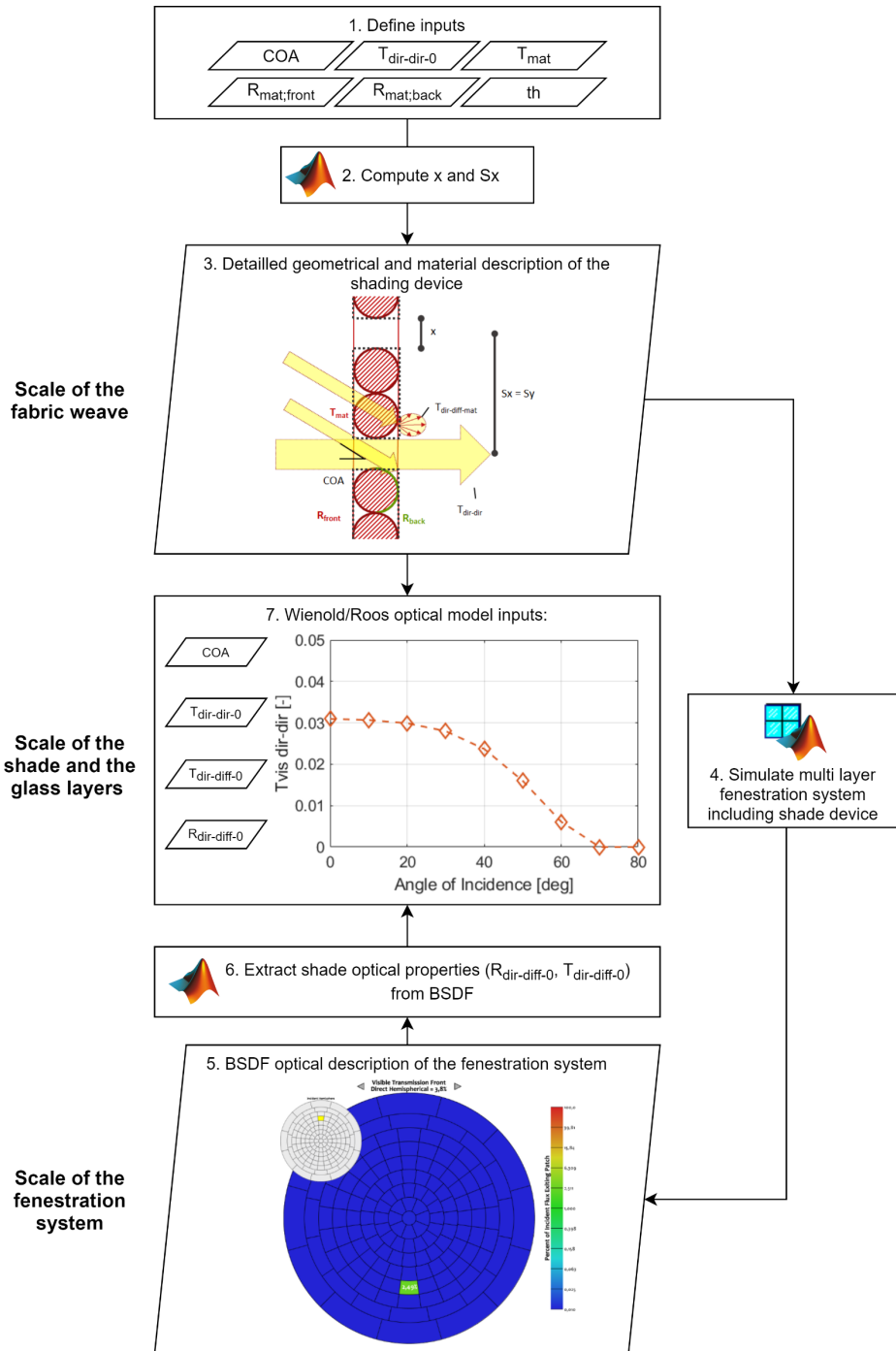
Figure 7.9 Parametrisation workflow for providing each optical model with consistent inputs

7.5 Quality assurance

The following sections section highlight quality assurance of the new VTB features contained in VTB modules A.3, B.3.1 and B.4 as well as the overall VTB configuration.

7.5.1 VTB Module A.3: Verification of the eDGPs$_{3PHS\text{-}Rpict}$ daylight glare prediction method

Wienold (2009b) validated the eDGPs approach, using Daysim for the $E_{v;glare}$ simulations and Rpict for simulating the luminance distribution, by comparing its DGP predictions of a situation with blind and roller shades to those from regular simulations using Rpict (DGP$_{Rpict}$). Additionally, the eDGPs$_{3PHS+Rpict}$ method where the 3PHS method is used to simulate $E_{v;glare}$ was validated by Abravesh et al. (2019) using measured luminance distributions by HDR cameras in an empirical setup with automated horizontal blinds. This research therefore focusses on verifying the implementation of the eDGPs$_{3PHS+Rpict}$ modelling approaches in the VTB.

A. Simple case where saturation is the dominant glare mechanism:
Largely overcast sky conditions, $T_{v\text{-dir-dir}}$: 0.8%, shade lowered partially to block sun from view, occupant 2.5 meters away from the façade facing the window at 45-degree
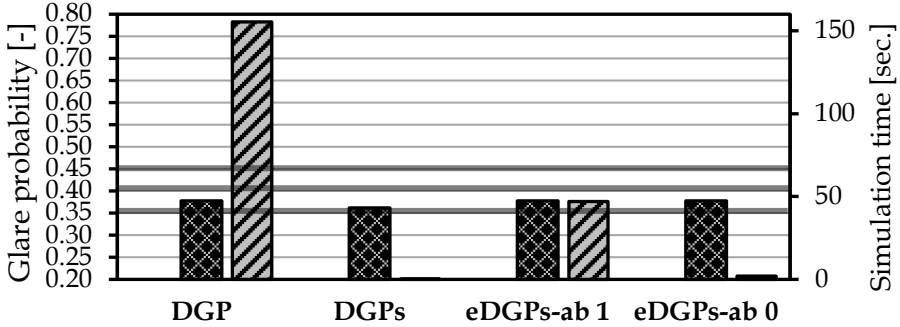
B. Complex case where contrast is the dominant glare mechanism:
Clear sky, high $T_{v\text{-dir-dir}}$:13%, shade lowered completely with sun visible through shade, occupant 2.5 meters away from the façade facing the window directly
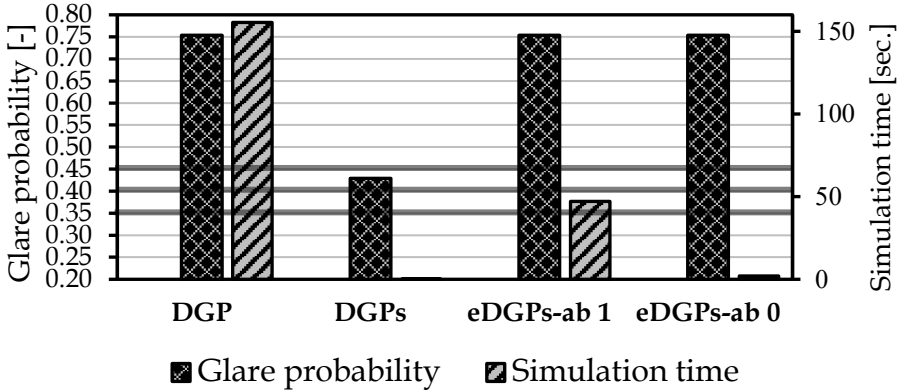
Figure 7.10 Comparison of predicted glare probability and the required simulation time for DGP_{Rpict}, $eDGPs_{3PHS\text{-}Rpict}$, and $DGPs_{3PHS}$ under two representative conditions

In this verification study, $eDGPs_{3PHS\text{-}Rpict}$ glare predictions will be compared to $DGPs_{Rpict}$ simulations with a higher number of ambient bounces (-ab 7), where $E_{v;glare}$ is computed from the HDR image. Two $eDGPs_{3PHS\text{-}Rpict}$ alternatives with a different number of ambient bounces in the rpict simulations (-ab 0 and -ab 1) are tested to evaluate the importance of this parameter. The results of this comparison are shown in Figure 7.10 and Figure 7.11 under two representative conditions. Figure 7.10 also shows DGPs predicted using the 3PHS method ($DGPs_{3PHS}$) to illustrate why a contrast-based glare metric is needed in this study. From this comparison the following can be concluded:

- The $eDGPs_{3PHS\text{-}Rpict}$ toolchain predicts the same glare probability as DGP_{Rpict}.
- The -ab 0 is sufficiently accurate in this application.

163

- The toolchain provides a computationally efficient method for predicting glare probability.
- There are large discrepancies between the DGPs$_{3PHS}$ approach and the contrast-based indicators. Only in the simple case does the DGPs$_{3PHS}$ method predict the correct 'perceptible' glare class.
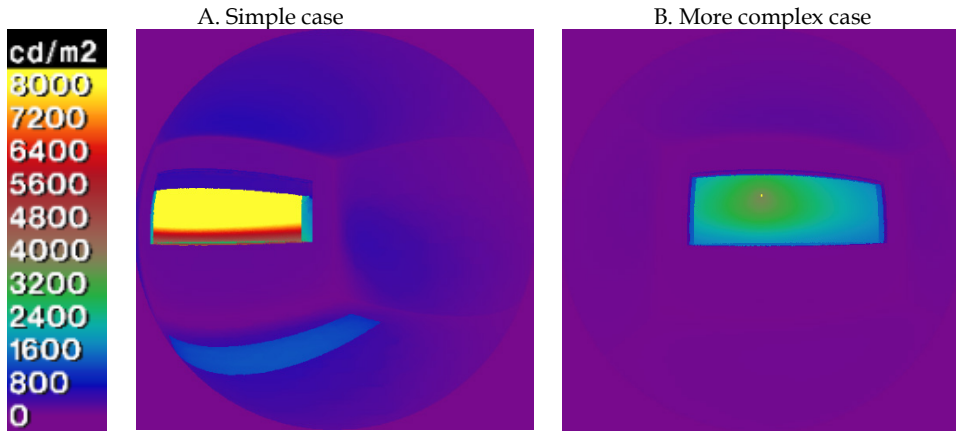
Figure 7.11 DGP$_{-Rpict}$ Luminance distributions for the cases shown in Figure 7.10

7.5.2 VTB Modules B.2, B.3.1 and B.4: Validation of the implementation and parametrisation of the optical models

The goal of the comparison in this section is to validate that the application of the LBNL perforated screen model and the Wienold-Roos fabric model give a realistic representation of the optical behaviour of the selected type of shading devices. Additionally, the optical model parametrisation approach will be validated. For both models, the predicted optical behaviour of the combined glazing and shading system will be compared to LBNL-Window simulations with the measured #20012 shading fabric from the CGDB.

Figure 7.12 is used to validate the perforated screen optical modelling approach that is used to generate BSDFs for the Radiance-3PHS and EnergyPlus-CFS simulations. The graph shows the $T_{v-dir-dir-\theta}$ and $T_{v-dir-diff-\theta}$ in relation to the angle of incidence (AOI) that is predicted using the measused BSDF (solid blue lines) and using the perforated shade model with different parameter settings (dashed lines). The graphs show optical properties for the combined glazing and shading system and in both cases the same glazing system is used, and the off-normal properties of the glazing system are simulated. For the measured fabric the OF, T_{vis} and R_{vis} of the overall fabric are known. However, the diffusing transmittance of the fabric thread (T_{mat}) and the COA are not known, and these properties have to be estimated for making this comparison. The graph shows that the predicted angular transmittance using

the perforated shade model is similar to the behaviour that is predicted using the measured BSDF and the best fit is achieved with a COA of 75° and a T_{mat} of 1.2%.
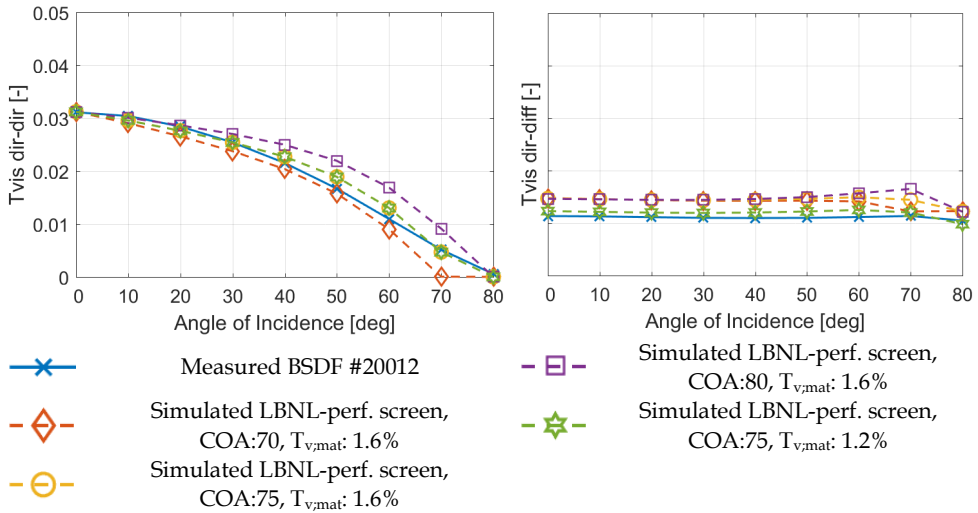
Figure 7.12 Validation of the optical model used within 3PHS and CFS. $T_{dir\text{-}dir\text{-}\theta}$ and $T_{dir\text{-}diff\text{-}\theta}$ predicted using LBNL-Window simulations with a measured BSDF compared to predictions using LBNL-Window and the perforated shade model with different estimated settings for unknown parameters

Figure 7.13 is used to validate the implementation of the Roos/Wienold fabric model used within the Rpict simulations. The graph shows $T_{dir\text{-}dir\text{-}\theta}$ predicted by LBNL-Window using the measured BSDF and by Radiance rtrace simulations using the Wienold-Roos model with different estimations of the unkown COA. Some discrepencies can be seen between the $T_{dir\text{-}dir\text{-}\theta}$ predicted by the Wienold-Roos model and the behaviour that is predicted using the measured BSDF within the 20-70 COA range. The magnitude of these differences is considered acceptable and within the margins of uncertainties in this research.
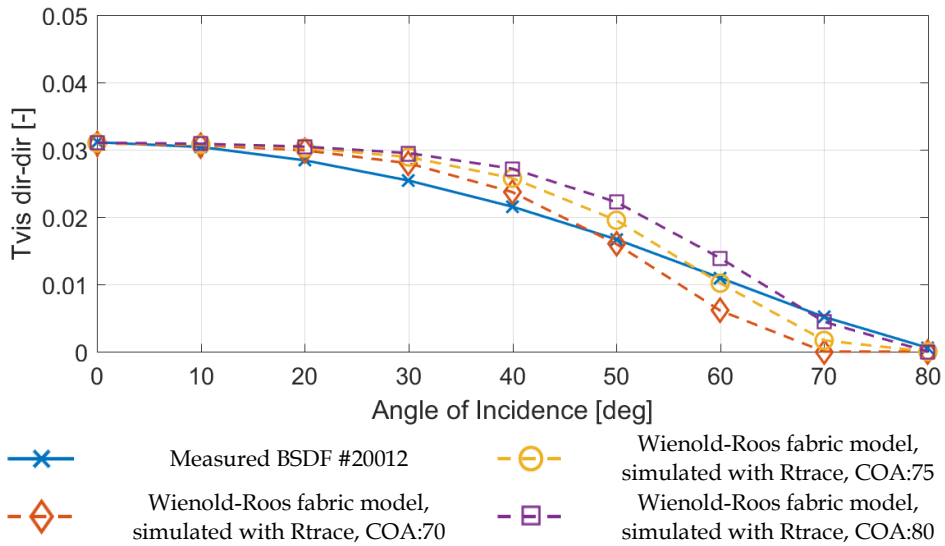
Figure 7.13 Validation of the Wienold-Roos optical model used within the rpict simulations. $T_{dir\text{-}dir\text{-}\theta}$ predicted using LBNL-Window with a measured BSDF compared to predictions using rtrace and the Wienold-Roos model with varying settings for unknown parameters

7.5.3 Verification of the overall VTB configuration: analyses of performance sensitivity to fabric design aspects

This section presents an analyses of performance sensitivity to the shading fabric's OF. Additionally, glare performance predictions using the eDGPs$_{3PHS\text{-}Rpict}$ will be compared to DGPs$_{3PHS}$ predictions for each of the investigated fabrics as well as for a corresponding set of fabrics that transmit daylight in a fully scattering manner. The goals of this sensitivity analyses are:

- To verify the overall VTB configuration.
- To illustrate why the eDGPs$_{3PHS\text{-}Rpict}$ approach is required in this study.
- To obtain insight into fit-for-purpose glare simulation methods by investigating the type of conditions where a simplified saturation-based approach to glare assessment could suffice.
- To investigate the performance effects of specifying the shading fabric's OF and verify the selection of the two chosen fabrics for the double roller blind system.

Figure 7.14 gives an overview of the optical characteristics of the seven investigated fabrics with a specular transmittance and a varying OF (diamonds). These fabrics have identical optical properties for the closed parts of the fabric (T_{mat}, R_{mat}, etc.) and an identical COA, but vary in terms of their OF and T_{vis}. In this sensitivity analyses,

the shade is controlled using the SC+ baseline strategy that employs only a single shade.
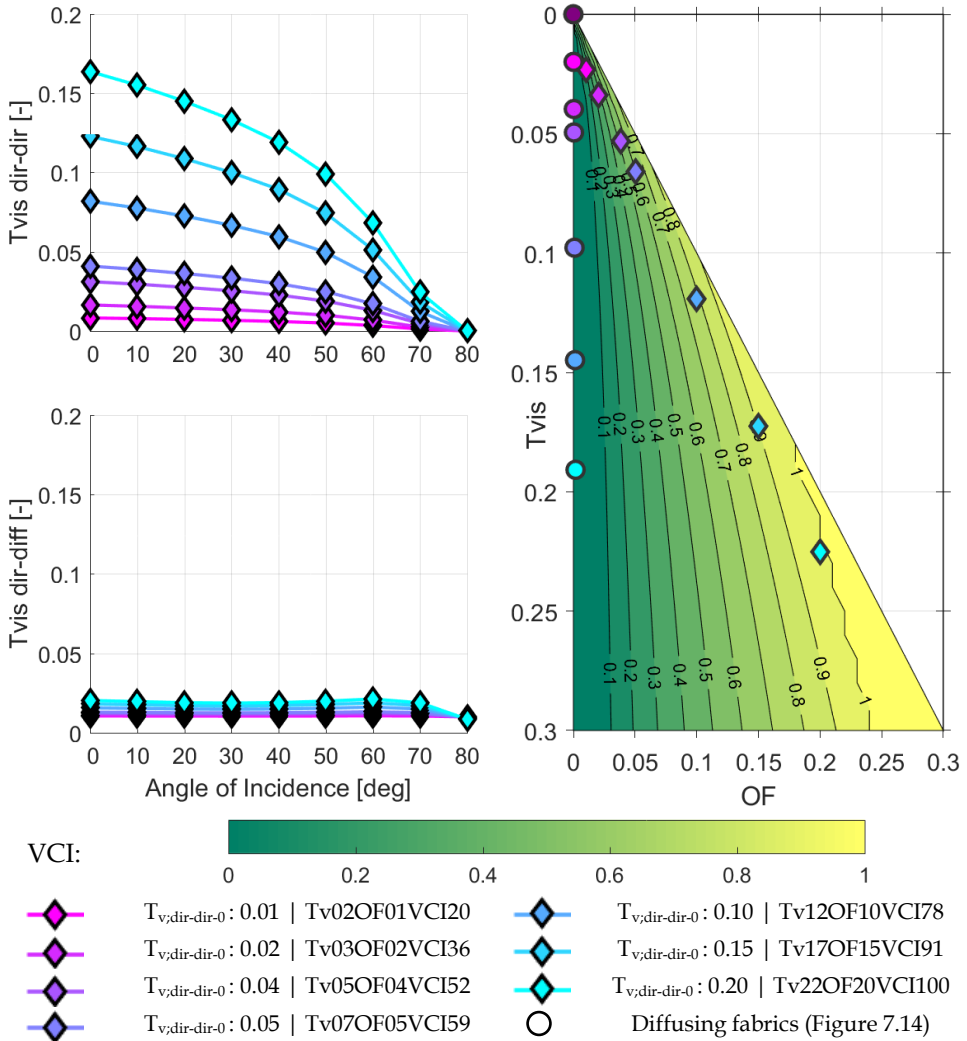
Figure 7.14 Simulated $T_{v;dir-dir-\theta}$ and $T_{v;dir-diff-\theta}$ using BSDF of measured fabrics (left) and VCI (right) for a selection of fabrics from the IGDB

Figure 7.15 shows simulated energy, daylighting and glare performance for each of the fabrics. The graph shows the sensitivity of energy performance to varying the fabric's OF. The 1% OF fabric (Tv02OF01VCI90) has an E_{prim} that is 12 kWh/m² (16%) higher than that of the 20% OF fabric (Tv22OF20VCI100). This difference can mainly be attributed to the effects of the OF on the E_{prim} for lighting (14 kWh/m²). The small differences in heating and cooling energy consumption are caused mainly by

reductions in heat gains from electric lighting. Glare and daylighting performance are both very sensitive to the fabric's OF. Compared to the least open Tv02OF01VCI20 fabric, the most open Tv22OF20VCI100 fabric offers 47% more $sDA_{300/50}$ but also leads to 11% more $eDGPs_{0.40exc-45deg}$ and 11% more $eDGPs_{0.35exc-0deg}$. Generally, these results correspond with known principles from building physics, and it is concluded that the VTB configuration functions as intended. Additionally, the following observations can be made about these results:

- All performance aspects are very sensitive to the fabric's OF.
- There is a strong trade-off between daylighting and energy performance on the one hand and visual comfort on the other.
- To provide a high degree of glare protection and meet the defined $eDGPs_{0.35exc-0deg} \leq 5\%$ performance criterion, requires a fabric with an OF as low as 1%.
- For the double roller blind system, the use of the Tv22OF20VCI100 fabric for the front shade and the Tv05OF04VCI52 for the back shade allows for maximal daylighting admission when only one of the shades is lowered, whilst providing the required degree of glare protection when both shades are lowered (i.e.: a combined OF lower than 1%).
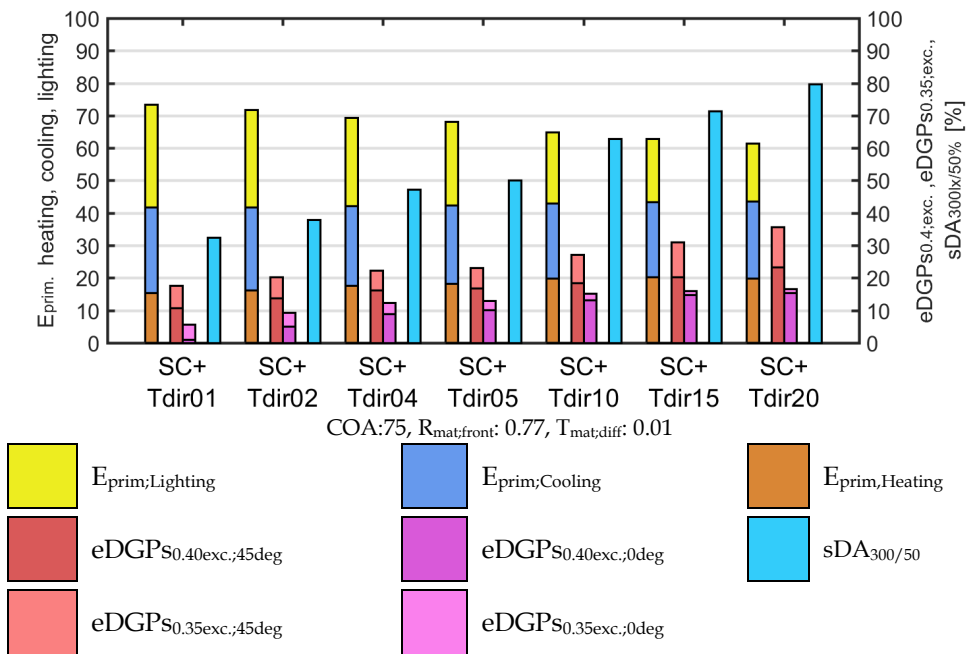
Figure 7.15 Performance sensitivity to fabric openness. Annual simulation of the SC+ control strategy assuming fabrics with a specular transmittance and a varying openness

Figure 7.16 shows the comparison of glare predictions using the two glare simulation methods. In the two graphs, predictions using the saturation-based

DGPs$_{3PHS}$ method are plotted in relation to predictions using the eDGPs$_{3PHS-Rpict}$ method, that also explicitly describes contrast and adaptation as glare mechanisms. Figure 7.16A shows the results for the seven specularly transmitting fabrics that are plotted as diamonds in Figure 7.14. Figure 7.16B shows a similar sensitivity analyses with results for the 8 fully diffusing fabrics, whose optical properties are shown as circles in Figure 7.14.

A. Fabrics with rectangular openings, specular transmittance, COA 75, T$_{mat}$: 1%
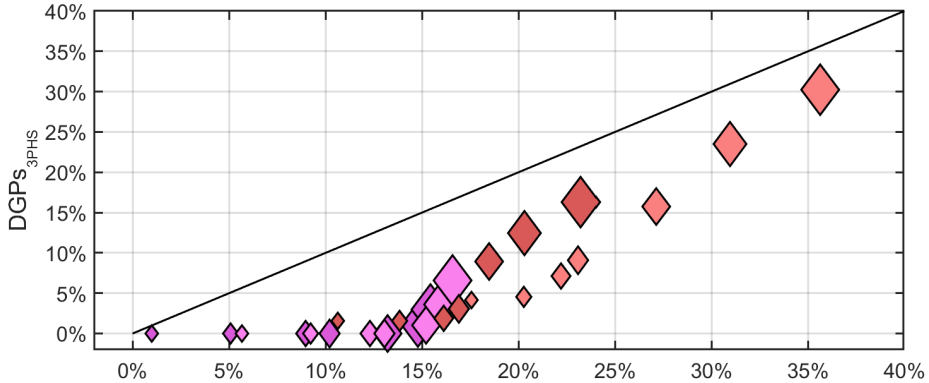
B. Fully diffusing fabrics
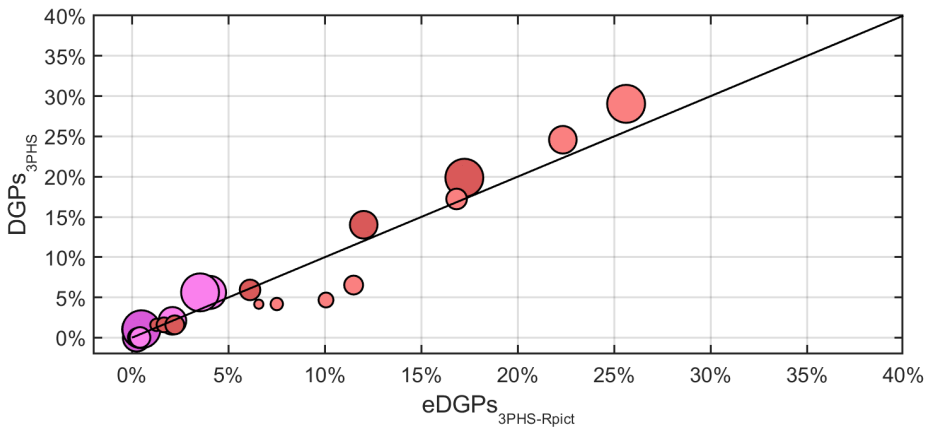
Legend:

◇ Specular fabric, 0.4 DGP exceedance - 0 deg. view. dir. ○ Diffusing fabric, 0.4 DGP exceedance - 0 deg. view. dir.
◇ Specular fabric, 0.35 DGP exceedance - 0 deg. view. dir. ○ Diffusing fabric, 0.35 DGP exceedance - 0 deg. view. dir.
◆ Specular fabric, 0.4 DGP exceedance - 45 deg. view. dir. ● Diffusing fabric, 0.4 DGP exceedance - 45 deg. view. dir.
◆ Specular fabric, 0.35 DGP exceedance - 45 deg. view. dir. ● Diffusing fabric, 0.35 DGP exceedance - 45 deg. view. dir.

◇	◇	◇	◇	◇	◇	◇		○	○	○	○	○	○	○
SC+	SC+	SC+	SC+	SC+	SC+	SC+		SC+	SC+	SC+	SC+	SC+	SC+	SC+
Tdir:01	Tdir:02	Tdir:04	Tdir:05	Tdir:10	Tdir:15	Tdir:20		Tdiff:00	Tdiff:01	Tdiff:02	Tdiff:04	Tdiff:05	Tdiff:10	Tdiff:15	Tdiff:20

Figure 7.16 Glare performance sensitivity for two types of fabrics of varying overall transmittance using the DGPs$_{3PHS}$ approach and the eDGPs$_{3PHS-RPICT}$ approach

The diffusing fabrics behave similarly to the #7023 shading fabric from the CGDB, shown in Figure 7.4, and fully scatter incoming daylight in all directions. The visual transmittance of the diffusing fabrics was specified such that $T_{v;dir-hem-0}$ of the diffusing fabrics matches the $T_{v;dir-dir-0}$ of the specularly transmitting fabrics. The specular and the fully diffusing fabrics represent two extremes in terms of the types of shading devices that are possible and provide some insights into the factors that influence a fit-for-purpose glare performance simulation approach.

For the specularly transmitting fabrics (Figure 7.16 A) a substantial difference can be observed between the $DGPs_{3PHS}$ and the $eDGPs_{3PHS-Rpict}$ visual comfort predictions. Especially for the fabrics with a low to intermediate OF (2-10% $T_{v;dir-dir-0}$) the discrepancy between the two methods is large. For the 4% OF fabric, the $DGPs_{3PHS}$ method leads to an error of 14% in terms of $DGP_{0.40exc-45deg}$ and 12% in terms of $DGP_{0.35exc-0deg}$. It is only for the fabric with the 1% OF, and a viewing direction where the occupants are facing their monitor (0-Deg), that the error in the glare performance predictions remains small (2% $DGP_{0.40exc-0deg}$ and 6% $DGP_{0.35exc-0deg}$). The fact that the error is largest for the fabrics with an intermediate OF can be explained by the fact that these fabrics in particular, can lead to high contrast indoor daylight conditions where the sun is visible through the shade but overall $E_{v;glare}$ at the position of an occupant is low.

For the fully diffusing fabrics, the error caused by using the $DGPs_{3PHS}$ method is much smaller (Figure 7.16B) because the sun is never visible through the shades and saturation is the dominant mechanism causing glare. The cases with high transmittance fabrics now show the largest discrepancies between $eDGPs_{3PHS-Rpict}$ and $DGPs_{3PHS}$, where the latter approach slightly overpredicts the glare sensation because the adaptation effect is not considered. Amongst the diffusing shades, the 20% $T_{v;dir-diff-0}$ shade gives a maximum error of 3% in terms of $DGP_{0.40exc-45deg}$ and 2% in terms of $DGP_{0.35exc-0deg}$. For the diffusing fabrics with a low transmittance (0-5% $T_{v;dir-diff-0}$), the errors are negligible in terms of $DGP_{0.40exc-45deg}$ and $DGP_{0.35exc-0deg}$. Only when the 'perceptible' glare criterion (DGP≥0.35) is used and comfort is assessed for the 45-degree viewing angle, small but possibly problematic errors occur (2% $DGP_{0.35exc-45deg}$ error for the 0% $T_{v;dir-diff-0}$ fabric and 5% $DGP_{0.35exc-45deg}$ error for the 3% $T_{v;dir-diff-0}$ fabric).

The following conclusions can be drawn from this analysis:

- Using the $DGPs_{3PHS}$ method for assessing glare in cases with fabrics with a specular component to daylight transmittance leads to substantial errors (14% $DGP_{0.40exc-45deg}$ and 12% $DGP_{0.35exc-0deg}$).
- This shows the $eDGPs_{3PHS-Rpict}$ method should be used to assess the double roller blind system in this study.
- For assessing the performance of fully diffusing fabrics, the simplified $DGPs_{3PHS}$ method can suffice as long as the shade is controlled such that occupants are not exposed to direct sunlight.

- Fully diffusing fabrics distribute daylight evenly and prevent high luminance specular transmission. Although this characteristic is very favourable in terms of effective daylighting, it is less desirable in terms of view through the shading device, e.g., all the investigated diffusing shades have a VCI of 0 (Figure 7.14).
- The investigated fabric types represent two extremes. For fabric types that show an intermediate type of behaviour (e.g., #6005 in Figure 7.4), the importance of the contrast related terms in the DGP algorithm is likely to become bigger as the specular component to daylight transmission increases.

7.6 Development and performance evaluation of the multi-state double roller blind strategy

In this section, the performance of the double roller blind concept will be assessed. A sun tracking control strategy based on classification trees (SCtree) is developed for the double roller blind system in Section 7.6.1. The performance effects of the double roller blind system with the SCtree strategy, and the baseline strategies are simulated and evaluated in Section 7.6.2. In Section 7.6.3, the SCtree strategy will be refined further by adding additional control rules that are aimed at reducing potentially disturbing shade actuations.

7.6.1 Control strategy development using classification trees

This section presents how the method, discussed in Section 7.4, was used to develop a control strategy based on classification trees generated from simulation results. Additionally, the classification trees are verified, and an initial assessment is made of the effectivity of the approach.

The control modes for the double roller blind system follow a similar logic as in Chapter 5. To clarify these control modes, they will be designated using two terms. The term *shade mode* (SM) will be used to define which and how many of the shading devices are lowered and dynamically operated. These shade modes are constrained to have all shades fully raised (SM1), only the front shade activated (SM2), only the back shade activated (SM3), or both shades activated (SM4). The term shade position (SP) will be used to define a set of control logics that determine the position of the active shading devices. The following SP are considered: fully raising the active shades (SP1), operating the active shades according to the sun-tracking SC logic SP2), operating them to the maximum eye-level EL logic (SP3), or lowering all active shades to the work plane height (SP4).

These SM and SP are combined into the eight unique control modes shown in Table 7.5. The control modes are ordered in this table according to the amount of solar energy that is admitted, from the most open control mode (SM1CM1: all shades fully raised) to the most closed one (SM4CM4: both shades lowered to the work plane height). The table also clarifies how possibly disturbing shade actuations are quantified for the double roller blind system. The large shade actuations are instances where the system switches between SM (a horizontal transition in Table 7.5). The large shade movements are instances where the system switches between different SP (a vertical transition).

Using the described method, a set of classification trees were developed using annual simulations of the control modes in Table 7.5, the sensor variables (S) in Table

7.6 as predictors and the true performance classification (PC_{true}). Based on the defined performance goals, PC_{true} is computed using Equation 7.4:

$$PC_{true(t)} = eDGPs_{0deg(t)} \geq 0.39 \mid eDGPs_{45deg(t)} \geq 0.34 \qquad (7.4)$$

Where $eDGPs_{0deg(t)}$: Glare performance prediction in the 0-degree viewing direction at t.
$eDGPs45_{deg(t)}$: Glare performance prediction in the 45-degree viewing direction at t.
t: time step

Each control mode has its own classification tree that is called at each control interval and predicts, based on S, whether the glare performance criterion ($eDGPs_{0deg} \geq 0.34$ or $eDGPs_{0deg} \geq 0.39$) would be exceeded if the corresponding control mode were activated. The control strategy then activates the most open SMSP control mode, that does not lead to glare.

Table 7.5 Possible modes of operation for the double roller blind system.

Shade Mode:		No shades activated	Only front shade is activated	Only back shade is activated	Both shades are activated	
Shade Position:		◄ Large shade actuation (SA) ►				
AU: Active shades are fully raised	▲ Large shade movement (ShMv) ▼	SM1SP1				Admit less solar energy ▼
SC: Active shades follow sun tracking control logic			SM2SP2	SM3SP2	SM4SP2	
EL: Active shades follow eye-level control logic			SM2SP3	SM3SP3	SM4SP3	
Otherwise, **WP:** Both shades are lowered to work plane height					SM4SP4	
		Admit less solar energy ►				

SM: Shade Mode that defines what shades are active. **SP:** Shade Position that defines the placement of the currently active shades.

Table 7.6 Predictor variables used to grow classification trees in this study

$EWF_{(SMSP)}$	Ev	γ	α
Exposed window fraction (EWF_{shFshB}) that would result if the SMSP control mode were activated	Vertical illuminance at window sensor	Solar azimuth	Solar altitude

Figure 7.17 shows the resulting CT$_{\text{SM1SP1}}$ classification tree for SM1SP1 (all shades up). To illustrate the effectivity of the classification tree in detecting a risk of glare this approach can be compared to the control threshold optimisation approach, presented in Chapter 5, that is used to the develop the baseline SC+ strategy. Figure 7.18 shows results from an annual simulation of the CM1SP1 control mode. The graph shows eDGPs for the two viewing directions in relation the simulated E$_v$ sensor readings and graphically illustrates the confusion matrix approach that is used to optimise the control thresholds of the SC+ baseline. Here, a single 4500 lux control threshold determines PC$_{\text{detected}}$ which defines when glare is detected and one of the more closed control modes is activated. For the SC+ baseline the control thresholds were optimised by selecting a control threshold that lies close to the point where the horizontal eDGPs$_{45\text{deg}}$ ≥ 0.4 line intersects the part of the scatter plot where the relationship between E$_v$ and eDGPs$_{45\text{deg}}$ is nearly linear. This point was found by accepting a small (0.2%) number of FN, omitting these instances from the dataset, and then selecting the highest control threshold that meets the eDGPs$_{45\text{deg}}$ ≥ 0.4 condition. Although this approach identifies control thresholds with beneficial performance trade-offs, the effectivity of this approach is limited by the constraints that are posed by using a single sensor and a single control threshold, as can be seen from the large number of FP (25.7%).
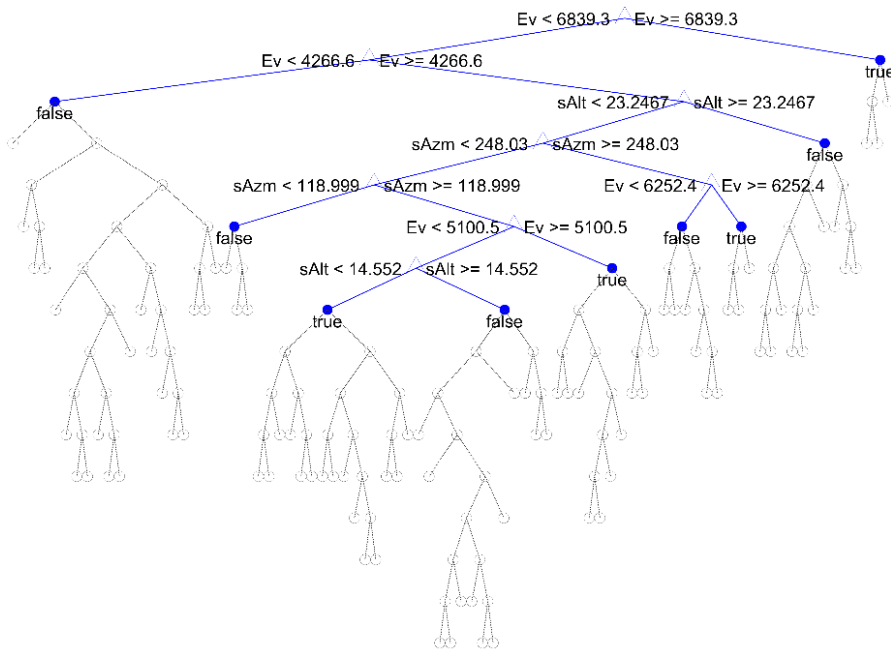
Figure 7.17 Graphical representation of the classification tree CT$_{\text{SM1CM1}}$. For clarity only the first 20 levels of the 25-level decision tree are shown in blue with the corresponding conditions. The full 25 level decision tree was used in the control strategy
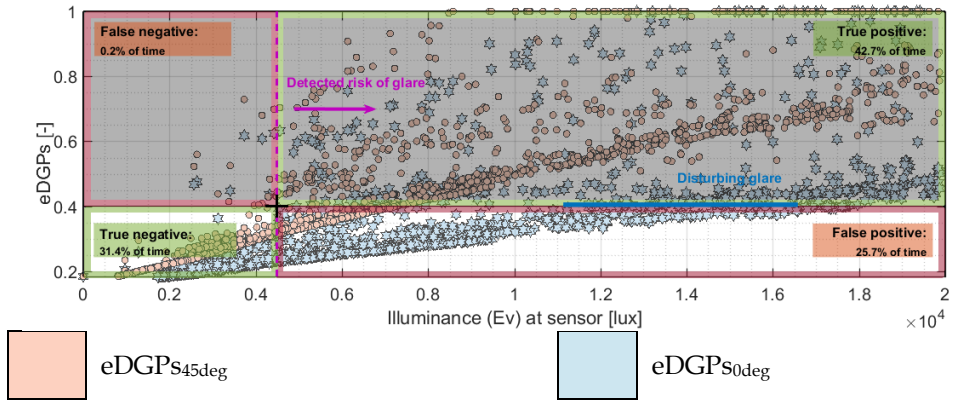
Figure 7.18 Confusion matrix control threshold optimisation method used for the SC+ control strategies. Simulated glare predictions and Ev sensor readings for SM1CM1
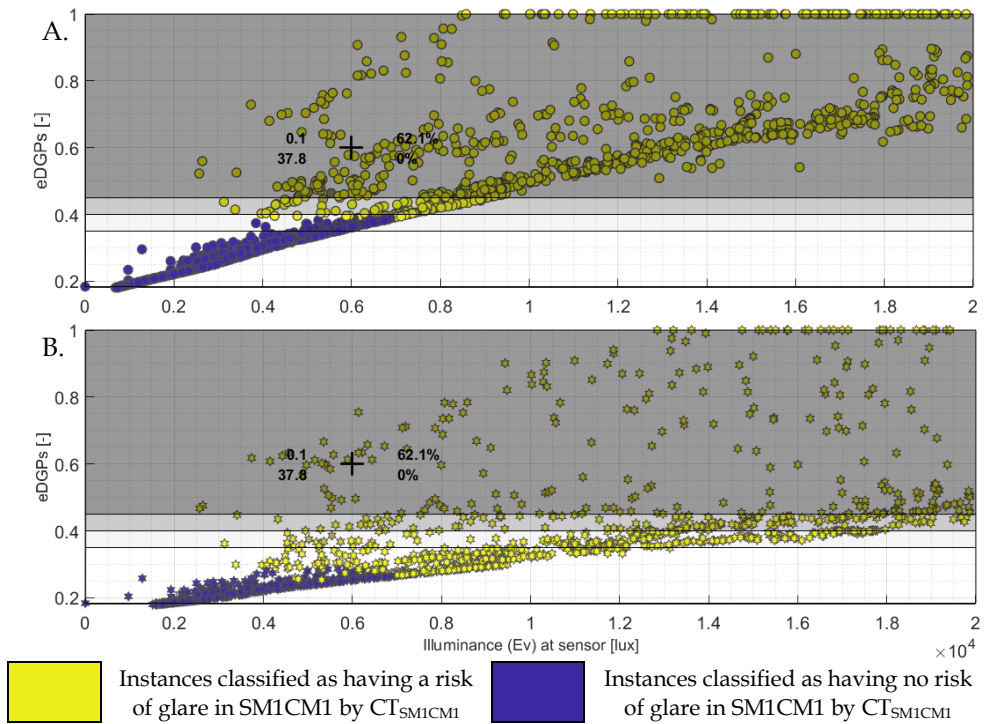
Figure 7.19 Classification of glare performance by CT_{SM1CM1} and evaluation of its effectivity in a confusion matrix. on matrix.
A. 45-degree viewing direction. B. 0-degree viewing direction

Figure 7.19 shows the same simulation results but now the colour of the markers indicates the classification of glare risk associated to SM1CM1, predicted by the

175

CT$_{SM1CM1}$ classification tree based on the sensor variables. For clarity the two viewing directions are shown in two images. The black cross indicates the number of instances contained within each of the confusion matrix quadrants. Because the CT uses multiple predictors, and the PC$_{true}$ now uses a two-fold conditional statement, the confusion matrix can no longer be represented as in Figure 7.18 and the cross is placed arbitrarily in the image. The graph shows that the CT$_{SM1CM1}$ is verry effective at distinguishing instances with a risk of glare from conditions where both shades can safely be raised, and leads to only 0.1% FN.

The graphical representation of CT$_{SM1CM1}$ in Figure 7.17 gives some insights into how the classification tree identifies glare conditions and suggests some analogies to the initial method using confusion matrices. The first two levels of the decision tree classify glare conditions using control thresholds that are close to those that are found with the confusion matrix approach. In Figure 7.18, the 6839 lux threshold is close to the horizontal coordinate of the point where the disturbing (0.4 eDGPs) glare line intersects the linear part of eDGPs$_{45deg}$ plot as well as the point where the perceptible (0.35 eDGPs) glare line intersect the linear part of the eDGPs$_{0deg}$ plot. Using this point in the confusion matrix approach would provide a verry high accuracy. The 4267-lux threshold that is used in the second classification tree level, is very close to the SC+ baseline threshold, and provides a more conservative approach that eliminates most FN. It is mainly in the range between 4267 and 6839 lux where the lower levels of the decision tree refine control decisions using information about the sun's position. It is also this range, that contains nearly all false positive control decisions of the SC+ strategy. These hard-to-predict visual comfort conditions, are where the classification tree approach offers its performance benefits.

The same process was repeated to create and verify the classification trees for the other control modes. Figure 7.20 shows scatter plots of glare performance in relation to E$_v$ sensor readings for the control modes where only the front shade is used to track the sun (SM2SP2), and where both shades are used to track the sun (SM4SP2). Additionally, four graphs are shown that test the effectivity of the corresponding classification trees. As was found in Chapter 5, classifying visual comfort conditions is more complex for the sun-tracking strategies and approaching this through an E$_v$ sensor threshold alone leads to many FN and provides unsatisfactory outcomes. The graphs show, however, that the classification tree approach can accurately (99.9%[4]) classify visual comfort conditions in these complex cases.

Based on these results it is concluded that the classification tree approach functions as intended and that it leads to classification trees that can classify visual comfort conditions with a high accuracy.

---

[4] The accuracy is a result of the classification tree settings and is related to the depth of the classification tree. The following settings where used: Maximum categories: 10, Maximum number of splits: 1, Minimum leave size: 1, Minimum parent size: 10, Merge leaves.
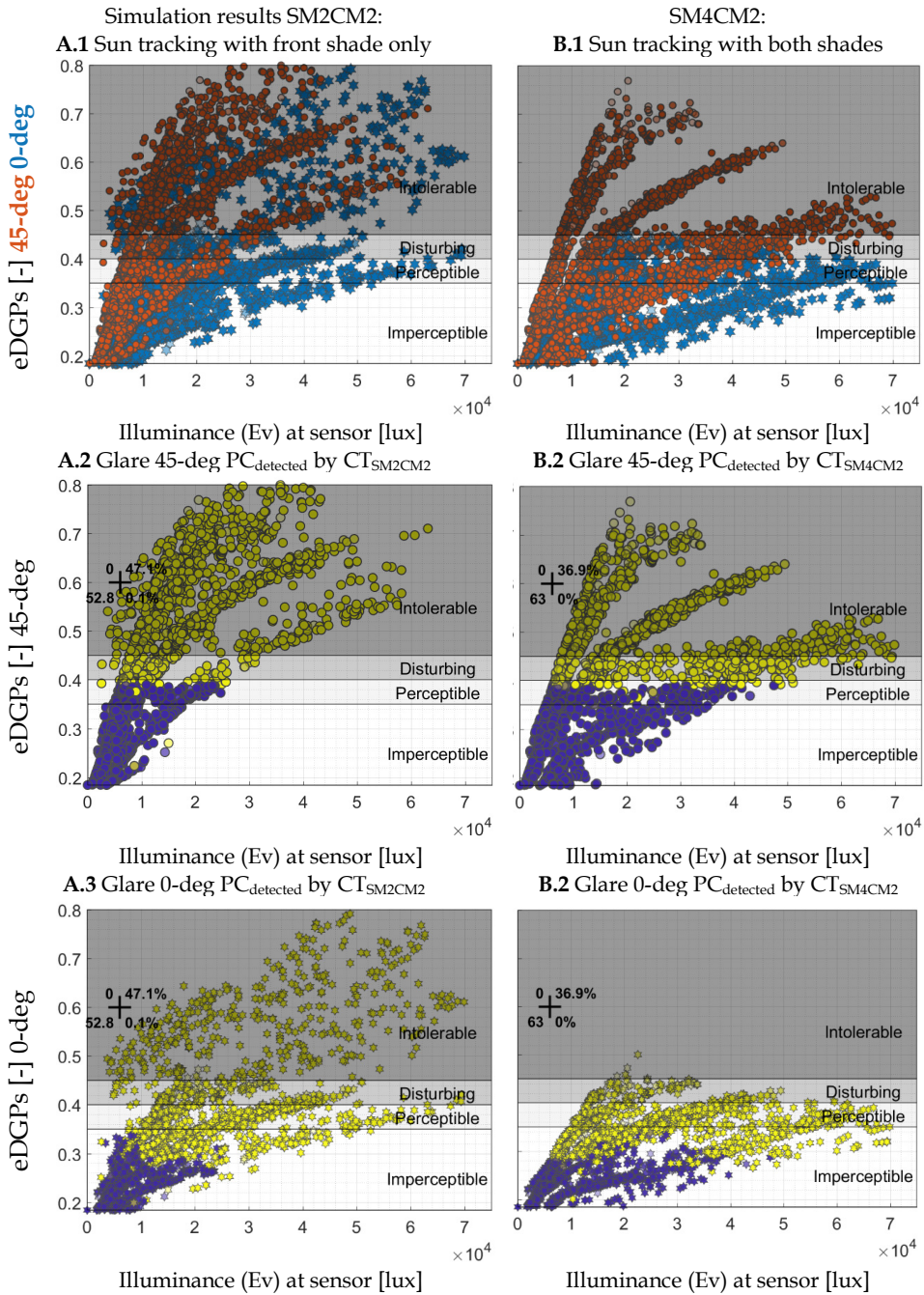
Figure 7.20 Simulated glare performance for the SM2CM2 and SM4CM2 control modes and evaluation of the effectivity of the corresponding classification trees

7.6.2 Performance assessment of the double roller blind system

In this section, the performance of the double roller blind system will be assessed in relation to different variations of the baseline strategies. Figure 7.21 shows a summary of all performance indicators resulting from an annual simulation of each alternative. The double roller blind system (SCtree-FrBck) is controlled using the database of classification trees that were developed in Section 7.6.1. Fabric Tv22OF20VCI100 is used for the front shade and fabric Tv07OF05VCI59 is used for the back shade.

All the baselines represent systems that utilise only a single shade. Three variations to the advanced SC+ baseline are presented: One where only the Tv22OF20VCI100 front shade is used (SC+Frnt), one where only the Tv07OF05VCI59 back shade is used (SC+Bck), and one where both shades are operated in a synchronised manner (SC+FrntBck). In this last alternative, the two shades are considered representative for a conventional system that uses a single shade that offers similar optical characteristics to that of the double roller blind system when both shades are lowered. This alternative is designed to give the same degree of glare protection as the SCtree-FrBck alternative but does so using less sophisticated controls and with more limitations to the optical states that the system can take. Both shades are also used simultaneously to represent a single shade of equivalent optical characteristics in the two conventional baseline strategies.

Figure 7.21 shows that the SCtree-FrBck double roller blind strategy performs substantially better than the conventional BL strategies for nearly all performance indicators. Compared to these two baselines the SCtree-FrBck strategy leads to 21.6 – 45.8 kWh/m^2 (29-62%) less E_{prim}, 40-69% more $sDA_{300lx50\%}$, 14% less $eDGPs_{0.40exc-45deg}$ and 10% less $eDGPs_{0.35exc-0deg}$. The SCtree-FrBck strategy leads to less time where both shades are raised above 1.2 meters (15% lower $EWF_{shFshB;40\%;exc.}$) compared to the BL200W alternative. Compared to the BL4500lx alternative, however, the SCtree-FrBck strategy offers an improvement of 19% in terms of $EWF_{shFshB;40\%;exc.}$. If the time where occupants have a view through one of the high openness shades is included in the assessment of view, the SCtree-FrBck leads to a substantial improvement compared to the baselines, offering a 20-54% higher total sum for EWF_{shFshB} + EWF_{shF} + EWF_{shB}.

Figure 7.21 shows that the SCtree-FrBck strategy combines the most beneficial performance features of the three SC+ alternatives. The energy, daylighting and view performance of the SCtree-FrBck strategy come close to that of the SC+Frnt strategy whilst offering a similar degree of protection against glare as the SC+FrBck strategy. Compared to the SC+FrBck strategy, the SCtree-FrBck strategy offers a reduction of 24.6 kWh/m^2 (33%) in E_{prim}, 45% more sDA, 1% less $eDGPs_{0.40exc-45deg}$ and identical performance in terms of $eDGPs_{0.35exc-0deg}$. With regards to view, the SCtree-FrBck strategy offers slightly more time where both shades are above 1.2 meters (3% more $EWF_{shFshB;40\%;exc.}$) and substantially more time with a view if view-through the high openness shades is included (38% more total EWF_{shFshB} + EWF_{shF} + EWF_{shB}).
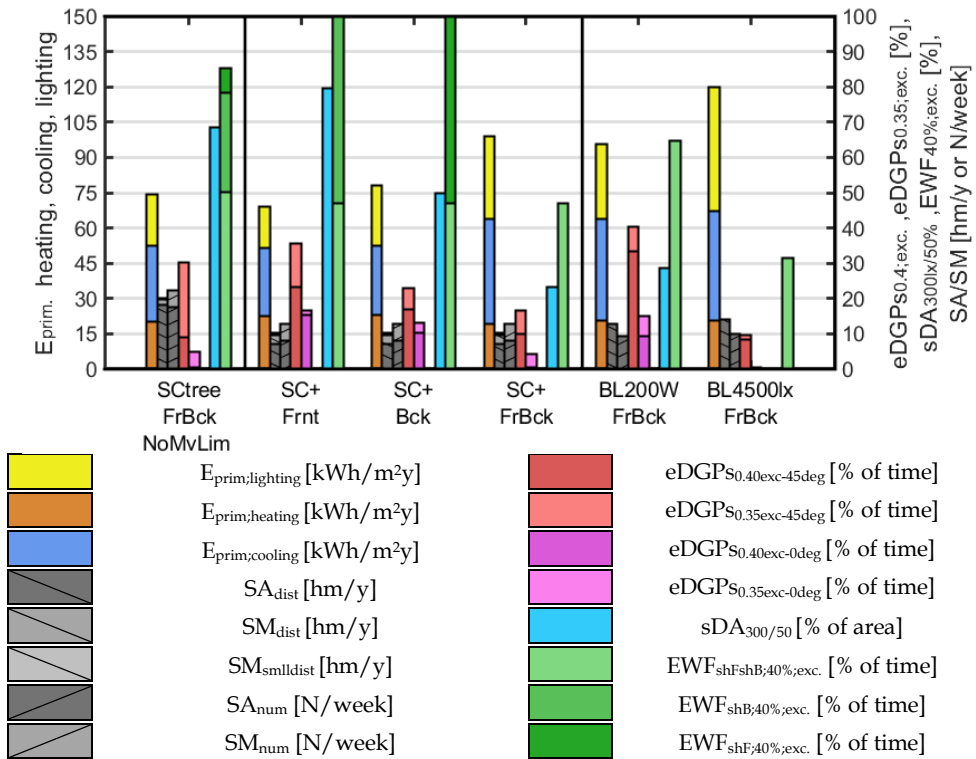
Figure 7.21 Summary of whole building performance for the double roller blind system controlled using classification trees (SCtree FrBck) in relation to multiple baseline shading strategies

These results show that the classification tree control approach makes beneficial performance trade-offs in activating the different control modes. This approach does, however, cause the SCtree-FrBck strategy to take more frequent control actions that could potentially be disturbing to occupants. In an average workday, the SCtree-FrBck strategy makes 2-3 more large shade movements and actuations (SA_{num} + SM_{num}). The SCtree-FrBck strategy also performs less well than the other strategies when 'disturbance' is quantified using the total distance travelled by the shading devices. In total the shading devices travel $6\text{-}10 \cdot 10^2$ meters more in a year with SCtree-FrBck strategy than with the other strategies. In the following section, further control rules will be explored that are aimed at limiting the frequency of these large movements whilst preserving the performance benefits that the SCtree-FrBck strategy offers.

7.6.3 Control refinement

Figure 7.22 B and C show how the two shading devices are positioned within the SCtree-FrBck and the SC+ strategies throughout a representative day with sky conditions alternating between completely clear and partly cloudy. Graph C shows that the SCtree strategy leads to multiple instances during this day where one of the shades is activated and another is deactivated, the type of actuation that is quantified by the SA indicator as being possibly disturbing. In this section the performance effects of additional heuristic control rules, aimed at limiting the frequency of these type of movements, will be explored.

To reduce the number of possibly disturbing large shade movements where two shades are alternated, the alternating shade actuations (SA) will be counted for each day and a limitation is set to the number of times per day the control strategy can execute this type of actuation. In this study, preventing discomfort glare is given priority. Therefore, limitations to the number of disturbing movements will only be set for movements where the system is actuated to a more open position and one or both shades are raised to admit more daylight. Disturbing 'opening' movements are thus quantified as instances where the system selects a lower SM than at the previous control interval, corresponding to a transition in control modes from right to left in Table 7.5. Once the maximum number of large movements has been reached for a particular day, the available modes of operation shown in Table 7.5 will be limited. Now, shade modes (SM) that have a lower number than that in the previous control interval can no longer be chosen, meaning that the system can no longer fully raise any shading device that has been activated since the limitation was reached. The system is, however, still free to change the shade position (SP) of the already active shades or activate another shade, increasing the SM number compared to the previous time step. The control strategy will still use classification trees to predict whether glare would for each of the possible modes of operation and activate the most open mode that is allowed whilst respecting the aforementioned limitation. At the beginning of each day the counter is reset, and the system is controlled without limitations until the maximum number of large actuations is reached.

The behaviour of this control concept is shown in Figure 7.22 C and D, where the maximum number of large shade deactivations is limited to respectively 3 or 1 such movements per day. Figure 7.23 shows the effects on daylighting and visual comfort performance across the day. The graphs show that the additional control rules effectively reduce the number of potentially disturbing shade activations but also have a negative effect on daylighting performance.

A. Sky conditions expressed in terms of solar radiation
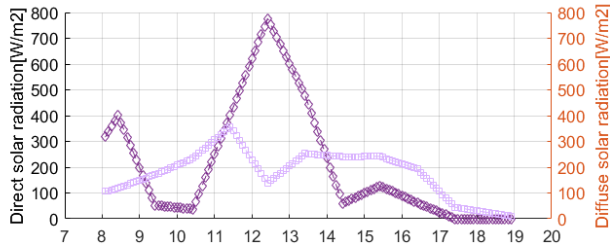
Shade positions:

B. SC+ control with optimised thresholds, single roller blind
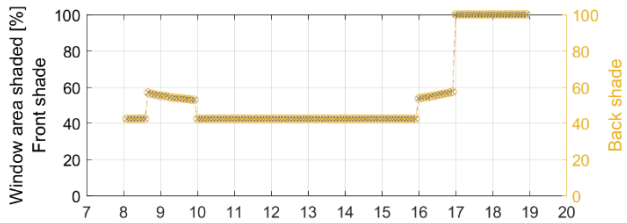
C. SCtree control, double roller blind, no limitation to large movement
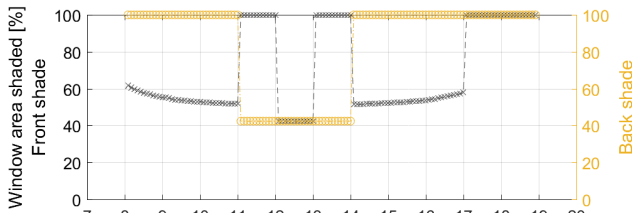
D. SCtree control, double roller blind, maximum 3 large opening movements
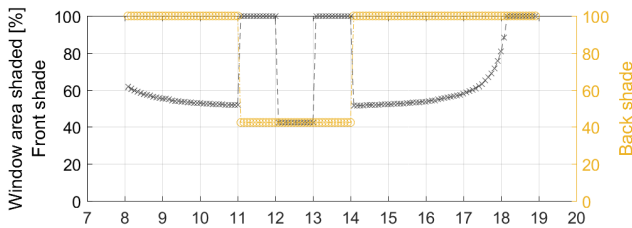
E. SCtree control, double roller blind, maximum 1 large opening movement
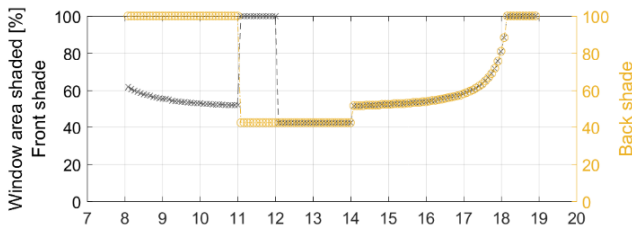
Figure 7.22 Shade movements in relation to outdoor conditions. Simulation results for the 4th of April, a day sky conditions alternating between clear and partly overcast.

Direct normal solar radiation [W/m²]

Diffuse horizontal solar radiation [W/m²

Window area shaded by front shade [%]

Window area shaded by back shade [%]

$eDGPs_{45deg}$

$eDGPs_{0deg}$

$D_{t;area;300lx}$

Shade positions:

B. SC+ control with optimised thresholds, single roller blind
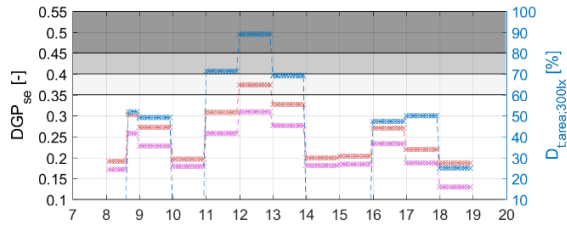
C. SCtree control, double roller blind, no limitation to large movement
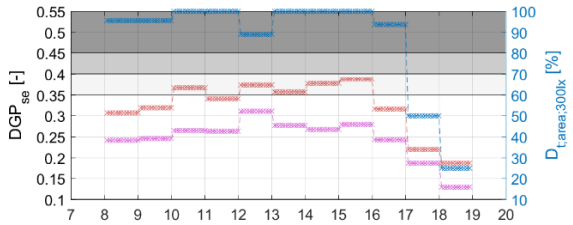
D. SCtree control, double roller blind, maximum 3 large opening movements
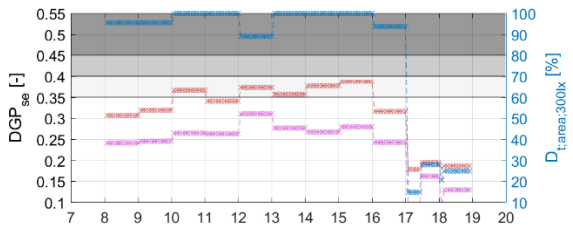
E. SCtree control, double roller blind, maximum 1 large opening movement
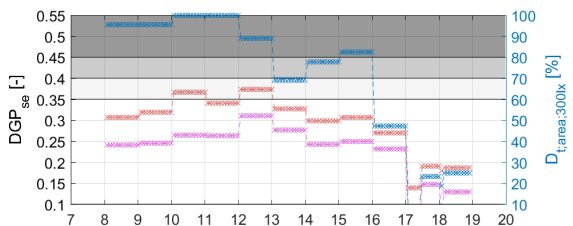
Figure 7.23 Daylighting and glare performance of the SCtree double roller blind strategy and the SC+ single roller blind baseline. Simulation results for the 4th of April

Figure 7.24 shows the performance effects of these additional control rule across a full year. The figure shows that by limiting the number of allowed opening actuations to 1 per day (SCtree-FrBck-Mx1Mv), the number of potentially disturbing instances can be reduced to an extent that the system performs similar to baseline strategies. In terms of the number of large shade actuations (SA$_{num}$) the system now leads to an average of 8 actuations per week compared to 8-10 for the baseline scenarios. If all type of shade movements, including large movements with a single set of activated shades (ShMv$_{num}$), are counted as being equally disturbing then the SCtree-FrBck-Mx1Mv strategy performs slightly worse (16 N/week SA$_{num}$+ShMv$_{num}$) than the baselines (9-13 N/week SA$_{num}$+ShMv$_{num}$).
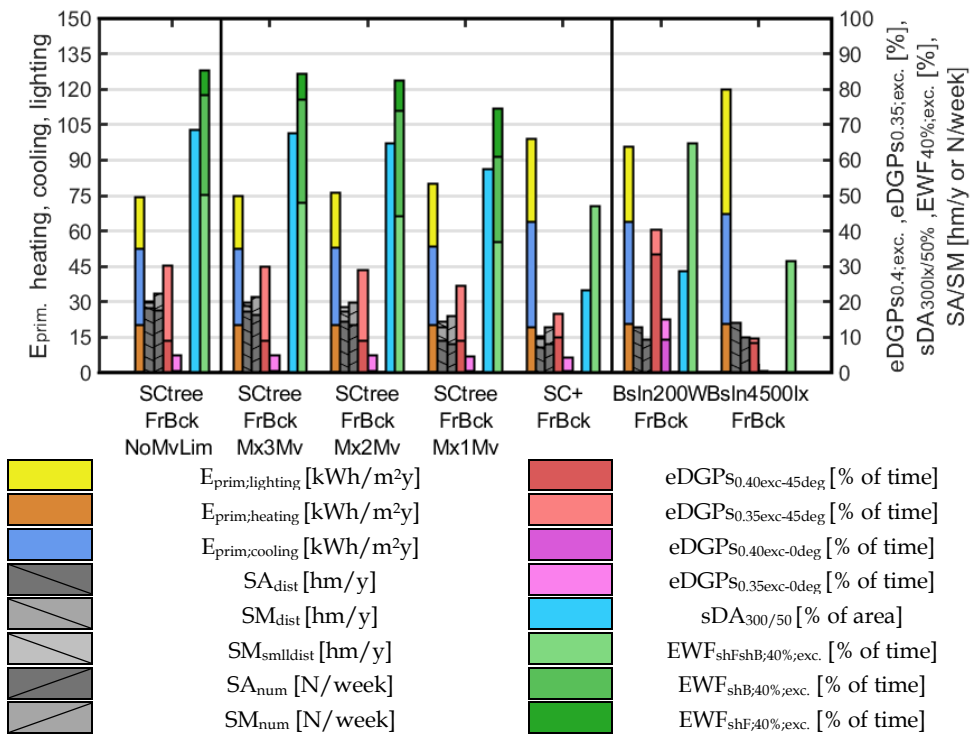
Figure 7.24 Performance effects of limiting the number of shade activations per day in the SCtree-FrBck strategy. NoMvLim: no limatations, Mx3Mv: maximum 3 shade deactivations, Mx2Mv: maximum 2 deactivations, Mx1Mv: maximum 1 deactivation

The graph also indicates a trade-off between limiting the number of potentially disturbing shade actuations on the one hand, and daylighting, energy and view performance on the other. Compared to the SCtree strategy without limitations, the SCtree-FrBck-Mx1Mv strategy leads to 11% less sDA$_{300lx/50\%}$, 7% more E$_{prim}$ and 11% lower total EWF$_{shFshB}$+EWF$_{shF}$+EWF$_{shB}$. The system, however, still performs

substantially better than all the baseline strategies. With SCtree-FrBck-Mx1Mv leading to 29-57% more $sDA_{300lx/50\%}$, a 20-50% lower E_{prim} and 10-43% more total $EWF_{shFshB}+EWF_{shF}+EWF_{shB}$.

7.7 Application discussion and conclusion

The application study showed that the double roller blind system offers substantial performance improvements over conventional automated solar shading solutions, as well as the advanced single roller shade strategy from Chapter 5. The system leads to improved energy performance, with E_{prim} being 15.8-45.8 kWh/m^2 (20-62%) lower, offers a greater admission of daylight, resulting in a 29-69% higher $sDA_{300lx50\%}$, provides superior protection against daylight discomfort glare, with 1-25% less $eDGPs_{0.40exc-45deg}$ and 0-10% less $eDGPs_{0.35exc-0deg}$, and increases the total time that occupants experience a view to the outdoors, expressed in terms of a 10-54% higher $EWF_{shFshB}+EWF_{shF}+EWF_{shB}$. The double roller blind system improves all these performance aspects simultaneously and offers little need for compromise. The extent of these performance improvements does depend, however, on the number of large shade movements and activations that is considered acceptable (the control alternatives from Figure 7.24) and the baseline that the system is compared to.

The results of this study indicate promising directions for the further development of the double roller blind system. The performance of the double roller blind system is constrained by the characteristics of the two fabrics that are used. The results in Section 7.5.3 show that all performance aspects are highly sensitive to the optical properties of the applied fabrics (variation: 16% E_{prim}, 47% more $sDA_{300/50}$ and 11% more $eDGPs_{0.40exc-45deg}$). This suggests that the performance of the double roller blind can likely be improved if these properties are optimised for specific applications. Additionally, using different fabric typologies for the two shades could offer more beneficial performance trade-offs. For instance, Section 7.5.3 showed that diffusing fabrics offer less view-through but are more effective at mitigating discomfort glare. Figure 7.24 shows that the Tv07OF05VCI59 back shade is below seated eye-level for 22-39% of office hours depending on the control alternative that is selected. By using a more diffuse shade, a trade-off can be made between improving daylighting performance and the degree of view to the outdoors during these hours.

The double roller blind concept also offers opportunities for dynamically adjusting the amount of solar radiation that is reflected or absorbed by the shading system largely independently of the amount of daylight that is admitted. Two roller blinds could be used, for instance, that are identical in their visual transmittance behaviour but differ in their solar reflectance. This system could switch the amount of solar energy that is admitted without compromising on the amount of admitted daylight. This application would, however, offer less freedom to dynamically adjust the amount of daylight that is admitted, compared to the concept that was assessed in this study. Another application could be using a high solar absorptance, low visible

transmittance fabric for the inner shade and a high solar reflectance, high visible transmittance fabric for the outer shade. In controlling such a system, there will be strong, and sometimes counter-intuitive trade-offs in balancing the admission of daylight and solar energy that could be navigated using the classification tree method.

Finally, it should be noted that different control modes could be explored to improve the performance of the system further. These could include strategies where the shades are both activated but positioned independently from each other.

7.8 Concluding remarks

This study showed how the VTB can be used to assess the performance effects of systems with a time-varying and highly specular visual transmittance. The study also presented a VTB configuration that allows developers to test the whole-building performance effects associated to detailed fabric design aspects. Additionally, a set of VTB modules and features were developed and verified:

- The $eDGPs_{3PHS-Rpict}$ method (A.3) for computationally efficient simulation of daylight discomfort glare for cases where both contrast and saturation are relevant mechanisms.
- A set of optical models (B.2, B.3.1, B.4) that allow the shading system to be described at different levels-of-scale, and a set of functions that facilitate the definition of consistent input parameters for each model.

The comparison between the $eDGPs_{3PHS-Rpict}$ and $DGPs_{3PHS}$ discomfort glare predictions in Section 7.5.3 showed the inaccuracies in predicting glare performance with the DGPs indicator for shading systems that are characterised by a high specular transmittance. Only in the cases where a diffusing shading device with a low visual transmittance is used (max. 1-2% T_{vis}) and the system is controlled to prevent occupants from being exposed to direct sunlight (i.e.: as in the other chapters of this thesis), does the DGPs indicator provide reliable performance predictions.

This study showed the VTB configuration was able to describe the behaviour of shades with weave patterns that form rectangular openings, leading to partly specular light transmittance. Additionally, the toolchain was tested for completely diffuse shading fabrics. In its current form, the VTB can be used to evaluate the performance effects of fabric design properties for some, but not all, shade typologies. There are multiple limitations to the current toolchain that should be considered in this context. For assessing the double roller blind system, the LBNL-Window perforated screen model is used. This approach simplifies the complex woven structure of the type of fabrics to a screen with uniformly spaced rectangular or circular openings. The model explicitly describes direct transmittance through an opening ($T_{dir-dir}$) and fully diffuse transmittance through the shade material ($T_{dir-diff;mat}$). It does not, however, explicitly describe light entering openings and being

scattered by the outside of the shade thread ($T_{dir\text{-}diff;scat}$). The study in Section 7.5.2 showed that this simplification did not lead to substantial errors (0.1% in $T_{dir\text{-}diff}$ for CGDB-#: 20012). The reason for this is that this study focusses on shading devices with a high COA and VCI resulting from a small shade thickness in relation to the size of the openings. For these types of fabrics, the contribution of $T_{dir\text{-}diff;scat}$ to the overall diffuse transmittance is relatively small (i.e., 0.1% $T_{dir\text{-}diff\text{-}90°\theta}$ versus 3.2% $T_{dir\text{-}diff\text{-}90°\theta}$ for CGDB-#: 20012). For cases where $T_{dir\text{-}diff;scat}$ is likely to have a larger contribution (low COA, large thickness) the LBNL-Window woven shade model can be used. This model however assumes a particular pattern to the fabric weave that was found to not fit well with the type of fabrics investigated in this study.

Although the $eDGPs_{3PHS+Rpict}$ approach was shown to substantially decrease simulation time (98.7%) in relation to DGP_{Rpict}, the efficiency of the approach should be reviewed in relation to other computationally efficient methods. Here, a comparison with the Radiance 5phase method (Geisler-Moroder et al. 2016) and the GLANCE method (Giovannini et al. 2020) is recommended for future research.

This study also presented and tested an extended version of the support method based on classification trees. The study showed that this approach led to a control strategy that is able to classify complex visual comfort conditions and exploit the large number of optical states that the double roller blind system offers. In addition to fulfilling the requirements that were defined in the introduction, the classification tree approach offers opportunities for including user feedback in the control logic. User overrides and sensor data collected during operation could, for instance, be stored within the control system. Such data could then be used to periodically update the control system by uploading new classification trees that were developed with the inclusion of measured data in the training data.

In developing the classification trees in this study, the emphasis lay on mitigating discomfort glare whilst keeping the system in the most open possible state. Other performance aspects, however, can also be included as parameters driving the decisions of the classification tree. This requires formulating these performance aspects in terms of PC_{true} using a criterion classifying instantaneous performance, as was done in Chapter 5.

One limitation of the classification tree approach is that it focusses on instantaneous performance effects. This makes the system less suited for addressing performance aspects that involve transient or historical effects. These limitations can potentially be overcome, however, using additional heuristic control rules, as was illustrated by the study focussed on limiting large shade movements.

Finally, this chapter provided some insights into the causal relationships between shading design parameters and building performance effects:

- Section 7.5.2 showed that detailed shading fabric characteristics are very defining for whole building performance. This shows that there is potential in leveraging these properties to improve building performance.
- Additionally, this shows that there are uncertainties associated to building performance predictions if these detailed fabric characteristics are not known or specified.
- Specifically, the fabric OF was shown to be an important design parameter that should receive more attention.
- The results in section 7.6.1 showed that performance effects of design features and control behaviour are intrinsically linked. In this application study, control behaviour was optimised for shading designs but only a small number of fabric alternatives were investigated. This application study indicates that co-optimisation of design features and dynamic control behaviour are a promising research direction and further research is recommended on investigating this concept with a larger design space of shading fabric design features.

8 Co-optimisation of façade design and automated solar shading systems

8.1 Introduction

Building designers have many options to choose from for managing the admission of solar energy into office buildings, including fixed shading devices (e.g., overhangs and shading fins), glazing properties and dynamic solar shading devices. Because of the fragmented responsibilities within the façade design and delivery process, separate parties often make decisions regarding facade design and control aspects, and decision-making is done in a consecutive manner (Attia et al. 2018). This process tends to follow a stepped (optimisation) approach (Figure 8.1 left), starting at the highest level-of-scale with the design of windows (e.g., position in the façade and window-to-wall ratio) and static shading devices, followed by the selection of glazing and the positioning of dynamic shading devices and ending at the lowest level-of-scale with the specification of a control strategy and control settings for automated shading devices. At each stage, design choices are optimised in an isolated manner where previously made design choices on higher scale levels are considered irreversible and by making simplifying assumptions regarding yet to be made design choices at lower scale levels. In early-stage façade design, for instance, dynamically operated shading device are often assumed not to be present, or a simple control strategy is assumed.

Interior shading devices are often not considered in the facade design phase at all. Building designers have traditionally had a thermally driven approach to specifying solar shading devices and focussed mainly on the ability of such devices to limit and control the admission of solar energy into the building (Van Gessel et al. 2005; Konis and Selkowitz 2017). Dynamic shading devices on the interior of the glazing system, have therefore not been treated as an integral part of the building skin. Such shading devices are often viewed to be functional for glare protection only and the design, installation and operation of such devices is still often considered the responsibility of the users of the building rather than that of the building design and development team. Moreover, standards for energy performance assessment usually assume no interior shading devices are present or assume simplified shading control strategies and to not account for the effects that the operation of shading devices has on lighting energy consumption.

Also, in the scientific literature on simulation-based façade design optimisation simplifying assumptions are usually made. In the majority of studies it is assumed that dynamically operated shading devices are not present (Méndez Echenagucia et al. 2015; Mangkuto et al. 2016; Pilechiha et al. 2020; Susorova et al. 2013) and only few of such studies quantify the effects of the façade design on daylight glare or the effects of user interactions with dynamic shading devices (Huang and Niu 2016; Ochoa et al. 2012b). Also, the number of studies that consider the operation of

automated shading devices within the selection of optimal façade design configurations is limited (Goia et al. 2013a; Goia 2016; Atzeri et al. 2018).

Research on an adaptive opaque facade by (Favoino et al. 2017) and (Jin and Overend 2014), pointed out that the performance of such an adaptive system depends on interactions between design and control features and an optimal outcome requires that these aspects are considered simultaneously in the optimisation process. Earlier research on this topic by (Talami et al. 2020), compared the design outcomes resulting from a sequential optimisation versus a simultaneous (co-) optimisation approach and concluded that the former does not necessarily lead to globally suboptimal outcomes. The research however, explored only the design of windows, opaque fabric materialisation, and the selection of HVAC systems and setpoints. The study did not investigate dynamic shading controls.
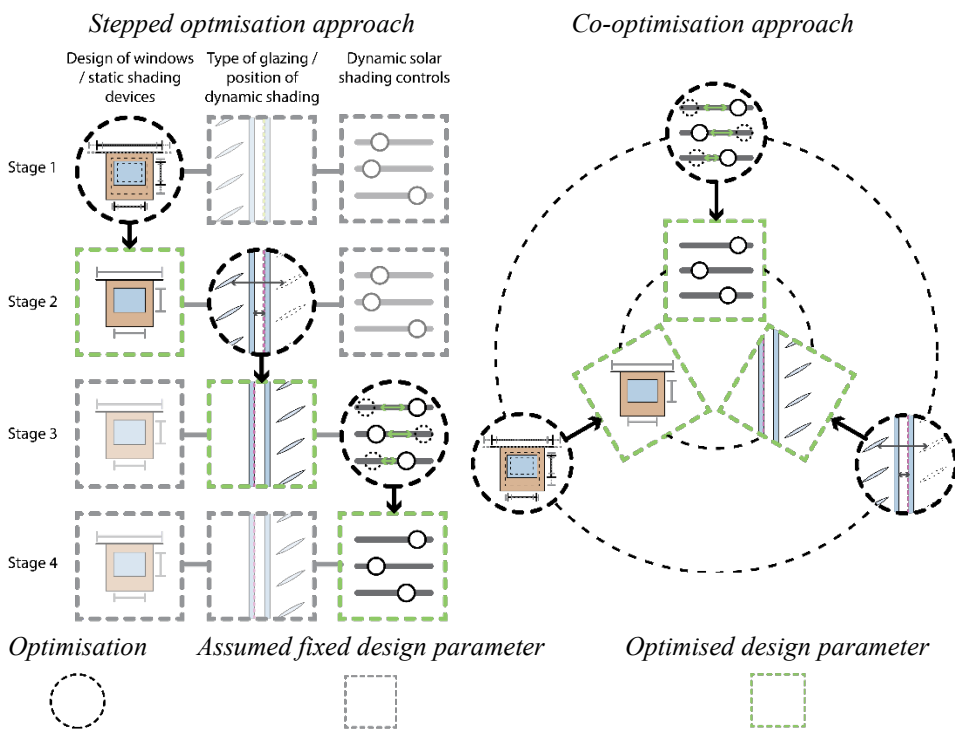
Figure 8.1 The current practice of stepped optimisation (left) of façade design features and solar shading controls and the proposed co-optimisation approach (right)

This chapter focuses on design optimisation of the façade, and optimisation of the applied control rules and control parameters (the B and E levels-of-scale in Table

2.1). The application study will test the hypothesis that co-optimisation of static façade design features and dynamic solar shading control behaviour leads to high-performance solutions that would be missed with a stepped optimisation approach. In this co-optimisation approach (Figure 8.1 right), control features (e.g., control rules and parameters) and design features (e.g., size of the window, static shading devices) are investigated simultaneously to select beneficial combined configurations. By optimising control behaviour to a specific façade design alternative, a building-aware control strategy will be obtained (Motamed et al. 2020; Coffey 2013). The expectation is that such a building-aware strategy can make use of daylight more effectively by employing knowledge of the building's design features. Dynamic shading devices could, for instance, be safely opened without this causing glare when direct sunlight is blocked by static shading systems. This application study explores the potential of such synergies and investigates the question of whether it is important to consider these synergies early on in the façade design process. The goal of this application study is to illustrate how the VTB can applied to facilitate such a co-optimisation process and create building-aware control strategies that exploit unique façade design features.

An additional consideration in this study is that in performing early-stage optimisation studies, practitioners inevitably have to make a great number of assumptions related to yet undecided HVAC systems, and the carbon intensity of grid electricity and other fuels (Atzeri et al. 2018; Jin and Overend 2014). A commonly applied approach for assessing the environmental impacts associated to building electricity consumption, that was also used in the previous chapters, is to simulate the building's end-use electricity consumption and multiply this by an average carbon intensity or primary fossil energy factor (PEF_{nonRE}) that represents the site-to-source efficiency across a year for a particular geographical area (Zirngibl 2020). This approach works fine in a context where electricity is predominantly generated from fossil fuels. It is, however, much less suited in situations where electricity is generated using fuels of varying carbon intensity or intermittent renewable sources (Cubi et al. 2015; St-Jacques et al. 2020; Magni and Ochs 2020). In such a context, the carbon intensity of consumed grid electricity depends greatly on the time-of-use. Additionally, buildings that are designed today, are likely to experience significant changes associated to the current energy transition ambitions of many European countries. Such buildings will experience changes in the characteristics of the electricity grid that services them in the coming decades. Additionally, the energy transition could involve the electrification of heating systems and the type and efficiency of HVAC systems that are representative for newly built buildings is changing. This study will therefore also investigate the effects of (i) different assumptions regarding the future grid load and source

composition, and (ii) the type of applied HVAC systems on energy performance predictions and optimal design outcomes.

To summarise, the goals of this study within the overall research are to:

- Develop and test a VTB configuration for co-optimisation of automated shading controls and static façade design features.
- Develop and test a method for quantifying the consequences of uncertainties regarding future electricity grid characteristics.
- Obtain insight into how interactions between shading controls and static building features affect building performance outcomes.
- Obtain insight into how HVAC system configurations and assumptions regarding future electricity grid characteristics influence performance trade-offs in the design and control of facades with automated shading systems.

The research presented in this chapter was presented, in part, in a IBPSA Building Simulation 2021 conference paper (De Vries et al. 2021a).

8.2 The concept: co-optimization of static and dynamic façade solar control features

This application study takes the perspective of a façade designer who has the following simulation purpose:

i.   To obtain insight into performance trade-offs to support early-stage façade design choices
ii. To select a façade design configuration that offers beneficial trade-offs.
iii. Although the exact control behaviour of the dynamic shading system can be specified at a later stage the designer does not want to regret early-stage façade design choices later.
iv. To select a robust façade design configuration that delivers beneficial energy performance effects regardless of changes in the PEF_{nonRE} of consumed grid electricity resulting from changes in the energy infrastructure servicing the building throughout its lifetime.

The application study is focussed on the optimisation of the façade design of the south facing reference office cell (Section 4.2). Different façade design configurations will be evaluated, varying in terms of the design of a horizontal louvre system, the size and position of the glazed area, the type of glazing and the position of the dynamic shading device in relation to the window.

The façade design configuration of the office cell will be optimised assuming either conventionally controlled dynamic solar shading solutions or an advanced building

aware alternative based on the sun-tracking vertical-blind (STVB) strategy from Chapter 6. The combined configuration of the static horizontal louvre system and the dynamic STVB is aimed at utilizing the strengths of each type of shading system in blocking direct sunlight at different solar positions. Section 6.5.2 showed that a weakness of the STVB system is that, in order to block direct sunlight at solar positions characterized by a low VPPA (Figure 6.1), the blinds have to close fully. For this south facing façade, this situation occurs daily at solar noon (Figure 8.2). At these sun positions, an overhang or horizontal louvre is more effective at obstructing direct sunlight whilst preserving a large unobstructed view of the sky. The concept behind the building aware STVB strategy is that the control strategy detects conditions where the static shading devices offer sufficient glare protection and chooses a more open vertical blind position at these instances. Table 8.1 gives an overview of the main goals and assumptions in this study in addition to the characteristics of the shading system that is investigated.

Low α, high γ* | Vertical blinds   High α, low γ* | Vertical blinds

High α, low γ* | Horizontal overhang
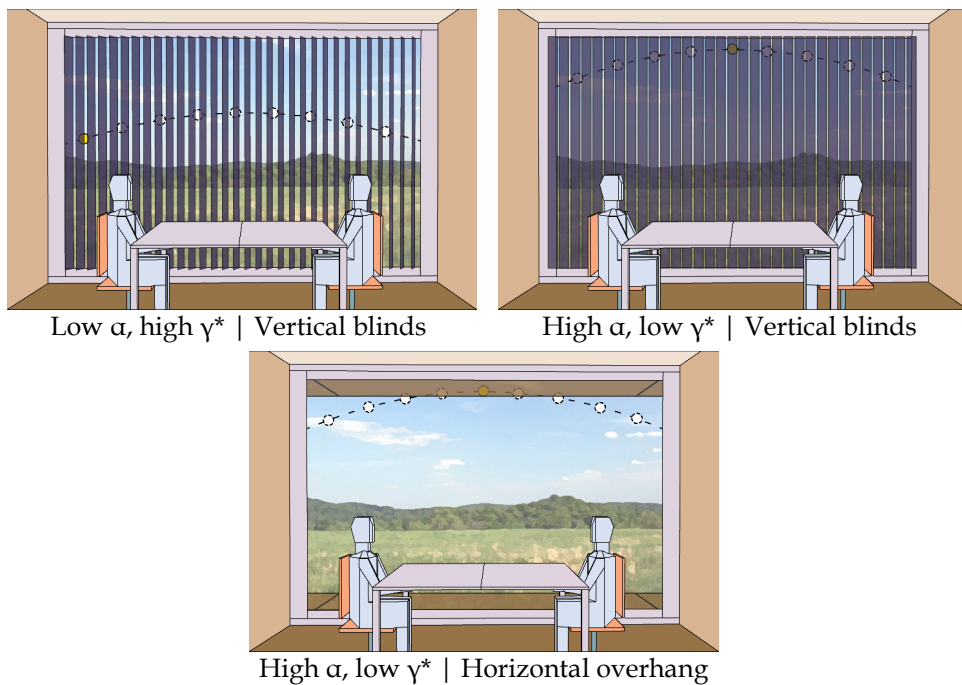
Figure 8.2 Combination of the dynamic STVB and static horizontal solar shading devices

Table 8.1 Goals, assumptions and system characteristics in application study 4

Optimise / investigate:	Assume:	System:
Control rules and parameters	Sensors	Variable rotation angle blind system
Façade design	Shading material	Constant thermal/optical properties
Energy systems	Motorisation system	Complex control logic

8.3 Methodology and simulation strategy

Figure 8.3 gives an overview of the methodology that is followed in this application study. In the first part of the study, the performance of each façade design is simulated for each of the baseline control strategies and each of the individual control modes of the STVB strategy. These simulation results will be used to investigate the performance effects of each façade design parameter for each control strategy and verify the overall VTB configuration (Section 8.5.2). Additionally, quality assurance tests are executed to verify the method for quantifying uncertainties regarding future electricity grid characteristics (8.4.2) and validate the detailed energy systems model (Appendix D).

The method for developing detection algorithms using classification trees based on simulation results, discussed in Chapter 7, is used to develop a building-aware STVB-Ctree control strategy (presented in Section 8.4.1) and the performance of this strategy is simulated. The performance trade-offs in selecting facade design options are then investigated assuming different strategies for the operation of the shading system to assess whether it is important to consider automated control strategies and control optimisation in early design stages. Finally, the influence of different assumptions regarding the applied HVAC systems and the future electricity grid characteristics on façade design performance trade-offs are tested.
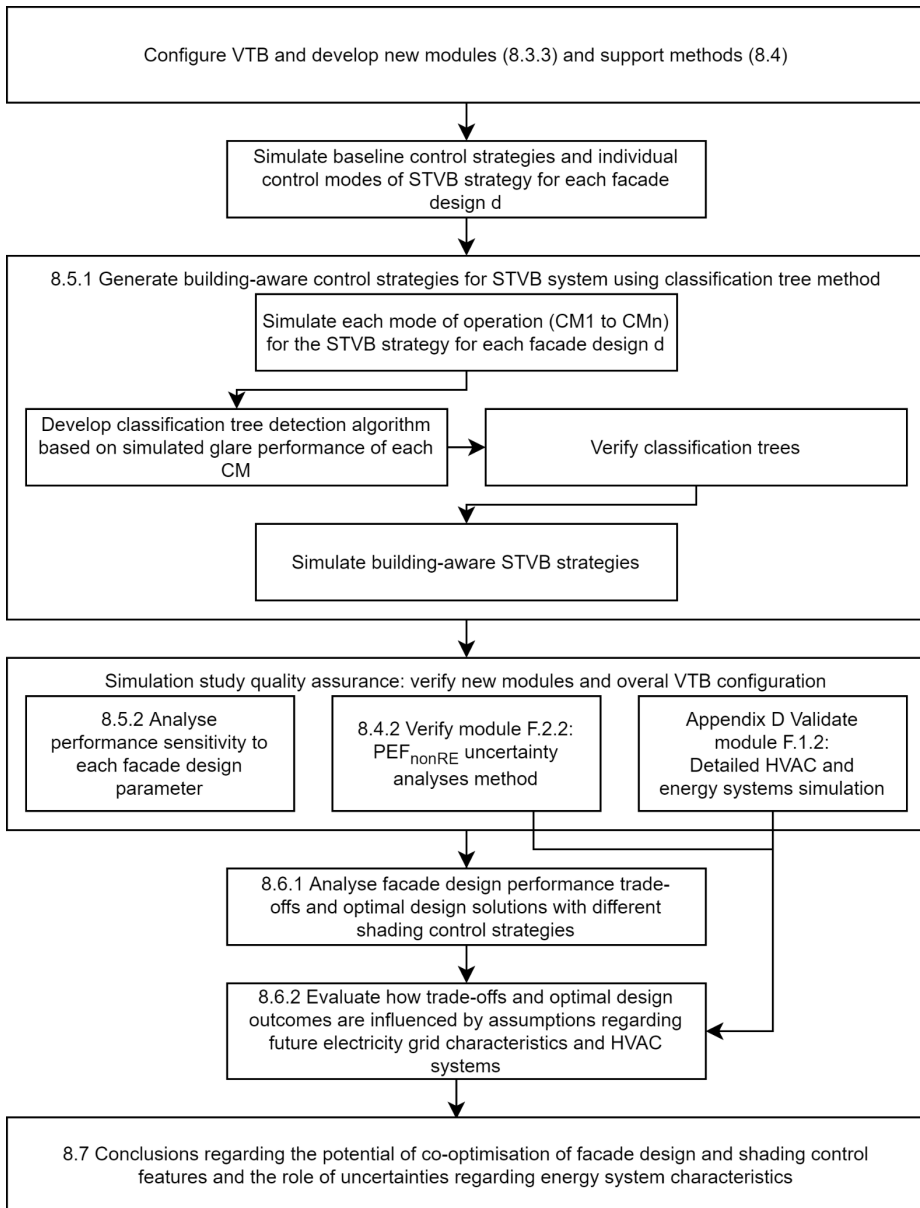
Figure 8.3 Overview of the methodology followed in the fourth application study

8.3.1 The investigated design space

Figure 8.4 gives an overview of all the combinations of façade design configurations and dynamic shading control strategies that will be evaluated in the study.

195
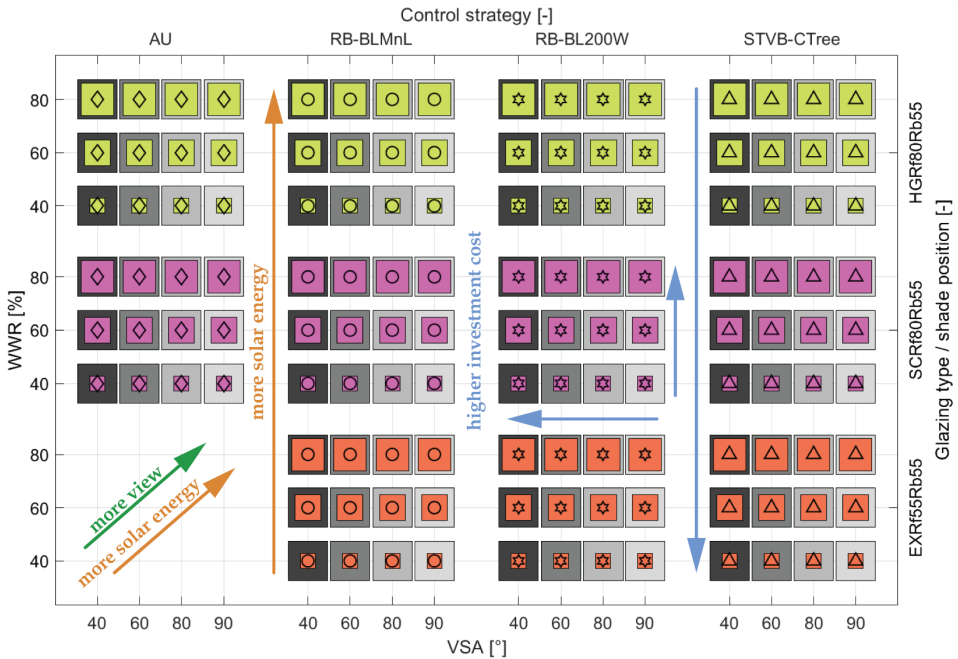
Figure 8.4 Façade design and control strategy alternatives that are investigated in this study. Arrows indicate how these design choices are related to the admission of solar energy, view to the outdoors and investment costs

The design space includes four shading control strategies. In the always up (AU) strategy, it is assumed to no dynamic solar shading is present. This assumption is commonly made in façade optimisation studies in literature. In practice, a solar exposed office space that is delivered without operable shading devices leads to high levels of discomfort glare (Chapter 5) and manually operated shading devices are likely to be installed during operation. To represent this situation, a manually operated roller blind strategy will be used (RB-BLMnl). This strategy is described using the LightSwitch model, developed by Reinhart (2004) on the basis of observed user interactions with an electronically adjustable blind system, controlled by occupants in cellular office spaces (Reinhart and Voss 2003). In the RB-BLMnl strategy, users lower the roller blind fully whenever the horizontal illuminance on the desks of the occupants exceeds 8000 lux, or when one of the occupants experiences glare as proposed by Wienold (2009a). In this study, 'disturbing' glare in either of the two viewing directions is used as criterion to close the shading device (DGPs ≥ 0.4). Additionally, the conventional full-close, full-open RB-BL-200W/m^2 automated control strategy is included amongst the baselines.

The design space includes 36 façade design configurations based on all combinations of 4 horizontal louvre designs (Figure 8.5), 3 glazing and shading device configurations (Figure 8.6) and 3 window designs (Figure 8.7) with varying window-to-wall ratios (WWR). Figure 8.5 shows the four louvre designs. Each design is described using a vertical shading angle (VSA) that indicates the part of the sky that is obstructed (Whitsett and Fajkus 2018; Lyons et al. 2017). The VSA is defined here as the angle between the furthest edge of the louvre and the vertical façade surface. The VSA90 alternative refers to a situation without any exterior louvres. The VSA describes the shading devices in a generic way that specifies only the geometric relationships. Although a set of specific designs is tested in this study, each VSA alternative can be considered representative for a range of design solutions that are equivalent in terms of the part of the sky that is obstructed. In a MSc research, Bodde (2020) showed that many varying louvre designs with the same VSA can lead to similar daylighting performance.

| VSA 90° | VSA 80° | VSA 60° | VSA 40° |
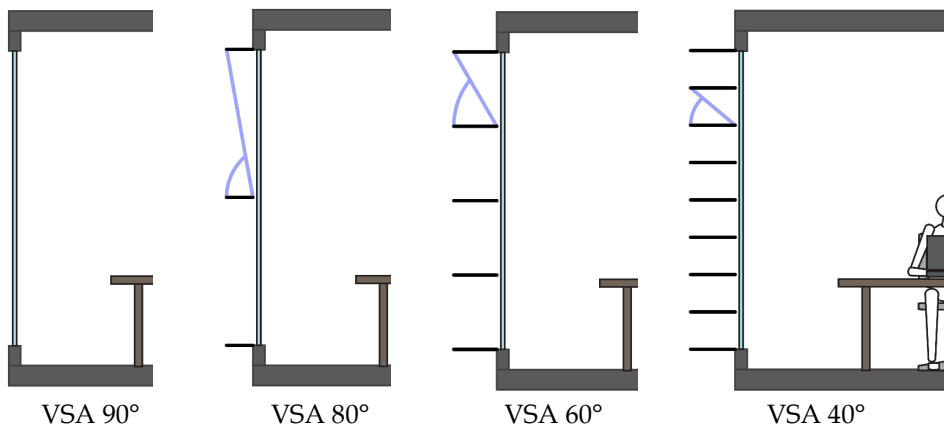
Figure 8.5 The four louvre designs and the vertical shading angle (VSA) that is used to describe them

HG-Rf80Rb55:	SC-Rf80Rb55	EX-Rf55Rb55
High solar gain glazing	Solar control glazing	High solar gain glazing
Coating in position 2	Coating in position 2	Coating in position 3
Interior shading, $R_{f;sol}$:0.8	Interior shading, $R_{f;sol}$:0.8	Exterior shading, $R_{f;sol}$:0.55
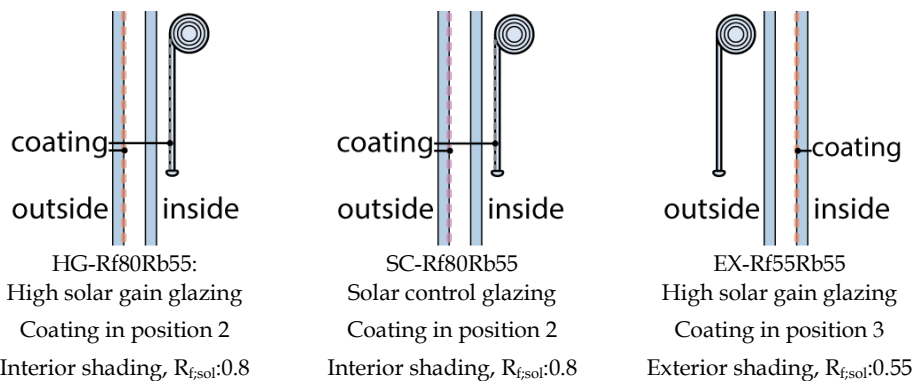
Figure 8.6 The 3 glazing and dynamic shading configurations. A roller blind indicates the position of the shading system. In the STVB strategy a vertical blind is used

The three glazing and dynamic shading device configurations vary in terms of the amount of solar energy that is admitted (Figure 8.6). The HG-Rf80Rb55 alternative uses high solar gain glazing combined with a metallised interior shading system, SC-Rf80Rb55 uses solar control glazing with the same metallised fabric, and the EX-Rf55Rb55 uses high gain glazing with a non-metallised exterior shading system. All shading fabrics have an identical visual and solar transmittance.
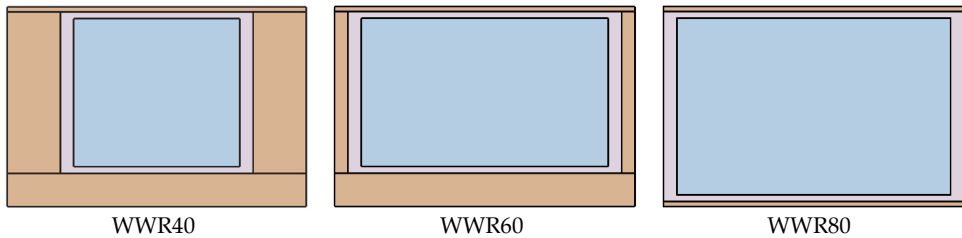
WWR40	WWR60	WWR80
Window-to-wall ratio: 40%	Window-to-wall ratio: 60%	Window-to-wall ratio: 80%

Figure 8.7 Façade elevations showing the three different window-to-wall ratios. The three designs are based on recommendations given by Reinhart et al. (2013). From left to right: 40, 60 and 80% WWR

8.3.2 Performance aspects and indicators

In this study, daylight sufficiency, visual comfort and energy performance will be assessed in a quantitative manner. Energy performance is quantified as primary energy consumption (E_{prim}) for cooling, heating, and lighting. In some graphs a total E_{prim} is presented that includes energy consumption for equipment which is identical for all alternatives (45 kWh/m²). Daylighting performance across a year is assessed using $sDA_{300/50\%}$ and D_{300lx} is used to evaluate instantaneous daylighting performance. The blinds are assumed to have no specular daylight transmittance (0% $T_{dir-dir-\theta}$) and DGPs is used as a glare performance indicator. The same user positions and viewing directions are used as in the previous application studies. For the most critical 0-degree viewing direction 'perceptible' glare is used as a desired performance criterion (DGPs ≤ 0.35) and less than 'disturbing' glare is required for the 45-degree viewing direction (DGPs ≤ 0.40).

The daylighting and glare performance requirements are also combined in this study in the visual comfort time (VCT) indicator. This indicator expresses the share of occupied time where sufficient daylight was available (D_{300lx} ≥ 50%) and none of the occupants experienced glare ($DGPs_{0deg}$ ≤ 0.35 | $DGPs_{45deg}$ ≤ 0.40).

Investment costs and the degree of view to the outdoors will be assessed in a qualitative manner. Figure 8.5 indicates in a qualitative and relative manner how

each design alternative influences the degree of view to the outdoors and investment costs. Larger windows and less exterior shading devices increase visual contact with the exterior. Bigger windows and more exterior shading devices are generally more costly. Additionally, low costs are associated to HG-Rf80Rb55, intermediate costs to SC-Rf80Rb55 and high costs to EXT-Rf55Rb55.

The exposed window fraction (EWF), computed as discussed in Section 6.3.1, is used in this study for analysing the operation of shading devices resulting from different shading control strategies and façade designs. Here, it is only used for analysing control behaviour and not to assess view to the outdoors.

8.3.3 Configuration of the virtual testbed

Figure 8.8 shows the configuration of the VTB for this study. The parts that are new in this configuration are:

- A set of functions that can be used to estimate time-of-use dependent PEF_{nonRE} profiles that correspond with the weather data for the particular location (F.2.2 in Figure 8.8).
- A detailed heat pump model for describing interactions between the effects of advanced shading controls on heating and cooling loads and time-varying HVAC system performance (F.1.2).
- A set of functions for creating classification tree detection algorithms using simulation results for a large façade design space.
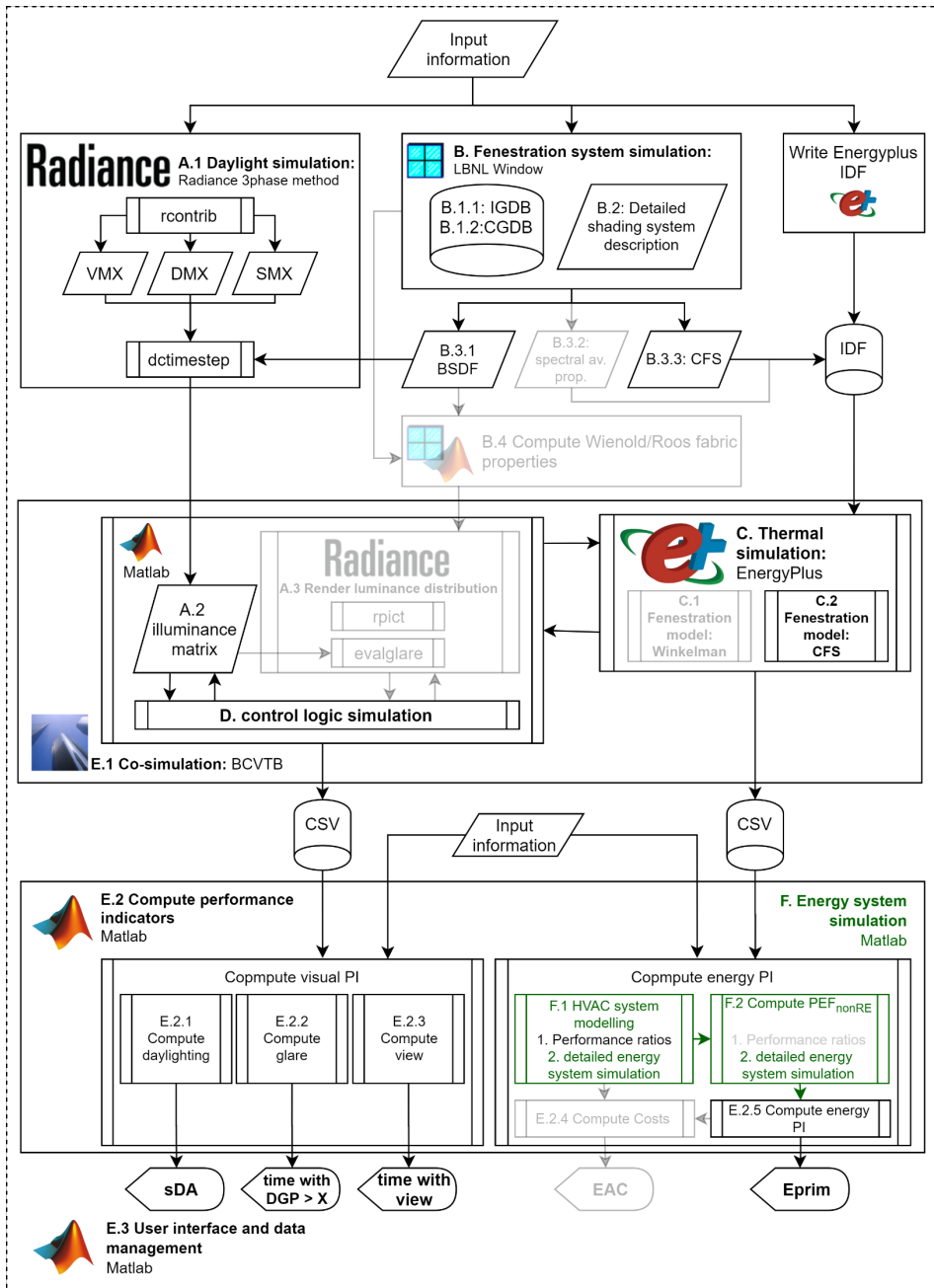
Figure 8.8 Configuration of the VTB for this study. VTB components that are not used in this configuration are shown in light grey. New VTB modules that will be tested in this chapter are shown in green. The input information refers to the geometry and parameters that are specified in Sections 4.2 and 8.3.4

8.3.4 Assumptions and simulation input parameters

This study largely uses the same assumptions as in Chapter 6. Additional input parameters are shown in Table 8.2.

Table 8.2 Simulation parameters and assumptions

		EnergyPlus	Radiance
Fenestration	Interior shading device	LBNL-Window venetian blind model	
	Exterior shading device	Lambertian reflector, $R_{vis/sol}$: 0.2	
	SC-Rf80Rb55	Layer 1: IGDB# 21056, Layer 2: IGDB# 1608, Layer 3: VB	
	HG-Rf80Rb55	Layer 1: IGDB# 11560, Layer 2: IGDB# 1608, Layer 3: VB	
	EXT-Rf55Rb55	Layer 1: VB, Layer 2: IGDB# 1608, Layer 3: IGDB# 11560	
		CFS	BSDF

In this application study, E_{prim} will be computed for assuming two different HVAC system configurations (Table 8.3). Initially, the conventional HVAC system configuration is used, that is also assumed in the earlier chapters of this research. This system is representative for a situation with a gas-based heating system and cooling system that uses a relatively inefficient chiller with an outdoor air condenser. The system is described in a simplified manner using Equation 2.3 and the constant efficiencies presented in Table 4.1. In Section 8.6.2, also the effects of a more efficient all-electric HVAC concept will be explored. This second HVAC system configuration assumes a non-ducted air source heat pump for both heating and cooling. A detailed model is used to simulate the indoor and outdoor temperature dependent behaviour of the heat pump. In Appendix D the model is described in more detail and the implementation of the model is validated through inter model comparison that was performed within the IEA SHC Task-56 framework.

Table 8.3 Summary of heating and cooling system performance indices

HVAC conventional	$\eta_{cool,deliv}$: 0.7	Air-based cooling delivery system
	$SEER_{cool}$: 3	Chiller with outdoor air condenser
	η_h: 0.95	Natural gas condensing boiler
HVAC all-electric	$SEER_{cool}$: 6.6	Non-ducted air source heat pump
	SPF_{heat}: 4.8	Non-ducted air source heat pump

8.4 Support methods

The following sections present the support methods, and new ways of applying them, that were developed for this application study.

8.4.1 Application of the classification-based control development method: building features as control input parameters

Figure 8.9 shows how the method for developing control strategy classification trees based on simulation results, presented in detail in Section 7.6, is applied in this study. In the earlier application of the method, a set of classification trees was developed using performance classifications (PC_{true}) based on glare simulation results for a single building. In the present application, the PC_{true} will be created using glare performance predictions of the entire façade design space.

Instantaneous performance (P) and sensor measurements (S) are simulated for each control mode (CM) and each design (D), that is described using its design characteristics (DC). For each CM the PC_{true} is then defined and a classification tree (CT) is developed using P, S and DC as predictors. In the operational phase of the control strategy, a set of building features (DC) are obtained as input parameters to the control strategy and used along with sensor measurement and solar position data as predictors for the CT.
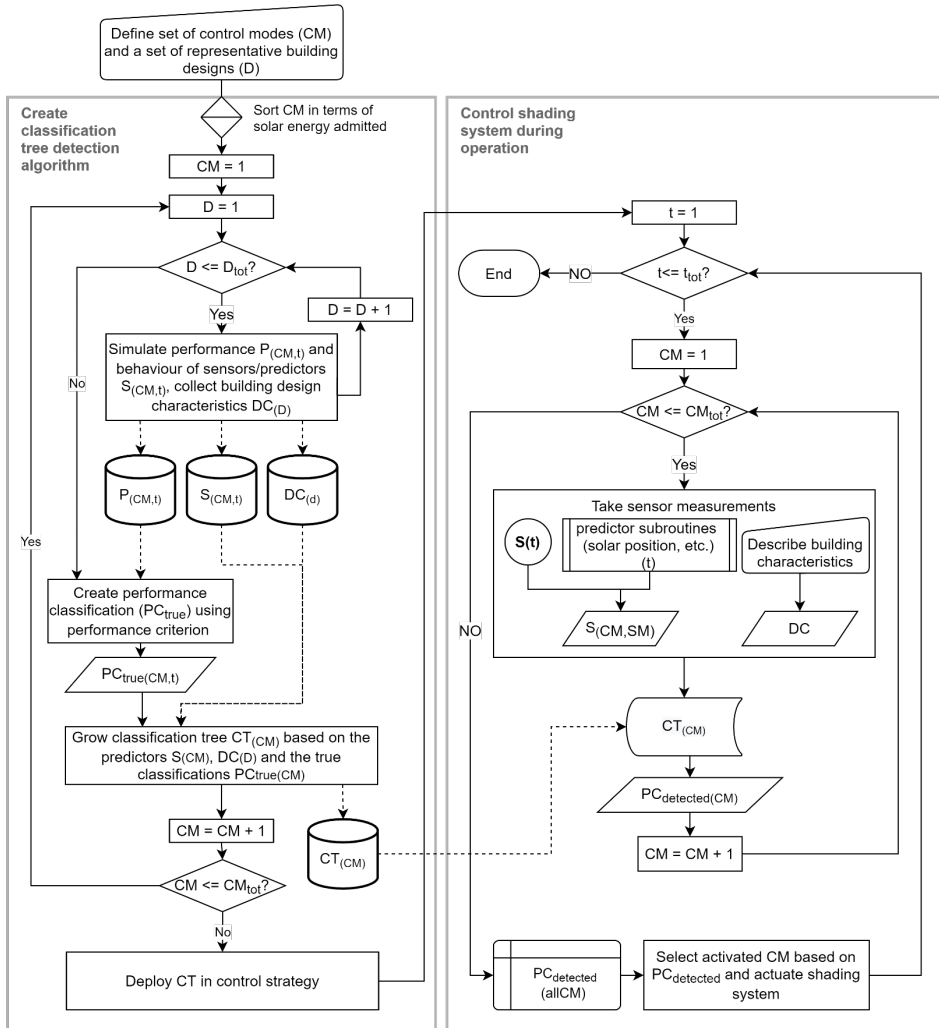
Figure 8.9 Configuration of the method for developing control strategy classification trees for a set of representative building applications that are described using design characteristics (DC)

8.4.2 A Method for developing PEF$_{nonRE}$ profiles to represent future grid electricity uncertainties

Several methods have been proposed in literature for deriving hourly emission factors, representative for the current characteristics of grid regions, from measured grid load and generation data (Cubi et al. 2015; St-Jacques et al. 2020). These methods, however, do not directly provide insight into the performance of different building designs when the grid load and source composition of the electricity grid

changes in the future. Ochs and Dermentzis (2018) proposed an approach for developing monthly PEF$_{nonRE}$, representing possible future electricity grid scenarios, using estimated grid load and generation curves together with assumptions regarding the source composition of the annually produced electricity in these scenarios. Ochs and Dermentzis (2018) and Magni and Ochs (2020) applied the method in the selection of cost-optimal building technologies for reducing primary non-renewable energy consumption in an office building renovation. The research showed that different assumptions regarding future electricity grid solutions leads to different decisions regarding cost-optimal outcomes which indicates the importance of considering various future electricity grid scenarios when choosing amongst various energy saving technologies.

This research extends the method proposed by Ochs and Dermentzis (2018) to develop time-varying PEF$_{nonRE}$ profiles on the basis of the weather data used for building performance simulation. The method is developed to:

- Establish realistic connections between the time varying PEF$_{nonRE}$ and the weather data that is used in the building performance simulations.
- Be suited for the early-stage façade design context where there is little time available for detailed systems modelling, there is a lack of detailed information regarding energy systems and where practitioners are not subject matter experts on the topic of the local electricity grid.
- Reflect the range in expected energy performance associated to the uncertainty regarding the load characteristic and source composition of the future electricity grid.

The aim of this method is not to give a detailed and accurate description of the interactions between a particular building design and the electricity grid in a specific scenario. Rather, the method is primarily used in this research to explore the importance of addressing the uncertainties regarding future electricity grid characteristics. Additionally, the method can be used to identify robust design solutions that give beneficial performs across all plausible future electricity grid scenarios.

Figure 8.10 gives an overview of the developed method. The input for this algorithm is the weather data and a set of assumed scenarios that describe the annual source composition of grid electricity. Although it is clear that the composition of grid electricity is likely to change and many countries have pledged to implement specific fractions of renewables in the future, there is still much uncertainty about how such pledges will be fulfilled. This uncertainty is described in this research using the generation scenarios shown in A. In this study, estimations by Abels-Van Overveld et al. (2020) regarding the current

characteristics of the Dutch electricity grid are included (HighFossil21Ren) as well as projections for 2030 based on current national policies (HighWind64Ren). Also, scenarios are included that describe a situation where the national policy goal is fulfilled with higher fractions for solar (HighSolar64Ren) or nuclear[5] (HighNuclear64Ren) energy sources, in addition to scenarios with less (HighNucFos34Ren) and more (HighWind64Ren) renewable generation than is stated in current policies. A time step is then selected at which the PEF_{nonRE} should be computed. Within this time step the PEF_{nonRE} will be assumed constant. In this study, this will be done on a monthly basis but smaller time steps are also possible.

Figure 8.10 Overview of the method used for generating the monthly PEF_nonRE scenarios

---

[5] Nuclear here stands for types of electricity generation with low a low carbon intensity that does not vary across time

Figure 8.11 Input assumptions and results of the method for developing PEF$_{nonRE}$ profiles for consumed grid electricity

Multiple variables are taken from the weather data to generate a set of renewable generation and grid load unit fraction profiles. Average windspeed and global horizontal irradiation are used, respectively, to develop the wind and solar generation profiles. Outdoor dry bulb temperature is used to compute the number of heating- and cooling degree days (HDD and CDD) per period. A time step unit fraction profile (B) is computed for each of the variables by dividing the value at each time step by the annual sum for that variable using the equation:

$$p_{prof}(t) = \frac{P(t)}{\sum P(t)} \qquad (8.1)$$

Where P(t) is one of the environmental variables based on the weather data

206

The HDD and CDD profiles are linearly scaled and combined to form load profiles (C) that are considered representative for plausible future grid load scenarios. Here, the scenarios are made to represent different types and degrees of adoption of electrical heating solutions on a National scale as well as varying degrees of summer cooling. Potentially, also parameters like solar radiation or wind speed could be used in future research to represent changes in the efficiency of building skins.

For each generation scenario g and load scenario l, the energy that could be generated by each source $E_{gen;src(t,g,l)}$ is then computed using the equation:

$$E_{gen;src(t,l,g)} = f_{gen;src;g} \cdot p_{gen;src(t)} \cdot \sum E_{load(t,l)} \tag{8.2}$$

Where: $E_{gen;scr(t)}$: energy generated by source src,
$f_{gen;scr}$: annual fraction of load covered by source in generation scenario g,
$p_{gen;scr(t)}$: generation profile, $E_{load(t,:)}$: grid load at time step t for load scenario l

The computed $E_{gen;src(t,g,l)}$ does not account for curtailment of renewables and ramping down of fossil sources. In the next step, a merit order is therefore assumed. Here, the order of the different sources in terms of carbon intensity (PEF$_{src}$ in) is used as a merit order. The $E_{gen;src(t,g,l)}$ including curtailment is computed by looping through this merit order and subtracting the energy generated by each source from the remaining grid load.

The time step primary energy factors (PEF$_{src(t)}$) are now computed for each source using Equation and the PEF$_{src}$ factors (). The PEF$_{src(t)}$ contributions of the different sources are then summed at each time step to obtain the total PEF$_{(t)}$. This procedure is repeated for each g and l scenario to obtain PEF$_{nonRE(t)}$ profiles, shown in D, that together describe the range of uncertainty regarding the future electricity grid. The colour of the lines in this graph shows the average annual PEF$_{nonRE}$, denoted as avPEF$_{nonRE}$, that can be used to identify each scenario.

$$PEF_{nonRE(t,l,g)} = \frac{E_{gen;src(t,l,g)}}{E_{load(t,l)}} \cdot PEF_{src} \tag{8.3}$$

$PEF_{nonRE(t,l,g)}$: Non-renewable primary energy factor for src in scenario g and l at time step t, PEF_{src}: PEF for source src

Table 8.4 Assumed PEF for each source

PEF$_{gas}$	2.48	PEF$_{wind}$	0.05	PEF$_{const;RE}$	0.02
PEF$_{coal}$	2.56	PEF$_{solar}$	0.10		

8.5 Quality assurance

This section highlights quality assurance of some of the new VTB features. Section 8.5.1 presents how the classification tree method was applied to develop a building-aware STVB-CTree strategy. Additionally, the glare classifications made by the classification trees are analysed to verify their correct functioning. The goal of Section 8.5.2 is to verify the correct functioning of the overall VTB configuration using a sensitivity analysis. In this sensitivity analysis the effects of each design parameter on the different performance indicators will be evaluated.

8.5.1 Verification of the classification-based support method in this application

Table 8.5 shows the selected control modes for the STVB-CTree control strategy. The first three (Op-Mx-Mn) follow the same control logic as was presented in Chapter 6. To be able to meet the more stringent DGPs$_{45deg}$ ≤ 0.40 visual comfort goal in this study, a fourth **Cls** control mode is added that closes the blinds 30 degrees (bRA) beyond the Mn sun tracking approach (Appendix F, Table F.1). This control mode is activated when the CTs predict that all other control modes lead to glare. Table 8.6 shows the variables that are used as predictors in creating the CT's and for classifying glare conditions during operation. Here, also the WWR, VSA and glazing and dynamic shading configuration are used as predictor variables and assigned as control inputs. Using the described method, a set of classification trees was developed using annual simulations of the control modes in Table 8.5, the sensor variables (S) and design characteristics (DC) in Table 8.6 as predictors, and the true performance classification (PC$_{true}$). PC$_{true}$ is computed using the equation:

$$PC_{true(t)} = eDGPs_{0deg\,(t)} \geq 0.39 \mid eDGPs_{45deg\,(t)} \geq 0.34 \qquad (8.4)$$

As in Chapter 7 the STVB-CTree control strategy activates the most open control mode that does not lead to glare.

Figure 8.12 (left) shows the simulated glare performance and Ev sensor data that was used to develop the classification tree CM2. In the graph, simulation results of all façade design alternatives are shown. The right part of the image shows the classification made by CT$_{CM2}$ based on the predictor variables. The graph shows that the classification tree functions as intended.

Table 8.5 Control modes for the STVB-CTree system

Control mode:	**Op:** Most open blind rotation	**Mx:** Most open sun tracking	**Mn:** Most closed sun tracking	**Cls:** Close beyond sun tracking
STVB-CTree	CM1	CM2	CM3	CM4
Admit less solar energy ▶				

Table 8.6 Predictor variables used to grow classification trees in this study

Sensed and computed variables (S)			
EWF(CM)	Ev	γ	α
Exposed window fraction that would result if CMn were activated	Vertical illuminance at window sensor	Solar azimuth	Solar altitude

Control inputs based on building design characteristics (DC)		
WWR	VSA	ShGlz
Window-to-wall ratio	Vertical shading angle	Shading and glazing configuration
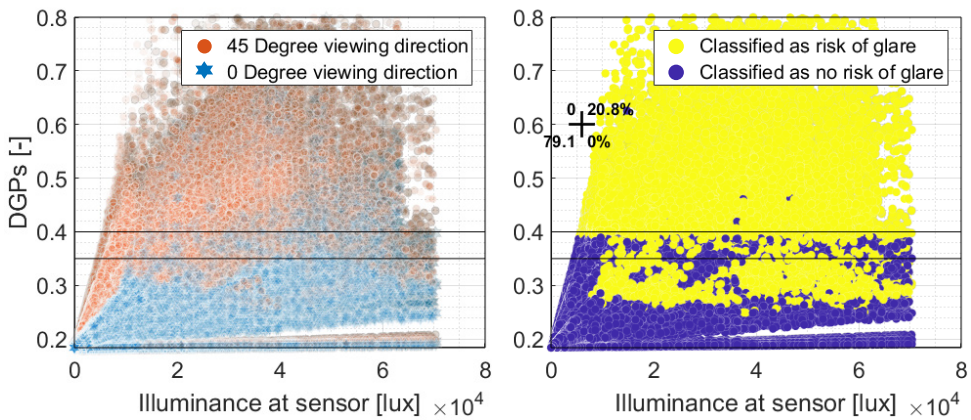
Figure 8.12 Simulated glare performance predictions and predicted classifications for control mode CM2. Simulation results for all building designs. Left: The glare performance data used to grow the classification tree for CM2 in relation to the Ev sensor measurements that are used as one of the predictors. Right: Classifications by CT$_{CM2}$ based on simulated predictors and building design characteristics

8.5.2 Verification of VTB configuration: evaluate performance sensitivity to design parameters

Figure 8.13 shows the sensitivity of each performance indicator to the different façade design aspects for the AU control scenario. The graph shows that E$_{prim}$ strongly depends on the chosen WWR (8-30 kWh/m²), particularly if HG glazing is used (30 kWh/m²). VSA has a smaller effect on E$_{prim}$ (1-10 kWh/m²). It is only for the 80% WWR and HG glazing designs that the presence and dimensioning of the horizontal louvres has a substantial effect on E$_{prim}$ (10 kWh/m²). The reason for this is that although larger louvres help reduce cooling energy demand, they also increase lighting energy consumption. Consequently, the louvres help reduce E$_{prim}$

in cases with extremely high solar gains (e.g., large window and HG glazing) but increase E_{prim} in cases with low solar gains (e.g., small window and SC glazing).

Because no dynamic shading device is assumed to be present, $sDA_{300lx/50\%}$ is close to 100% in most design alternatives. It is only in the design cases with a small window and the largest VSA40 louvre dimensioning that a substantial decrease (25%) in $sDA_{300lx/50\%}$ occurs. Glare performance is highly dependent on the chosen WWR and louvre design (35% variation in $DGPs_{0.35exc-0deg}$) where the louvre VSA has the strongest influence (27% variation). Because the SC glazing has a 10% lower visual transmittance it leads to a 0-10% lower $DGPs_{0deg}$, with the magnitude of the improvement depending on the other design variables. The results indicate that a situation without dynamic shading devices is very undesirable and unlikely to be accepted in practice as it leads to conditions with glare for 10-50% of occupied hours.

The VCT indicator, that considers both daylighting and visual comfort, is relatively insensitive (11% VCT) to the chosen WWR because the benefits of larger windows are offset by an increasing number of instances with discomfort glare. Increasing the size of the louvres, however, improves VCT regardless of the type of glazing of WWR that is used.

Figure 8.14 shows the performance sensitivity to façade design aspects for the dynamically operated shading cases. The results show that the effects of the chosen horizontal louvre design on energy performance depend strongly on the control strategy that the design is paired with. With the RB-BL strategy, a lower VSA (bigger/more louvres) generally increases E_{prim} (10 kWh/m^2 variation) due to increased lighting energy consumption. It is only for a design with an 80% WWR and HG glazing that adding a VSA80 exterior louvre helps reduce E_{prim} (4 kWh/m^2 in relation to VSA90).
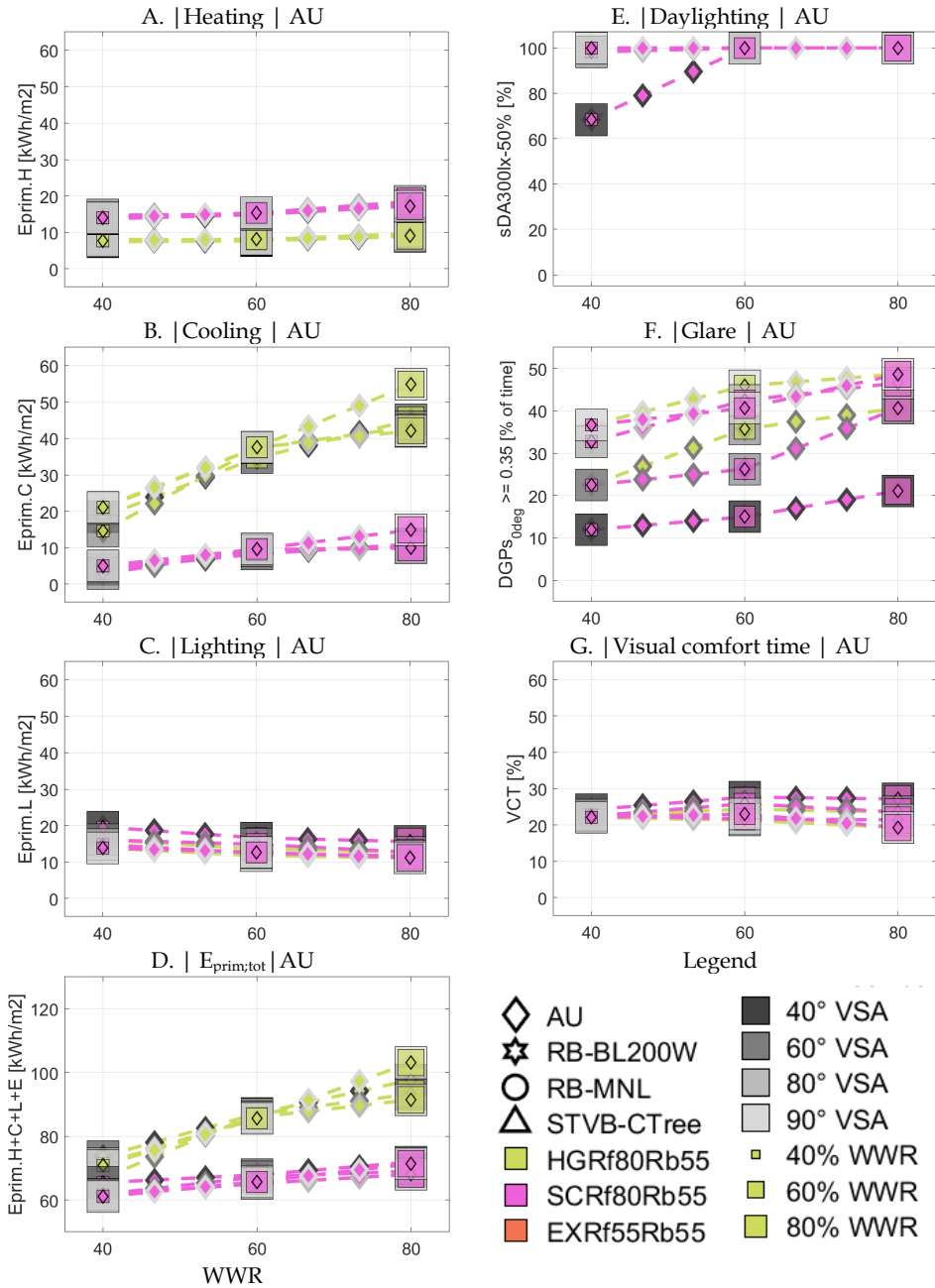
Figure 8.13 Sensitivity of each performance indicator to the different façade design aspects assuming no dynamic shading is present (AU).
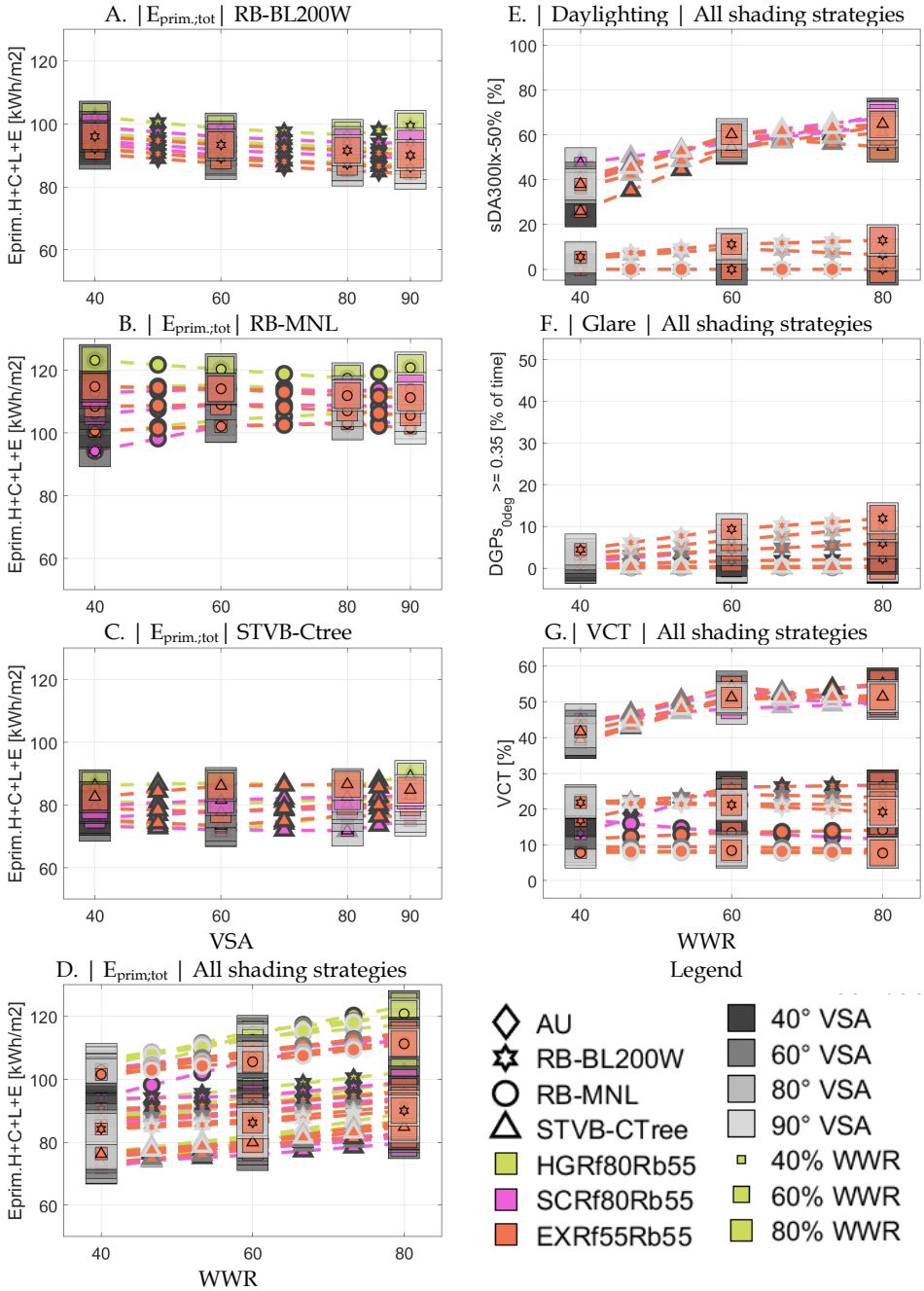
Figure 8.14 Performance sensitivity for the dynamically operated shading cases

If dynamic shading devices are operated according to the RB-MNL strategy, VSA becomes strongly defining for E_{prim} outcomes (~30 kWh/m² variation) and contrasting patterns can be observed. For the designs with small windows (40% WWR), increasing the louvre depth (lower VSA) reduces cooling energy consumption because more solar radiation is blocked by the louvres. Additionally, the low VSA louvres help reduce the number of instances with glare, preventing users from closing the dynamic shading device. Consequently, a lower VSA also leads to less heating and lighting energy consumption in these cases (~10 kWh/m² lower overall E_{prim}). For the design with an 80% WWR and HG glazing, however, choosing a lower VSA increases cooling energy because the more frequently opened shading devices lead to excessive solar heat gains cases (~8 kWh/m² higher overall E_{prim}). Many of the other designs lie between these two extremes and appear relatively insensitive to VSA because the two aforementioned effects cancel each other out. With the STVB-CTree strategy, E_{prim} is less sensitive to the chosen louvre design (~4 kWh/m² variation) and minima tend to vary depending on other design choices.

With the two automated shading strategies (RB-BL and STVB-CTree), E_{prim} becomes less sensitive to the WWR (7-11 kWh/m² variation) and there is a smaller penalty for using a larger window than with the AU and RB-Mnl strategies. With the STVB-CTree strategy, SC glazing consistently offers the lowest E_{prim}. This in contrast to the pattern that can be observed with the other control strategies where EX glazing usually offers the lowest E_{prim}. The reason for this is that with the STVB-CTree strategy, direct solar radiation is blocked more often than with the other strategies, in order to prevent discomfort glare. When STVB-CTree strategy is used to control an exterior shading device in the EX-configuration this leads to lower solar heat gains in winter and, consequently, a larger increase in heating energy consumption than with the other control strategies. With the STVB-CTree strategy, the SC-configuration leads to the lowest E_{prim} because it offers the best trade-off between cooling and heating energy consumption.

For all cases with dynamically operated shading, overall VCT depends on an interplay of exterior louvre design and window size and various contradictory patterns can be observed. The RB-BL and RB-Mnl strategies lead to poor daylighting performance and hence the strategies do not offer much improvement in VCT (0-13%) over the situation with no glare protection devices (AU). These results suggest that amongst the dynamically operated alternatives, only RB-BL leads to a substantial number of instances with perceptible glare, particularly for the cases with an 80% WWR and 90VSA (12% $DGPs_{0deg}$). The results also show the difficulties of quantifying glare for a manually operated strategy that is driven by visual discomfort. The RB-Mnl strategy is predicted to lead to very little $DGPs_{0.35exc-0deg}$ because when glare occurs it is resolved in the next time step. The VCT indicator

therefore gives a more representative indication of the effects of a manual strategy on visual comfort conditions.[6] As with the AU strategy, the RB-BL and RB-Mnl strategies offer a poor trade-off between glare and daylighting performance as is witnessed by the relative insensitivity of the VCT indicator to façade design choices (1-11% variation). With these strategies, using a larger window can even lead to a depreciation in VCT (0-5%) and only leads to an improvement (9-11% VCT) for the cases that also deploy the most/deepest louvres. This is not the case for the STVB-CTree strategy where design choices have a larger effect on VCT (8-19% variation). With this strategy, choosing a larger window increases $sDA_{300lx/50\%}$ without also increasing $DGPs_{0.35exc-0deg}$. Consequently, VCT is substantially higher (4-16%) with larger window sizes (60-80% WWR), particularly for the cases that include exterior louvres.

The presented results can be explained with known principles from building physics and it is concluded that the VTB configuration functions as intended. The results provided insights into the combined effects of façade design choices and control behaviour on performance indicators and suggest that optimal design configurations vary depending on the type of assumed dynamic shading controls.

---

[6] The number of user operations or instances with discomfort glare were found to be a suited additional indicator for investigating this in detail

8.6 Co-optimisation of static façade design features and dynamic solar shading controls

8.6.1 Co-optimisation versus stepped optimisation

Figure 8.15 shows VCT and E_{prim} for each of the investigated combinations of façade design options and dynamic shading strategies. In this figure, daylighting and glare performance are only shown through the combined VCT indicator and E_{prim} gives the total primary energy consumption for heating, cooling, lighting and office equipment. In Figure 8.15A, the groups belonging to the four control strategies are highlighted. Desirable design and control solutions, that combine low energy consumption with a high degree of visual comfort can be found in the lower right of the graph.

To assess whether different assumptions regarding the operation dynamic shading devices lead to different optimal multi-criteria trade-off design solutions, the optimal solutions for each control group will be compared. At this stage, a group of pareto optimal solutions will be identified without assuming a preference between the two performance indicators. A pareto optimal solution here refers to a design solution that offers better performance for one of the two indicators than that of any other design solution that has the same or better performance in terms of the other performance indicator (Radford and Gero 1980). In this case, this means that for any design solution within the pareto optimal group, improving VCT by changing the design can only be done at the cost of a less favourable E_{prim} and vice versa. In Figure 8.15B, the pareto optimal solutions for each control group are highlighted. These pareto optimal solutions were identified using the weighted sum method (Yang 2014), described in detail in Appendix E.
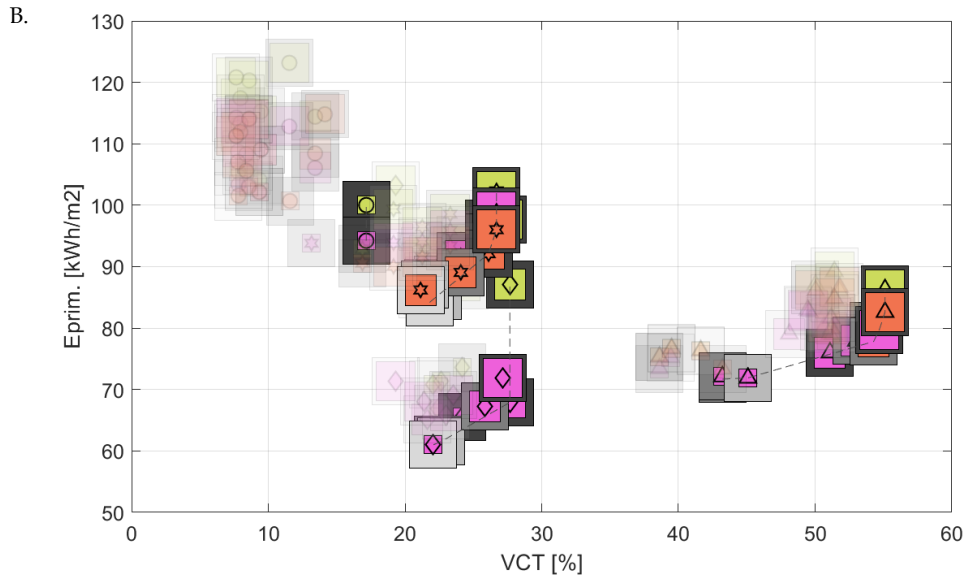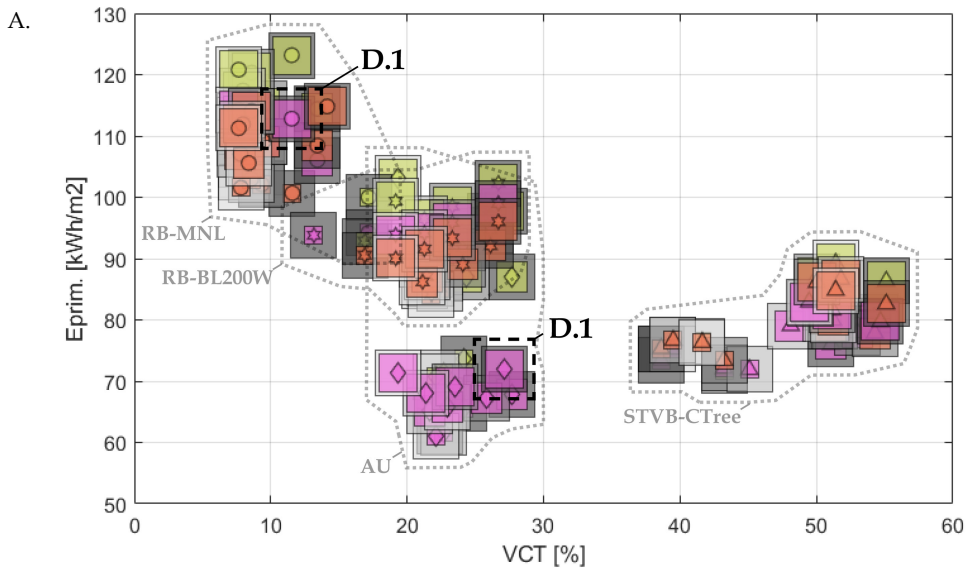
Figure 8.15 A: VCT and total E_prim (including equipment) for all façade design options and dynamic shading control strategies. B: Pareto optimal solution highlighted for each group

Some initial observations can be made based on these graphs:

- For the investigated office space, the chosen strategy for operating the dynamic shading devices is more defining for VCT and E_{prim} than any of the façade design choices.
- E_{prim} is very sensitive to façade design choices for the groups with no dynamic shading (AU) or manually operated devices (RB-MNL). In these groups there is a maximum difference of 29-42 kWh/m^2 in E_{prim} amongst the façade design alternatives. E_{prim} is relatively insensitive (17-18 kWh/m^2), however, to façade design choices for the groups that employ automated shading strategies (RB-BL and STVB-CTree).
- Façade design choices can lead up to 17% difference in VCT for the STVB-CTree strategy whereas these choices lead to only 7-8% of difference for the other strategies.
- Particularly, the design solutions with large windows (80%WWR) and deep louvres (low VSA) stand out as offering beneficial VCT performance for the STVB-CTree strategy.
- The different groups of dynamic shading strategies lead to different pareto optimal façade design configurations.

Figure 8.15 indicates the importance of considering the presence of dynamically operated glare protection devices in earl-stage façade design. The D.1 markers that outline the SC-40VSA-80%WWR design configuration in Figure 8.15A, give an example of this using the preferences of a fictive designer. If the designer makes the commonly made assumption that no dynamic shading is present (the AU group) whilst performing the façade design optimisation study, they will find that the SC-40VSA-80%WWR design configuration (D.1) offers beneficial trade-offs between E_{prim} and VCT and might therefore choose this design option. A situation without shading devices, however, leads to an unacceptable degree of glare (AU in Figure 8.13) and it is likely that manually operated shading devices (RB-Mnl) will be installed during the building's operation. Within the manually operated RB-Mnl group, however, the D.1 design is far from optimal and more beneficial performance would have been achieved with a smaller 40%WWR (7 kWh/m^2 less E_{prim} and 2% more VCT). Identifying this design option would have required that the RB-Mnl strategy was considered in the initial design optimisation.

The results for the RB-BL and STVB-CTree strategies provide some insights into the question of whether it is necessary to co-optimise an automated shading control strategy when making early-stage façade design decisions. Potentially, a simplified stepped design approach could be taken where the simple RB-BL strategy is assumed in early design stages, a particular façade configuration is selected, and the control strategy is later optimised (STVB-CTree) in relation to the chosen design. The

difference between the stepped and the co-optimised design approaches is clarified in Figure 8.16 which shows only the regions containing the RB-BL and STVB-CTree groups from the previous graphs.

A. BL-200W/m2 control strategy
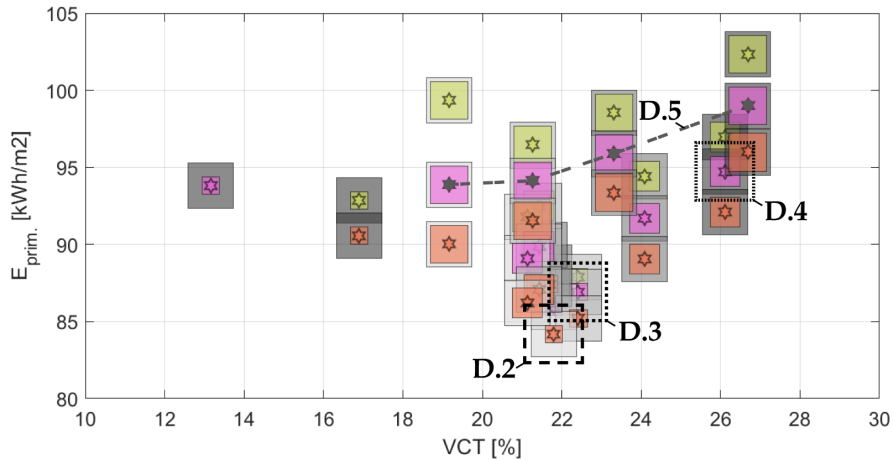
B. STVB-Ctree control strategy
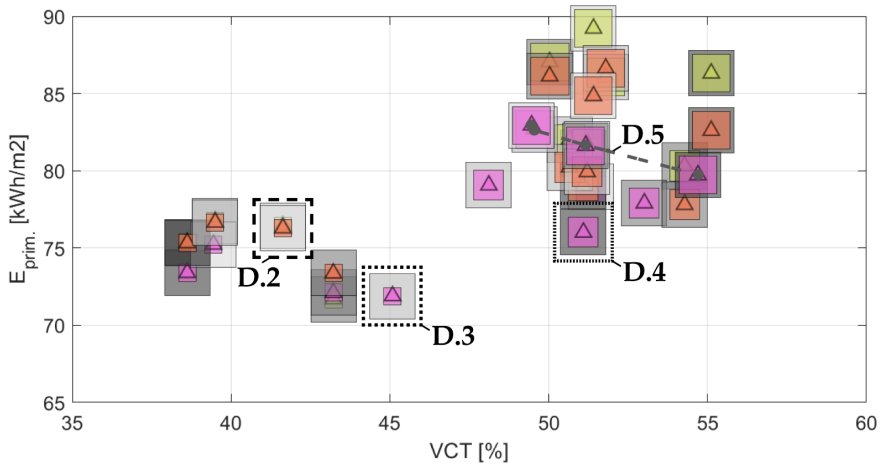
Figure 8.16 VCT and $E_{prim.}$ for heating, cooling, lighting and equipment for all façade design alternatives and the STVB-Ctree and BL shading control strategies

A designer might prioritise energy performance over visual comfort, assume the RB-BL in the early-stage design evaluation and select the EX-90VSA-40%WWR design (marker D.2 in Figure 8.16A). At a later stage, when control strategies for automated shading devices are being specified, a design team might select the STVB-CTree

strategy because it leads to a 17% lower E_{prim} and 23% more VCT compared to the RB-BL strategy that was assumed earlier. Although this stepped approach leads to incremental performance improvements it does not guarantee ideal outcomes and the design team can potentially miss high performance solutions. Figure 8.16B shows, for instance, that the SC-90VSA-40%WWR design (marker D.3) offers a 6% lower E_{prim} and 4% more VCT whilst requiring a lower investment cost due to the less expensive interior position of the shading device. Alternatively, the SC-60VSA-60%WWR design (marker D.4) offers 11% more VCT for similar energy performance (2% less E_{prim}) and a larger view to the outdoors. These two alternative design solutions are likely overlooked in the stepped design approach because of their less favourable performance when the simple RB-BL strategy is assumed.

The graph also shows that the two dynamic control strategies lead to different and contradictory conclusions regarding the relationships between particular design aspects and their building performance effects. With the RB-BL strategy, the EX glazing configuration consistently comes out as offering the best energy performance amongst the glazing alternatives. With the STVB-CTree strategy, however, the less expensive SC glazing with interior shading leads to lower heating energy consumption and total E_{prim} than EX in most cases. The two strategies also lead to contradictory effects of the horizontal louvre VSA on E_{prim}. Increasing the depth of the louvres for the SC-80%WWR designs, for instance, leads to a higher E_{prim} with the RB-BL strategy but reduces E_{prim} when the STVB-CTree strategy is used.

Figure 8.17 and Figure 8.18 help explain these contradictory effects. The temporal maps show the EWF and D_{300lx} for the RB-BL and STVB-CTree strategies. This comparison is shown for the SC-80%WWR design with no exterior louvres (90VSA Figure 8.17) or the louvre design that is most obstructing (40VSA Figure 8.18). The plots show that for the RB-BL strategy, adding exterior louvres is detrimental for daylighting performance. Consequently, the louvres increase lighting energy consumption and lead to a higher E_{prim} (Appendix C).
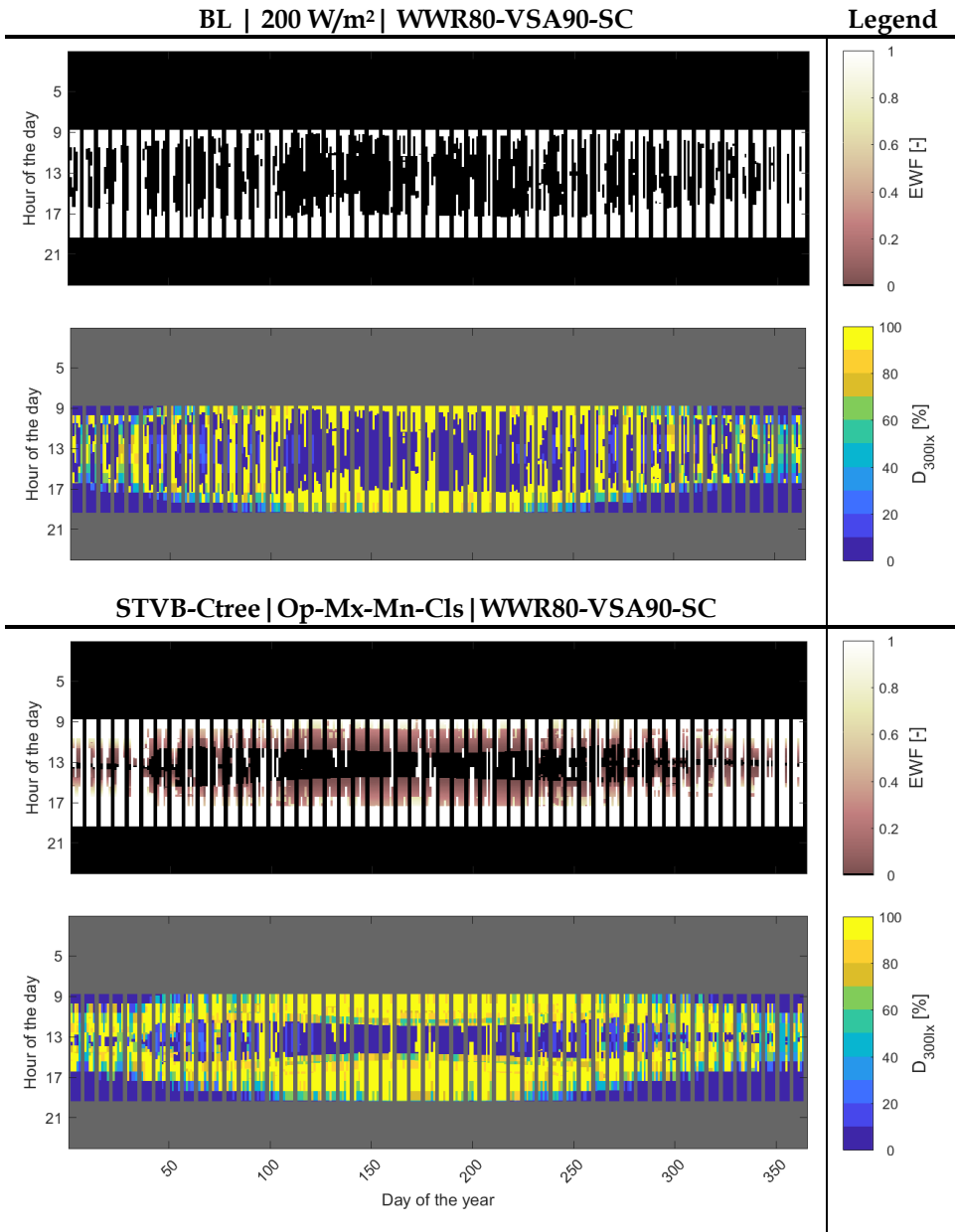
Figure 8.17 Temporal maps showing instantaneous behaviour and performance effects at each time step for the RB-BL and STVB-CTree strategies with no horizontal louvres
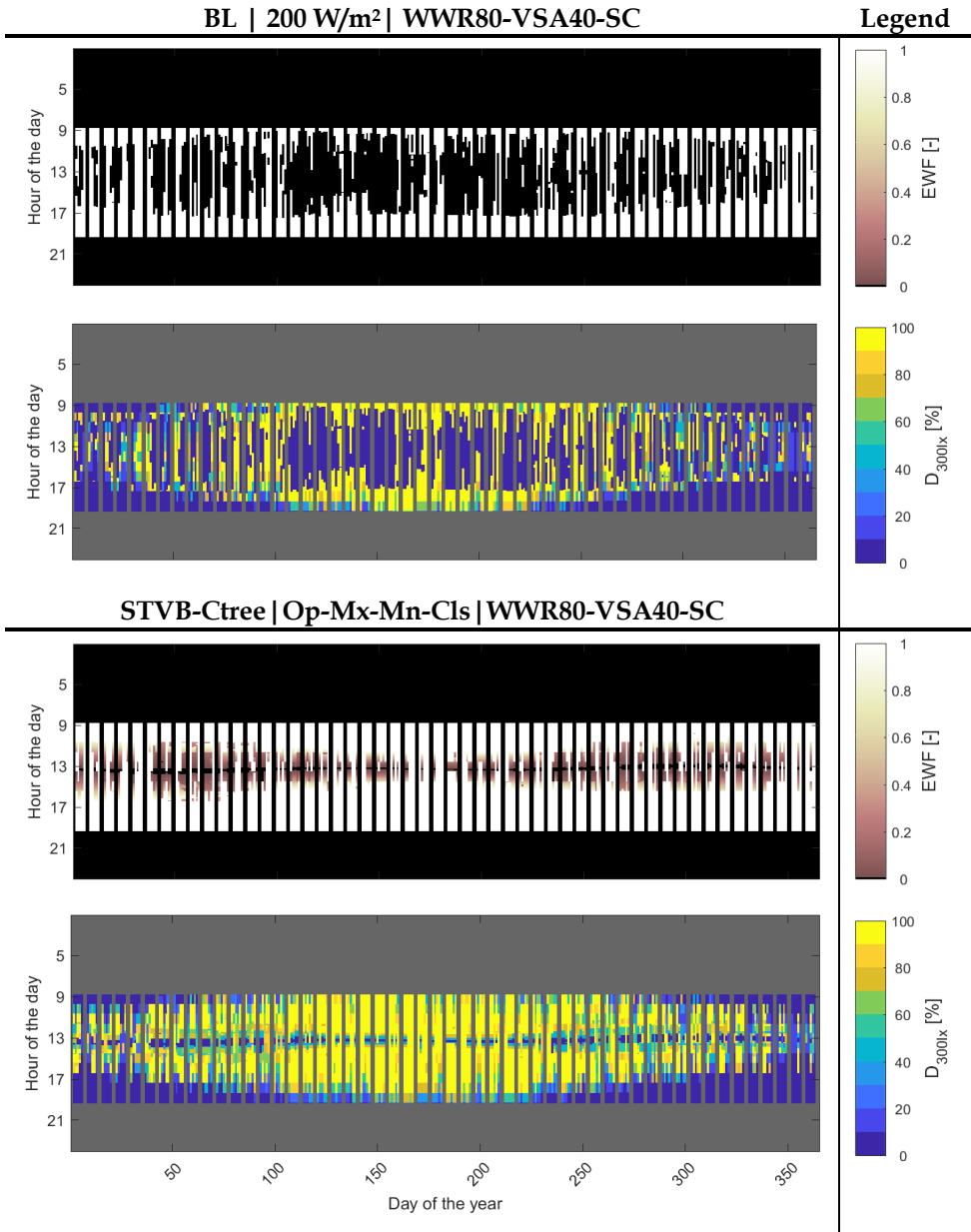
Figure 8.18 Temporal maps showing instantaneous behaviour and performance effects at each time step for the RB-BL and STVB-CTree strategies with 40VSA horizontal louvres

With the STVB-CTree strategy, however, adding louvres increases the admission of daylight. Figure 8.17 shows that in the case without louvres the vertical blinds are closed to prevent glare for a period of more than 2 hours around solar noon each day when the sun is directly in front of the façade. The louvres block the sun from view when solar altitude is higher than 40 degrees and lower the illuminance perceived by the occupants. This allows the STVB-CTree to choose more open shading positions and with the 40VSA louvre design, the blinds now only have to close fully for a short 15 to 30-minute period around solar noon. Consequently, lighting energy consumption and total E_{prim} are reduced (Appendix C). The CTree strategy leverages the presence of static shading devices, and knowledge of such building features within the control strategy, for more effective daylight utilisation. Hence the strategy causes to façade design features to affect the building's performance in a different manner.

8.6.2 Sensitivity of design outcomes to future energy system scenarios

This section evaluates how the assumptions regarding the type and efficiency of applied HVAC systems and future electricity grid characteristics influence performance trade-offs in the selection of façade design configurations. Here, E_{prim} is computed for each design alternative using the PEF_{nonRE} profiles, presented in section 1.1.1, and the two HVAC system configurations (Table 8.3).

Figure 8.19A shows a plot of VCT versus E_{prim} for the RB-BL and STVB-CTree strategies. Here, however, the range of E_{prim} resulting from the different PEF_{nonRE} scenarios is given where the markers indicate the minimum and maximum E_{prim} of the range for each façade design and shading control combination. Figure 8.19B shows the same results but each E_{prim} outcome is shown with a circle and the colour of the circles indicates the $avPEF_{nonRE}$ of the corresponding PEF_{nonRE} scenario. The maximum E_{prim} marker ($avPEF_{nonRE}$: 1.99) in Figure 8.19A represents the situation under current Dutch electricity grid characteristics (HighFossil21Ren+LoWintPeak) and the minimum E_{prim} marker ($avPEF_{nonRE}$: 0.53) represents the situation resulting from a high renewables future with large difference in PEFnonRE between winter and summer (HighWndSol85Ren+HiWintPeak).

The results show that the characteristics of the electricity grid strongly influence the relative merits of different design solutions in terms of their carbon intensity. In the grid scenarios that include more renewables, that are characterised by a low $avPEF_{nonRE}$, glazing configurations that admit more solar energy (HG) now lead to the lowest E_{prim}.

A. Conventional HVAC systems
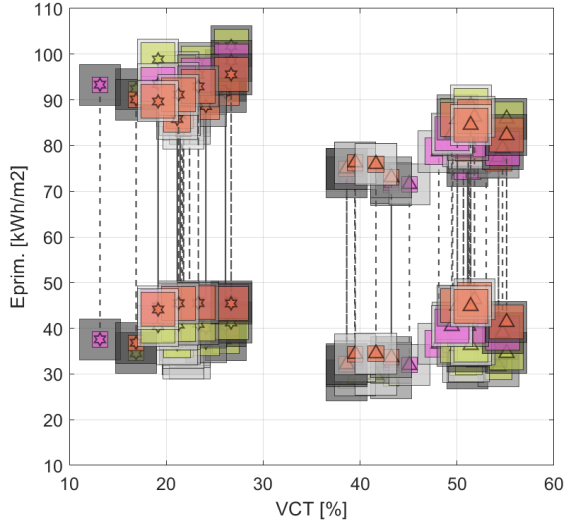
B. PEF$_{nonRE}$
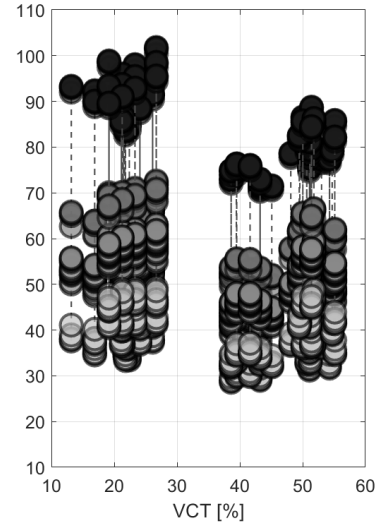
C. All-electric HVAC systems

D. PEF$_{nonRE}$

△ Minimum and maximum E$_{prim}$ across all PEF$_{nonRE}$ scenarios

--- Range in E$_{prim}$ resulting from all PEF$_{nonRE}$ scenarios

⬤ E$_{prim}$ resulting from a particular PEF$_{nonRE}$ scenario
Colour scale of circles (right): Average annual PEF$_{nonRE}$ of the scenario

0.53 ▮ 1.99
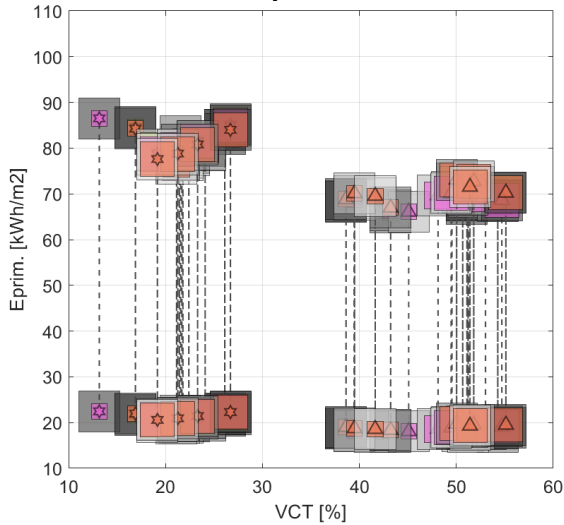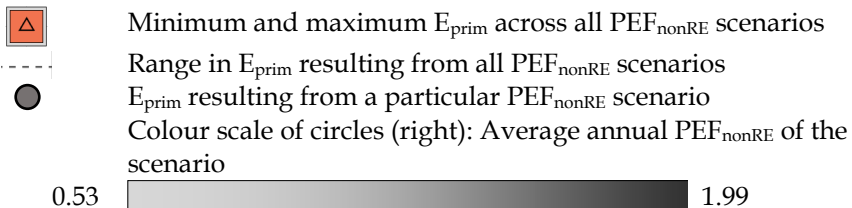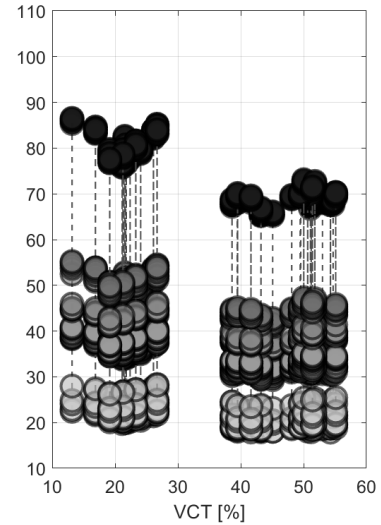
Figure 8.19 Left: VCT and range of E$_{prim}$ resulting from the PEF$_{nonRE}$ scenarios for the RB-BL and STVB-CTree strategies. Right: The same plot all E$_{prim}$ outcomes with the corresponding average annual PEF$_{nonRE}$ plotted as the colour of each marker.

Figure 8.19C shows the same comparison but now for a building design that includes the all-electric HVAC concept. In the current 1.99 $avPEF_{nonRE}$ context, the change to more efficient heating and cooling systems reduces the influence of façade design choices on E_{prim}. The graph also shows that in a situation where the all-electric HVAC concept is combined with a future scenario with a high penetration of renewables in the electricity grid, façade design choices no longer have a substantial influence on E_{prim} (1-3 kWh/m² variation) and only the chosen shading control strategy has a meaningful effect (4-6 kWh/m² variation).

To understand the reasons for these changes in the relationship between façade design parameters and their effects on E_{prim}, Figure 8.20 shows a breakdown of the heating, cooling and lighting components to E_{prim} for the different PEF_{nonRE} and HVAC system scenarios. The graphs show the 90VSA-80%WWR design with varying glazing configurations for the RB-BL and STVB-CTree control strategies.

In the current context, with a carbon intensive electricity grid and conventional HVAC systems, reducing cooling energy consumption is an important consideration in reducing E_{prim}. For the RB-BL strategy, the EX glazing configuration therefore comes out best. For the STVB-CTree strategy, however, SC offers the most beneficial trade-offs between heating, cooling and lighting. For this strategy, EX leads to a higher E_{prim} than SC because the exterior position of the blinds, combined with visual comfort driven control strategy, causes low passive solar heat gains in winter and less favourable heating energy consumption in relation to only limited reduction in cooling energy consumption. The same trade-offs between heating and cooling energy consumption can be observed in the situation where a high efficiency all-electric HVAC concept is used. In this case, however, the contribution of lighting to the overall E_{prim} is more dominant and the differences amongst the investigated glazing alternatives a relatively small (~3 kWh/m² variation). In this case, designers would be more inclined to choose for the relatively less expensive HG or SC glazing configurations.

In the electricity grid scenario with more renewables the fossil intensity of consumed grid electricity greatly reduces. Additionally, the presence of more PV generation causes the PEF_{nonRE} to be more favourable in the summer months, reducing the relative importance of cooling. For the cases with the conventional HVAC system, where natural gas boilers are used, this has the consequence that heating energy consumption becomes defining for E_{prim}. Consequently, maximizing passive solar heat gains becomes the most important design considerations and the HG glazing configuration offers the lowest E_{prim} for both control strategies. For the cases with the all-electric high efficiency HVAC systems, a transition to an electricity grid scenario with an abundance of renewables leads to a drastic reduction of E_{prim} for all design and control alternatives.

Conventional HVAC systems
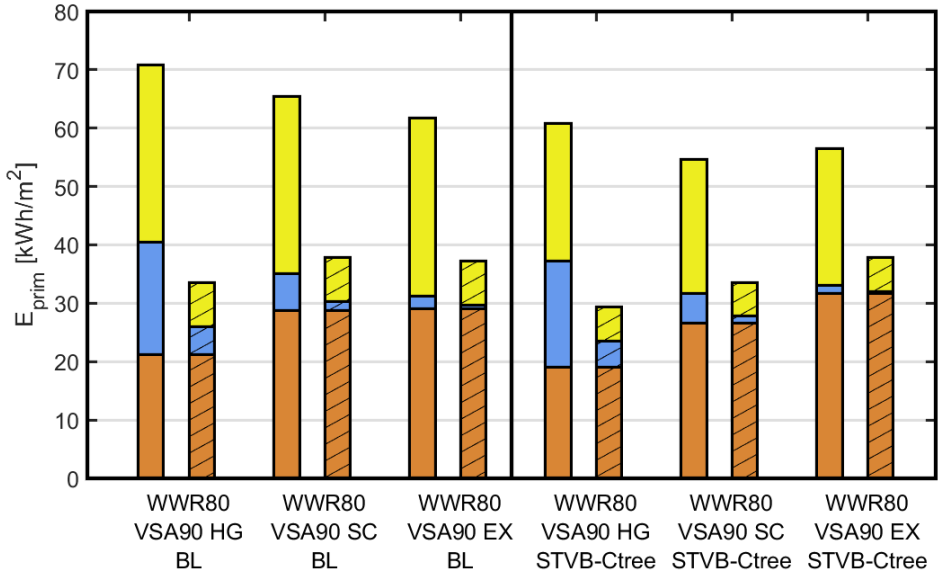
All-electric HVAC systems
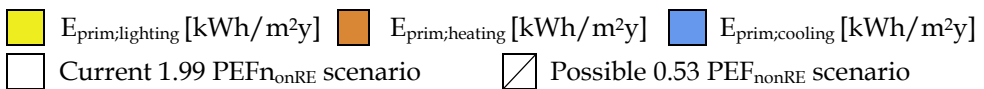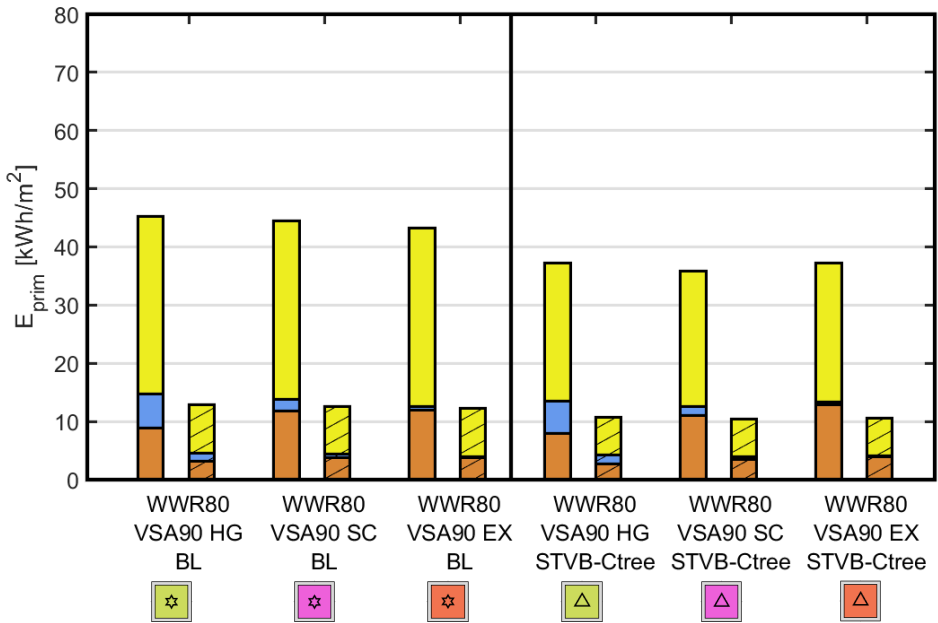
Figure 8.20 The E_{prim} components for the RB-BL and STVB-CTree strategies, the 80%WWR-90VSA façade design and various HVAC and grid electricity scenarios

225

In this situation there are no longer any substantial differences (≤1 kWh/m²) amongst the different façade design options in terms of E_{prim}. Additionally, lighting energy consumption is the most defining component of E_{prim} and the more favourable daylight utilisation of the STVB-CTree strategy does still lead to a reduction in E_{prim} (2-3 kWh/m²) compared to the RB-BL strategy.

8.7 Application discussion and conclusion

The application study of this chapter showed that the building-aware STVB-CTree strategy was able to exploit the presence of static shading devices, and the knowledge of such facade features within the control strategy, for more effective daylight utilisation. Due to this quality, the STVB-CTree strategy offered substantial improvements in energy performance (e.g., 17% lower E_{prim}), daylighting, and glare performance (23% more VCT) over the conventional RB-BL strategy. This study also points out the importance of considering the advanced STVB-CTree strategy early on in the design process because it leads to different conclusions regarding the relative merits of different façade design configurations. The example showed that by including the building aware strategy in early-stage design considerations, facade configurations could be identified that offered lower E_{prim} and lower cost, or similar E_{prim} with higher VCT and larger windows.

Additionally, this application study showed that:

- The sensitivity of the E_{prim} and VCT performance indicators to façade design choices varied strongly depending on what shading strategy was assumed.
- The different groups of dynamic shading strategies lead to different conclusions regarding pareto optimal façade design configurations.
- The different control strategy groups indicated contradictory relationships between façade design parameters and building performance effects.

These results confirm that the co-optimisation of static façade design features and dynamic solar shading control behaviour can lead to high-performance solutions that would be missed with a stepped optimisation approach.

The application study also investigated how façade design performance trade-offs are influenced by assumptions regarding the characteristics of the future electricity grid combined with two types of HVAC systems. The results showed that varying assumptions regarding the nature of the future electricity grid and the type of HVAC system that is employed lead to different performance trade-offs and pareto optimal solutions as well as different conclusions regarding cause-and-effect relationships.

In the case that is characterised by fossil intensive grid electricity generation, gas-based heating systems and low efficiency cooling, reducing the operational greenhouse gas (GHG) emissions of the office space through façade design choices involves making trade-offs between reducing solar heat gains to reduce cooling energy consumption on the one hand, and admitting sufficient daylight and solar energy to reduce lighting and heating energy consumption on the other. Consequently, design options with exterior shading, solar controlled glazing and small windows lead to the lowest E_{prim}. If the more efficient all-electric HVAC concept is used, lighting energy consumption becomes most defining for E_{prim} and effective daylight utilisation becomes the most important design consideration. E_{prim} becomes less sensitive to the size of the window and the type of glazing configuration but remains sensitive to the type of shading control strategy and the dimensioning of exterior louvres.

The scenarios with a higher penetration of renewables, and particularly solar sources, in the electricity grid cause cooling energy consumption to become less defining for the operational GHG emissions. If a conventional gas-based heating system is used in these scenarios, reducing heating energy consumption by maximizing passive solar heat gains becomes a defining factor reducing E_{prim} and glazing configurations with a high SHGC come out more favourable. When this grid scenario is combined with the all-electric HVAC concept, this leads to a situation where the design of the louvres, the window and the glazing configuration no longer have a substantial influence on E_{prim} (1-3 kWh/m² variation) and only the chosen control strategy still has a meaningful effect (4-6 kWh/m² variation).

By analysing the effects of these assumptions on performance trade-offs and optimal design outcomes, a façade designer can select robust design configurations. For example, the STVB-CTree strategy performs better in terms of E_{prim} and VCT with all design options and all scenarios. For the cases with the STVB-CTree strategy, the SC-40VSA-80%WWR and HG-60VSA-60%WWR façade designs configurations offer beneficial trade-off between E_{prim} and VCT in all scenarios. Here, the SC-40VSA-80%WWR design has the benefit of offering a larger window and the HG-60VSA-60%WWR offer a more low-cost solution.

8.8 Concluding remarks

This application study showed how the VTB can be used to simultaneously optimise shading control behaviour and static façade design features. The study illustrated that all performance aspects are strongly influenced by the combined effects of the control behaviour of automated shading systems and static façade characteristics. In addition, the study points out that there is an opportunity cost associated with a

stepped optimisation process where advanced visual comfort-driven control strategies are only considered in the later stages, and not addressed integrally with façade design choices in the early-stage design phase. In such a stepped design approach, there is a risk that desirable design options are overlooked. In the application study these overlooked design options included designs that offered a lower energy consumption and a higher degree of visual comfort when they were combined with the building-aware control strategy. Additionally, these designs offered benefits like a lower investment cost and more view to the outdoors. To conclude, the study shows what can be gained by considering the control of automated shading devices as an integral part of the façade design process and provides a VTB configuration that facilitates such an integral approach.

The study also showed how the method for developing detection algorithms using classification trees can be used to create a generic yet building-aware control strategy. By developing the classification trees using simulation results of a large variety of building designs, the method was able to create a single control logic that can be customised to specific building applications by specifying only a limited number of easily obtainable design features as input parameters. This application of the presented method could allow control developers to deploy high performance strategies that are customised to particular buildings with relatively little commissioning effort. The application study illustrated that such a building-aware control strategy can exploit synergies between static shading systems and dynamic shading devices and lead to more effective daylight utilisation.

This study showed the importance of addressing uncertainties regarding future electricity grid characteristics in façade design optimisation. A method was presented and tested for quantifying these uncertainties and describing plausible interactions between the time-varying carbon intensity of grid electricity and the effects of various façade technologies on the building's energy consumption. The presented method offers some benefits over the existing approaches presented in the literature (Cubi et al. 2015; St-Jacques et al. 2020). In contrast to approaches that are based on the current grid characteristics, the presented method allows designers to also account for uncertainties regarding how these characteristics might change in the future. Additionally, the method allows designers to estimate time-varying PEF_{nonRE} profiles that correspond with the weather data for the particular location and matches the information, skill level and the time that is available in early-stage façade optimisation.

Finally, this chapter provided some additional insights relevant for the development and deployment of automated shading systems in high performance office building façades. In this study, E_{prim} and VCT were found to be more sensitive to the way in which dynamic shading devices are operated than to façade design choices

regarding the size of windows, the type of glazing and the design of static shading devices. More specifically, this study showed that the choice for the fine-tuned STVB-CTree automated shading control strategy was found to be more defining for E_{prim} than the position of the shading device within the overall glazing system. This observation is important because interior shading devices are generally more suited to be operated in a silent and fine-tuned manner using low-cost motorisation systems. Deploying such fine-tuned strategies in exterior shading systems might not be possible at scale. The results of this study show that, in the investigated cases, interior solar shading with the fine-tuned STVB-CTree strategy leads to a lower E_{prim} than exterior shading devices with conventional control strategies. These findings negate the commonly held view that interior shading devices are functional for glare protection only and show that substantial reductions E_{prim} can be missed (8-11 kWh/m² or 8-13%) if interior shading devices with advanced fine-tuned strategies are not considered based on their less favourable position within the glazing system alone.

Here, it is important to underline that this study did not explicitly investigate the performance effects of the different glazing and shading configurations on thermal comfort. Although the results showed that an interior shading device controlled with the STVB-CTree strategy leads to similar cooling energy consumption as an exterior shading device with a conventional control strategy, the perceived level of thermal comfort is not necessarily identical in both cases because the interior shading device leads to occupants being exposed to higher levels of radiant heat transfer from the blind and the inner window surfaces. A comparison of the effects of these alternatives on occupant thermal comfort conditions is therefore recommended for further research.

This study also indicated that a transition towards more efficient HVAC systems, electrification of heating systems, and a situation where more electricity demand is fulfilled using on-site or grid PV generation leads to changes in the factors that drive operational GHG emissions. Consequently, such a transition also calls for different guiding principles for the design of facades and automated shading controls that seek to minimise operational GHG emissions. In this new context, reducing solar heat gains becomes less important and effective daylight utilisation becomes a more important consideration.

This study also indicates the limitations of focussing on energy consumption alone in a context with a high penetration of renewable electricity generation. This calls for some caution in the interpretation of the presented conclusions regarding energy performance in this context. This study focussed on the building-level and assumed no absolute constraints or price signals related to local or national electricity grid capacity. The results in Section 8.6.2 indicate that there is little difference in E_{prim}

amongst the façade design options in the scenario with all-electric HVAC system and an abundance of renewable electricity generation. This suggests that improvements in the PEF_{nonRE} of electricity will decrease the relative importance of operational GHG emissions in relation to other performance aspects. In addition, there are likely to be large differences, for instance, in the extent to which these alternatives load the electricity grid and the associated operating costs if this factor is including in the price of consumed electricity. Addressing these issues in the building design and control development context in a more comprehensive energy performance assessment framework including aspects such as energy flexibility is therefore recommended for further research (Taveres-Cachat et al. 2018; Zeiler 2020).

9 Reflection

9.1 Introduction

Each application study deployed the VTB in a different manner. Additionally, each study investigated performance sensitivity only for a few parameters and many assumptions were made. The studies were executed in a consecutive manner and new insights were progressively obtained. This chapter reflects on some of the assumptions that were made in the earlier chapters and tries to explore the magnitude of the associated uncertainties in the results, using the results of later chapters.

9.2 Reflection on the four application studies

In chapters 5 and 8 a variable height roller shade model is developed using existing models that describe binary open-closed states and dividing the window plane into a number of horizontally oriented segments. This approach has been used in earlier research (Gunay et al. 2016; Subramaniam 2018; Atzeri et al. 2018) but its validity and modelling sensitivities had not yet been explored. A limitation of the variable height roller shade models in EnergyPlus (modules C.1 and C.2), is that they do not accurately describe buoyancy driven airflow in the cavity between the shade and glazing system. This limitation did not cause a substantial error in this research (Section 5.5.1: 0.5% in E_{prim}) but future applications of the VTB might require this aspect to be described in more detail.

All application studies investigate the performance of shading devices that employ metal coated fabrics. These systems are therefore characterised by different properties for the front- and back of the shading device. The most advanced VTB fenestration system modules (B.2, B.3.1, B.3.3, C.2, B.4) offer the most accurate description of such products as they allow different properties to be assigned to the two sides of a device. This feature is not supported, however, by the Winkelmann (2001) shade model (C.1) that is used in EnergyPlus in Chapter 5. Here, the asymmetric front and back emissivity of the shading device was simplified using single average emissivity for both sides of the shade which is likely to have caused some error in the predicted heating and cooling energy consumption that is not present in the later chapters (6, 7 and 8).

The VTB also employs the A.2 (eDGPs$_{3PHS-Rpict}$ simulation) and B.4 (Wienold/Roos optical model) modules that are specifically aimed at accurate glare performance prediction for shading systems that are characterised by a high specular transmittance. Additionally, Chapter 7 provided some insights in expected magnitude of the error that could be expected when glare is assessed using the DGPs$_{3PHS}$ approach for fabrics with various degrees of specular transmittance. The results from Section 7.5.3 can therefore be used to obtain an idea of error associated

to the use of the $DGPs_{3PHS}$ approach in the other chapters. This error depends strongly on the assumed viewing angle and is largest for the 1% $T_{v;dir-dir-0}$ fabric that is used in Chapter 5: up to 1.0% in terms of $DGP_{0.40exc-0deg}$, and up to 9.0% in terms of $DGP_{0.40exc-45deg}$. For the 0% $T_{v;dir-dir-0}$ blind that is used in Chapter 8, however, the error is expected to be very small: up to 0.2% in terms of $DGP_{0.40exc-0deg}$, and up to 0.3% in terms of $DGP_{0.40exc-45deg}$. Although this research showed that the $eDGPs_{3PHS+Rpict}$ approach is substantially faster than regular image based DGP_{Rpict} simulations (98.7% reduction), simulation time can still be a limiting factor for some applications. Investigating a large design space, such as in Chapter 8, would be difficult with the $eDGPs_{3PHS+Rpict}$ method. Other computationally efficient glare simulation methods, like the Radiance 5phase method (Geisler-Moroder et al. 2016) or the GLANCE method (Giovannini et al. 2020), might proof to be more satisfactory in such cases.

10 Conclusions and future research

10.1 Conclusions

Automated shading systems have the potential to substantially reduce building energy consumption, increase occupant exposure to natural daylight, reduce visual and thermal discomfort, and relieve occupants from manual operation. The realisation of this potential, however, requires a new generation of control strategies that is able to operate shading devices in a fine-tuned manner to addresses the visual comfort conditions of occupants and prevent excessive solar heat gains, whilst maximizing the admission of daylight. To further the development of such strategies, there is a need for tools and methods that facilitate informed decision-making in the R&D process of advanced solar shading strategies, as well as in the design process leading to their successful application.

Through literature review in Chapter 1 it was concluded that the currently available building performance simulation tools and methods have a number of limitations that need to be overcome if they are to contribute to the development and deployment of advanced automated solar shading strategies. The objective of this research was therefore to develop and test computational approaches for performance evaluation and optimisation of advanced solar shading concepts. This objective was divided into the following subobjectives:

O.1.To develop and test a virtual test bed for advanced automated shading strategies (VTB) aimed at analysing the performance of (i) advanced shading controls, (ii) materialisation and shading system design features, and (iii) applications of dynamic solar shading systems within performance-driven façade design processes.

O.2.To develop computational support methods, aimed at performance analysis, optimisation, and quality control in the application of the VTB.

O.3.To illustrate, through a series of application studies, how the VTB and the support methods can be used to identify scalable high-performance design and control solutions.

O.4.To better understand the causal relationships between solar shading design/control parameters and building performance effects.

These objectives were addressed through an iterative process involving four application studies that focused on the development and optimisation of a series of advanced shading concepts. The following sections discuss the outcomes of this research in relation to the subobjectives.

10.1.1 The virtual testbed for advanced automated shading strategies

The requirements for the VTB (Chapter 2) were defined based on a literature review and the findings of the four application studies.

Based on these requirements, a multi-domain and multi-scale VTB (Chapter 3) was developed that employs a co-simulation approach directed by BCVTB using EnergyPlus for transient thermal building simulations, a variety of Radiance methods for the simulation of indoor daylight conditions and discomfort glare, and Matlab for simulation of the control systems. A set of Matlab functions acts as a wrapper for the VTB, providing a flexible and versatile interface for interacting with the VTB. The VTB follows a modular structure that allows component models of varying levels-of-detail to be selected. The VTB was equipped with multiple shading and window models, that describe the combined fenestration system at different levels-of-scale. Additionally, the VTB provides an interface for various Radiance simulation methods for predicting visual comfort. Finally, the VTB provides varying methods for describing energy systems from simple performance ratios to detailed simulations with Matlab following a stepwise approach.

The main VTB components (EnergyPlus, Matlab, the Radiance 3PHS method), that are used throughout all VTB applications, were validated through inter-model comparison (in Chapter 4). All other VTB components were validated and verified in a series of quality assurance studies associated to particular VTB applications. Additionally, the correct functioning of different VTB configurations was verified in these studies.

The VTB is envisioned as a continuously evolving toolchain. New applications require different configurations from those presented in this research. Additionally, new desired functionalities could call for additional VTB modules. The contribution of this research is a prototype of the VTB. This prototype was developed using four application cases that address optimisation of design and control aspects on the five most relevant levels-of-scale, identified in Chapter 1, and takes the perspective of designers and developers in different positions of the façade design and delivery value chain. The prototype has therefore gone through usability testing in a broad variety of representative applications.

This research showed that the VTB is suited for evaluating advanced control concepts. The VTB can describe mutual interactions between indoor daylighting conditions, indoor thermal conditions, dynamic operation of shading systems, and energy systems. Additionally, the VTB was equipped with modules for describing partially closed shading devices (chapters 5, 6, 7 and 8) and alternating optical and thermal properties (chapters 6 and 7). This allows the VTB to be used to test multi-state control strategies involving fine-tuned control actuations. The VTB is also

suited for evaluating the performance effects of choices regarding design and materialisation of the shading system.

Although these functionalities were only tested for rotating vertical-blinds and vertically retracting roller shades, they can also be used to test fine-tuned strategies for other commonly used shading devices (e.g., screens or horizontal blinds) and systems with other degrees of freedom in their actuation (e.g., horizontally retracting). The current modelling approach is, however, limited to co-planer shading devices (Subramaniam 2018), that is: shading systems that do not project inward or outward from the façade. This limitation could be overcome using the Radiance method for developing F-matrices (Wang et al. 2018) that map flux transfer from the non-coplanar shading device to the façade. These F-Matrices could then be used for daylighting simulation using the Radiance five phase method and for thermal simulation using the CFS-module (C.2) with some modifications.

Additionally, the types of shading devices that the current VTB can describe is limited to the available algorithms in the LBNL-Window environment and the Wienold/Roos fabric optical model. These algorithms currently do not support describing solar shading devices with complex geometries (e.g., double curved blinds), materials that give highly specular reflections (De Michele et al. 2018), or fabric weave patterns that do not form evenly spaced rectangular or circular openings. For describing the effects of more complex or non-yet-existing solar shading products with the VTB high-resolution goniophotometer measurements would have to be available. Alternatively, the Radiance genBSDF program can be used to generate BSDFs of varying resolutions using detailed models of the proposed solution (Mcneil and Lee 2013; Molina et al. 2015; Bustamante et al. 2017). Both high-resolution goniophotometer measurements and the computationally efficient visual comfort simulation, however, remain challenging for systems that transmit or reflect daylight in a specular manner and are a field of active research (Ward et al. 2021).

10.1.2 Support methods for analyses and optimisation of automated shading strategies

In addition to the VTB, this research set out to develop a set of computational support methods, that facilitate the effective use of the VTB in identifying high-performance solutions, and illustrate approaches aimed at simulation study quality assurance. Together with the VTB these methods form a computational analyses and optimisation framework. The requirements for this framework were developed throughout the four application studies and are presented in Section 2.6.

This research proposed a support method for using the VTB to aid the development of comfort-driven solar shading controls. The support method was applied in multiple variations throughout the four application studies. What these variations have in common is that they map sensor measurements and building characteristics to performance effects and classify control decisions using statistical methods. This structured support method contributes to the body of knowledge on the simulation-based development of advanced shading strategies. The novelty of this approach can be found in the beneficial trade-off between (i) its replicability, (ii) its effectivity in finding control strategies that are based on performance goals and optimally exploit non-intrusive and non-ideal sensors, and (iii) the time, effort, and skill that are required of developers in its application. Many existing approaches (reviewed in Section 2.5: MPC, trial-and-error, etc.) tend to perform particularly well in only a subset of these three aspects. Because the support method places due emphasis on all three aspects, however, it allows the creation of control strategies that are potentially more scalable in the current context.

The method is applied for (i) the selection of sensor deployment strategies (Chapter 5) that offer beneficial trade-offs considering multiple performance aspects and (ii) identification of control algorithms that optimise comfort conditions using non-ideal sensors (Chapter 5 and Chapter 7). Additionally, the method can be used to develop control strategies that are customised to particular building designs by using simulation results of a large building design space as training data and design features as control inputs (Chapter 8). By applying the support method to various optimisation problems, shading systems, and buildings, this research has shown that the method is effective and generically applicable. Additionally, the support method was shown to require only a small number of simulations and relatively little effort from a developer. Therefore, the method fits well within the constraints in the current practice of shading control development. A limitation of the support method is that it optimises the immediate performance effects of control actions and does not accurately accredit the transient effects of shade actuations. This makes the method less effective at identifying control decisions that optimise energy performance and thermal comfort than it is at identifying decisions that optimise daylighting and visual comfort.

This research assumes that such constraints are present and that it is therefore desirable to minimise the complexity of the developed control strategies. Increased computing power and cloud computing technologies are likely to enable more complex model-based, performance weighing control features in the future but such strategies were not explored in the application studies. The current VTB is suited for developing and testing such control strategies, however, and this capability was tested by Ballegooijen (2020). In that research project, the VTB was used as a virtual building and connected to a single-board computer containing a MPC system

through an additional socket connection. The research showed that the VTB could be used to:

- Aid the development of simplified models for control purposes using results from detailed fenestration system simulations.
- Extract initial input parameters for reduced-order thermal models from detailed VTB simulations.
- Evaluate a MPC strategy before implementation in a real building and provide insights in its performance and behaviour for development purposes.

This research also presented a method for quantifying uncertainties regarding future electricity grid characteristics. The method enables designers to estimate time varying PEF_{nonRE} profiles that correspond with the weather data for the particular location. The method is designed for early stage building design where limited information, subject matter expertise, and time are generally available. The method greatly simplifies the dynamic relationship between weather conditions and generation of renewable electricity at the national level. The method also does not describe allocation of generation through market dynamics, the actual boundaries of bid zones and grid infrastructure, imports and exports, local grid infrastructure and grid capacity limitations. It is therefore not recommended to use the method outside of the context of early stage building design.

Finally, this research presented a method for providing consistent input parameters to the models that describe the optical behaviour of the window/shading system in different modelling domains. In this method the VTB is configured to use detailed subsystem simulations describing the optical behaviour of a woven fabric structure to compute the emergent behaviour, and corresponding input parameters, on the level of the shading device and on the level of the shading device and the overall fenestration system.

10.1.3 Application studies

Through the application studies, this research gave insight into the sensitivity of the outcomes of simulation-based performance prediction of advanced automated shading solutions to various modelling parameters and assumptions. A series of sensitivity analyses, presented as part of the application studies showed the importance of the chosen modelling resolution in discretising the optical states of the shading system, the assumed viewing direction of occupants, assumed optical properties and assumed energy system characteristics. Through these practical examples, this research provides guidance for the assessment of performance sensitivity and addressing input uncertainty.

The application studies also illustrated a fit-for-purpose approach where model complexity is tuned to the goals of the simulation study. The results of Chapter 7 provide insights into the conditions were the more advanced glare simulation method (eDGPs$_{3PHS+Rpict}$) should be used. Chapters 6 and 7 illustrated showed how optical and thermal models that describe the fenestration system can be selected depending on the characteristics of the shading device that will be assessed and the design features that the decision maker wants to investigate.

The application studies also provided practical examples of quality assurance tests that can be executed to confirm the correct functioning of the VTB and its individual modules.

Finally, the application studies illustrated how the simulation framework can be used to analyse and optimise solar shading design and control features at different levels-of-scale, i.e.: the sensor strategy, the control strategy, the design of the shading fabric and system, and the overall façade design configuration. A novel feature of the applications in this research is that control and design features are simultaneously optimised (chapters 6, 7 and 8) rather than being treated in isolation or consecutively addressed. Additionally, this research showed how computational experiments can be set up to allow building performance effects to be evaluated within a larger framework of design and control considerations to develop shading solutions that can be deployed successfully at scale.

10.1.4 Design, control and application of advanced automated shading solutions

Through the application studies, this research contributes insights into the causal relationships between solar shading design, control features and building performance effects.

All application studies investigated finetuned, visual comfort-driven shading control strategies for interior shading devices that seek to maximise daylight admission by closing shading devices only to the extent that is necessary to prevent daylight discomfort glare. These strategies were compared to conventional strategies that follow a full open and close behaviour. As expected, the visual comfort-driven strategies offered substantial improvements in daylighting performance and reduced discomfort glare. In terms of energy performance, the comfort-driven strategy in Chapter 5 led to a small increase in cooling energy consumption that was offset by substantial reductions in lighting energy consumption, and small reductions in heating. With the comfort-driven strategies in the other application studies, all energy demands were reduced in relation to the conventional strategies.

These findings give reason to reconsider the often thermally driven approach to the design of facades, the specification of solar shading devices and the development of control approaches. With regards the goal of reducing building energy consumption through façade design, and the development and application of automated shading devices, this research concludes the following:

- Effective daylight utilisation is a defining factor for building energy consumption. Maximizing the admission of natural daylight reduces lighting consumption. If some measures are taken to reduce extremely high solar heat gains (e.g., solar controlled glazing), reductions in lighting energy demands usually offset increased cooling loads. These reductions can even indirectly reduce cooling loads.
- Enabling optimal daylight utilisation requires fine-tuned shading system actuations rather than full open and close actions.
- Visual comfort-driven control strategies for automated shading systems can substantially reduce building energy consumption (14-35% less E_{prim}) whilst improving occupant exposure to daylight (56-75% more $sDA_{300lx/50\%}$) and reducing discomfort glare (8-25% less $DGP_{s0.40exc}$).
- The way in which dynamic shading devices are operated (e.g., manually, using conventional or comfort-driven control strategies) has a stronger impact on energy performance and visual comfort than other façade design features (e.g., the type of glazing, dimensioning of windows).
- If interior shading devices with advanced fine-tuned strategies are not considered based on their less favourable position within the glazing system alone, substantial improvements in energy performance can be missed (8-11 kWh/m² or 8-13% E_{prim}).
- In the current context, reducing the operational greenhouse gas (GHG) emissions of office buildings through façade design choices, involves making trade-offs between reducing solar heat gains to reduce cooling energy consumption on the one hand, and admitting sufficient daylight and solar energy to reduce lighting and heating energy consumption on the other. If some measures are taken to reduce extremely high solar heat gains (e.g., solar controlled glazing, highly reflective interior shading device, blocking direct sunlight through sun-tracking strategies) daylight sufficiency becomes the most driving factor for operational GHG emissions.
- A transition towards more efficient HVAC systems, electrification of heating systems, and a situation where more electricity demand is fulfilled using on-site or grid PV generation causes electrical lighting and heating to become more defining for the GHG emissions of office buildings. Under such conditions, reducing lighting and heating energy consumption by designing for daylight

sufficiency and effective utilisation of solar heat gains increase in their relative importance as façade design principles.

The application studies, provided examples of effective approaches for leveraging design and control aspects to improve the performance effects in the development and application of visual comfort-driven automated shading systems:

- The presented control strategies can be generalised to three generally applicable approaches to developing controls that maximise the admission of daylight whilst preserving visual comfort conditions: (i: Chapter 5) admitting daylight in parts of the space where this does not lead to visual discomfort, (ii: Chapter 6 and 8) admitting daylight only from parts of the sky where there is no direct sunlight, and (iii: Chapter 7) using a variable transmittance to admit more or less daylight in response to varying outdoor conditions. These approaches can be used to develop strategies for types of shading devices that were not investigated in this research (e.g., horizontal blinds).
- In the selection of light sensors for classifying visual comfort and solar heat gain conditions, the orientation, position, and part of the solar spectrum that is measured influence the effectivity of the sensor. Daylighting (9% $sDA_{300lx;50\%}$), View (3% $V_{1.2m;exc}$), and glare performance (3% $DGPs_{0.4;exc;45deg}$) are sensitive to choices amongst commonly used sensor configurations.
- Detailed shading fabric characteristics (e.g., OF, COA, etc.) are very defining for daylighting, glare and building energy performance (Section 7.5.2 showed 1-20% variation in OF lead to a difference of: 16% E_{prim}, 47% more $sDA_{300/50}$ and 11% more $eDGPs_{0.40exc-45deg}$).
- There is potential in leveraging these properties to improve building performance.
- There are large uncertainties associated to building performance predictions if these detailed fabric characteristics are not known or specified. This indicates the importance of addressing the uncertainties associated to yet undecided shading design parameters in early-stage façade design. Additionally, this finding points to the importance of having detailed shading product information available when specifying shading devices.
- There is an opportunity cost associated to not considering advanced visual comfort-driven control strategies in the early-stage design phase because options that require lower investment cost and more view to the outdoors are overlooked. Choosing a co-optimisation approach, where façade design features and shading control are simultaneously optimised, can also improve energy performance (2-6% lower E_{prim}) as well as the quality of the indoor visual environment (4-11% more VCT).

This research is connected to three of valorisation projects: the TKI-iDEEGO (De Vries and Loonen 2018) and TKI-ISC (De Vries and Loonen 2018) research projects, and a PDEng project focussed on strategies for stimulating market penetration of advanced solar shading systems, executed by Oindrila Ghosh (2021). In these research projects, the control strategies presented in Chapters 5 and 6 were evaluated in relation to conventionally controlled interior and exterior roller shades assuming various climates, glazing systems, shade fabrics, lighting power densities, façade orientations and HVAC system efficiencies. The findings of these studies regarding the relative merits of interior and exterior automated shading devices were found to be generally consistent with the conclusions presented in this research.

10.2 Limitations
10.2.1 Investigated simulation parameters
Although a variety of testing methods were presented for simulation study quality assurance, this research cannot claim to have addressed all parameters that influence the effectivity of simulation studies focused on assessing advanced automated shading strategies. Many performance sensitivities were not investigated explicitly in a formal manner but found to be of importance in casual observations. One such aspect is the resolution of the grid that is used to assess the indoor daylight distribution. The effects of the grid resolution were found to vary in a way that is strongly dependent on the pattern of daylight distribution that results from the type of shading system and how it is controlled. In this research, the grid resolution in each application study was chosen based on unstructured investigations.

10.2.2 The functionalities and applications of the VTB
Additional uncertainties arise from the use of hourly weather data in daylight simulations. Sky conditions show more sub-hourly variability than what is represented by such data and this could potentially be a cause of errors in predicting visual comfort and daylighting performance and, consequently, also in energy performance. The current VTB does not include methods for dealing with this uncertainty, because sub hourly datasets would not be available in the envisioned applications of the VTB and because of the identified uncertainties associated to the creation of synthetic sub-hourly data (Walkenhorst et al. 2002) in this application.

Although the current VTB allows automated control strategies to be benchmarked against manually operated alternatives, e.g. using the Reinhart (2004) model, it does not include models for explicitly describing user interactions with automated shading systems. Chapter 6 shows how assuming different control thresholds can be used to bracket and approximate the effects of user interactions with conventional strategies. Van Woensel (2018) combined a selection of models that describe occupant interactions with manually operated device with automated control strategies to quantify the potential influence of interactions on performance predictions. These automated control strategies included the conventional (BL) and advanced sun tracking roller blind (SC) strategies that are investigated in Chapter 5 of this work. The results showed that advanced comfort-driven control strategies lead to substantially less predicted interactions than with conventionally and manually operated shading systems, suggesting that performance predictions of advanced strategies are more robust. The research, however, also made clear that uncertainties related to the translation of such occupant behaviour models to new applications can be large. Additionally, Sadeghi et al. (2016) has shown that users interact differently with advanced strategies than with manually operated devices. More research on the interactions of occupants with various types of automated

shading systems is therefore needed to address this aspect in more detail within a simulation framework.

The current VTB configuration takes a simplified approach to assessing thermal comfort by addressing it through the analyses of cooling energy consumption of cooling systems with unlimited capacity. An important limitation of this approach is that it does not account for the effect that shading strategies have on indoor radiative temperatures and transmitted solar radiation that falls on occupants[7]. The current VTB can be used, however, with minor modifications for more detailed thermal comfort assessments.

The current VTB also does not explicitly assess the non-image forming aspects of human exposure to daylight that have been shown to be defining for positive effects on human health. These effects include regulation of the physical and behaviour rhythms related to sleep (Figueiro et al. 2018; Brainard et al. 2001; Thapan et al. 2001) and stimulating short term alertness (Cajochen et al. 2000). Although promising methods and indicators have been proposed for quantifying these effects within the building design domain (Aries et al. 2013; Geisler-Moroder and Dür 2010; Inanici et al. 2015; Jakubiec and Alight 2021), there is currently not sufficient scientific consensus regarding this topic (Rea and Figueiro 2016) to integrate this within the simulation framework.

Overall, this research approaches occupant satisfaction mainly indirectly and the VTB is aimed predominantly at predicting indoor environmental quality (IEQ) in terms of comfort in separate domains. Although this research presents these comfort aspects such that trade-offs can be investigated, it does allow for an integrated prediction of occupant satisfaction. Current research efforts show that occupant satisfaction is influenced by interactions in perceived comfort across these domains (Luna-Navarro et al. 2022; Chinazzo et al. 2019; Pierson et al. 2018) as well as the degree of personal control that is available to occupants (Luna-Navarro et al. 2022; Day et al. 2020). The current state of the knowledge on occupant satisfaction is not sufficient, however, to integrate this into a single metric.

10.2.3 The generalisation of the observed causal relationships

Some limitations should be noted in the concluded causal relationships between control and design aspects and building performance effects. The application studies were all focussed on a cellular, perimeter office space with a south-facing window orientation in the oceanic (Cfb) climate of the Netherlands. Additionally, the reference office assumptions are representative for a reasonably energy efficient building built according to minimum Dutch building code requirements in the 2014-

---

[7] The investigated sun-tracking strategies are designed to prevent this

2021 period. Additionally, only a limited number of façade design variations and HVAC system configurations are explored in this research.

An important limitation to the reported improvements in building energy performance for the presented visual comfort driven control strategies is that this finding assumes the presence of daylight dimming of electric lighting. Here, it should be noted that the application studies in this research assume continuous dimming controls to be present and describe this dimming strategy using a simplified and idealised approach that does not consider a ballast loss factor or standby power consumption.

10.3 Future research

The conclusions and limitations of this research suggest various additional directions for future research aimed at improving the computational framework and at the development of automated shading solutions for high performance building facades.

10.3.1 Open questions in computational performance assessment and optimisation of automated shading systems

With regards to the further improvement of the computational framework, the following directions are suggested for future research:

- The VTB can be extended with features that give detailed insight into the effects of automated shading strategies on thermal comfort, including the effects of directly transmitted solar radiation (Luna Navarro et al. 2019).
- The VTB can be extended with features for assessing the health effects of automated shading strategies related the human exposure to daylight including its the non-image forming aspects (Aries et al. 2013; Geisler-Moroder and Dür 2010; Inanici et al. 2015; Jakubiec and Alight 2021).
- Deploying the VTB to support research in experimental testbeds aimed at developing models for predicting occupant satisfaction and interaction with automated shading system, such as the one developed by Luna-Navarro and Overend (2021) provides a promising point of departure for future research in this direction.
- The framework can be extended with experimental design features and search algorithms for more effective uncertainty analysis and design optimisation (Hopfe 2009; Loonen 2018; Chi et al. 2017).
- The VTB can be extended with features for describing new modelling domains. For instance, Shi (2020) showed that being able to actively ventilate the cavity between the window and an interior shading device can greatly reduce cooling energy consumption. The research by Shi (2020) assumed simple control strategies and did not investigate performance effects in the visual domain. The VTB could be extended with detailed airflow modelling features to find control strategies that optimally exploit this feature.
- Exploring the use of other statistical classification approaches within the presented support method, such as support vector machines (Xie and Sawyer 2021).
- The inclusion of additional computationally efficient glare performance prediction methods in the VTB aimed at different fit-for-purpose applications.

- The inclusion of more versatile multi-scale optical modelling approaches for describing more complex types of shading devices. This also requires more research on high-resolution goniophotometer measurements (Ward et al. 2021).

10.3.2 Towards automated shading solutions for high performance building facades

The suggested directions for future research into advanced automated shading strategies can be grouped into the following themes:

Co-optimisation of design and control features: This research showed that the performance effects of façade design choices, the specifications of shading device properties, and the control behaviour of shading systems are intrinsically linked. Further research into the co-optimisation of these features is therefore recommended.

Multi-scale design of automated shading solutions: This research illustrated the potential of leveraging detailed shading material design features to influence performance effects. Promising future application of the VTB in this direction could be aimed at developing:

- Systems and materials with a directionally selective transmittance. Using horizontal blinds made from expanded metal, for instance, could improve view to the outdoors and could be designed to admit more daylight from parts of the sky without direct sunlight.
- Systems that employ different materials throughout different parts of the window plane. The vertical blind could, for instance, be equipped for a high transmittance diffusing part at the top of the façade, and a low transmittance lower part with a higher degree of view-through.
- Systems that leverage optical interactions between multiple dynamically operated shading devices, for instance by exploiting their combined cut-off behaviour (Bueno et al. 2020) or light polarisation.

Automated shading systems as part of advanced façade concepts: This research focussed on interior and exterior shading devices. The VTB can also be used to evaluate more advanced configurations, including:

- Shading devices positioned between glazing layers (Ballegooijen 2020).
- Actively ventilated glazing and shading cavities (Shi 2020).
- Multi-sectional facades that employ different shading technologies and control behaviour at different zones of the façade (Hu and Olbina 2011).

Solar-powered internet-of things enabled façade technologies: In the stakeholder consultations, plug and play façade technologies that require as little physical wired power and communication infrastructure as possible were identified as a promising product development direction. Several PV and battery powered shading products that offer wireless communication are currently coming to market that have a competitive advantage over the traditional wired approach. Additionally, the ability to share sensor information between connected devices could provide increased abilities to improve indoor comfort conditions or reduce the number of sensors. Considerations related to this theme formed the background of the application studies in this research. The VTB could also be used to support research and development of such concepts more actively and the VTB was tuned to this application in a series of related research activities. To give some examples:

- The support method was used to map measurements (E_v) of the window illuminance sensor to simulated work plane illuminance and a strong correlation was found when also the shades position was factored in. This indicates that the window sensor could also be used to control daylight dimming of interior lighting and that the presented support method could be used to define controls for this purpose.
- Van Der Sommen (2020) showed that operational extraction of geometrical information regarding nearby sunlight obstructions (e.g., buildings, trees) from window illuminance sensor measurements for control purposes was possible using an online simulation framework and classification algorithms. The research was unclear, however, about the performance potential of this concept.
- Shi (2020) showed that coordinated operation of automated shading systems and mechanical ventilation systems could improve building energy performance but more research into suited control strategies is needed.
- The use of presence and occupant position data in open plan offices for localised shading and lighting control, such as admitting more daylight and dimming lighting in zones where no occupants are seated.

12 References

Abels-van Overveld, M., D. Blomjous, P. Boot, G.J. van den Born, C. Brink, B. Daniels, E. Drissen, et al. 2020. "Klimaat-en Energieverkenning 2020." Den Haag: PBL.

Abravesh, M., B. Bueno, S. Heidari, and T.E. Kuhn. 2019. "A method to evaluate glare risk from operable fenestration systems throughout a year." *Building and Environment* 160:106213.

Allen, M., A. Luna-Navarro, O. Babasola, R. Hartwell, M. Overend, and J. Blanco Cadena. 2019. User-centred control of automated shading for intelligent glass facades. In Glass Performance Days 2019, Tampere:

Arasteh, D., C. Kohler, and B. Griffith. 2009. "Modeling Windows in Energy Plus with Simple Performance Indices." Berkeley: LBNL.

Aries, M.B.C., M.P.J. Aarts, and J. van Hoof. 2013. "Daylight and health: A review of the evidence and consequences for the built environment." *Lighting Research & Technology* 47 (1):6-27.

Aries, M.B.C., J.A. Veitch, and G.R. Newsham. 2010. "Windows, view, and office characteristics predict physical and psychological discomfort." *Journal of Environmental Psychology* 30 (4):533-41.

Arnesano, M., B. Bueno, A. Pracucci, S. Magnagni, O. Casadei, and G.M. Revel. 2019. Sensors and control solutions for Smart-IoT façade modules. In 2019 IEEE International Symposium on Measurements & Networking (M&N) 2019, Catania: IEEE.

ASHRAE. 2001. "International Weather for Energy Calculations (IWEC Weather Files) Users Manual and CD-ROM." In. Atlanta: ASHRAE.

ASHRAE. 2014. "ASHRAE Guideline 14: Measurement of energy, demand and water savings." Atlanta: ASHRAE.

Aslihan, T., and S.L. Eleanor. 2006. "Effects of Overhangs on the Performance of Electrochromic Windows." *Architectural Science Review* (4):349-56.

Attia, S., S. Bilir, T. Safy, C. Struck, R. Loonen, and F. Goia. 2018. "Current trends and future challenges in the performance assessment of adaptive façade systems." *Energy and Buildings* 179:165-82.

Atzeri, A.M., A. Gasparella, F. Cappelletti, and A. Tzempelikos. 2018. "Comfort and energy performance analysis of different glazing systems coupled with three shading control strategies." *Science and Technology for the Built Environment* 24 (5):545-58.

Bakker, L., B. Cazes, and R. Belliard. 2019. "Potential impact of high performance glazing on energy and CO2 savings in Europe." Delft: TNO.

Bakker, L.G., E.C.M. Hoes-van Oeffelen, R.C.G.M. Loonen, and J.L.M. Hensen. 2014. "User satisfaction and interaction with automated dynamic facades: A pilot study." *Building and Environment* 78:44-52.

Bakker, L.G., and D. van Dijk. 2015. "Besparingen op verwarmingsenergie door thermische isolatie van zonweringen." Delft: TNO.

Bakker, L.G., L. Zonneveldt, and E.C.M. Oeffelen (van). 2011. "Energiegebruik, comfort en zonwering MKB-kennisoverdracht." Delft: TNO.

Ballegooijen, M. 2020. "Development of a digital test environment for R&D support of complex multi-state facades with advanced controls." MSc thesis, Eindhoven University of Technology.

Barnaby, C.S., J.L. Wright, and M.R. Collins. 2009. "Improving load calculations for fenestration with shading devices." *ASHRAE transactions* 115 (2):31-44.

Beck, W., D. Dolmans, G. Dutoo, A. Hall, and O. Seppänen. 2010. *Solar Shading REHVA Guidebook 12*. Forssa, Finland.

Bian, Y., T. Leng, and Y. Ma. 2018. "A proposed discomfort glare evaluation method based on the concept of 'adaptive zone'." *Building and Environment* 143:306-17.

Bittner, K., and I. Spence. 2003. *Use case modeling*. *The Addison-Wesley Object Technology Series*. Boston: Addison Wesley.

Bluyssen, P.M., M. Aries, and P. van Dommelen. 2011. "Comfort of workers in office buildings: The European HOPE project." *Building and Environment* 46 (1):280-8.

Bodde, K. 2020. "Coupled design optimization of façade design and automated shading control for improving visual comfort in office buildings." MSc thesis, Eindhoven University of Technology.

Böke, J., U. Knaack, and M. Hemmerling. 2020. "Prototype of a cyber-physical façade system." *Journal of Building Engineering* 31:101397.

Bonato, P., and R. Fedrizzi. 2019. "IEA SHC Task 56 - Building Integrated Solar Envelopes: Common Challenges and Trends for the Future." In *IEA SHC Newsletter*. Paris: IEA SHC.

Bonato, P., R. Fedrizzi, M. D'Antoni, M. Meir, A. Kostro, A. Hafner, A.V. Souto, B. Arregi, B. Copertaro, and B. Wilkinson. 2019. "State-of-the-art and SWOT analysis of building integrated solar envelope systems: deliverables A. 1 and A. 2." Paris: IEA SHC.

Brainard, G.C., J.P. Hanifin, J.M. Greeson, B. Byrne, G. Glickman, E. Gerner, and M.D. Rollag. 2001. "Action Spectrum for Melatonin Regulation in Humans: Evidence for a Novel Circadian Photoreceptor." *The Journal of Neuroscience* 21 (16):6405-12.

Breiman, L., J. Friedman, C.J. Stone, and R.A. Olshen. 1984. *Classification and regression trees*. Boca Raton: CRC press.

Brembilla, E., and J. Mardaljevic. 2019. "Climate-Based Daylight Modelling for compliance verification: Benchmarking multiple state-of-the-art methods." *Building and Environment* 158:151-64.

Buckman, A.H., M. Mayfield, and S. B.M. Beck. 2014. "What is a Smart Building?". *Smart and Sustainable Built Environment* 3 (2):92-109.

Bueno, B., J.M. Cejudo Lopez, A. Katsifaraki, and H.R. Wilson. 2018. "A systematic workflow for retrofitting office façades with large window-to-wall ratios based

on automatic control and building simulations." *Building and Environment* 132:104-13.

Bueno, B., J. Wienold, A. Katsifaraki, and T.E. Kuhn. 2015. "Fener: A Radiance-based modelling approach to assess the thermal and daylighting performance of complex fenestration systems in office spaces." *Energy and Buildings* 94:10-20.

Bueno, B., H.R. Wilson, S. Sunkara, A. Sepúlveda, and T.E. Kuhn. 2020. "Simulation-based design of an angle-selective and switchable textile shading system." *Building and Environment* 184.

Bui, D.-K., T.N. Nguyen, A. Ghazlan, N.-T. Ngo, and T.D. Ngo. 2020. "Enhancing building energy efficiency by adaptive façade: A computational optimization approach." *Applied energy* 265:114797.

Bustamante, W., D. Uribe, S. Vera, and G. Molina. 2017. "An integrated thermal and lighting simulation tool to support the design process of complex fenestration systems for office buildings." *Applied energy* 198:36-48.

Cajochen, C., J.M. Zeitzer, C.A. Czeisler, and D.-J. Dijk. 2000. "Dose-response relationship for light intensity and ocular and electroencephalographic correlates of human alertness." *Behav Brain Res* 115 (1):75-83.

Carli, I. 2006. "Window 6 verification results." Amhest: LBNL and Carli Inc.

CEN. 2017a. "EN 14500 - Blinds and shutters — Thermal and visual comfort — Test and calculation methods ". Brussels: European Committee for Standardization.

CEN. 2017b. "EN 14501 - Blinds and shutters — Thermal and visual comfort — Performance characteristics and classification." Brussels: European Committee for Standardization.

CEN. 2017c. "prEN 14501 Blinds and shutters—Thermal and visual comfort—Performance characteristics and classification." Brussels: Comité Européen de Normalisation.

Chan, Y.-C., and A. Tzempelikos. 2013. "Efficient venetian blind control strategies considering daylight utilization and glare protection." *Solar energy* 98:241-54.

Chi, D.A., D. Moreno, P.M. Esquivias, and J. Navarro. 2017. "Optimization method for perforated solar screen design to improve daylighting using orthogonal arrays and climate-based daylight modelling." *Journal of Building Performance Simulation* 10 (2):144-60.

Chinazzo, G., J. Wienold, and M. Andersen. 2019. "Daylight affects human thermal perception." *Scientific Reports* 9 (1):13690.

Choi, S.-J., D.-S. Lee, and J.-H. Jo. 2017. "Method of Deriving Shaded Fraction According to Shading Movements of Kinetic Façade." *Sustainability* 9 (8):1449.

Coffey, B. 2012. "Using building simulation and optimization to calculate lookup tables for control." PhD thesis, University of Colorado.

Coffey, B. 2013. "Approximating model predictive control with existing building simulation tools and offline optimization." *Journal of Building Performance Simulation* 6 (3):220-35.

Cohen, R., P. Ruyssevelt, M. Standeven, W. Bordass, and A. Leaman. 1999. Building intelligence in use: Lessons from the Probe project. In Intelligent Buildings: Realising the Benefits 1999, Watford, UK: BRE.

Correia da Silva, P., V. Leal, and M. Andersen. 2015. "Occupants' behaviour in energy simulation tools: lessons from a field monitoring campaign regarding lighting and shading control." *Journal of Building Performance Simulation* 8 (5):338-58.

Crawley, D.B., L.K. Lawrie, F.C. Winkelmann, W.F. Buhl, Y.J. Huang, C.O. Pedersen, R.K. Strand, et al. 2001. "EnergyPlus: creating a new-generation building energy simulation program." *Energy and Buildings* 33 (4):319-31.

Cubi, E., G. Doluweera, and J. Bergerson. 2015. "Incorporation of electricity GHG emissions intensity variability into building environmental assessment." *Applied energy* 159:62-9.

Curcija, C., S. Vidanovic, R. Hart, J. Jonsson, R. Powles, and R. Mitchell. 2018. "WINDOW Technical Documentation." Berkeley: Lawrence Berkeley National Laboratory; Windows and Envelope Materials Group.

D'Antoni, M., P. Bonato, D. Geisler-Moroder, R. Loonen, and F. Ochs. 2019. "IEA SHC Task 56 - System Simulation Models, part C Office Buildings." Paris, France: International Energy Agency.

Dariush, K.A., M.S. Reilly, and D.R. Michael. 1989. "A Versatile Procedure for Calculating Heat Transfer Through Windows." *ASHRAE transactions* 95.

Daum, D., and N. Morel. 2010. "Assessing the total energy impact of manual and optimized blind control in combination with different lighting schedules in a building simulation environment." *Journal of Building Performance Simulation* 3 (1):1-16.

Day, J.K., C. McIlvennie, C. Brackley, M. Tarantini, C. Piselli, J. Hahn, W. O'Brien, et al. 2020. "A review of select human-building interfaces and their relationship to human behavior, energy use and occupant comfort." *Building and Environment* 178:106920.

de Klijn-Chevalerias, M., R. Loonen, A. Zarzycka, D. de Witte, M. Sarakinioti, and J. Hensen. 2017. Assisting the development of innovative responsive façade elements using building performance simulation. In Proceedings of the Symposium on Simulation for Architecture and Urban Design 2017, Toronto: Society for Computer Simulation International.

De Michele, G., R. Loonen, H. Saini, F. Favoino, S. Avesani, L. Papaiz, and A. Gasparella. 2018. "Opportunities and challenges for performance prediction of dynamic complex fenestration systems (CFS)." *Journal of Facade Design and Engineering* 6 (3):101-15.

De Vries, S.B., and R.C.G.M. Loonen. 2018. "TKI iDEEGO: Intelligent energieregelsysteem voor maximale energiebesparing en comfort met geautomatiseerde binnenzonwering." Eindhoven: Unit Building Physics and Services, Eindhoven University of Technology, TKI Urban Energy.

De Vries , S.B., and R.C.G.M. Loonen. 2018. "TKI ISZ: Intelligente sturing van zonwering voor optimale gebouwprestaties." Eindhoven: Unit Building Physics and Services, Eindhoven University of Technology, TKI Urban Energy.

De Vries, S.B., R.C.G.M. Loonen, and J.L.M. Hensen. 2019. Sensor selection and control strategy development support for automated solar shading systems using building performance simulation. In Building Simulation 2019, Rome IBPSA.

De Vries, S.B., R.C.G.M. Loonen, and J.L.M. Hensen. 2021a. The influence of uncertainties in grid electricity primary energy conversion factors on multi-criteria trade-off solutions in façade design optimisation In Building Simulation 2021a, Brugge: IBPSA.

De Vries, S.B., R.C.G.M. Loonen, and J.L.M. Hensen. 2021b. "Multi-state vertical-blinds solar shading – Performance assessment and recommended development directions." *Journal of Building Engineering* 40:102743.

De Vries, S.B., R.C.G.M. Loonen, and J.L.M. Hensen. 2021c. "Simulation-aided development of automated solar shading control strategies using performance mapping and statistical classification." *Journal of Building Performance Simulation*:1-23.

Denz, P., W. Priedemann, and L. Anders. Year. ACT Façade–Interior sun shading for energy efficient fully glazed façades. In Façade 2018 - COST TU1403 Adaptive Facades Network Final Conference Year, Lucerne: TU Delft Open.

Do, C.T., and Y.-C. Chan. 2020. "Evaluation of the effectiveness of a multi-sectional facade with Venetian blinds and roller shades with automated shading control strategies." *Solar energy* 212:241-57.

Do, C.T., and Y.-C. Chan. 2021. "Daylighting performance analysis of a facade combining daylight-redirecting window film and automated roller shade." *Building and Environment* 191:107596.

Favoino, F., F. Fiorito, A. Cannavale, G. Ranzi, and M. Overend. 2016a. "Optimal control and performance of photovoltachromic switchable glazing for building integration in temperate climates." *Applied energy* 178:943-61.

Favoino, F., F. Goia, M. Perino, and V. Serra. 2016b. "Experimental analysis of the energy performance of an ACTive, RESponsive and Solar (ACTRESS) façade module." *Solar energy* 133:226-48.

Favoino, F., Q. Jin, and M. Overend. 2017. "Design and control optimisation of adaptive insulation systems for office buildings. Part 1: Adaptive technologies and simulation framework." *Energy* 127:301-9.

Favoino, F., M. Overend, and Q. Jin. 2015. "The optimal thermo-optical properties and energy saving potential of adaptive glazing technologies." *Applied energy* 156:1-15.

Fawcett, T. 2006. "An introduction to ROC analysis." *Pattern recognition letters* 27 (8):861-74.

Fedrizzi, R. 2020. "Technology Position Paper: Building Integrated Solar Envelope Systems for HVAC and Lighting." Paris: IEA SHC.

Fedrizzi, R., and T.E. Fassaden. 2018. "Task 56-Building Integrated Solar Envelope Systems for HVAC and Lighting."

Figueiro, M., M. Kalsher, B. Steverson, J. Heerwagen, K. Kampschroer, and M. Rea. 2019. "Circadian-effective light and its impact on alertness in office workers." *Lighting Research & Technology* 51 (2):171-83.

Figueiro, M.G., M. Kalsher, B.C. Steverson, J. Heerwagen, K. Kampschroer, and M.S. Rea. 2018. "Circadian-effective light and its impact on alertness in office workers." *Lighting Research & Technology* 51 (2):171-83.

Finlayson, E.U., D.K. Arasteh, C. Huizenga, M.D. Rubin, and M.S. Reilly. 1993. "WINDOW 4.0: Documentation of calculation procedures." Berkeley, USA: Lawrence Berkeley National Laboratory.

Fontoynont, M., B. Bueno, J. de Boer, R. Delvaeye, B. Deroisy, D. Geisler-Moroder, N. Gentile, T. LUO, D. Neves Pimenta, and P. Reinhold. 2021. "Survey on opportunities and barriers in lighting controls." Paris: IEA SHC Task 61 / EBC Annex 77.

Garretón, J.A.Y., E.M. Colombo, and A. Pattini. 2018. "A global evaluation of discomfort glare metrics in real office spaces with presence of direct sunlight." *Energy and Buildings* 166:145-53.

Gehbauer, C., D.H. Blum, T. Wang, and E.S. Lee. 2020. "An assessment of the load modifying potential of model predictive controlled dynamic facades within the California context." *Energy and Buildings* 210.

Geisler-Moroder, D., and A. Dür. 2010. "Estimating Melatonin Suppression and Photosynthesis Activity in Real-World Scenes from Computer Generated Images." *Conference on Colour in Graphics, Imaging, and Vision* 2010 (1):346-52.

Geisler-Moroder, D., E.S. Lee, and G.J. Ward. 2016. "Validation of the five-phase method for simulating complex fenestration systems with radiance against field measurements." Lawrence Berkeley National Lab.(LBNL), Berkeley, CA (United States).

Ghosh, O. 2021. "Strategies for stimulating market penetration of advanced solar shading systems." PDEng Thesis, Technische Universiteit Eindhoven.

Giovannini, L., F. Favoino, V.R.M. Lo Verso, V. Serra, and A. Pellegrino. 2020. "GLANCE (GLare ANnual Classes Evaluation): An approach for a simplified spatial glare evaluation." *Building and Environment* 186:107375.

Giovannini, L., F. Favoino, A. Pellegrino, V.R.M. Lo Verso, V. Serra, and M. Zinzi. 2019. "Thermochromic glazing performance: From component experimental characterisation to whole building performance evaluation." *Applied energy* 251:113335.

Goia, F. 2016. "Search for the optimal window-to-wall ratio in office buildings in different European climates and the implications on total energy saving potential." *Solar energy* 132:467-92.

Goia, F., M. Haase, and M. Perino. 2013a. "Optimizing the configuration of a façade module for office buildings by means of integrated thermal and lighting simulations in a total energy perspective." *Applied energy* 108:515-27.

Goia, F., M. Perino, and V. Serra. 2013b. "Improving thermal comfort conditions by means of PCM glazing systems." *Energy and Buildings* 60:442-52.

Greenguard. 2013. "UL Environment 2821 - UL GREENGUARD Certification Program Method for Measuring and Evaluating Chemical Emissions From Building Materials, Finishes and Furnishings." In. Illinois: UL Standards.

Gunay, H.B., W. O'Brien, and I. Beausoleil-Morrison. 2016. "Implementation and comparison of existing occupant behaviour models in EnergyPlus." *Journal of Building Performance Simulation* 9 (6):567-88.

Gunay, H.B., W. O'Brien, I. Beausoleil-Morrison, and B. Huchuk. 2014. "On adaptive occupant-learning window blind and lighting controls." *Building Research & Information* 42 (6):739-56.

Haldi, F., and D. Robinson. 2010. "Adaptive actions on shading devices in response to local visual stimuli." *Journal of Building Performance Simulation* 3 (2):135-53.

Hart, R., H. Goudey, and D.C. Curcija. 2018. "Experimental validation and model development for thermal transmittances of porous window screens and horizontal louvred blind systems." *Journal of Building Performance Simulation* 11 (2):190-204.

Hashemloo, A., M. Inanici, and C. Meek. 2015. "GlareShade: a visual comfort-based approach to occupant-centric shading systems." *Journal of Building Performance Simulation* 9:1-15.

Hellinga, H., and T. Hordijk. 2014. "The D&V analysis method: A method for the analysis of daylight access and view quality." *Building and Environment* 79:101-14.

Henninger, R.H., and M.J. Witte. 2011. "EnergyPlus testing with ASHRAE 1052-RP Toolkit–Building fabric analytical tests." Washington: Department of Energy.

Henninger, R.H., and M.J. Witte. 2013. "EnergyPlus Testing with Building Thermal Envelope and Fabric Load Tests from ANSI/ASHRAE Standard 140-2011." Washington: Department of Energy.

Heschong, L. 2003a. "Windows and classrooms: A study of student performance and the indoor environment." Fair Oak: California Energy Commission.

Heschong, L. 2003b. "Windows and offices: A study of office worker performance and the indoor environment." Fair Oak: California Energy Commission.

Heschong, L., K. Wymelenberg van den, M. Andersen, N. Digert, L. Fernandes, A. Keller, J. Loveland, H. McKay, R. Mistrick, and B. Mosher. 2012. "Approved Method: IES Spatial Daylight Autonomy (sDA) and Annual Sunlight Exposure (ASE)." IES-Illuminating Engineering Society.

Hopfe, C.J. 2009. "Uncertainty and sensitivity analysis in building performance simulation for decision support and design optimization." PhD Thesis, Eindhoven University of Technology.

Hu, J., and S. Olbina. 2011. "Illuminance-based slat angle selection model for automated control of split blinds." *Building and Environment* 46 (3):786-96.

Huang, Y., and J.-l. Niu. 2016. "Optimal building envelope design based on simulated performance: History, current status and new potentials." *Energy and Buildings* 117:387-98.

Huchuk, B., H.B. Gunay, W. O'Brien, and C.A. Cruickshank. 2016. "Model-based predictive control of office window shades." *Building Research & Information* 44 (4):445-55.

Hutchins, M. 2015. "High performance dynamic shading solutions for energy efficiency and comfort in buildings." Abingdon: Sonnergy, ESSO.

IEA. 2019. "The Critical Role of Buildings " Paris: International Energy Agency.

Inanici, M., M. Brennan, and E. Clark. Year. Spectral daylighting simulations: Computing circadian light. In Proceedings of BS2015: 14th Conference of International Building Performance Simulation Association, Hyderabad, India Year:

ISO. 2001. "ISO 15099: Thermal Performance of Windows, Doors and Shading Devices—Detailed Calculations." Geneva: ISO.

Jacobson, I. 1987. "Object-oriented development in an industrial environment." *ACM SIGPLAN Notices* 22 (12):183-91.

Jain, A., F. Smarra, M. Behl, and R. Mangharam. 2018. "Data-Driven Model Predictive Control with Regression Trees—An Application to Building Energy Management." *ACM Trans. Cyber-Phys. Syst.* 2 (1):Article 4.

Jakubiec, J.A., and A. Alight. 2021. Spectral and Biological Simulation Methods for the Design of Healthy Circadian Lighting. In Building Simulation 2021, Brugge: IBPSA.

Jakubiec, J.A., and C.F. Reinhart. 2011. DIVA 2.0: Integrating daylight and thermal simulations using rhinoceros 3D, DAYSIM and EnergyPlus. In Building Simulation 2011, Sydney: IBPSA.

Jakubiec, J.A., and C.F. Reinhart. 2012. "The 'adaptive zone'–A concept for assessing discomfort glare throughout daylit spaces." *Lighting Research & Technology* 44 (2):149-70.

Jankowski, S., J. Covello, H. Belini, J. Ritchie, and D. Costa. 2014. "IoT Primer, The Internet of Things: Making Sense of the Next Mega-Trend." The Goldman Sachs Group, Inc.

Jia, M., A. Komeily, Y. Wang, and R.S. Srinivasan. 2019. "Adopting Internet of Things for the development of smart buildings: A review of enabling technologies and applications." *Automation in construction* 101:111-26.

Jin, Q., and M. Overend. 2014. "A prototype whole-life value optimization tool for façade design." *Journal of Building Performance Simulation* 7 (3):217-32.

Karlsen, L., P. Heiselberg, and I. Bryn. 2015. "Occupant satisfaction with two blind control strategies: Slats closed and slats in cut-off position." *Solar energy* 115:166-79.

Katsifaraki, A., B. Bueno, and T.E. Kuhn. 2017. "A daylight optimized simulation-based shading controller for venetian blinds." *Building and Environment* 126:207-20.

Killian, M., and M. Kozek. 2016. "Ten questions concerning model predictive control for energy efficient buildings." *Building and Environment* 105:403-12.

Klems, J.H. 1994. "A New Method for Predicting the Solar Heat Gain of Complex Fenestration Systems I. Overview and Derivation of the Matrix Layer Calculation." *ASHRAE transactions* 100, Part 1.

Knoop, M., O. Stefani, B. Bueno, B. Matusiak, R. Hobday, A. Wirz-Justice, K. Martiny, T. Kantermann, M.P.J. Aarts, and N. Zemmouri. 2019. "Daylight: What makes the difference?". *Lighting Research & Technology*.

Konis, K. 2013. "Evaluating daylighting effectiveness and occupant visual comfort in a side-lit open-plan office building in San Francisco, California." *Building and Environment* 59:662-77.

Konis, K., and E.S. Lee. 2015. "Measured daylighting potential of a static optical louver system under real sun and sky conditions." *Building and Environment* 92:347-59.

Konis, K., and S. Selkowitz. 2017. *Effective Daylighting with High-Performance Facades*. Cham, Switzerland: Springer.

Konstantzos, I., Y.-C. Chan, J.C. Seibold, A. Tzempelikos, R.W. Proctor, and J.B. Protzman. 2015a. "View Clarity Index: a new metric to evaluate clarity of view through window shades." *Building and Environment* 90:206-14.

Konstantzos, I., A. Tzempelikos, and Y.-C. Chan. 2015b. "Experimental and simulation analysis of daylight glare probability in offices with dynamic window shades." *Building and Environment* 87:244-54.

Konstantzos, I., A. Tzempelikos, N.M. Murchison, and R.W. Proctor. 2016. "Daylight Glare Evaluation When the Sun is Within the Field of View Through Window Shades."

Kristl, Ž., M. Košir, M.T. Lah, and A. Krainer. 2008. "Fuzzy control system for thermal and visual comfort in building." *Renewable energy* 33 (4):694-702.

Kuhn, T.E. 2017. "State of the art of advanced solar control devices for buildings." *Solar energy* 154:112-33.

Kwon, M., H. Remøy, A. van den Dobbelsteen, and U. Knaack. 2019. "Personal control and environmental user satisfaction in office buildings: Results of case studies in the Netherlands." *Building and Environment* 149:428-35.

LaFrance, M. 2013. "Technology Roadmap: Energy efficient building envelopes." Paris: IEA Energy Technology Policy Division.

LBNL. 2019a. "Optics: A PC program for analyzing the optical behaviour of fenestration products." *Windows and Daylighting Group, Lawrence Berkeley Laboratory, Berkeley, California, USA*.

LBNL. 2019b. "Window 7.6: A PC program for analyzing window thermal performance of fenestration products." *Windows and Daylighting Group, Lawrence Berkeley Laboratory, LBNL-35298, Berkeley, California, USA*.

Lee, E., D. DiBartolomeo, and S. Selkowitz. 1998. "Thermal and daylighting performance of an automated venetian blind and lighting system in a full-scale private office." *Energy and Buildings* 29 (1):47-63.

Loonen, R.C.G.M. 2018. "Approaches for computational performance optimization of innovative adaptive façade concepts." PhD thesis, Eindhoven university of technology.

Loonen, R.C.G.M., M.L. de Klijn-Chevalerias, and J.L.M. Hensen. 2019. "Opportunities and pitfalls of using building performance simulation in explorative R&D contexts." *Journal of Building Performance Simulation* 12 (3):272-88.

Loonen, R.C.G.M., F. Favoino, J.L.M. Hensen, and M. Overend. 2017. "Review of current status, requirements and opportunities for building performance simulation of adaptive facades." *Journal of Building Performance Simulation* 10 (2):205-23.

Loonen, R.C.G.M., S. Singaravel, M. Trčka, D. Cóstola, and J.L.M. Hensen. 2014. "Simulation-based support for product development of innovative building envelope components." *Automation in construction* 45:86-95.

Loonen, R.C.G.M., M. Trčka, D. Cóstola, and J.L.M. Hensen. 2013. "Climate adaptive building shells: State-of-the-art and future challenges." *Renewable and Sustainable Energy Reviews* 25:483-93.

Loutzenhiser, P.G., H. Manz, C. Felsmann, P.A. Strachan, and G.M. Maxwell. 2007. "An empirical validation of modeling solar gain through a glazing unit with external and internal shading screens." *Applied Thermal Engineering* 27 (2):528-38.

Lucas, R.J., S.N. Peirson, D.M. Berson, T.M. Brown, H.M. Cooper, C.A. Czeisler, M.G. Figueiro, et al. 2014. "Measuring and using light in the melanopsin age." *Trends in neurosciences* 37 (1):1-9.

Luckiesh, M., and S.K. Guth. 1949. "Brightnesses in visual field at borderline between comfort and discomfort." *Illuminating engineering* 44 (11):650-70.

Luna-Navarro, A., G.R. Hunt, and M. Overend. 2022. "Dynamic façades – An exploratory campaign to assess occupant multi-domain environmental satisfaction and façade interaction." *Building and Environment* 211:108703.

Luna-Navarro, A., R. Loonen, M. Juaristi, A. Monge-Barrio, S. Attia, and M. Overend. 2020. "Occupant-Facade interaction: A review and classification scheme." *Building and Environment*.

Luna-Navarro, A., and M. Overend. 2021. "Design, construction and validation of MATELab: A novel outdoor chamber for investigating occupant-facade interaction." *Building and Environment* 203:108092.

Luna Navarro, A., J. Blanco Cadena, F. Favoino, M. Donato, T. Poli, M. Perino, and M. Overend. 2019. Occupant-Centred Control Strategies For Adaptive Facades:

Preliminary Study Of The Impact Of Shortwave Solar Radiation On Thermal Comfort. In Building Simulation 2019: 16th Conference of IBPSA 2019, Rome, Italy: IBPSA.

Lyons, P., C. Curcija, and J. Hetzel. 2017. "Fenestration." In *Handbook - Fundamentals*, 1-68. Atlanta, USA: ASHRAE.

Magni, M., and F. Ochs. 2020. Analysis of the impact of different HVAC configurations and control strategies on primary energy and cost savings for an office building. In IEA Heat Pump Conference 2020, Jeju, Korea: IEA HPT TCP.

Magni, M., F. Ochs, S. de Vries, A. Maccarini, and F. Sigg. 2021. "Detailed Cross Comparison of Building Energy Simulation Tools Results using a reference office building as a case study." *Energy and Buildings*:111260.

Mahdavi, A. 2001. "Simulation-based control of building systems operation." *Building and Environment* 36 (6):789-96.

Mahdavi, A., A. Mohammadi, E. Kabir, and L. Lambeva. 2008. "Occupants' operation of lighting and shading systems in office buildings." *Journal of Building Performance Simulation* 1 (1):57-65.

Mahdavi, A., B. Spasojevic, and K. Brunner. 2005. Elements of a simulation-assisted daylight-responsive illumination systems control in buildings. In Building Simulation 2005, Montréal: IBPSA.

Mangkuto, R.A., D.K. Dewi, A.A. Herwandani, M.D. Koerniawan, and Faridah. 2019. "Design optimisation of internal shading device in multiple scenarios: Case study in Bandung, Indonesia." *Journal of Building Engineering* 24:100745.

Mangkuto, R.A., M. Rohmah, and A.D. Asri. 2016. "Design optimisation for window size, orientation, and wall reflectance with regard to various daylight metrics and lighting energy demand: A case study of buildings in the tropics." *Applied energy* 164:211-9.

Mardaljevic, J. 2019. Aperture-based daylight modelling: Introducing the 'View Lumen'. In Building Simulation 2019, Rome: IBPSA.

Mashaly, I.A., V. Garcia-Hansen, M.E. Cholette, and G. Isoardi. 2021. "A daylight-oriented multi-objective optimisation of complex fenestration systems." *Building and Environment* 197:107828.

Maurer, C., C. Hubschneider, J. Hollick, M. Meir, P. Lemarchand, R. Garay, K. Tilmann, and V. Aegesen. 2020. "Task 56 - Report on the development of strategies for market penetration." Paris: IEA SHC.

McNeil, A. 2020. "A photographic method for mapping angular locations of exterior solar obstructions." *Journal of Building Engineering* 29:101170.

McNeil, A., and E.S. Lee. 2013. "A validation of the Radiance three-phase simulation method for modelling annual daylight performance of optically complex fenestration systems." *Journal of Building Performance Simulation* 6 (1):24-37.

Meerbeek, B., M. te Kulve, T. Gritti, M. Aarts, E. van Loenen, and E. Aarts. 2014. "Building automation and perceived control: A field study on motorized exterior blinds in Dutch offices." *Building and Environment* 79:66-77.

Méndez Echenagucia, T., A. Capozzoli, Y. Cascone, and M. Sassone. 2015. "The early design stage of a building envelope: Multi-objective search through heating, cooling and lighting energy performance analysis." *Applied energy* 154:577-91.

Mettanant, V. 2013. "Daylight performance of an automated vertical blinds system." *Journal of Science and Technology Mahasarakham University* 32 (1):123-8.

Mitchell, R. 2017. "Complex glazing database (CGDB) version 10.0." In. Berkeley: Lawrence Berkeley National Laboratory.

Mitchell, R. 2018. "International glazing database (IGDB) version 59.0." In. Berkeley: Lawrence Berkeley National Laboratory.

Mohelnikova, J. 2009. "Materials for reflective coatings of window glass applications." *Construction and Building Materials* 23 (5):1993-8.

Molina, G., W. Bustamante, J. Rao, P. Fazio, and S. Vera. 2015. "Evaluation of radiance's genBSDF capability to assess solar bidirectional properties of complex fenestration systems." *Journal of Building Performance Simulation* 8 (4):216-25.

Motamed, A., B. Bueno, L. Deschamps, T.E. Kuhn, and J.L. Scartezzini. 2020. "Self-commissioning glare-based control system for integrated venetian blind and electric lighting." *Building and Environment* 171.

Newsham, G., J. Brand, C. Donnelly, J. Veitch, M. Aries, and K. Charles. 2009. "Linking indoor environment conditions to job satisfaction: a field study." *Building Research & Information* 37 (2):129-47.

Nezamdoost, A., and K. Van Den Wymelenberg. 2017. "A daylighting field study using human feedback and simulations to test and improve recently adopted annual daylight performance metrics." *Journal of Building Performance Simulation* 10 (5-6):471-83.

Niessink, R.J.M., and J. Gerdes. 2018. "Primaire fossiele energiefactor elektriciteit op bovenwaarde (HHV) voor toepassing in de energieprestatienorm NTA 8800." Amsterdam: ECN and TNO, BZK RVO, EZK.

NREL. 2014. "Reference Solar Spectral Irradiance: ASTM G-173." Golden: NREL, Renewable Resource Data Center.

O'Brien, W., K. Kapsis, and A.K. Athienitis. 2013. "Manually-operated window shade patterns in office buildings: A critical review." *Building and Environment* 60:319-38.

O'Brien, W., and B. Gunay. 2015. Mitigating office performance uncertainty of occupant use of window blinds and lighting using robust design. In Building Simulation 2015, Hyderabad, India: IBPSA.

Ochoa, C.E., M.B.C. Aries, and J.L.M. Hensen. 2012a. "State of the art in lighting simulation for building science: a literature review." *Journal of Building Performance Simulation* 5 (4):209-33.

Ochoa, C.E., M.B.C. Aries, E.J. van Loenen, and J.L.M. Hensen. 2012b. "Considerations on design optimization criteria for windows providing low energy consumption and high visual comfort." *Applied energy* 95:238-45.

Ochs, F., and G. Dermentzis. 2018. Evaluation of Efficiency and Renewable Energy Measures Considering the Future Energy Mix. In International Building Physics Conference 2018, Syracuse, USA:

Ochs, F., M. Magni, M. Hauer, D. Geisler-Moroder, P. Bonato, S.B. de Vries, R.C.G.M. Loonen, et al. 2020a. "IEA SHC Task 56 - System Simulation Results - Deliverable DC2." Paris: IEA SHC, IEA SHC.

Ochs, F., M. Magni, E. Venturi, S. de Vries, H. Martin, B. Paolo, E. Taveres-Cachat, D. Venus, D. Geisler-Moroder, and N. Abdelnour. 2020b. "IEA SHC Task 56 - Design Guidelines." Paris: IEA SHC.

Oh, M.H., K.H. Lee, and J.H. Yoon. 2012. "Automated control strategies of inside slat-type blind considering visual comfort and building energy performance." *Energy and Buildings* 55:728-37.

Oldewurtel, F., A. Parisio, C.N. Jones, D. Gyalistras, M. Gwerder, V. Stauch, B. Lehmann, and M. Morari. 2012. "Use of model predictive control and weather forecasts for energy efficient building climate control." *Energy and Buildings* 45:15-27.

Perez, R., P. Ineichen, R. Seals, J. Michalsky, and R. Stewart. 1990. "Modeling daylight availability and irradiance components from direct and global irradiance." *Solar energy* 44 (5):271-89.

Perez, R., R. Seals, and J. Michalsky. 1993. "All-weather model for sky luminance distribution—Preliminary configuration and validation." *Solar energy* 50 (3):235-45.

Pierson, C., J. Wienold, and M. Bodart. 2018. "Review of Factors Influencing Discomfort Glare Perception from Daylight." *Leukos* 14 (3):111-48.

Pilechiha, P., M. Mahdavinejad, F. Pour Rahimian, P. Carnemolla, and S. Seyedzadeh. 2020. "Multi-objective optimisation framework for designing office windows: quality of view, daylight and energy efficiency." *Applied energy* 261:114356.

Piscitelli, M.S., S. Brandi, G. Gennaro, A. Capozzoli, F. Favoino, and V. Serra. 2019. Advanced Control Strategies For The Modulation of Solar Radiation In Buildings: MPC-enhanced Rule-based Control. In Building Simulation 2019, Rome IBPSA.

Radford, A.D., and J.S. Gero. 1980. "Tradeoff diagrams for the integrated design of the physical environment in buildings." *Building and Environment* 15 (1):3-15.

Rea, M., and M. Figueiro. 2018. "Light as a circadian stimulus for architectural lighting." *Lighting Research & Technology* 50 (4):497-510.

Rea, M.S., and M.G. Figueiro. 2016. "Light as a circadian stimulus for architectural lighting." *Lighting Research & Technology* 50 (4):497-510.

Reinhart, C., T. Rakha, and D. Weissman. 2014. "Predicting the Daylit Area—A Comparison of Students Assessments and Simulations at Eleven Schools of Architecture." *Leukos* 10 (4):193-206.

Reinhart, C.F. 2004. "Lightswitch-2002: a model for manual and automated control of electric lighting and blinds." *Solar energy* 77 (1):15-28.

Reinhart, C.F. 2018. *Daylighting Handbook II - Daylight Simulations Dynamic Facades*. Boston: Building Technology Press.

Reinhart, C.F., J.A. Jakubiec, and D. Ibarra. 2013. Definition of a reference office for standardized evaluations of dynamic façade and lighting technologies. In Building Simulation 2013, Chambéry:

Reinhart, C.F., and K. Voss. 2003. "Monitoring manual control of electric lighting and blinds." *Lighting Research & Technology* 35 (3):243-58.

Rizi, R.A., and A. Eltaweel. 2021. "A user detective adaptive facade towards improving visual and thermal comfort." *Journal of Building Engineering* 33:101554.

Roos, A., P. Polato, P.A. Van Nijnatten, M.G. Hutchins, F. Olive, and C. Anderson. 2001. "Angular-dependent optical properties of low-e and solar control windows—: Simulations versus measurements." *Solar energy* 69:15-26.

Roudsari, M.S., M. Pak, and A. Smith. 2013. Ladybug: a parametric environmental plugin for grasshopper to help designers create an environmentally-conscious design2013, Lyon: IBPSA.

Sabine, H., and S.L. Eleanor. Year. Potential energy savings with exterior shades in large office buildings and the impact of discomfort glare. In Fourth BEST Conference Building Enclosure Science & Technology (BEST4) Year, Kansas City, Missouri: NIBS.

Sadeghi, S.A., P. Karava, I. Konstantzos, and A. Tzempelikos. 2016. "Occupant interactions with shading and lighting systems using different control interfaces: A pilot field study." *Building and Environment* 97:177-95.

Sadeghi, S.A., S. Lee, P. Karava, I. Bilionis, and A. Tzempelikos. 2018. "Bayesian classification and inference of occupant visual preferences in daylit perimeter private offices." *Energy and Buildings* 166:505-24.

Saini, H., R.C.G.M. Loonen, and J.L.M. Hensen. 2018. "Simulation-based performance prediction of an energy-harvesting facade system with selective daylight transmission." In *VIII International Congress on Architectural Envelopes (ICAE 2018)*, 213-9.

Santos, L., A. Leitão, and L. Caldas. 2018. "A comparison of two light-redirecting fenestration systems using a modified modeling technique for Radiance 3-phase method simulations." *Solar energy* 161:47-63.

Saxena, M., L. Heschong, K. Van Den Wymelenberg, S. Wayland, and I.P. Analytics. 2010. 61 flavors of daylight. In ACEEE Summer Study on Energy Efficiency in Buildings 2010, Pacific Grove: ACEEE.

Seong, Y.-B. 2015. "HELIOS-EX: Blind control simulator and method with a consideration of adjacent buildings." *Indoor and Built Environment* 24 (1):37-51.

Seong, Y.B., M.S. Yeo, and K.W. Kim. 2014. "Optimized control algorithm for automated venetian blind system considering solar profile variation in buildings." *Indoor and Built Environment* 23 (6):890-914.

Shen, E., J. Hu, and M. Patel. 2014. "Energy and visual comfort analysis of lighting and daylight control strategies." *Building and Environment* 78:155-70.

Shen, H., and A. Tzempelikos. 2012. "Daylighting and energy analysis of private offices with automated interior roller shades." *Solar energy* 86 (2):681-704.

Shen, H., and A. Tzempelikos. 2017. "Daylight-linked synchronized shading operation using simplified model-based control." *Energy and Buildings* 145:200-12.

Shi, A. 2020. "Simulation-based Performance Evaluation of Buildings with Window-frame Integrated Ventilation and Advanced Solar Shading." MSc thesis, Eindhoven University of Technology.

Silva da, P.C., V. Leal, and M. Andersen. 2012. "Influence of shading control patterns on the energy assessment of office spaces." *Energy and Buildings* 50:35-48.

St-Jacques, M., S. Bucking, and W. O'Brien. 2020. "Spatially and temporally sensitive consumption-based emission factors from mixed-use electrical grids for building electrical use." *Energy and Buildings* 224:110249.

Stevens, S. 2001. "Intelligent facades: Occupant control and satisfaction." *International journal of solar energy* 21 (2-3):147-60.

Subramaniam, S. 2018. "Parametric modeling strategies for efficient annual analysis of daylight in buildings." PhD thesis, The Pennsylvania State University.

Sun, Y., Y. Wu, and R. Wilson. 2018. "A review of thermal and optical characterisation of complex window systems and their building performance prediction." *Applied energy* 222:729-47.

Susorova, I., M. Tabibzadeh, A. Rahman, H.L. Clack, and M. Elnimeiri. 2013. "The effect of geometry factors on fenestration energy performance and energy savings in office buildings." *Energy and Buildings* 57:6-13.

Tabadkani, A., A. Roetzel, H.X. Li, and A. Tsangrassoulis. 2020a. "A review of automatic control strategies based on simulations for adaptive facades." *Building and Environment* 175:106801.

Tabadkani, A., A. Roetzel, H. Xian Li, A. Tsangrassoulis, and S. Attia. 2021. "Analysis of the impact of automatic shading control scenarios on occupant's comfort and energy load." *Applied energy* 294:116904.

Tabadkani, A., A. Tsangrassoulis, A. Roetzel, and H.X. Li. 2020b. "Innovative control approaches to assess energy implications of adaptive facades based on simulation using EnergyPlus." *Solar energy* 206:256-68.

Talami, R., J. Wright, and B. Howard. 2020. A comparison between sequential and simultaneous whole-building design optimization for building performance. In Building Simulation and Optimization 2020, Loughborough, UK:

Taveres-Cachat, E., F. Favoino, R. Loonen, and F. Goia. 2021. "Ten questions concerning co-simulation for performance prediction of advanced building envelopes." *Building and Environment* 191:107570.

Taveres-Cachat, E., S. Grynning, and F. Goia. 2018. *Solar efficiency index of building envelopes and load matching in low energy buildings*.

Taveres-Cachat, E., G. Lobaccaro, F. Goia, and G. Chaudhary. 2019. "A methodology to improve the performance of PV integrated shading devices using multi-objective optimization." *Applied energy* 247:731-44.

Thapan, K., J. Arendt, and D.J. Skene. 2001. "An action spectrum for melatonin suppression: evidence for a novel non-rod, non-cone photoreceptor system in humans." *J Physiol* 535 (Pt 1):261-7.

The MathWorks Inc. 2017. "Matlab." Natick, Massachusetts.

Tokura, M., T. Iwata, and M. Shukuya. 1996. "Experimental study on discomfort glare caused by windows part 3: Development of a method for evaluating discomfort glare from a large light source." *Journal of Architecture and Planning* 61 (489):17-25.

Trčka, M., and J.L.M. Hensen. 2010. "Overview of HVAC system simulation." *Automation in construction* 19 (2):93-9.

Tsangrassoulis, A., V. Bourdakis, V. Geros, and M. Santamouris. 2006. "A genetic algorithm solution to the design of slat-type shading system." *Renewable energy* 31 (14):2321-8.

Turan, I., C. Reinhart, and M. Kocher. 2019. Evaluating Spatially-Distributed Views in Open Plan Work Spaces. In Building Simulation 2019, Rome: IBPSA.

Tzempelikos, A. 2008. "The impact of venetian blind geometry and tilt angle on view, direct light transmission and interior illuminance." *Solar energy* 82 (12):1172-91.

Tzempelikos, A., A.K. Athienitis, and P. Karava. 2007a. "Simulation of façade and envelope design options for a new institutional building." *Solar energy* 81 (9):1088-103.

Tzempelikos, A., B. O'Neill, and A. Athienitis. 2007b. Daylight and luminaire control in a perimeter zone using an automated venetian blind. In Conference on Building Low Energy Cooling and Advanced Ventilation Technologies in the 21st Century 2007b, Crete:

Tzempelikos, A., and H. Shen. 2013. "Comparative control strategies for roller shades with respect to daylighting and energy performance." *Building and Environment* 67:179-92.

van der Sommen, W. 2020. "Context-aware solar shading strategies: performance potential and support vector machine learning approaches." MSc thesis, Eindhoven University of Technology.

van Gessel, F., A. Reitsma, J. Reymers, A. Zegelaar, J. Roeten, and N. Zimmermann. 2005. *Jellema 4C - Omhulling, Gevelopeningen*: ThiemeMeulenhoff.

van Moeseke, G., I. Bruyère, and A. De Herde. 2007. "Impact of control rules on the efficiency of shading devices and free cooling for office buildings." *Building and Environment* 42 (2):784-93.

van Uffelen, G.M. 2014. "Gelijkwaardigheidsverklaringen Verosol zonweringscreens." Mook, The Netherlands: Peutz.

van Woensel, R. 2018. "Automated solar shading and occupant behavior - The impact of occupant behavior modeling on the simulation-based performance

prediction of automated solar shading systems." Eindhoven University of Technology.

Walkenhorst, O., C. Reinhart, J. Luther, and J. Timmer. 2002. "Dynamic annual daylight simulations based on one-hour and one-minute means of irradiance data." *Solar energy* 72 (5):385-95.

Wang, T., G. Ward, and E.S. Lee. 2018. "Efficient modeling of optically-complex, non-coplanar exterior shading: Validation of matrix algebraic methods." *Energy and Buildings* 174:464-83.

Ward, G., R. Mistrick, E.S. Lee, A. McNeil, and J. Jonsson. 2011. "Simulating the Daylight Performance of Complex Fenestration Systems Using Bidirectional Scattering Distribution Functions within Radiance." *Leukos* 7 (4):241-61.

Ward, G., R. Shakespeare, C. Ehrlich, J. Mardaljevic, E. Phillips, and P. Apian-Bennewitz. 1998. *Rendering with Radiance: the art and science of lighting visualization*. Edited by Brian Barsky, *The Morgan Kaufmann series in computer graphics and geometric modeling*. San Francisco: Morgan Kaufmann Publishers.

Ward, G.J., T. Wang, D. Geisler-Moroder, E.S. Lee, L.O. Grobe, J. Wienold, and J.C. Jonsson. 2021. "Modeling specular transmission of complex fenestration systems with data-driven BSDFs." *Building and Environment* 196:107774.

Wargocki, P.S., O. , J. Andersson, A. Boerstra, D. Clements-Croome, K. Fitzner, and S.O. Hanssen. 2007. *Indoor climate and productivity in offices*. Rotterdam: REHVA/ISSO.

WELL. 2019. "The WELL Building Standard v2 with Q1 2019 Addenda." New York: WELL Building Institute.

Werner, M., D. Geisler-Moroder, B. Junghans, O. Ebert, and W. Feist. 2017. "DALEC– a novel web tool for integrated day-and artificial light and energy calculation." *Journal of Building Performance Simulation* 10 (3):344-63.

Wetter, M. 2011. "Co-simulation of building energy and control systems with the Building Controls Virtual Test Bed." *Journal of Building Performance Simulation* 4 (3):185-203.

Wetter, M., P. Haves, and B. Coffey. 2008. "Building Controls Virtual Test Bed." Lawrence Berkeley National Laboratory.

Whitsett, D., and M. Fajkus. 2018. *Architectural Science and the Sun: The poetics and pragmatics of solar design*. New York: Routledge.

Wienold, J. 2007. Dynamic simulation of blind control strategies for visual comfort and energy balance analysis. In Building Simulation 2007, Beijing, China: IBPSA.

Wienold, J. 2009a. *Daylight glare in offices*. Freiburg, Germany Fraunhofer and Universität Karlsruhe (TH).

Wienold, J. 2009b. Dynamic daylight glare evaluation. In Building Simulation 2009b, Glasgow, Scotland: IBPSA.

Wienold, J., and J. Christoffersen. 2006. "Evaluation methods and development of a new glare prediction model for daylight environments with the use of CCD cameras." *Energy and Buildings* 38 (7):743-57.

Wienold, J., F. Frontini, S. Herkel, and S. Mende. 2011. Climate based simulation of different shading device systems for comfort and energy demand. In Building Simulation 2011 2011, Sidney: IBPSA.

Wienold, J., T. Iwata, M. Sarey Khanie, E. Erell, E. Kaftan, R.G. Rodriguez, J. Yamin Garreton, T. Tzempelikos, I. Konstantzos, and J. Christoffersen. 2019. "Cross-validation and robustness of daylight glare metrics." *Lighting Research & Technology*:1477153519826003.

Wienold, J., T.E. Kuhn, J. Christoffersen, and M. Andersen. 2017. Annual glare evaluation for fabrics. In PLEA 2017, Edinburg: PLEA.

Winkelmann, F.C. 2001. Modeling windows in EnergyPlus. In Building Simulation 2001, Rio de Janeiro:

Wu, Y., J.H. Kämpf, and J.-L. Scartezzini. 2019a. "Automated 'Eye-sight' Venetian blinds based on an embedded photometric device with real-time daylighting computing." *Applied energy* 252:113317.

Wu, Y., T. Wang, E.S. Lee, J.H. Kämpf, and J.L. Scartezzini. 2019b. "Split-pane electrochromic window control based on an embedded photometric device with real-time daylighting computing." *Building and Environment* 161.

Xie, J., and A.O. Sawyer. 2021. "Simulation-assisted data-driven method for glare control with automated shading systems in office buildings." *Building and Environment* 196:107801.

Yang, X.-S. 2014. "Chapter 14 - Multi-Objective Optimization." In *Nature-Inspired Optimization Algorithms*, edited by Xin-She Yang, 197-211. Oxford: Elsevier.

Yao, J., D.H.C. Chow, R.-Y. Zheng, and C.-W. Yan. 2016. "Occupants' impact on indoor thermal comfort: a co-simulation study on stochastic control of solar shades." *Journal of Building Performance Simulation* 9 (3):272-87.

Yi, Y.K., and A.M. Malkawi. 2009. Thermal efficiency of the window shade. In Proceedings of 11th International Building Simulation Conference 2009, Glasgow: IBPSA.

Yun, G., D.Y. Park, and K.S. Kim. 2017. "Appropriate activation threshold of the external blind for visual comfort and lighting energy saving in different climate conditions." *Building and Environment* 113:247-66.

Yun, S.-I., H.-R. Kim, D.Y. Park, and J.-W. Jeong. 2020. "Sensor minimization method for integrated daylighting control by a mathematical approach." *Energy and Buildings* 214:109891.

Zeiler, W. 2020. "Demand-Side Energy Flexibility Management of Office Buildings." In *Renewable Energy and Sustainable Buildings: Selected Papers from the World Renewable Energy Congress WREC 2018*, edited by Ali Sayigh, 209-20. Cham: Springer International Publishing.

Zirngibl, J. 2020. "prEN 17423 Reporting of Primary Energy Factors and CO2 emission coefficient." *REHVA Journal* February.

13 Curriculum Vitae

Samuel de Vries was born on 26th of May 1987 in Amsterdam, The Netherlands. In 2014, Samuel obtained a MSc degree in Architecture (cum laude and with distinction) from Delft University of Technology. His graduation research focused on mapping the urban metabolism and energy infrastructure of Amsterdam and the design of a multi-functional recreational, agricultural and energy producing landscape. Samuel worked as a freelance architect (2014-2015), a green building consultant at Metabolic B.V. (2015-2016), and as a sustainability and energy consultant at DPA Cauberg-Huygen (2016-2017).

In June 2017, Samuel started a PhD project at Eindhoven University of Technology in the Unit Building Services. His PhD research developed a computational framework for the analyses and optimisation of automated solar shading systems. Samuel's research work is aimed at the application of modelling and simulation strategies to aid decision making in the design of buildings and products that enable a high degree indoor environmental quality whilst minimizing environmental impacts. To date, Samuel de Vries has (co-)authored 4 journal papers, 1 book chapter, and 4 conference papers.

From June 2021, Samuel is employed as a researcher in energy technologies and systems at Amsterdam University of Applied Sciences (HvA).

14 List of publications

Journal articles

de Vries, S.B., R.C.G.M. Loonen, and J.L.M. Hensen. 2021a. "Multi-state vertical-blinds solar shading – performance assessment and recommended development directions." *Journal of Building Engineering*:102743.

de Vries, S.B., R.C.G.M. Loonen, and J.L.M. Hensen. 2021b. "Simulation-aided development of automated solar shading control strategies using performance mapping and statistical classification." *Journal of Building Performance Simulation*:1-23.

Butt, A.A., **S.B. de Vries**, R.C.G.M. Loonen, J.L.M. Hensen, A. Stuiver, J.E.J. van den Ham, and B.S.J.F. Erich. 2021. "Investigating the energy saving potential of thermochromic coatings on building envelopes." *Applied energy* 291:116788.

Magni, M., F. Ochs, **S.B. de Vries**, A. Maccarini, and F. Sigg. 2021. "Detailed Cross Comparison of Building Energy Simulation Tools Results using a reference office building as a case study." *Energy and Buildings*:111260.

Book chapters

Loonen, R.C.G.M., **S.B. de Vries**, and F. Goia. 2022. "Inverse Design for Advanced Building Envelope Materials, Systems, and Operation." In *Rethinking Building Skins*, edited by Eugenia Gasparri, Arianna Brambilla, Gabriele Lobaccaro, Francesco Goia, Annalisa Andaloro and Alberto Sangiorgio. Sawston, U.K.: Elsevier.

Conference contributions

de Vries, S.B., R.C.G.M. Loonen, and J.L.M. Hensen. 2021. The influence of uncertainties in grid electricity primary energy conversion factors on multi-criteria trade-off solutions in façade design optimisation. In Building simulation 2021, Brugge: IBPSA.

de Vries, S.B., R.C.G.M. Loonen, and J.L.M. Hensen. 2019. Sensor selection and control strategy development support for automated solar shading systems using building performance simulation. In Building simulation 2019, Rome IBPSA.

Magni, M., F. Ochs, P. Bonato, M. D'Antoni, D. Geisler-Moroder, **S.B. de Vries**, R.C.G.M. Loonen, A. Maccarini, A. Afshari, and C. Toni. 2019. Comparison of Simulation Results for an Office Building Between Different BES Tools – The Challenge of Getting Rid of Modeller Influence and Identifying Reasons for Deviations. In Building simulation 2019, Rome: IBPSA

D'Antoni, M., D. Geisler-Moroder, P. Bonato, F. Ochs, M. Magni, **S.B. de Vries**, R.C.G.M. Loonen, and R. Fedrizzi. 2018. Definition of a reference office building for simulation based evaluation of solar envelope systems. In EuroSun - 12th International Conference on Solar Energy for Buildings and Industry 2018, Rapperswil, Switzerland: ISES

15 Propositions

1. Visual comfort-driven control strategies for automated solar shading systems can substantially reduce building energy consumption whilst improving occupant exposure to daylight and reducing discomfort glare.

   This doctoral dissertation p.236-237

2. Interior shading devices offer an opportunity to deploy such comfort-driven automated shading strategies at economies of scale because (i) they are particularly suited to be actuated in a fine-tuned manner using silent and low-cost motorisation systems, and (ii) they are a commonly accepted element of contemporary office buildings.

   Lessons learned from collaboration with stakeholders from the shading and façade industry during the PhD research

3. If we want a built environment with minimal carbon emissions in the Netherlands, we should be less worried about the existence of fully glazed office buildings and more focussed on how these facades are operated. The '*blinds closed – lights on*'* situation we tend to find in contemporary office buildings is a squandering of solar exergy and defeats the point of having a window.

   This doctoral dissertation p.211-223

   * Cohen, R., P. Ruyssevelt, M. Standeven, W. Bordass, and A. Leaman. 1999. "Building intelligence in use: lessons from the probe project." *UK, Usable Buildings, London, UK*.

4. Co-optimisation of automated shading controls and static façade features leads to more beneficial building performance outcomes than a stepped, or isolated, optimisation approach. In particular, a balanced combination of static and dynamic shading devices can give a sum that is larger than its parts.

   This doctoral dissertation p.211-223, p.225

5. "*Fast and frugal heuristics*"* are a highly effective tool in designing buildings. They are, however, inextricably connected to the context wherein they were formed and should therefore be reviewed when this context changes. One of the most useful applications of building performance simulation is to use it to continuously test our design heuristics and provide task cues that indicate when a heuristic is appropriate.

   *Raworth (2017) who summarises Gigerenzer et al. (1999): "… *heuristics, the unconscious mental shortcuts we take every time we use a 'rule of thumb' to make decisions. Over millennia, the human brain has evolved to rely on quick decision-making tools in a fastmoving and uncertain world and in many contexts those heuristics lead us to make better decisions than exact calculations would do.*"

   Raworth, K. 2017. *Doughnut economics: seven ways to think like a 21st-century economist*. London: Random House Bussiness Books.

   Gigerenzer, G., et al. 1999. *Simple heuristics that make us smart, Evolution and cognition*. New York: Oxford University Press.

6. 'Sustainable growth' within a system with finite resources is a 'contradictio in terminis'. An important assumption underlying the assertion that growth cannot be sustainable, however, is that our future is not fundamentally different from our past.

   Smil, V. 2019. *Growth: from microorganisms to megacities.* Cambridge, Massachusetts: Mit Press.
   Steffen, W., K. Richardson, J. Rockström, S.E. Cornell, I. Fetzer, E.M. Bennett, R. Biggs, et al. 2015. "Planetary boundaries: Guiding human development on a changing planet." *Science* 347 (6223):1259855.

7. The scientific method is aimed at what 'is' or what 'could' be and not on what 'should' be. Obfuscating the moral grounds for political decisions with supposed scientific grounds feeds into pseudo-scepticism regarding the scientific method and 'should' be avoided if we want to work towards a common societal understanding about what 'is'.

   David Humes 1739 in *A Treatise of Human Nature - Being an attempt to introduce the experimental method of reasoning into moral subject.* London: John Noon.

8. Tinkering* activates subconscious abilities, builds confidence, and helps overcome paralysis caused by a lack of initial knowledge. As such, it is one of the most fast paced and gratifying methods for learning and an effective strategy to many of life's challenges.

   * (i) to repair, adjust, or work with something in an unskilled or experimental manner, (ii) to work in the manner of a tinker. "Tinker." Merriam-Webster.com. Merriam-Webster, 2022. Web. 12

   * "*Ik rotzooi maar wat aan*" - Karel Appel in *De werkelijkheid van Karel Appel*, 1961 a documentary by Jan Vrijman

9. We should foster tinkering in science and education. With the added condition that: "*The first rule of intelligent tinkering is to save all the parts.*"*

   *Paul R. Ehrlich 1971 in *Saturday Review,* 5 June, New York: Saturday Review Press.

10. What we call individual achievement stems as much from support and an enabling social ecosystem as it does from individual capabilities and persistence.

16 Acknowledgements

The final proposition of this dissertation is that 'what we call individual achievement stems as much from support and an enabling social ecosystem as it does from individual capabilities and persistence'. This proposition also holds true for this dissertation. The presented work would not have been possible without the support and interactions of my own social ecosystem and I am very grateful for this.

First and foremost, I would express my deep appreciation for my promotor Jan Hensen and co-promotor Roel Loonen. I owe you gratitude for giving me this opportunity and for the many ideas that have formed this dissertation.

Jan, I would like to thank you for stimulating my own critical reflection and for sharing your knowledge about the scientific method. Some things cannot be taught but can only be shown. Thank you for showing me how to navigate to the core of a problem and making it relevant to society. I also thank you for challenging me to reflect on my own career path and goals, aspects that I was sometimes reluctant to consider. Your attention to the personal development and conditions of young researchers, whilst always stimulating us to be ambitious in our research is greatly appreciated.

Roel, thank you for the many creative exchanges, directions, and practical solutions. The PhD process is much like tracking across a very jagged landscape and you are a very pleasant fellow traveller and guide. Our weekly sessions often led to great leaps forward across difficult terrain. I very much appreciated your encouragement and calm attitude during the climbs across the steepest inclines. Finally, thank you for indulging me in my sometimes unnecessary but educational scenic routes, whilst also pointing me to the map and destination when required.

I would like to thank the other members of the committee for their valuable suggestions and comments that helped improve this dissertation: prof.dr.ir. Myriam Aries, prof.dr. Francesco Goia, prof.dr. Mauro Overend, prof.ir. W. Zeiler, and prof.dr.ir. Akke Suiker.

This research would also not have been possible without the collaboration with our industry partners Kindow and Verosol.

I owe Sam Kin from Kindow my deepest appreciation for sharing his insights into the great diversity of topics that are relevant to technology development and deployment in the solar shading industry. These insights formed the basis for the constraints and the inspiration for the application studies in this research. Sam, thank you for sharing your knowledge, insights, creative ideas, and overall 'yes-we-can' attitude. I would also like to thank Koen Hees for his insights into mechatronics, and Yapkan Choi for sharing his extensive programming skills. The development

Appendices
Appendix A.　　　Supplemental material to Chapter 5

AU:
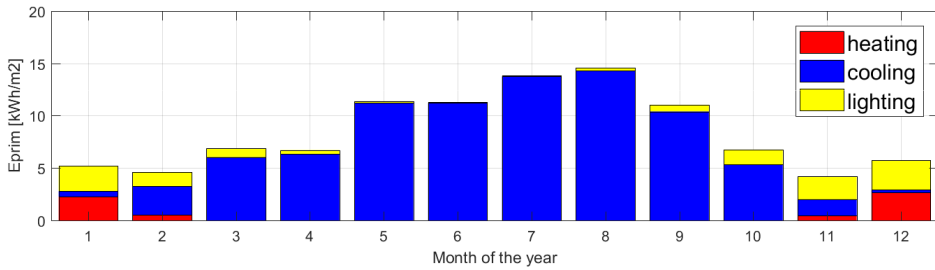
AD:
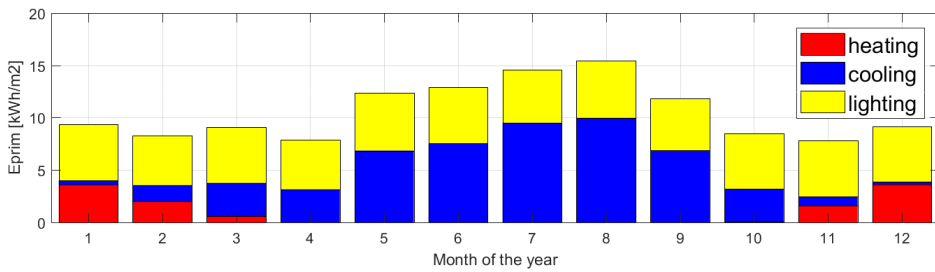
SC:
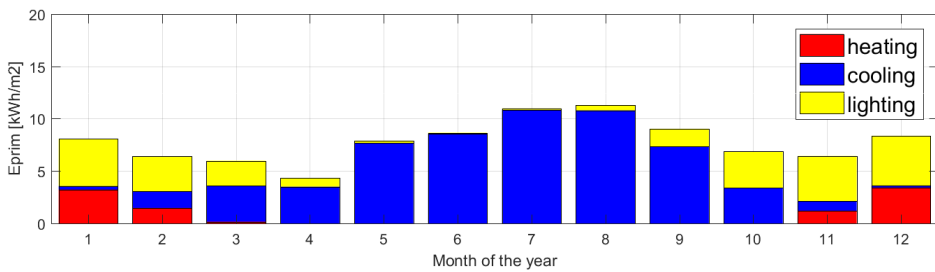
Figure A.1 Monthly primary energy consumption for heating, cooling, and lighting for the AU, AD and SC cases.
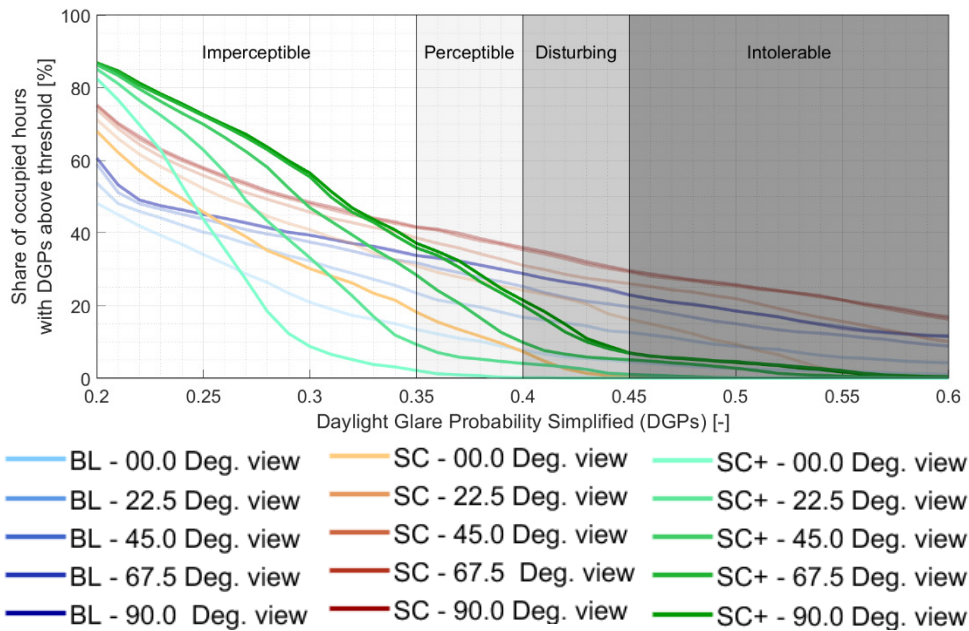
Figure A.2 Glare duration curve for the SC, BL, SC+$_{LoMiHi}$ control strategies. DGPs simulation results for different viewing directions varying between the direction where the occupants are facing the window (00.0 Deg.) to the direction where the occupants are facing a sidewall (90.0 Deg.).

Figure A.3 Façade elevations showing the three different window-to-wall ratios tested in this additional study. The three designs are based on recommendations given by Reinhart, Jakubiec and Ibarra [38]. From left to right: 40, 60 and 80% WWR.

Switch between CM1AU and CM2SC

Threshold based on:	Threshold:	80% Window to wall ratio		60% Window to wall ratio		40% Window to wall ratio	
		6400 lux		7100 lux		8400 lux	
	Glare:	TPR:	97%	TPR:	97%	TPR:	97%
		ACC:	98%	ACC:	98%	ACC:	97%
		DGPs	33%	DGPs	29%	DGPs	24%
		DGPs	8%	DGPs	1%	DGPs	0%
		0.4:45deg		0.4:45deg		0.4:45deg	
		0.4:45deg		0.4:45deg		0.4:40deg	
	sDA:	Actual:	100%	Actual:	78%	Actual:	60%
		Ideal:	100%	Ideal:	78%	Ideal:	60%
	Eprim:	Negative	Positive	Negative	Positive	Negative	Positive
DGPs45deg[2%] >= 0.4	kWh/m2	TNe: 7.9	FPe: 3.8	TNe: 9.0	FPe: 5.3	TNe: 9.3	FPe: 6.4
		FNe: -1.1	TPe: -8.1	FNe: -1.0	TPe: -6.2	FNe: -0.8	TPe: -3.0
		totNe: 6.8	totPe: -4.3	totNe: 8.0	totPe: -0.9	totNe: 8.5	totPe: 3.4
	Saved:	Actual: 6.8	Ideal: 11.7	Actual: 8.0	Ideal: 14.3	Actual: 8.5	Ideal: 15.7

Switch between CM2SC and CM3EL

Threshold based on:	Threshold:	80% Window to wall ratio		60% Window to wall ratio		40% Window to wall ratio	
		31600 lux·m		31700 lux·m		49900 lux·m	
	Glare:	TPR:	100%	TPR:	100%	TPR:	100%
		ACC:	80%	ACC:	85%	ACC:	95%
		DGPs	11%	DGPs	13%	DGPs	18%
		DGPs	0%	DGPs	0%	DGPs	0%
		0.4:45deg		0.4:45deg		0.4:45deg	
		0.4:0deg		0.4:0deg		0.4:0deg	
	sDA:	Actual:	63%	Actual:	44%	Actual:	26%
		Ideal:	69%	Ideal:	46%	Ideal:	26%
	Eprim:	Negative	Positive	Negative	Positive	Negative	Positive
DGPs0 deg >= 0.40 and sensor value * unshaded height	kWh/m2	TNe: 7.9	FPe: 0.8	TNe: 10.7	FPe: 1.6	TNe: 13.8	FPe: 0.8
		FNe: 0.0	TPe: -1.1	FNe: 0.0	TPe: 0.0	FNe: 0.0	TPe: 0.0
		totNe: 7.9	totPe: -0.3	totNe: 10.7	totPe: 1.6	totNe: 13.8	totPe: 0.8
	Saved:	Actual: 0.3	Ideal: 1.1	Actual: -1.6	Ideal: 0.0	Actual: -0.8	Ideal: 0.0

Table A.1 Summary of optimised thresholds and effectivity scores for the I-Ev sensor for switching between the different control modes of the CM1AU2SC3EL strategy for each of the three façade design cases
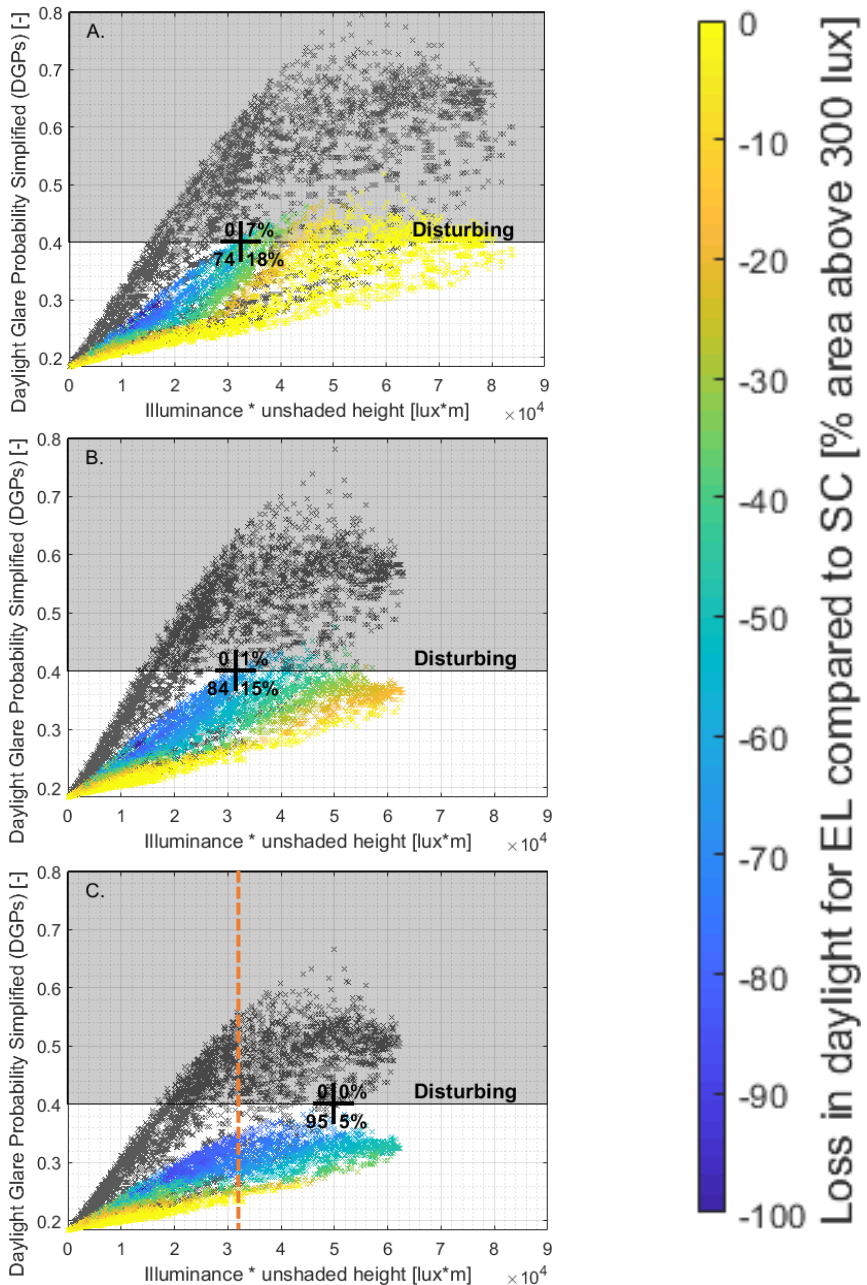
Figure A.4 Simulated glare performance for the SC case in relation to manipulated sensor measurements for each WtW scenario. Graphs illustrate the thresholds for switching between CM$_{2SC}$ and CM$_{3EL}$ that are obtained using the same approach as in Figure 5.15. Orange line: generic threshold obtained using the WtW80% case. A = WtW 80%, B = WtW 60%, C = WtW 40%
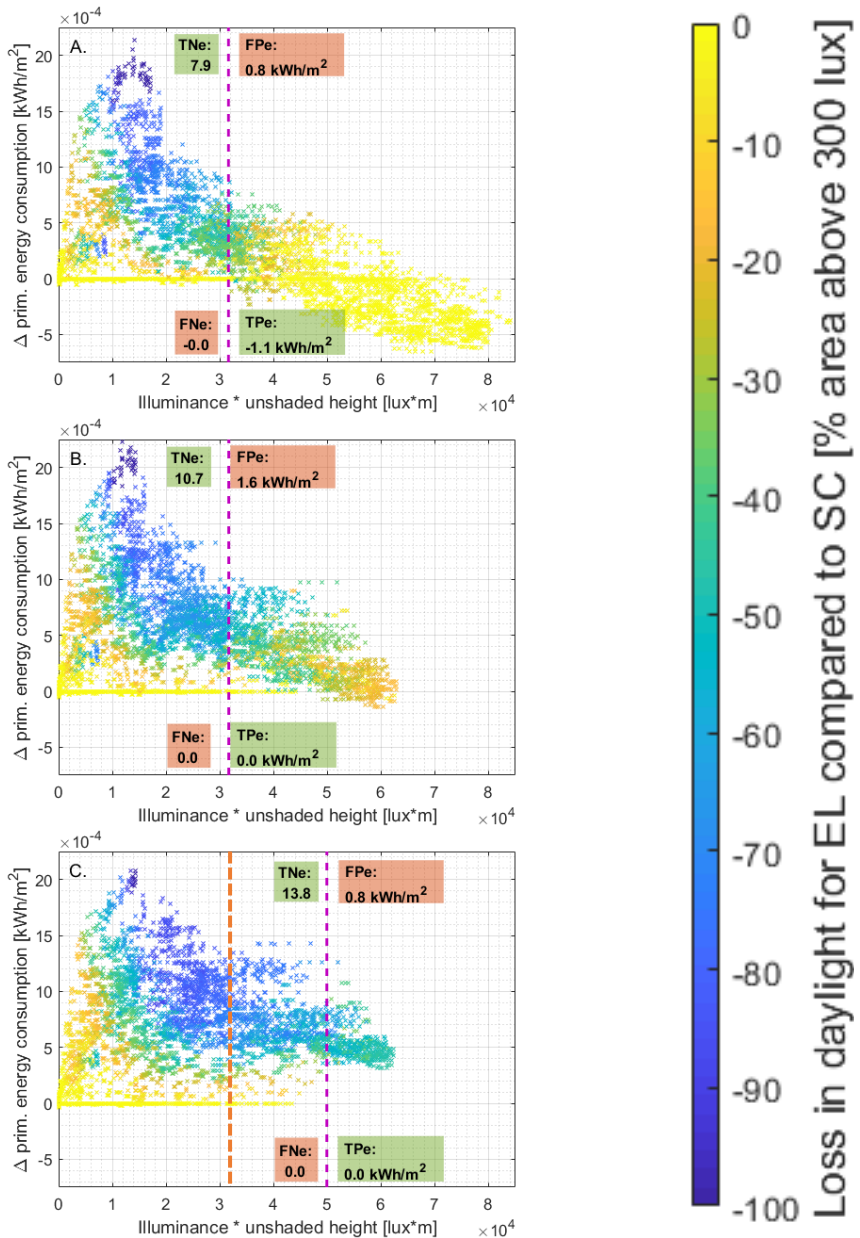
Figure A.5 Simulated E_{prim} for the SC case in relation to manipulated sensor measurements for each WtW scenario. Purple line: thresholds for switching between CM_{2SC} and CM_{3EL} optimised for the specific façade design.
Orange line: generic threshold obtained using the WtW80% case.
A = WtW 80%, B = WtW 60%, C = WtW 40%
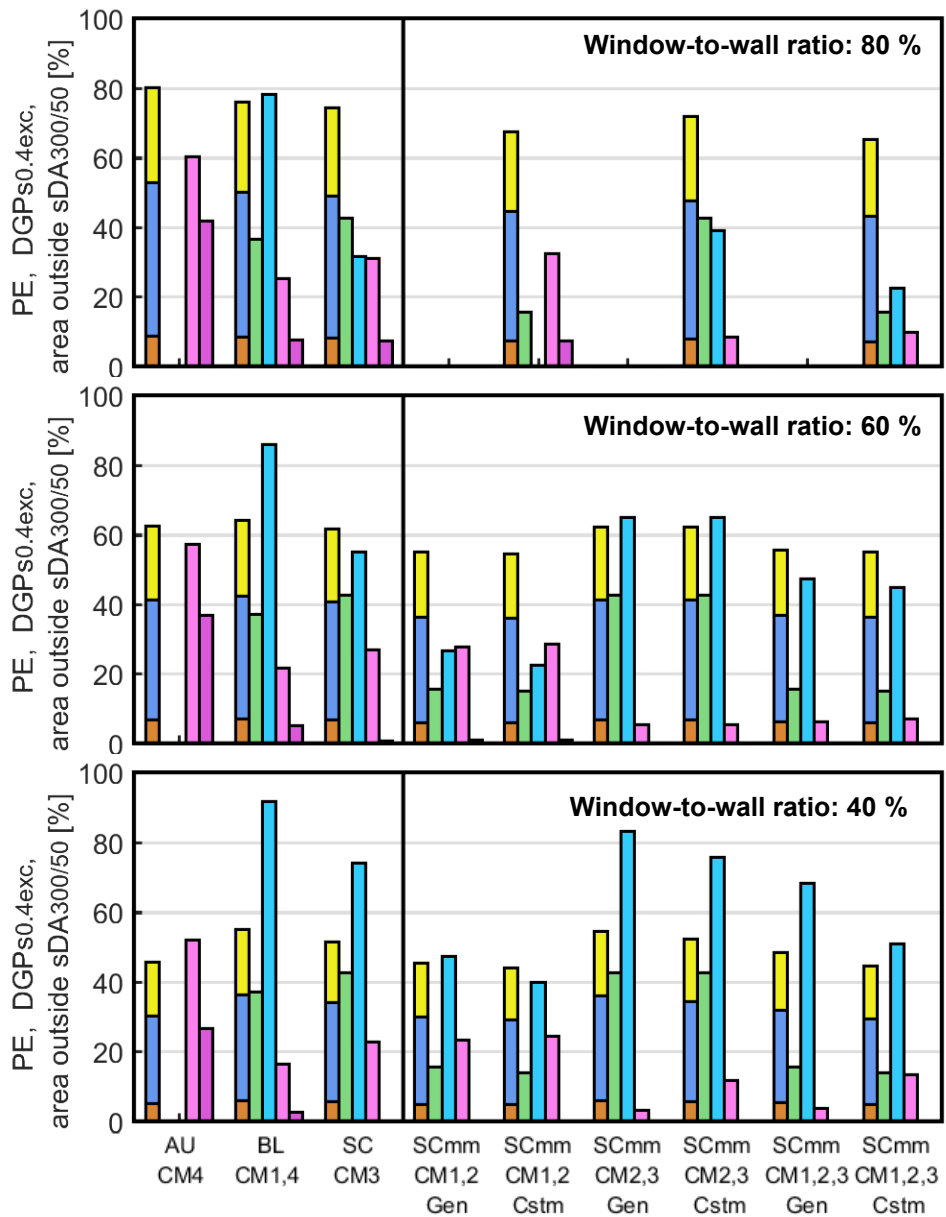
Figure A.6 Summary of whole building performance of the multi-mode and baseline strategies for the 80,60 and 40% window-to-wall ratio cases. Gen: Generic threshold defined using WWR 80%, Cstm: Threshold customised to specific façade design case

Appendix B.   Supplemental material to Chapter 6
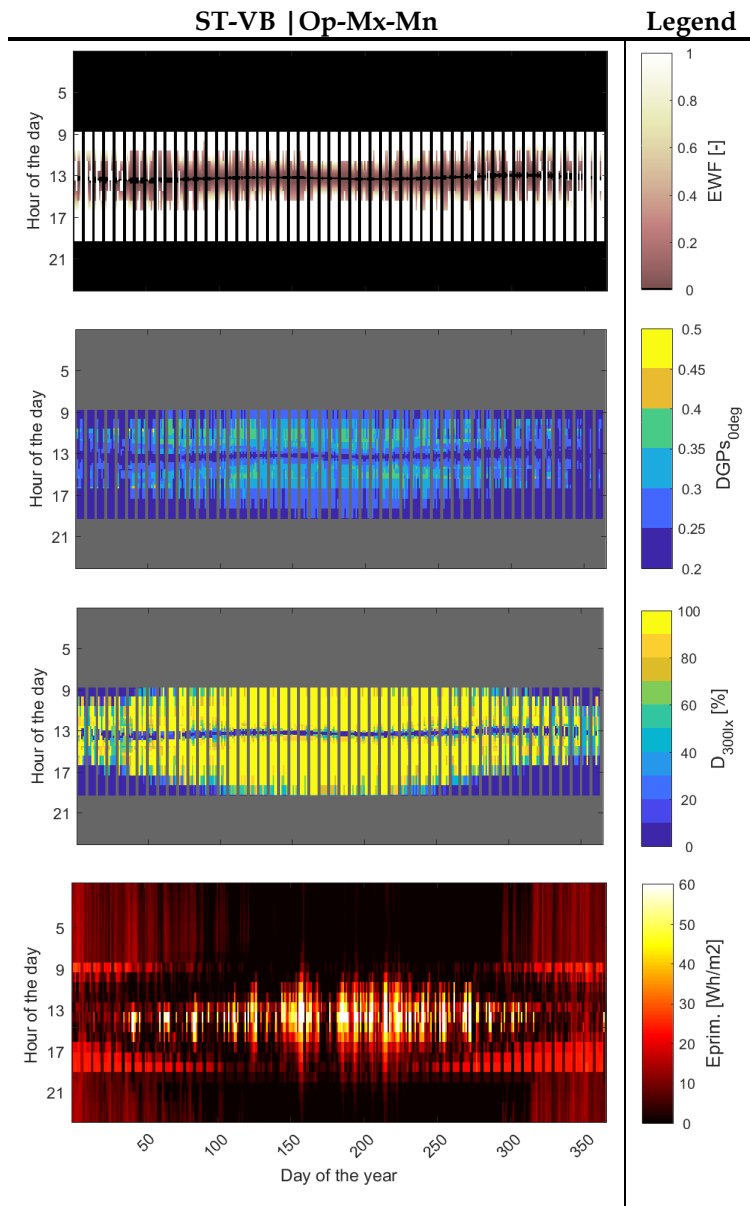
Figure B.1 Temporal maps showing instantaneous behaviour and performance effects at each time step for the 5ST-VB-Op-Mx-Mn-Reflect if morning-Rf80Rb55 strategy

BL | 200 W/m² | WWR80-VSA90-SC　　　　**Legend**
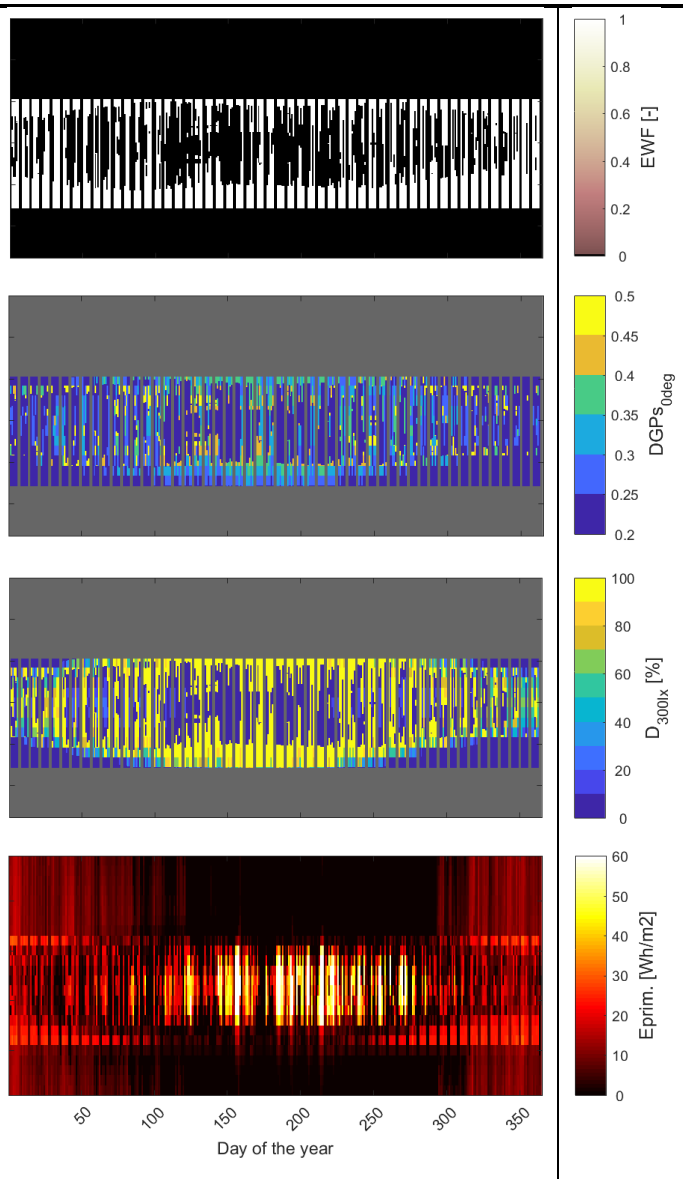
Figure B.2 Temporal maps showing instantaneous behaviour and performance effects at each time step for the 14BL strategy
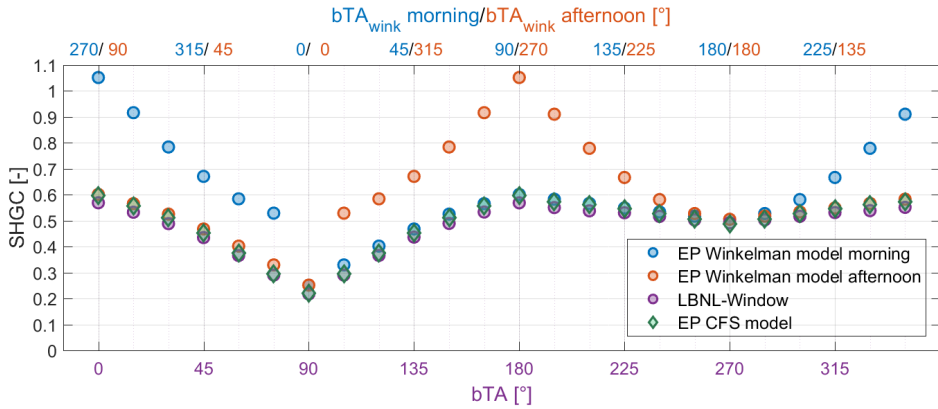
Figure B.3 SHGC in relation to the bRA predicted by LBNL-Window and EnergyPlus using the CFS or Winkelman blind models. The graph shows that rotating the back of the blind towards the sun goes beyond the range of applicability of the Winkelman model and leads to inaccurate predictions

RB-BL | CTree | 80%WWR | SC | 90 VSA   Legend
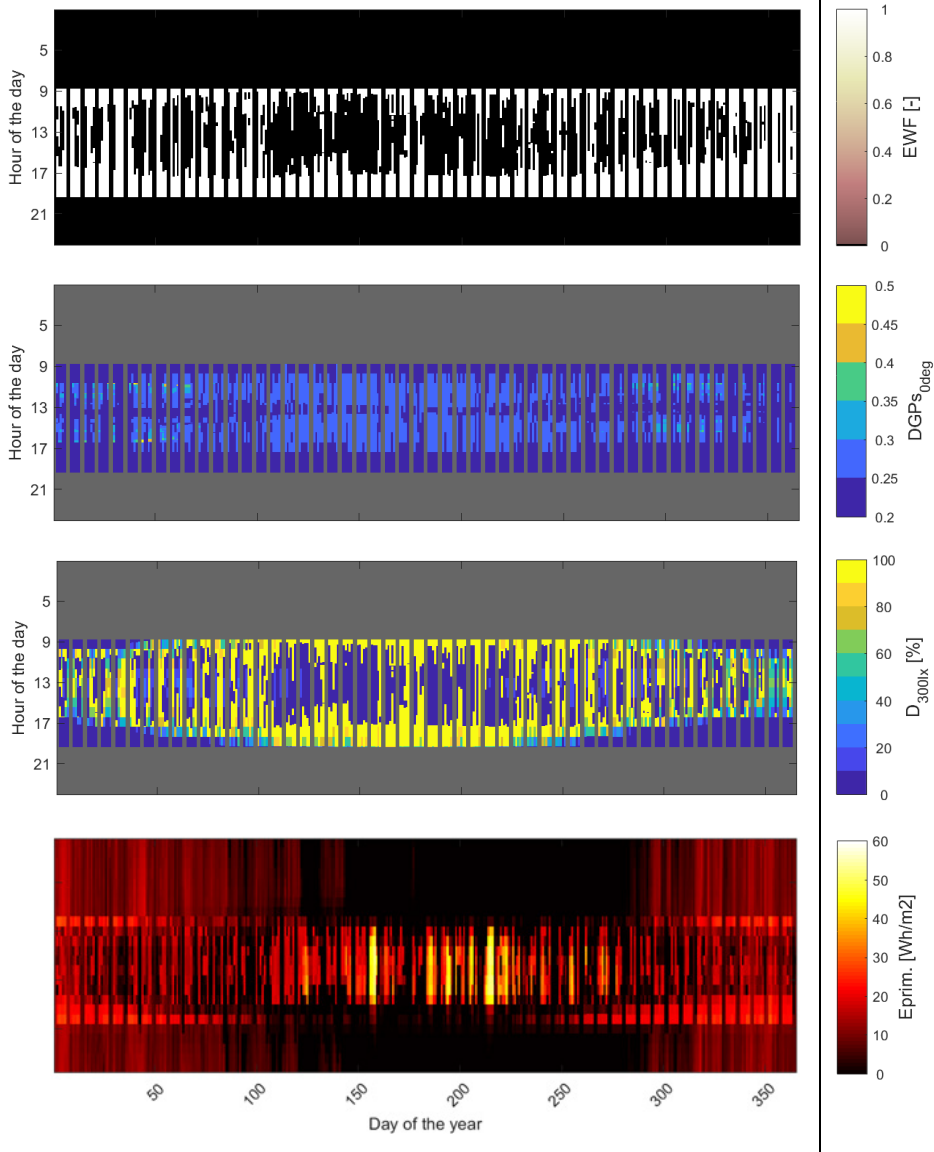
Figure C.1 Temporal maps showing instantaneous behaviour and performance effects at each time step for the STVB-CTree strategy with no horizontal louvres
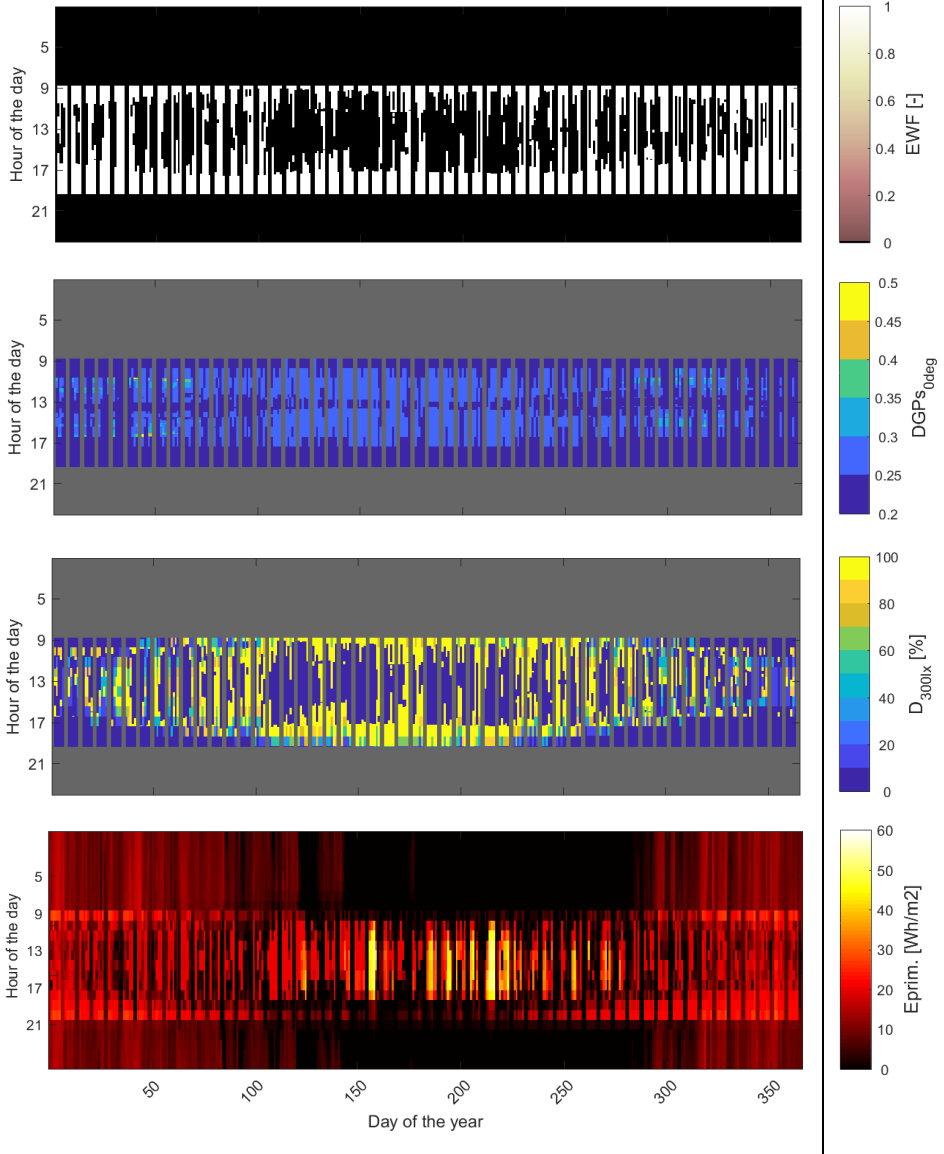
Figure C.2 Temporal maps showing instantaneous behaviour and performance effects at each time step for the STVB-CTree strategy with 40VSA horizontal louvres
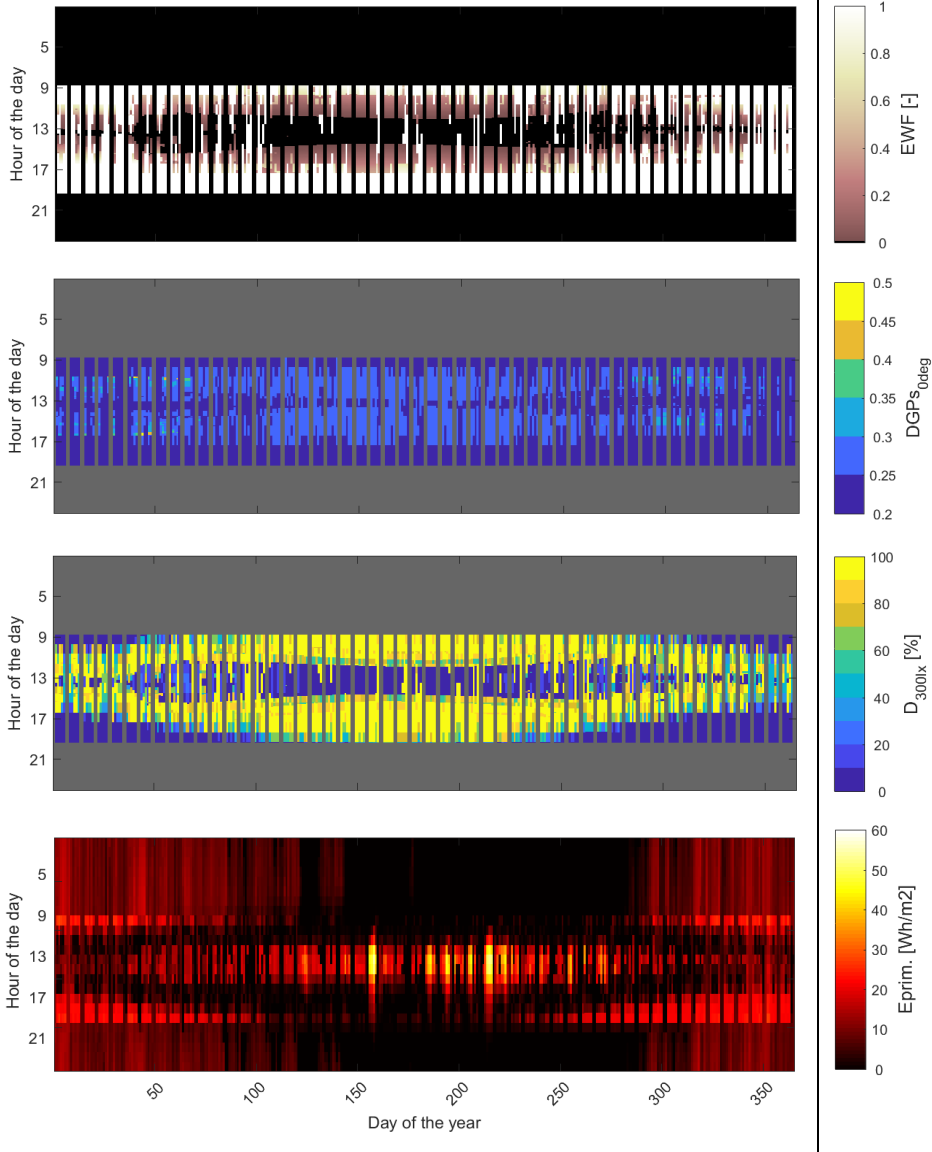
Figure C.3 Temporal maps showing instantaneous behaviour and performance effects at each time step for the STVB-CTree strategy with no horizontal louvres
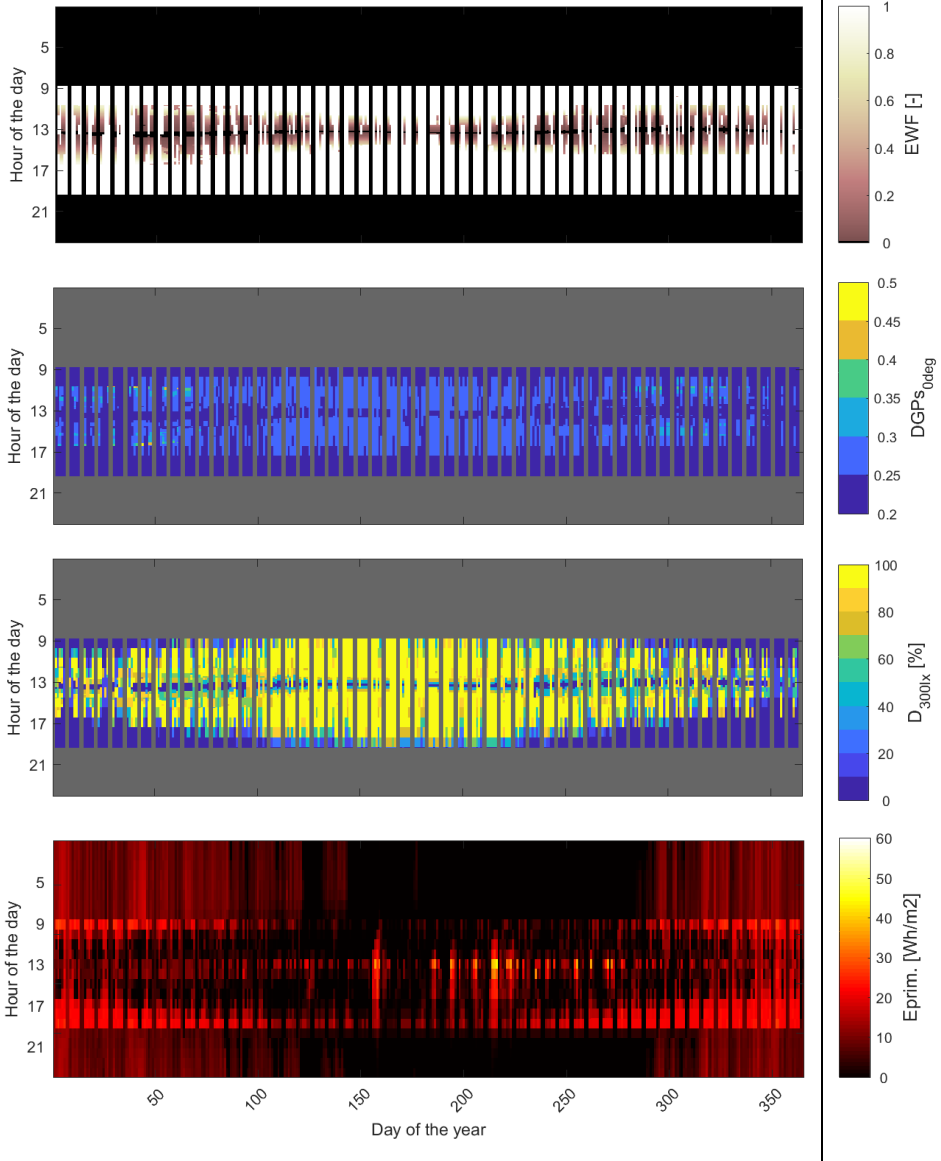
Figure C.4 Temporal maps showing instantaneous behaviour and performance effects at each time step for the STVB-CTree strategy with 40VSA horizontal louvres

Appendix D.   Module F.1.2 for detailed energy system simulation: validation through inter model comparison

This appendix presents an inter model comparison study aimed at validating the VTB modules for detailed energy system simulations. These modules include a detailed non-ducted air-source heat pump model and a façade integrated PV system with accompanying DC/AC inverter. The behaviour of these detailed energy systems is modelled using a stepped approach where a Matlab function computes system efficiencies from a set performance maps using indoor and outdoor temperatures, heating and cooling loads and vertical irradiance simulated by EnergyPlus. The Matlab functions use a set of performance maps. To validate the VTB model implementation the performance predictions of the reference office are compared to simulation made with Simulink-IBK that employs more detailed system models of the same products. This comparison is discussed in more detail in Ochs et al. (2020a).
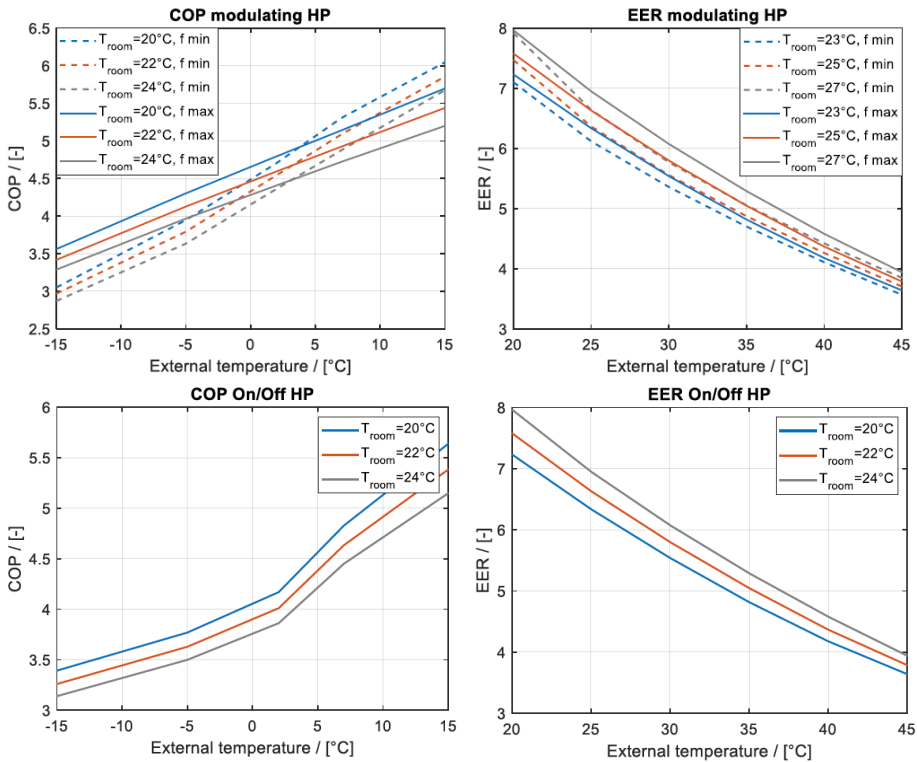
Figure D.1 Heat pump performance maps. Top: modulating mode that is used outside of occupied hours. Bottom: silent on/off mode that is used during occupied hours

The simulation results by the two tools (Figure D.2 and Figure D.3) show sufficient agreement to conclude that the detailed system models were correctly implemented in the VTB.

A. Stockholm | Heatpump electricity consumption for heating and cooling
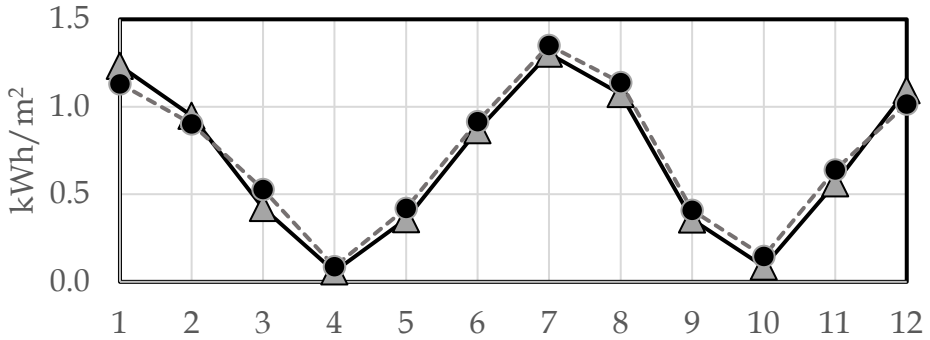
B. Stuttgart | Heatpump electricity consumption for heating and cooling
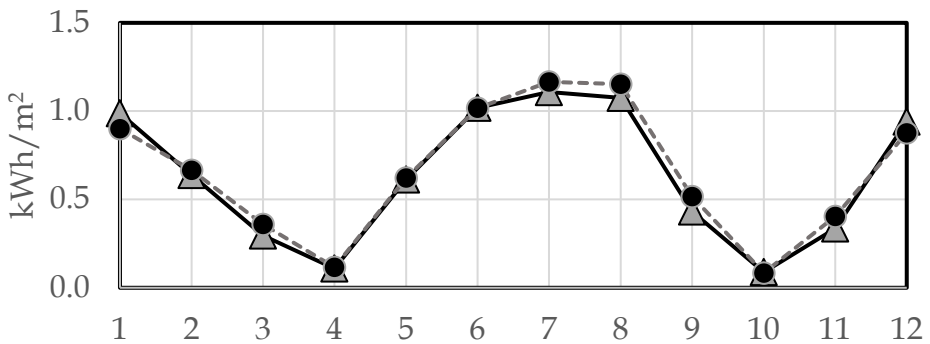
C. Rome | Heatpump electricity consumption for heating and cooling
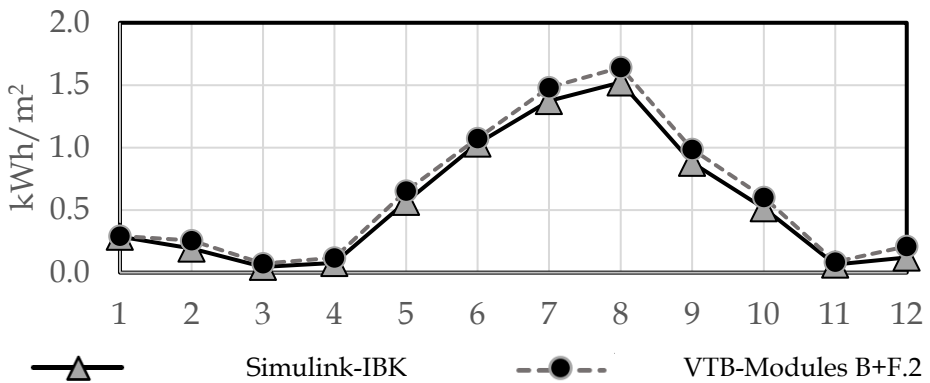
Simulink-IBK   VTB-Modules B+F.2

Figure D.2 Inter model comparison of predicted heat pump electricity consumption between the detailed VTB module F.2 heat pump model and Simulink-IBK

A. Stockholm | PV post inverter AC electricity production
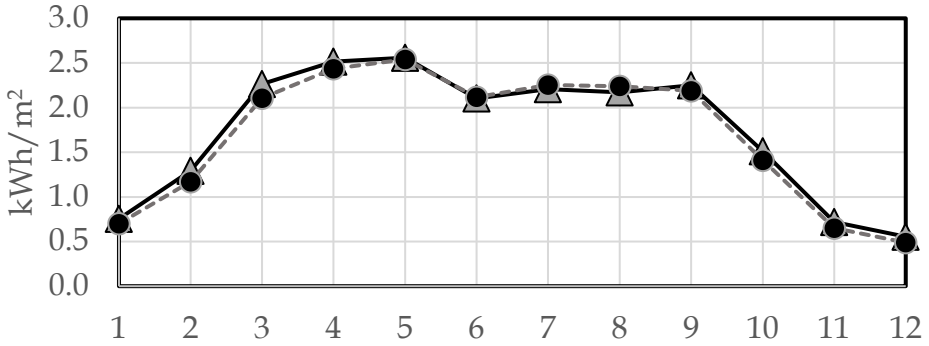
B. Stuttgart | PV post inverter AC electricity production

C. Rome | PV post inverter AC electricity production
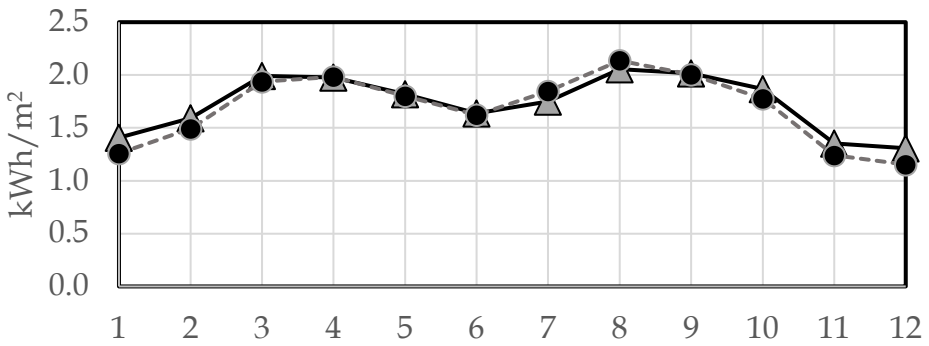
Simulink-IBK   VTB-Modules B+F.2
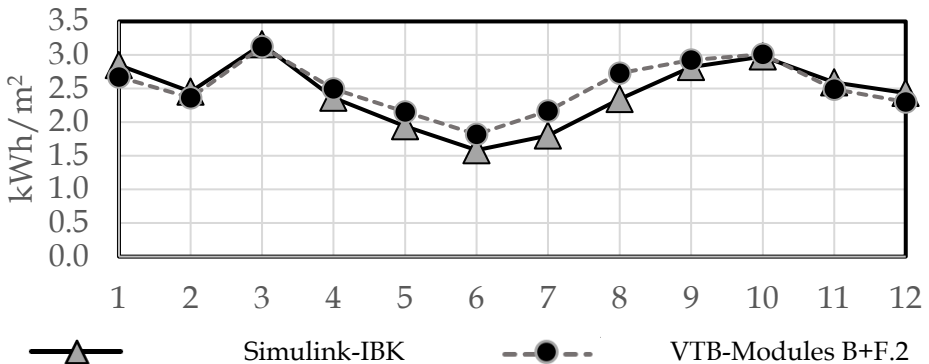
Figure D.3 Inter model comparison of predicted AC electricity production between the detailed VTB module F.2 PV+inverter model and Simulink-IBK

Appendix E. Multi-objective optimisation using the weighted sum method

For identifying solutions that offer optimal performance trade-offs in Chapter 8 the weighted sum method is used (Yang 2014). In the weighted sum method, multiple weighted performance indicators are be summed in one scalar. In this study, this scalar is defined as a penalty score (PF) which is to be minimised. PF is computed from VCT and E_{prim} using the equation:

$$PF_{d;c} = w_1 \cdot VCT_{d;c} + w_2 \cdot E_{prim;d;c} \tag{0.1}$$

$PF_{d;c}$: Penalty for design alternative d and control approach c, w_{vct}: relative performance weight attributed to the VCT indicator, $VCT_{d;c}$: Visual comfort time, $E_{prim;d;c}$: Primary energy consumption for heating, cooling, lighting and equipment.

Two vectors of weighting coefficients, w_{vct} and w_{Eprim} are used to represent different sets of priorities (w) in terms of the trade-offs that are considered desirable between the two performance indicators. These sets of priorities and the corresponding vectors are shown in the following equation:

$$w = w_{vct} + w_{Eprim}, \quad \text{with: } w_{vct} = \begin{bmatrix} 1.00 \\ 0.92 \\ \vdots \\ 0.08 \\ 0.00 \end{bmatrix}, w_{Eprim} = \begin{bmatrix} 0.00 \\ 0.08 \\ \vdots \\ 0.92 \\ 1.00 \end{bmatrix} \tag{0.2}$$

Sets of performance weights w

The optimal design solution ($D_{opt;d;w;c}$) for a particular set of weighting coefficients is found by selecting the design option (d) that gives the minimum PF. This process is repeated for every set of weighting coefficient to find solutions that define the pareto front. To test whether different control approaches lead to different optimal façade solutions, a set of pareto optimal solutions will be obtained for each control strategy individually. These steps are described by the equation:

$$\left[PF_{opt;d;w;c}, D_{opt;w;c} \right] = \min_i \{ PF_{d;w;c} \}_{i=1}^d \quad \textbf{for:} \text{ every } c \text{ and } w \tag{0.3}$$

$PF_{opt;d;w;c}$: Minimum penalty value amongst all design options for control c and weight set w, $D_{opt;w;c}$: Optimal façade design configuration for c and w.

Solutions that are close to the pareto front offer acceptable performance trade-offs and can potentially offer characteristics, that are not described by the selected performance indicators, which make them more desirable than pareto optimal

solutions. Therefore, solutions that are close to the pareto front will be included in a 'near-optimal' group of solutions that is found by selecting solutions with a $PF_{d;w;c}$ that is within 2% of the minimum $PF_{opt;d;w;c}$ for set of weights using equation:

$$\left[D_{n-opt;w;c} \right] = \left| PF_{d;w;c} - PF_{opt;d;w;c} \right| \leq PF_{opt;d;w;c} \cdot 0.02 \text{ \textbf{for:} every } c \text{ and } w \qquad (0.4)$$

$$D_{n\text{-}opt;w;c}: \textit{Near optimal façade design configuration for c and w.}$$

Appendix F. Pseudo code for rule-based control strategies

Table F.1 Pseudo code for vertical blind strategies

ST-VB	**Sun-tracking vertical-blind strategy**
Op	**If $\gamma \leq WN_{\gamma}$:** $bRA_{Op} = 180$
	Else: $bRA_{Op} = 0$
Mx	**If $\gamma \leq WN_{\gamma}$:** $bRA_{Mx} = 90 + 2 * VPPA$
	Else: $bRA_{Mx} = 90 - 2 * VPPA$
Mn	**If $\gamma \leq WN_{\gamma}$:** $bRA_{Mn} = 90 + VPPA$
	Else: $bRA_{Mn} = 90 - VPPA$
Cls	**If $\gamma \leq WN_{\gamma}$:** $max(90, bRA_{Mn} - 30)$
	Else: $min(90, bRA_{Mn} + 30)$
Op-Mx	**If $E_v > 6400$ lx And VPPA < 90:** *set Mx*
	Else: *set Op*
Op-Mn	**If $E_v > 6400$ lx And VPPA < 90:** *set Mn*
	Else: *set Op*
Op-Mx-Mn	**If $E_v > 30000$ lx And VPPA < 90:** *set Mn*
	Else if $E_v > 6400$ lx And VPPA<90: *set Mx*
	Else: *set Op*
Reflect always	**Always:** *Reflecting side of blind always facing sun*
Reflect if morning	**If solar time is morning:**
	Reflecting side of blind facing sun
	Else:
	Absorbing side of blind facing sun
Reflect if afternoon	**If solar time is afternoon:**
	Reflecting side of blind facing sun
	Else:
	Absorbing side of blind facing sun
Reflect if cooling season	**If month is [Jan. Feb. Nov. Dec.]:**
	Absorbing side of blind facing sun
	Else:
	Reflecting side of blind facing sun
Reflect if cooling season or Ti>23	**If month is [Jan. Feb. Nov. Dec.] and Ti < 23°C:**
	Absorbing side of blind facing sun
	Else:
	Reflecting side of blind facing sun
Start retracted	**If first occupied hour of the day and $E_v < 6400$ lx:**
	fully retract blind
	If $E_v > 6400$ lx:
	expand blinds and start sun-tracking response
	if $E_v < 6400$ lx and blinds have already been expanded today:
	most open blind rotation

STVB-CTree	**ST-VB strategy controlled using classification trees** *set lowest CM of CM$_{1;Op}$, CM$_{2;Mx}$, CM$_{3;Mn}$, CM$_{4;Cls}$ for which CT$_{CMx}$ predicts no glare*
BL	**Baseline:** conventional automated roller-blind strategy.
Up-Down 200 W/m²	**If I$_{g;v}$ > 200 W/m²:** *fully lower roller blind* **Else:** *fully raise roller blind*
Up-Down 6400 lx	**If E$_v$ > 6400 lx:** *fully lower roller blind* **Else:** *fully raise roller blind*
sh	Shade height (from bottom of floor to bottom of shade)
1;AU	**Set** *sh = mxSh (maximum shade height)*
1; SC	**Solar cut-off:** control logic for roller blinds *cuttOffHeight = tan(a) · wpd / (cos(γ-180)) + wph* **Set:** *sh = cuttOffHeight*
2;EL	**Set** *sh = min(cuttOffHeight, 1.2)*
4;AD	**Set** *sh = mnSh (minimum shade height)*
SCmm	Multi-mode solar cut-off control strategy
I-Ev	**If Ev < 6400 lx:** *Set AU*
CM1,2,3	**Else if Ev · (sh-mnSh)/(mxSh-mnSh) < 31,600 lx · m:** *Set SC* **Else:** *Set EL*
SC+	As SCmm-CM1,2,3 but with control threshold that are optimised for the specific shading fabric and building
STVB-FrBck	**Double roller blind controlled using classification trees** *set lowest SMSP of:* *SM1SP1, SM2SP2, SM2SP3, SM3SP2, SM3SP3, SM4SP2, SM4SP3, SM4SP4* *for which: CT$_{SMSP}$ predicts no glare, And which: is not restricted by large shade movement limitation*